FUNCTIONAL METAL PHOSPHONATES

A Dissertation

by

HOUSTON PHILLIPP PERRY

Submitted to the Office of Graduate Studies of
Texas A&M University
in partial fulfillment of the requirements for the degree of

DOCTOR OF PHILOSOPHY

December 2011

Major Subject: Chemistry

Functional Metal Phosphonates

FUNCTIONAL METAL PHOSPHONATES

A Dissertation

by

HOUSTON PHILLIPP PERRY

Submitted to the Office of Graduate Studies of
Texas A&M University
in partial fulfillment of the requirements for the degree of

DOCTOR OF PHILOSOPHY

Approved by:

Chair of Committee,	Abraham Clearfield
Committee Members,	Timothy Hughbanks
	Hongcai Zhou
	Jaime Grunlan
Head of Department,	David Russell

December 2011

Major Subject: Chemistry

ABSTRACT

Functional Metal Phosphonates. (December 2011)

Houston Phillipp Perry, B.S., Texas A&M University

Chair of Advisory Committee: Dr. Abraham Clearfield

The primary goal of the work described in this dissertation was the incorporation of functionality into metal phosphonates. This was done in one of several ways. The first involved using phosphonate ligands that had covalently attached organic functional groups. In some cases, these ligands undergo reactions during the solvothermal syntheses which can impart new chemical reactivity. Another method used to introduce functionality was to partially or completely substitute metal atoms within phosphonate clusters to create materials which may have interesting magnetic properties. By controlling the way these clusters pack in the solids, their magnetic properties may be able to be augmented. The final method used to impart functionality to metal phosphonates was the incorporation of N-donor and bulky aryl groups into the phosphonate ligands. These influences caused structural variations which exposed potentially active sites within the materials, including both Lewis acidic and basic sites, as well as Bronsted acid sites.

The first strategy was employed in the design of tetravalent metal phosphonates which have covalently incorporated bipyridine moieties. The materials are porous so that the bipyridine sites can chelate Pd atoms from solution, which can then be reduced to stable nanoparticles trapped within the phosphonate matrix. This approach was also used in the

synthesis of surface-functionalized divalent metal phosphonates which exhibit interesting amine uptake properties.

Solvent and cation substitution effects were used to control the packing and connectivity of phosphonate-based clusters. The selective substitution of metal atoms within the clusters may lead to interesting magnetic materials.

In other work, N-donor and bulky phosphonates were used to influence the structure of several Sn^{II} phosphonates, which resulted in the discovery of a new layered structure type. The effect of the Sn-N interaction on the structures is investigated, and found to have significant effects on the structural units formed and how they pack in the solid state.

The work presented herein represents only a small fraction of the rich chemistry of metal phosphonates. Creative researchers will continue to push boundaries and find new and interesting applications for phosphonate-based materials.

DEDICATION

I would like to dedicate the completion of this work to my family and friends. I thank my mother, Marie, and my father, Phillipp, for their love and support. I would also thank my brother, Brandon. I would especially like to thank my wife, Ruth, for her love, encouragement, and support during the course of this work. Thank you all.

Research is what I'm doing when I don't know what I'm doing. ~Wernher Von Braun

ACKNOWLEDGEMENTS

I would like to thank my committee chair, Dr. Clearfield, and my committee members, Dr. Hughbanks, Dr. Zhou, and Dr. Grunlan for their guidance and support throughout the course of this research. I would also like to thank Justin Law, who worked as an undergraduate researcher with me in the Clearfield lab. I have had many colleagues who have acted as both friends and mentors during my graduate education, including Dr. Jerzy Zon, Dr. Sharath Kirrumakki, Dr. Deyaun Kong, Dr. Aaron Celestian, Dr. Lev Zhakarov, Dr. Boris Shpeizer, Dr. Chris Fewox, Dr. Stacey Wark, Dr. Joy Heising, Dr. Sanjit Konar, Dr. Joseph Reibenspies, Dr. Nattamai Bhuvanesh, Dr. John Hogg, and Dr. Simon Teat. I couldn't have done it without them.

NOMENCLATURE

BET	Brunauer-Emmett-Teller
bpyBPAE	2,2’-bipyridyl-5,5’-(bis)phosphonate tetraethyl ester
DMSO	Dimethylsulfoxide
MePA	Methylphosphonic acid
PTFE	PolyTetraFluoroEthylene
PXRD	Powder X-Ray Diffraction
SAXS	Small-Angle X-ray Scattering
TEM	Transmission Electron Microscopy
TGA	Thermogravimetric Analysis

TABLE OF CONTENTS

CHAPTER Page

LIST OF FIGURES

FIGURE Page

FIGURE Page

FIGURE Page

FIGURE Page

FIGURE Page

FIGURE Page

LIST OF TABLES

CHAPTER I

INTRODUCTION

The current field of metal phosphonate chemistry is a diverse and expansive branch of chemistry. In the 1960's it was first noted that α-zirconium phosphate ($Zr(HPO_4)_2 \cdot H_2O$) had interesting ion-exchange properties,[1-3] similar to clays and other minerals. It was not until the structure was solved by powder X-ray diffraction that these properties could be fully explained.[4] Other tetravalent metals were found to form similar layered compounds.[5, 6] Soon, researchers recognized that phosphonates could be used in place of phosphate, thereby incorporating functional groups into the material.[7-13] This served as a way to modify the ion-exchange properties, proton conductivity, and exfoliation properties. The use of diphosphonic acids afforded a new class of materials in which the inorganic layers were crosslinked.[14-19] These compounds exhibited permanent porosity, high thermal stability, and were stable in acidic and mildly basic media. At the same time, a new field was growing exponentially as trivalent and divalent metals were combined with phosphonic acids of every conceivable variety.[20-26] High-throughput methods utilizing new phosphonic acids, templates, and co-crystallants have resulted in an enormous number of structurally diverse materials.[27-35]

This dissertation follows the style of the *Journal of the American Chemical Society*.

My efforts to advance the field of functional phosphonates have been divided among several projects, which involve different types of phosphonate materials. The first, covered in Chapter III, is the synthesis, characterization, and post-synthetic modification of robust Zr^{IV} and Sn^{IV} phosphonates that possess a covalently attached 2,2'-bipyridyl moiety. These materials are highly porous and can be loaded with nitrophilic metal ions, which may lend them to applications in separations or catalysis. Chapter IV is focused on novel carboxylic acid-functionalized Zn^{II} and Mn^{II} phosphonates. During hydrothermal syntheses, the ligand 4-(phosphono)benzonitrile in situ reactions that can transform it to a carboxylic acid or a carboxylate ester. The carboxylic acid-functionalized materials exhibit unusual amine uptake properties, which are discussed in context with those of other divalent metal phosphonates. Chapter V is concerned with the synthesis and characterization of phosphonate-based heptanuclear Zn, Co, and Mn clusters. The symmetry of the clusters, in addition to how they pack in the solid state, can be controlled by the choice of solvent and cation. Mixed-metal variants of these clusters were also obtained. Variations of these clusters which incorporate anisotropic metal ions may lead to compounds that exhibit single-molecule magnetism. Chapter VI explores structural variations in Sn^{II} phosphonates which are influenced by phosphonate bulk and the incorporation of N-donors into the phosphonate ligands. The relatively weak Sn-N interactions have significant effects on the final structures obtained.

M^{IV} Bipyridyl-bisphosphonates

Several tetravalent metal phosphonates based upon 4,4'-biphenyl-bis(phosphonic acid) have been reported in the literature by Clearfield[36-38] and others,[34, 39] and in general they are thoroughly characterized. The compounds can be made microporous by the inclusion of spacer groups, and have been shown to be catalytically active in Baeyer-Villiger oxidation reactions[38, 40] and terpene rearrangements.[41] Post-synthetic sulfonation of these robust compounds has produced solids that feature strong Brønsted acidity (close to that of 100% H_2SO_4), and exhibit high proton conductivity as solid membranes.[42, 43]

The ligand 2,2'-bipyridyl-5,5'-bis(phosphonic acid) (H_2O_3P-bipy-PO_3H_2) is a structural analogue of 4,4'-biphenyl-bis(phosphonic acid) that has additional capability as a bidentate chelator. This diphosphonic acid is a good candidate for the synthesis of functionalized metal phosphonates, since the structures and reactivity of the analogous Zr and Sn^{IV} biphenyl-diphosphonates have been previously studied. The work presented in Chapter III shows that this ligand can be effectively used to prepare highly porous Zr and Sn^{IV} phosphonates which are capable of binding Pd^{II} from solution. Upon reduction under hydrogen at elevated temperatures, Pd^0 nanoparticles form. The particles are limited to 2-4 nm by the porous phosphonate matrix, which prevents them from agglomerating without the use of stabilizers or surfactants.

Divalent Metal Phosphonocarboxylates

Carboxylic acids are another important functional group that can be incorporated into metal phosphonates. Many compounds based on phosphono-carboxylic acids have been reported in the recent literature.[44-53] In some cases, the carboxylic acids are deprotonated and contribute to the bonding within the structure, while in others, they remain uncoordinated and available for further reaction. The structures obtained when the carboxylate moieties are involved in bonding are interesting, but I am primarily interested in compounds in which the carboxylic acids are free. These types of compounds may further react with bases or metal ions to give materials with novel structures and properties.

In continuation of other work done previously in the Clearfield group on M^{II} phenylphosphonates, I synthesized the compounds $Zn(O_3PC_6H_5CN)H_2O$ and $Mn(O_3PC_6H_5CN)H_2O$ by reacting 4-(phosphonodiethyl)benzonitrile with Zn and Mn salts in water at low temperatures. The compounds obtained are isostructural, and the inorganic layers are identical to those present in $Zn(O_3PC_6H_5)H_2O$ and $Mn(O_3PC_6H_5)H_2O$. By performing the reactions at higher temperatures in water, I was able to achieve the complete hydrolysis of the nitrile group on the ligand to obtain the isostructural carboxylate-functionalized materials. Layered compounds with carboxylate ester surfaces were synthesized by performing the reactions in methanol at high temperatures. The work presented in Chapter IV covers the syntheses and unique amine uptake properties of these materials.

Phosphonate-based Heptanuclear M^{II} Clusters

Polynuclear metal clusters are of great current interest, particularly for their potential as single-molecule magnets (SMMs).[54, 55] Such compounds may have applications in high-density data storage and quantum computing. The majority of these clusters utilize some combination of alkoxides, N-donors, cyanide, and carboxylates to bridge paramagnetic metal ions and form the clusters. However, paramagnetic metal clusters incorporating phosphonate groups are relatively scarce in the literature.[56-62]

In the course of research on compounds formed by transition metals with multifunctional phosphonic acids, I synthesized a series of heptanuclear metal cluster compounds. In these compounds, the central ion is octahedrally coordinated by oxygen atoms from each of the six phosphonate ligands. The six equivalent outer metal ions are five-coordinate in approximate trigonal bipyramidal geometry, and coordinated by oxygen atoms from three phosphonates, a pyridyl nitrogen atom, and another oxygen atom from the carboxylate. The charge of the $[Zn_7(L)_6]^{4-}$ cluster is balanced by four dimethylammonium cations produced by the thermal decomposition of the solvent.

Chapter V describes my work in developing analogues to these Zn clusters with other transition metals that have more interesting magnetic properties. Co^{II} and Mn^{II} seemed to be good candidates for isostructural substitution because they are divalent and are known to adopt both octahedral and trigonal bipyramidal coordination geometries. The packing of the clusters in the solid state can also be varied by changing the charge-balancing cation, which has resulted in several structures in which the clusters are

oriented in the same direction. This is a step towards achieving SMM behavior by increasing the anisotropy. The clusters show promise as magnetically interesting materials for two reasons. First, they contain an odd number of metal ions, so if each one has unpaired electrons, the cluster will have $S \neq 0$. Also, the connectivity of the cluster is unique in that the central metal ion is coupled to each of the external metal ions by oxygen bridges, while the external metal ions are coupled to each other (and the central ion) by phosphonate bridges. This situation presumably results in stronger coupling between the external metal ions and the central ion than between the external ions. This geometry may prove to support unusual magnetic behavior.

Sn^{II} Phosphonates

Sn^{II} compounds are typically studied for their applications in catalysis.[63] One of the goals in this area of research is the incorporation of this functionality into a porous framework.[64, 65] As an exercise in crystal engineering, I chose to systematically vary two factors which affect the structures of Sn^{II} phosphonates. The first factor is the presence of a functional group, in addition to the phosphonate, which may weakly interact with the Sn^{II} atoms to stabilize certain structures. The ligands chosen were pyridine derivatives, which can interact with Sn^{II} atoms by dative bonding. While pyridine-based ligands were shown to interact with the Sn^{II} atoms, weaker bases like nitriles were not observed to engage in this type of bonding.

The second factor which was varied to obtain different structures was the bulk of the phosphonate ligand. Sn^{II} phosphonates typically form layered structures, with the

pendant phosphonate groups decorating the surfaces of inorganic layers.[66, 67] By using bulky ligands, it may be possible to preclude the formation of layers for other structures which better accommodate the bulk of the organic moiety. This may result in structures which have new and interesting architectures, and potentially more accessible Sn^{II} sites.

CHAPTER II

PREPARATION OF PHOSPHONIC ACIDS

General Information

Zirconyl chloride octahydrate was purified by recrystallization from 6M HCl and acetone. Palladium tetrakis(triphenylphosphine) was obtained from Pressure Chemical Company (Pittsburgh, PA). Triethylamine, diethyl phosphite, toluene, Sn^{II} oxalate, Sn^{II} chloride, 3-bromopyridine, 4-bromopyridine, 4-bromotoluene, 3,5-dimethyl bromobenzene, 4-bromo-*t*-butylbenzene, 3,5-di-*t*-butyl benzyl bromide, 9-bromophenanthrene, and benzylphosphonic acid were purchased from Sigma Aldrich. 5,5'-Dibromo-2,2'-bipyridine was obtained by bromination of 2,2'-bipyridine dihydrobromide.[68] Triethylamine was dried over KOH pellets, while toluene and diethylphosphite were distilled and stored over 3 Å sieves. The n-alkylamines used in the work presented in Chapter IV were obtained from Sigma Aldrich and dried over 3 Å sieves. Water was distilled and deionized. Toluene, triethylamine, and diethylphosphite were dried or distilled prior to use. All other starting materials were used as received. 4-Pyridylphosphonic acid[69] and 6-methyl-2-pyridylphosphonic acid[70] were synthesized as described in the literature. Naphthylphosphonic acid and 4,4'-biphenyl(bis)phosphonic acid were kindly provided by Dr. Jerzy Zon of the University of Wroclaw, Poland.

Arylphosphonic Acids

p-Tolylphosphonic acid ($H_2O_3PC_6H_4CH_3$)

$Pd(PPH_3)_4$ (3.47 mmol, 4.0 g) and a stirbar were sealed under dry nitrogen in a 1 liter Schlenck flask topped with a reflux condenser. The top of the condenser was sealed with a septum through which liquid reagents and solvents were added. A balloon attached to a needle was put in the septum to allow for pressure relief. After flushing the entire setup with dry nitrogen, 100 ml toluene was added and the flask was put in an oil bath at 90 °C. *p*-Bromotoluene (0.146 mol, 25 g) was added by syringe, followed by triethylamine (0.165 mol, 23 ml) and diethylphosphite (0.163 mol, 21 ml). The resulting yellow solution refluxed at 110 °C for 18 hours. The mixture was then cooled to room temperature and 100 ml acetone added to further precipitate the Et_3NHBr, which was removed by filtration. The solvents were removed under reduced pressure to give a brownish-orange oil, to which 20 ml acetone was added before it was placed in a freezer at -4 °C. After 24 hours, additional Et_3NHBr which had precipitated was removed by filtration, and the acetone removed under reduced pressure. The brown oil was vacuum-distilled, and the fraction which was collected at 170 °C was kept and identified as diethyl *p*-tolylphosphonate. This colorless oil was added to a 500 ml flask along with 100 ml water and 100 ml concentrated HCl, and the flask placed in an oil bath at 130 °C. After 48 hours, the solution was cooled to room temperature. A white precipitate formed, which was collected by filtration. The remaining solution was dried on a rotary evaporator at 65 °C for several hours, which provided a white solid that was collected

and further dried in an oven at 90 °C. The combined precipitates were identified as *p*-tolylphosphonic acid and used without further purification. Yield: 20.6 g, 82%.

3,5-Dimethylphenylphosphonic acid ($H_2O_3PC_6H_3(CH_3)_2$)

$Pd(PPH_3)_4$ (3.0 mmol, 3.5 g) and a stirbar were sealed under dry nitrogen in a 1 liter Schlenck flask topped with a reflux condenser. The top of the condenser was sealed with a septum through which liquid reagents and solvents were added. A balloon attached to a needle was put in the septum to allow for pressure relief. After flushing the entire setup with dry nitrogen, 100 ml toluene was added and the flask was put in an oil bath at 90 °C. 3,5-dimethylbromobenzene (0.135 mol, 25 g) was added by syringe, followed by triethylamine (0.151 mol, 21 ml) and diethylphosphite (0.147 mol, 19 ml). The resulting yellow solution refluxed at 110 °C for 18 hours. The mixture was then cooled to room temperature and 100 ml acetone added to further precipitate the Et_3NHBr, which was removed by filtration. The solvents were removed under reduced pressure to give a brownish-orange oil, to which 20 ml acetone was added before it was placed in a freezer at -4 °C. After 24 hours, additional Et_3NHBr which had precipitated was removed by filtration, and the acetone removed under reduced pressure. The brown oil was vacuum-distilled, and the fraction which was collected at 180 °C was kept and identified as diethyl (3,5-dimethylphenyl)lphosphonate. This colorless oil was added to a 500 ml flask along with 100 ml water and 100 ml concentrated HCl, and the flask placed in an oil bath at 130 °C. After 48 hours, the solution was cooled to room temperature. A

white precipitate formed, which was collected by filtration and air dried for 24 hours. Yield: 18.4 g, 73%.

4-t-butyl phenylphosphonic acid

4-*t*-butyl-bromobenzene (73.0 mmol, 15.65 g) was heated to 150 °C under a dry nitrogen atmosphere. $NiCl_2$ (3.65 mmol, 0.47 g) was added and the mixture was continuously stirred for the remainder of the reaction. Triethyl phosphite (15.6 ml, 91.25 mmol) was added dropwise over a period of 12 hours. Upon addition of a drop of triethyl phosphite, the reaction would turn a reddish-brown color, gradually changing to greenish-blue over the course of a few minutes. After all the triethylphosphite was added, the reaction maintained a dark purple color. After stirring for another 12 hours at 150 °C, the product and residual triethylphosphite were removed by vacuum distillation at 190 °C. This yielded a colorless oil, which was put under vacuum at 155 °C to remove the residual triethylphosphite. This oil did not have the odor of triethyl phosphite. It was refluxed in 50 ml 6 M HCl and 10 ml ethanol for 18 hours. Upon cooling, a white solid precipitated and was collected by filtration, washed with H_2O, and dried in an oven at 80 °C. The yield of this portion was 4.2 g. Additional portions were obtained by removing the water from the remaining solution in vacuo, resulting in the precipitation of a white solid which was collected and dried in the same manner as the first portion. The total yield was 11.63 g, 74%.

Di-t-butylbenzylphosphonic acid

Di-t-butylbenzylbromide (2.5 g, 8.8 mmol) was refluxed at 160 °C in 10 ml triethylphosphite overnight. Excess triethylphosphite was removed under reduced pressure to yield a pale yellow oil. This oil was refluxed in 50 ml 6 M HCl for 48 hours. After cooling, a white solid was collected by filtration and washed with ~250 ml H_2O. This was then dried in an oven at 90 °C. Yield: 2.03 g, 81%.

Phosphonic Acids with N-Donors

3-Pyridylphosphonic acid

$Pd(PPh_3)_4$ (2.0 mmol, 2.31 g) was placed, with a stirbar, in a 500 ml Schlenk roundbottom flask to which was then affixed a Vigreux column sealed with a septum. A needle with a balloon attached as a pressure moderator was inserted into the septum. The sealed system was then repeatedly evacuated and flushed with dry nitrogen. Toluene (30 ml) was added into the top of the condenser through the septum by syringe, and the setup was placed in an oil bath at 90 °C with stirring. Once the solid had dissolved, 3-bromopyridine (0.1 mol, 15.8 g), triethylamine (0.12 mol, 16.7 ml) and diethyl phosphite (0.12 mol, 15.5 ml) were added sequentially in the same manner as the toluene. The yellow solution was stirred and heated at 115 °C for 12 hours, during which a white precipitate appeared. After cooling, 100 ml acetone was added and the mixture was filtered to remove the majority of the Et_3NHBr. The solvent was then removed under reduced pressure, and 50 ml acetone was added. After cooling to -5 °C, the mixture was filtered again to remove residual Et_3NHBr, and the acetone removed under reduced

pressure. The clear brown oil was dissolved in CH_2Cl_2, dried over $MgSO_4$, and the solvent removed under reduced pressure. Column chromatography on silica gel eluted with ethyl acetate afforded 13.9g (65% yield) diethyl 3-pyridylphosphonate. The ester was then hydrolyzed under acidic conditions according to published procedures. 3-Pyridylphosphonic acid was dried *in vacuo* and used without further purification.

Diethyl 4-cyanophenylphosphonate

$Pd(PPh_3)_4$ (1.25 mmol, 1.44 g) and 4-bromobenzonitrile (50.0 mmol, 9.1 g) were placed, with a stirbar, in a 500 ml Schlenk roundbottom flask to which was then affixed a Vigreux column sealed with a septum. A needle with a balloon attached as a pressure moderator was inserted into the septum. The sealed system was then repeatedly evacuated and flushed with dry nitrogen. Toluene (50 ml) was added into the top of the condenser through the septum by syringe, and the setup was placed in an oil bath at 100 °C with stirring. A white precipitate slowly began to form. After ~20 minutes, an additional 10 ml toluene was added to loosen the mixture and facilitate stirring. The mixture was refluxed for 20 hours, then cooled to ambient temperature before washing three times with 50 ml portions of H_2O. The clear yellow organic phase was dried over $MgSO_4$ and the solvent then removed under reduced pressure. Column chromatography on silica gel eluted with hexanes/ethyl acetate (1:1) afforded 7.2 g (79% yield) diethyl 4-cyanophenylphosphonate. The diethyl ester was used directly in the hydrothermal reaction without further purification.

Tetraethyl 2,2'-bipyridinediyl-5,5'-bis(phosphonate) (bpyBPAE)

This compound was synthesized in a manner derived from that of Penicaud et al.[71]. 5,5'-Dibromo-2,2'-bipyridine (0.025 mol, 7.85 g) and $Pd(PPh_3)_4$ (1.25 mmol, 2.88 g) were sealed under dry nitrogen with a stirbar in a 500 ml Schlenck flask topped with a reflux condenser. The top of the condenser was sealed with a septum through which liquid reagents and solvents were added. A balloon attached to a needle was put into the septum to allow for pressure relief. After flushing the entire setup with dry nitrogen, 60 ml toluene was added and the flask was put in an oil bath at 90 °C. After the catalyst had dissolved, triethylamine (0.055 mol, 7.7 ml) and diethyl phosphite (0.055 mol, 7.1 ml) were added, and the resulting yellow solution refluxed at 110 °C for 18 hours. We found that when performed on this scale, it was not necessary to add additional triphenylphosphine (as was done by Penicaud et al.), and doing so only complicated the purification. The mixture was then cooled to room temperature and 60 ml acetone added to further precipitate the Et_3NHBr, which was removed by filtration. The solvents were removed under reduced pressure to give a brownish-yellow oil, to which 10 ml acetone was added before it was placed in a freezer at -4 °C. After 24 hours, additional Et_3NHBr which had precipitated was removed by filtration, and the acetone removed under reduced pressure. The oil obtained was purified by column chromatography (Rf = 0.2) on silica gel (60 Å, 32-63 μm) using a 3:2 mixture of hexanes/ethyl acetate, which yielded the target compound as a white crystalline solid. This compound had the same ^1H NMR spectrum as was described in the literature [71] and was used without further purification. Yield: 7.27 g, 68%.

CHAPTER III

POROUS ZIRCONIUM AND TIN PHOSPHONATES AS SUPPORTS FOR PALLADIUM NANOPARTICLES

Introduction

Zirconium and tin phosphonates have been extensively researched because of their great potential as functional materials.[72-74] These compounds are typically layered, as they are derivatives of α-zirconium phosphate,[4, 75] which itself is an enormously useful material in ion exchange,[73] catalysis,[76-79] and the synthesis of polymer composites.[80-82] Phosphonate derivatives have the potential to be just as useful, because instead of –OH, they can possess one or more of many different functional groups which can impart new and varied reactivity. In addition to monophosphonate derivatives, crosslinked phosphonates utilizing phenylphosphonic and biphenyldiyl-4,4'-disphosphonic acids can be synthesized as porous solids, and have been post-synthetically sulfonated to form solid-acid catalysts.[42, 83]

Massiot and coworkers reported two Zr-based compounds incorporating 2,2'-bipyridyl.[84] The first was a layered material in which phosphite spacer groups separated the bipyridyl pillars, resulting in a porous structure that exhibited a surface area of 330 m^2/g. This was obtained by solvothermal synthesis in mixtures of DMSO and HF. The second material was also layered, synthesized by a topotactic exchange reaction between γ-zirconium phosphate and 2,2'-bipyridinediyl-5,5'-diphosphonic acid. This material had similar surface area, but the pores were smaller (~5 Å) and more uniform. Both

compounds were shown to be thermally stable and capable of coordinating divalent metals with the bipyridine moieties.

It was observed that even with excess metal present in solution, only a fraction of the bipyridyl sites were occupied in the γ-zirconium phosphate-based material. This indicates that not all of the porosity of the material is accessible, due to bottlenecks in the porous structure or blocking of the channels by the transition metal and its associated ligand sphere. This is in contrast with the results found for the hydrothermally-synthesized compound, which showed nearly complete occupation of the bipyridyl sites. The average pore size is much larger than that of the γ-zirconium phosphate-based material, which may allow more of the bipyridine moieties present to come into contact with metal ions in solution.

Recently, Yaghi and coworkers reported the microporous compound Al(OH)(bpydc), in which 2,2'-bipyridine-5,5'-dicarboxylate (bpdyc) coordinates aluminum only through the carboxylate moieties, leaving the bipyridyl sites open and available for insertion of Pd^{II} or Cu^{II} salts.[85] This material shows a BET surface area in excess of 2000 m^2/g and thermal stability to 400 °C in TGA under a nitrogen atmosphere, which may prove useful in applications such as heterogeneous catalysis and gas sorption.

Thompson and coworkers reported a unique, non-coordinating material based on 4,4'bipyridinium-N,N'-(bis)ethylphosphononate derivatives.[86] The positive charges of the bipyridinium crosslinkers were balanced by halide anions, which could be exchanged for Pd^{II} and Pt^{II} complex anions. These metal ions could then be reduced to make

nanoparticles by bubbling H_2 through an aqueous suspension at 50 °C. This was probably the first work in which metallic nanoparticles were put into a zirconium phosphonate framework. The metals were not complexed by the framework, but ion-exchanged into the material as a charge-balancing anion.

I set out to synthesize a series of porous frameworks, based on Zr and Sn phosphonates, that contained the 2,2'-bipyridyl moiety. The Clearfield group has had considerable success using a spacer group to increase the surface area of Zr and Sn phosphonates[17, 38], so I chose to use methylphosphonic acid as a spacer. Phosphinic acid or phosphoric acid are smaller, which could potentially result in more accessible internal voids, but phosphinic acid is easily oxidized to phosphoric acid, and phosphoric acid could potentially protonate the bipyridyl groups within the material. It was my interest to incorporate 2,2'-bipyridyl functionality into a robust phosphonate framework, and determine how varying the ratio of crosslinker to spacer would affect the surface area, porosity, ion-chelating ability, and the formation of nanoparticles within the pores.

This paper describes my work with Zr and Sn phosphonates which utilize 2,2'-bipyridinediyl-5,5'-diphosphonate as a pillar and methylphosphonate as a spacer ligand to facilitate the formation of pores within the layers. Materials were obtained that have remarkably high surface areas for Zr and Sn phosphonates, which were synthesized at relatively low temperatures without using mixtures of HF and DMSO. The materials readily complex divalent metals, which can be easily reduced to form uniformly-sized nanoparticles dispersed throughout the phosphonate matrix. These particles need no stabilizers or surfactants and are stable to 450 °C.

Syntheses and Characterization

Synthesis of Zr1-Zr6

$ZrOCl_2 \cdot 8H_2O$ (0.5 mmol, 0.161 g) was put in a PTFE-lined pressure vessel of 20 ml internal volume. To this was added the appropriate amounts of **bpyBPAE** and methylphosphonic acid (**MePA**) (given in Table 1). 50% Ethanol/water was added (15 ml) before adding 3 mmol HCl. The pressure vessels were then sealed and heated at 120 °C for 3 days. After cooling, the products were collected by filtration (on 0.2 μm filters) as white powders, which were washed thoroughly with water and ethanol before drying overnight in an oven at 90 °C. Yields were about 85% based on Zr.

Syntheses of Sn1-Sn6

$SnCl_4 \cdot 5H_2O$ (0.5 mmol, 0.175 g) was dissolved in 15 ml of a 50% ethanol/water solution inside a PTFE-lined pressure vessel of 20 ml internal volume. The appropriate amounts of **bpyBPAE** and **MePA** (given in Table 2) were added before 8 mmol HF. The pressure vessels were then sealed and heated at 140 °C for 3 days. After cooling, the products were collected by filtration (on 0.2 μm filters) as white gels, which were washed thoroughly with water and ethanol before drying overnight in an oven at 90 °C. Yields ranged from 60% (for **Sn1**) to 95% (for **Sn6**).

Table 1 Synthetic parameters and BET surface areas for compounds Zr1-Zr6.

Sample Name	Initial Reaction Mixture					Surface Area (m^2/g)	Percent Micropores
	$ZrOCl_2 \cdot 8H_2O$ (mmol)	bpyBPAE (mmol)	MePA (mmol)	Ratio Me:bpy	HCl (mmol)		
Zr1	0.5	0.125	0.75	6:1	3	-	-
Zr2	0.5	0.167	0.67	4:1	3	-	-
Zr3	0.5	0.25	0.5	2:1	3	528	93
Zr4	0.5	0.33	0.33	1:1	3	472	92
Zr5	0.5	0.375	0.25	2:3	3	462	92
Zr6	0.5	0.5	0	0:1	3	353	96

Surface areas of **Zr1** and **Zr2** were not determined because the samples were biphasic.

Table 2 Synthetic parameters and BET surface areas for compounds Sn1-Sn6.

Sample Name	Initial Reaction Mixture					Surface Area (m^2/g)	Percent Micropores
	$SnCl_4 \cdot 5H_2O$ (mmol)	bpyBPAE (mmol)	MePA (mmol)	Ratio Me:bpy	HF (mmol)		
Sn1	0.5	0.125	0.75	6:1	8	515	77
Sn2	0.5	0.167	0.67	4:1	8	434	80
Sn3	0.5	0.25	0.5	2:1	8	388	85
Sn4	0.5	0.33	0.33	1:1	8	363	85
Sn5	0.5	0.375	0.25	2:3	8	357	85
Sn6	0.5	0.5	0	0:1	8	323	82

Pd uptake of Zr3, Zr6, Sn1, and Sn6

To a solution of $Pd(O_2CCH_3)_2$ (0.2 mmol, 0.045 g) in acetone (20 ml) was added 0.10 g of the Zr or Sn phosphonate. The dark yellow mixture was stirred for 16 hours, then collected by filtration and washed thoroughly with acetone before drying in air.

Reduction of the Pd-loaded Materials

The Pd-loaded materials were reduced by heating under an atmosphere of hydrogen in nitrogen. The reductions were performed at 250, 300, 350, 400, and 450 °C. The material was placed in an alumina crucible inside of a long glass tube, which was then inserted into a tube furnace so that the sample was about ¾ of the way into the furnace. The tube was purged with nitrogen as the furnace was heated to the desired temperature. About ten minutes after the furnace came to temperature, the flow gas was switched to 10% H_2 in N_2. After 6 hours, the furnace was switched off and the sample was left under a flow of nitrogen until it was cool enough to handle. The black powder obtained was removed from the crucible and stored in a vial.

Experimental Details

Powder X-ray diffraction data were collected on a Bruker D8 Focus diffractometer using a Cu source (Kα = 1.54184Å) operated at a potential of 40 kV and a current of 40 mA. The detector was equipped with a Lynxeye wire detector. Nitrogen (77.4 K) surface area measurements were performed using an Autosorb-6 instrument

(Quantachrome Instruments, Boyton Beach, FL). The samples were outgassed for 18 hours at 180 °C under turbomolecular pump vacuum prior to the adsorption analysis. Surface areas were calculated on the basis of the BET model. Thermogravimetric analyses were performed with a TA Q500 instrument at a heating rate or 10 °C/min under air. TEM images were acquired using a JEOL 2010 transmission electron microscope operated at an acceleration voltage of 200 kV. SAXS data were collected on a Bruker Nanostar SAXS using a fine-focus Cu source (Kα = 1.54184Å) operated at a potential of 40 kV and a current of 30 mA. The samples were mounted on Mylar tape and data were collected at room temperature. Guinier analyses were performed using the program PRIMUS and R_g confirmed by using the program GNOM.[87] Uv-Vis spectra were acquired using an Ocean Optics USB4000 spectrometer with an Ocean Optics ISS light source. Elemental analyses were performed by Atlantic Microlab (Norcross, GA), Robertson Microlit Labs (Ledgewood, NJ), and Anderson Analytical (College Station, TX).

Powder X-ray Diffraction and TEM

PXRD of the compounds showed that they are practically amorphous and that there is little long-range order. As with many other crosslinked phosphonates that are structural derivatives of α-ZrP, the interlayer spacing gives rise to characteristic peaks which are dependent upon the *d*-spacing. For **Zr1** and **Zr2** (Figure 1), a peak at about 10° 2θ indicates the presence of a second phase, most likely $Zr(O_3PCH_3)_2$, which has a *d*-spacing of ~ 8.9 Å. This phase was only detected in **Zr1** and **Zr2**. The rest of the compounds in the series showed only the peak at ~13.5 Å corresponding to the *d*-spacing of the bipyridyl-pillared phase. The compounds **Sn1**-**Sn6** are all single phase, and exhibit a *d*-spacing of about 13.5 Å, similar to the Zr compounds (Figure 2). This interlayer distance is practically identical to that of the biphenyl-pillared analogues, indicating that these are similar pillared-layer type materials.

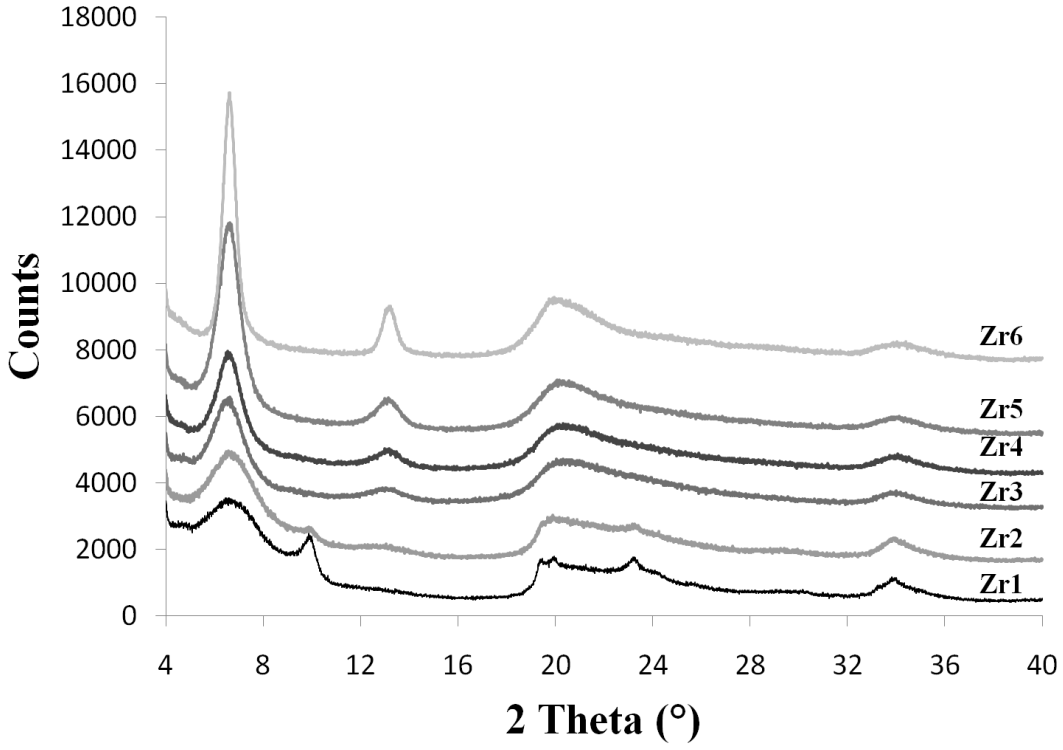

Figure 1 PXRD of Zr1-Zr6

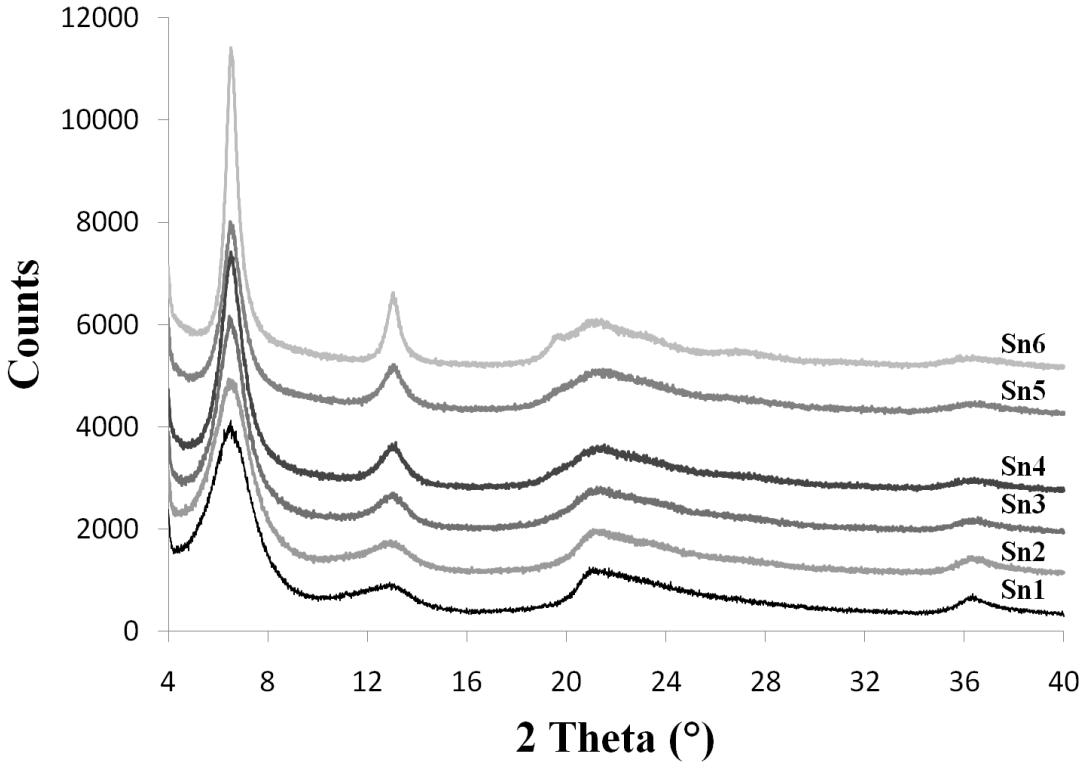

Figure 2 PXRD of Sn1-Sn6

TEM imaging revealed significantly different particle morphologies for the Zr and Sn samples. The Zr compounds consisted of small particles (~ 15 nm) in which distinct layers were observed (Figure 3). The distance between these layers matched the *d*-spacing obtained from PXRD. The stacks of layers became larger and visibly more ordered going from **Zr3**-**Zr6**, as the amount of methylphosphonic acid spacer was decreased. Overall, the zirconium compounds showed greater short-range order than the Sn compounds, which showed no distinct particle shapes or layers. Furthermore, differences in the particle shape and size of the samples **Sn1** and **Sn6** (Figure 4) were not as obvious as for the Zr compounds, even at a magnification of 200,000X. In contrast with the Zr compounds, it seems that the individual particle size may even be smaller for the pure bipyridyl(bis)phosphonate than for the methylphosphonate-spaced material.

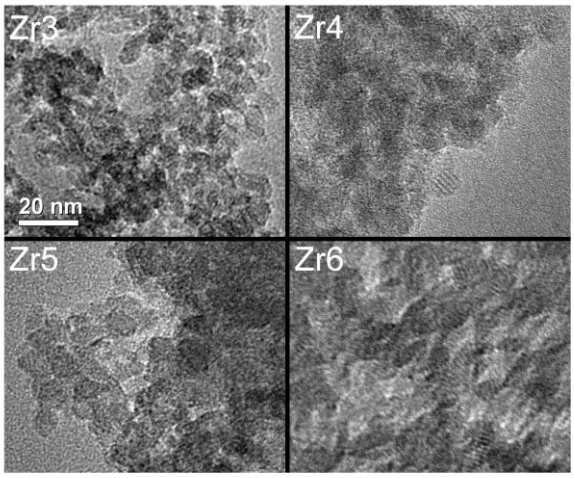

Figure 3 TEM images of Zr3-Zr6

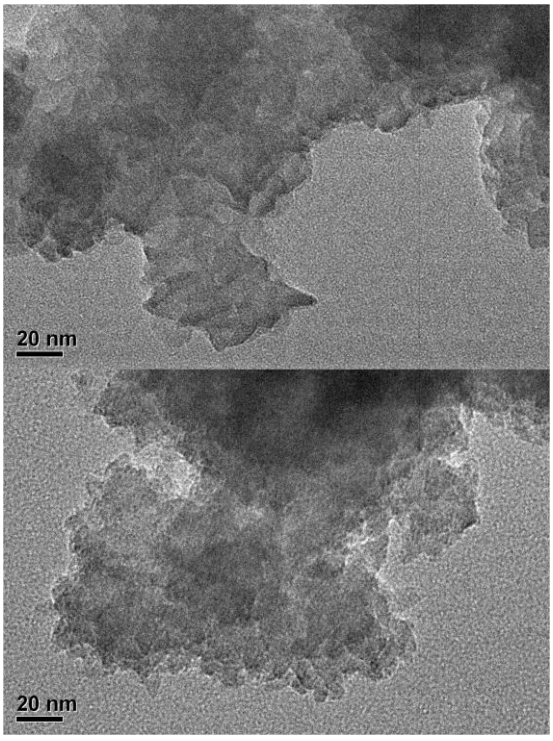

Figure 4 TEM images of Sn1(top) and Sn6 (bottom)

Surface Area and Isotherms

Surface areas for each of the compounds were determined by nitrogen sorption at 77 K. The measured surface areas are given in Table 1 and Table 2. Measurements were not performed for samples **Zr1** and **Zr2** because they contained the $Zr(O_3PCH_3)_2$ phase as an impurity. The decrease in surface area upon going from **Zr3** to **Zr6** correlates with smaller ratios of 2,2'-bipyridinediyl-5,5'-diphosphonate to methylphosphonate. However, it should be noted that even when no 'spacer' methylphosphonate groups were included in the compound (**Zr6** and **Sn6**), the materials still exhibited surface areas over 300 m^2/g. The desorption isotherms for all of the Zr compounds showed a strong hysteresis (Figure 5), which in poorly ordered materials of this type indicates a wide range of pore sizes and an interconnected network of pores in which desorption can be inhibited by 'bottleneck' effects and other pore-blocking phenomena. The range of pressures over which sorption occurred indicates a wide range of pore sizes spanning both the microporous and mesoporous ranges.

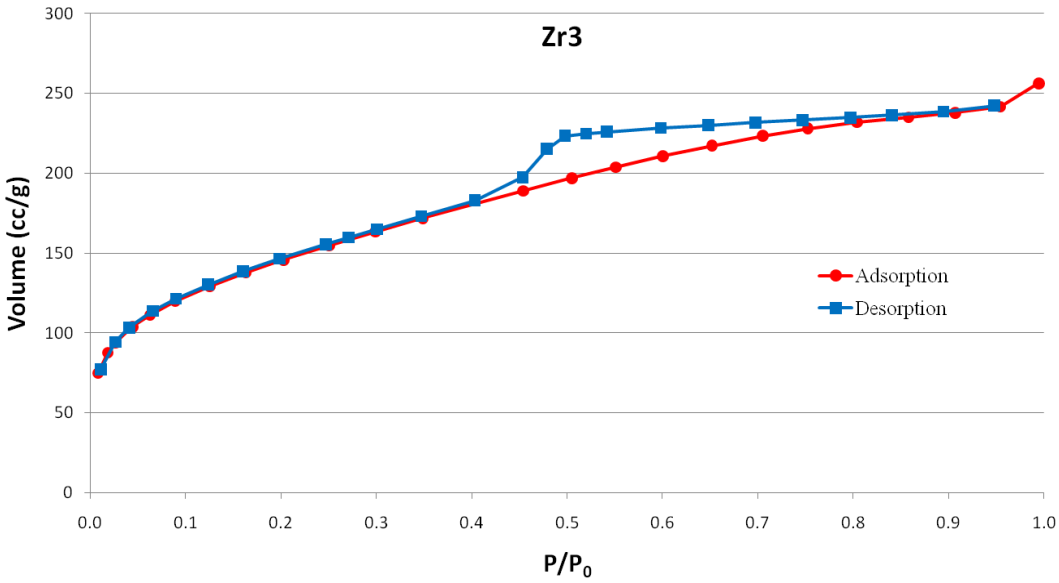

Figure 5 Nitrogen sorption and desorption isotherms at 77 K for Zr3

The compounds **Sn1**-**Sn6** exhibited a similar variation in surface area with respect to the bipyridyl(bis)phosphonate to methylphosphonate ratio, although they showed slightly lower surface areas, overall, than the Zr compounds. Hysteresis was observed in the desorption isotherm (Figure 6), but in contrast with the Zr compounds, the hysteresis seen for the Sn compounds was longer and much less pronounced, which is indicative of slit-shaped pores and micropores. The Sn compounds also showed a large uptake of nitrogen at just below P_0. This is most likely due to the condensation of nitrogen in the spaces between the small particles, which can effectively form large 'pores' that only fill at higher pressures. Nitrogen sorption-desorption isotherms for all materials are available in Appendix A.

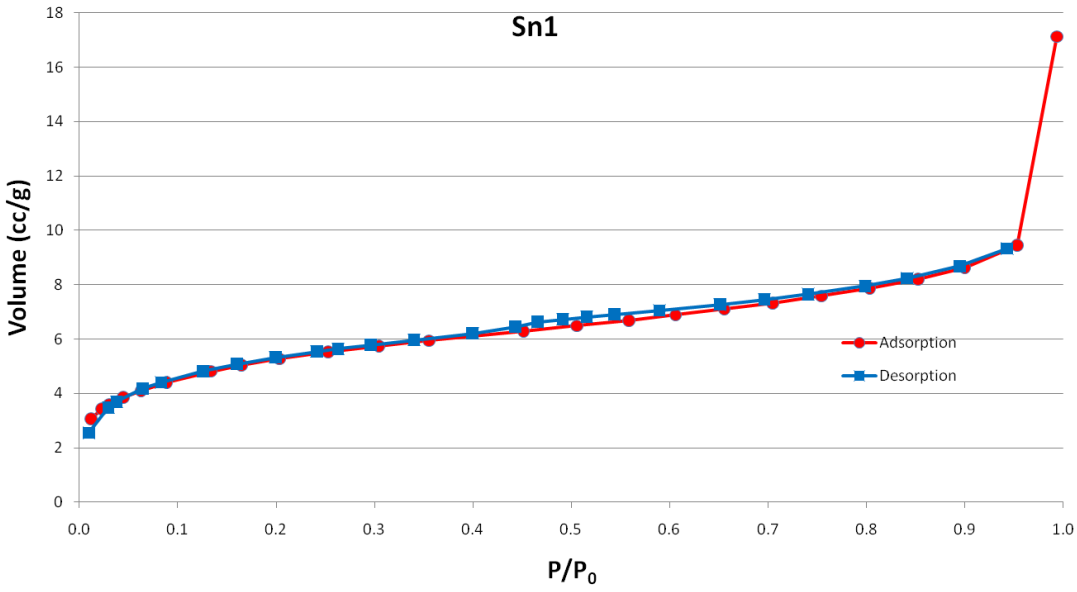

Figure 6 Nitrogen sorption and desorption isotherms at 77 K for Sn1

Composition by EA and TGA

From the elemental analyses and TGA measurements it was determined that the formulas for the Zr compounds closely matched the starting ratios of bpyBPAE to MePA (Table 3). Yields for these types of reactions are normally high, although in this case the yield was probably depressed by the high solubility of the phosphonic acids and the excess halide present in the reaction mixture. However, test reactions showed that removing HCl from the reaction mixture resulted in a less porous product. For compounds **Sn1** and **Sn2**, the ratio of bipyridylbisphosphonate to methylphosphonate was slightly higher than in the initial reaction mixture and the yields were lower. This was most likely due to the increased solubility of the Sn^{IV} in the presence of HF, as well as the high solubility of methylphosphonic acid. The addition of HCl (or no acid at all) to the Sn reactions resulted in products with lower porosity. It is likely that the concentration of HF decreases during the reaction as it diffuses through the PTFE liner and out of the reaction vessel, which slowly decreases the solubility of the Sn^{IV}.

Table 3 Elemental analyses and TGA weight loss for Zr3-Zr6 and Sn1-Sn6

Compound	Composition	%C (calcd.,found)	%H (calcd.,found)	%N (calcd., found)	TGA % weight loss (calcd., found)
Zr3	$Zr(O_3PC_{10}N_2H_6PO_3)_{0.5}(O_3PCH_3)(H_2O)_2$	19.10, 19.63	2.67, 2.07	3.71, 3.73	29.7, 30.3
Zr4	$Zr(O_3PC_{10}N_2H_6PO_3)_{0.66}(O_3PCH_3)_{0.68}(H_2O)_2$	22.02, 21.99	2.54, 2.55	4.66, 4.60	32.4, 33.2
Zr5	$Zr(O_3PC_{10}N_2H_6PO_3)_{0.75}(O_3PCH_3)_{0.5}(H_2O)_2$	23.53, 23.75	2.47, 1.78	5.15, 5.02	35.1, 34.6
Zr6	$Zr(O_3PC_{10}N_2H_6PO_3)(H_2O)_2$	27.34, 27.14	2.29, 1.87	6.38, 6.12	39.6, 39.8
Sn1	$Sn(O_3PC_{10}N_2H_6PO_3)_{0.31}(O_3PCH_3)_{1.38}$	15.59, 15.74	1.75, 2.12	2.52, 2.63	23.2, 22.2*
Sn2	$Sn(O_3PC_{10}N_2H_6PO_3)_{0.37}(O_3PCH_3)_{1.26}$	16.89, 16.74	1.72, 2.02	2.94, 2.98	24.7, 24.9*
Sn3	$Sn(O_3PC_{10}N_2H_6PO_3)_{0.5}(O_3PCH_3)$	19.54, 19.61	1.64, 2.03	3.80, 3.86	30.8, 30.9*
Sn4	$Sn(O_3PC_{10}N_2H_6PO_3)_{0.66}(O_3PCH_3)_{0.68}(H_2O)_{1.2}$	21.31, 21.41	2.06, 2.23	4.51, 4.41	33.9, 33.4*
Sn5	$Sn(O_3PC_{10}N_2H_6PO_3)_{0.75}(O_3PCH_3)_{0.5}(H_2O)_{1.8}$	22.23, 22.39	2.24, 2.17	4.86, 4.70	36.0, 36.0*
Sn6	$Sn(O_3PC_{10}N_2H_6PO_3)(H_2O)_{2.5}$	25.24, 25.08	2.33, 2.26	5.89, 5.43	38.5, 38.5*

All samples were dried at 105 °C prior to elemental analysis.

*TGA of the Sn materials revealed adsorbed water that was readily lost at low temperatures. The percentage weight loss values are calculated based on formulae that include more water molecules than those determined by CHN analysis: **Sn1** and **Sn2** each had two water molecules per formula unit, **Sn3** and **Sn4** each had three water molecules per formula unit, **Sn5** had 3.2 water molecules per formula unit, and **Sn6** had 2.5 water molecules per formula unit. Heating the samples at 105 °C was sufficient to remove the water from the highly porous compounds **Sn1**, **Sn2**, and **Sn3**, but was less effective for the less porous samples **Sn4**, **Sn5**, and **Sn6**. This is most likely due to the smaller amounts of spacer ligand in these compounds, which results in less well-connected inner pores, making it more difficult for trapped water to escape.

TGA analyses indicate that at all ratios of 2,2'-bipyridinediyl-5,5'-diphosphonate to methylphosphonate the compounds are stable to ~450 °C (see Appendix B). The total weight loss measured after the samples had been heated to 1000 °C was used to determine the formulations given in the experimental section, which were supported by the elemental analyses. All of the samples were dried at 90 °C overnight prior to CHN analyses, but this was insufficient to completely remove the water and particularly ineffective for the samples with less methylphosphonate spacer. The final products in the TGA were determined to be ZrP_2O_7 (for **Zr3**-**Zr6**) and SnP_2O_7 (for **Sn1**-**Sn6**). PXRD indicated poorly crystalline ZrP_2O_7 for Zr samples, while the Sn samples were amorphous. The initial loss is most likely surface water and water trapped within the pores close to the surface. The gradual weight loss of about 1% seen from 150 to 200 °C may be water split out from free P-OH and Zr-OH groups or water that is trapped in the interior of the particles. It should be noted that a distinct loss of water is measured during the initial heating, which is especially pronounced for **Zr4**-**Zr6** and **Sn4**-**Sn6**), the samples with the least amount of methyphosphonate spacer groups. Since these compounds have less methyl spacer and more crosslinking bipyridyl between the layers, the internal pores are presumably less connected, making it more difficult for the trapped water to escape.

Palladium Uptake and Reduction

Exposing **Zr3**, **Zr6**, **Sn1**, and **Sn6** to excess $Pd(O_2CCH_3)_2$ in acetone for a period of 16 hours yielded the Pd-loaded materials **Zr3 •0.13Pd(O$_2$CCH$_3$)$_2$**, **Zr6**

•0.16Pd(O_2CCH_3)$_2$, **Sn1 •0.16Pd(O_2CCH_3)$_2$**, and **Sn6 •0.28Pd(O_2CCH_3)$_2$**, respectively. These formulae were determined by measuring the M^{IV}:Pd ratios by ICP-MS. It was assumed that the acetate counterions accompanied the Pd^{II} into the materials for charge balance, but their presence could not be verified by IR. Recent work by Ha[88] describes the crystal structure of Pd(bipy)(O_2CCH_3)$_2$ •5H_2O, in which the Pd^{II} resides in a distorted square-planar configuration. While it would be impossible to obtain crystal structures of the Pd-loaded materials described herein, it is reasonable to assume that the Pd(O_2CCH_3)$_2$ is in a similar coordination environment within the Zr and Sn phosphonate materials. Powder X-ray diffraction patterns of the Pd-loaded materials were indistinguishable from those of the original materials. Upon heating to at least 250 °C in an atmosphere of 10% H_2 in N_2, each of these materials turned black. Further investigation by TEM showed that the Pd had been reduced and agglomerated within the materials to form particles in the range of 2-4 nm (Figure 7). The samples with higher loadings of Pd(O_2CCH_3)$_2$ yielded slightly larger and less dispersed nanoparticles after reduction(Figure 8). Even after reduction, there were no new features in the powder X-ray diffraction patterns. Reduction temperature (varied incrementally between 250 °C and 450 °C) did not affect the size or dispersion of the nanoparticles, as measured by TEM and small-angle X-ray scattering (SAXS).

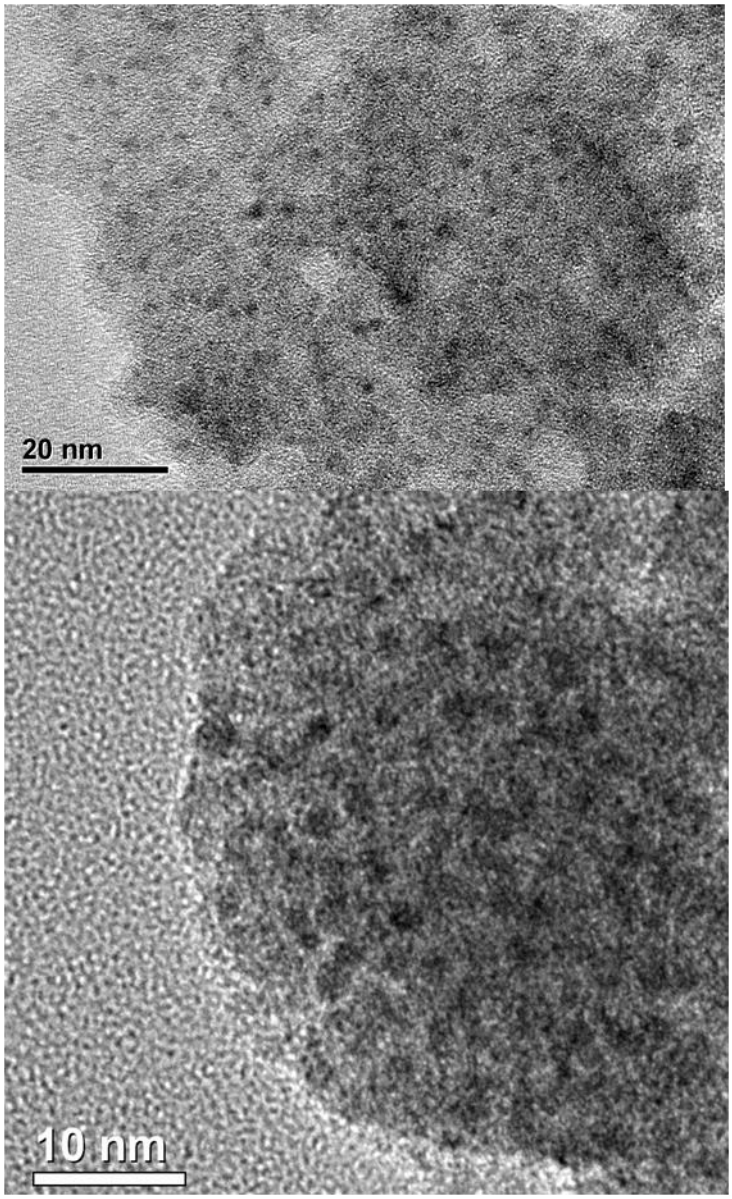

Figure 7 TEM images of Zr3 •0.13 Pd (top) and Sn3 •0.16 Pd (bottom) after reduction

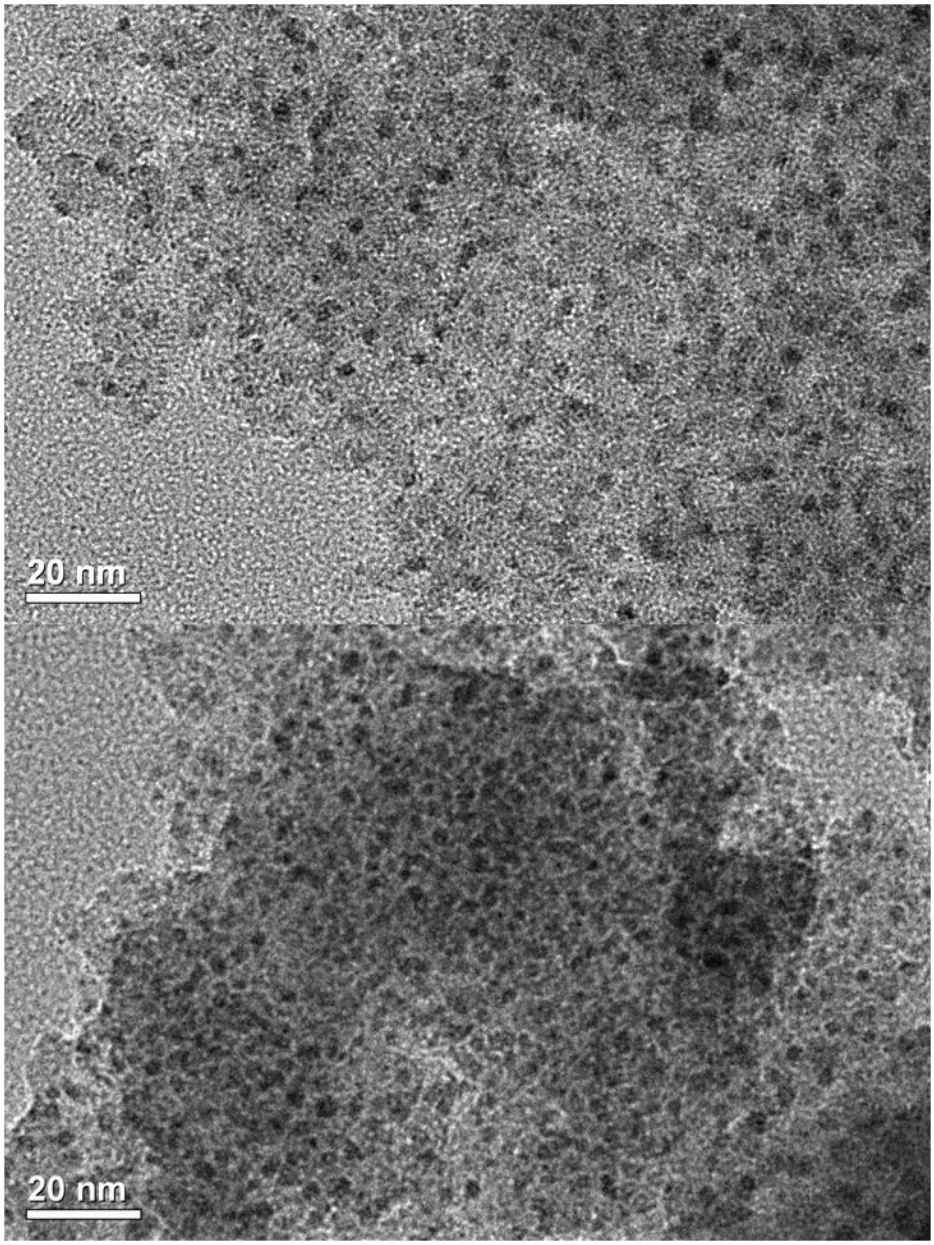

Figure 8 Zr •0.16 Pd (top) and Sn6 •0.28 Pd (bottom) with Pd nanoparticles made by reduction under 10% H_2 in N_2 at 350 °C

SAXS was used to further characterize the size of the Pd nanoparticles in the compound **Zr3 •0.13Pd** (Figure 9). This particular compound was chosen because TEM showed that the nanoparticles were fairly well-dispersed, a requirement for accurate SAXS analyses. The scattering pattern of **Zr3** was used as a background and subtracted so the resulting scattering would be due only to the Pd nanoparticles. The particle sizes were determined to be approximately 2-3 nm by Guinier analysis using the program PRIMUS, which is in good agreement with the Pd^0 particle sizes observed in the TEM images. Changing the temperature at which the reduction was carried out had no clear effect on the particle size.

UV-Vis absorption measurements were performed on suspensions of **Zr3**, **Zr3 •0.13Pd(O_2CCH_3)$_2$**, and **Zr3 •0.13Pd** as a means to monitor the coordination of Pd^{II} by the bipyridyl groups in the materials (Figure 10). The spectrum of **Zr3** prior to the coordination of $Pd(O_2CCH_3)_2$ shows two broad absorbance peaks at 250 nm and 290 nm. These are in reasonable agreement with the absorption peaks published for free 2,2'-bipyridine.[89] After uptake of $Pd(O_2CCH_3)_2$, **Zr3 •0.13Pd(O_2CCH_3)$_2$** also shows two absorbance peaks, but these have now been shifted to 261 nm and 330 nm as the bipyridine is coordinating the Pd^{II}. After reduction (**Zr3 •0.13Pd**), the peaks have shifted back to 250 nm and 290 nm, indicating that the bipyridine is no longer chelating the Pd^{II} (which has been reduced to Pd^0) and available for coordinating other metals.

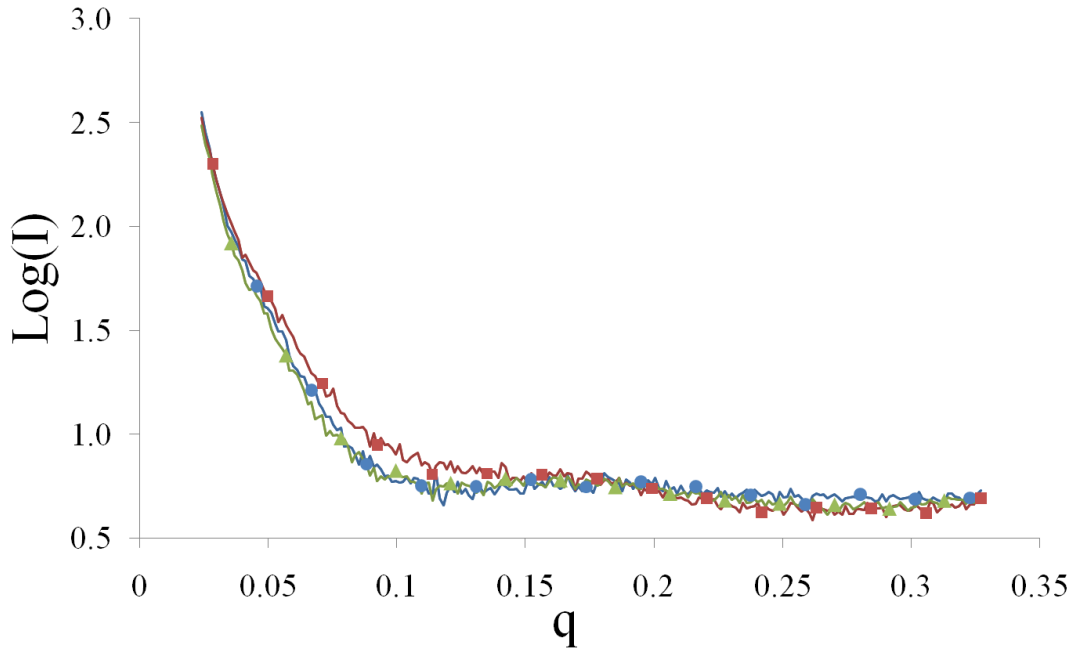

Figure 9 Log plots of scattering intensity vs. q for Zr3 ·0.13Pd reduced at three different temperatures: 250 °C (●) (Rg = 2.6 (0.35) nm), 300 °C (■) (Rg = 2.0 (0.5) nm), 350 °C (▲) (Rg = 2.2 (0.13) nm)

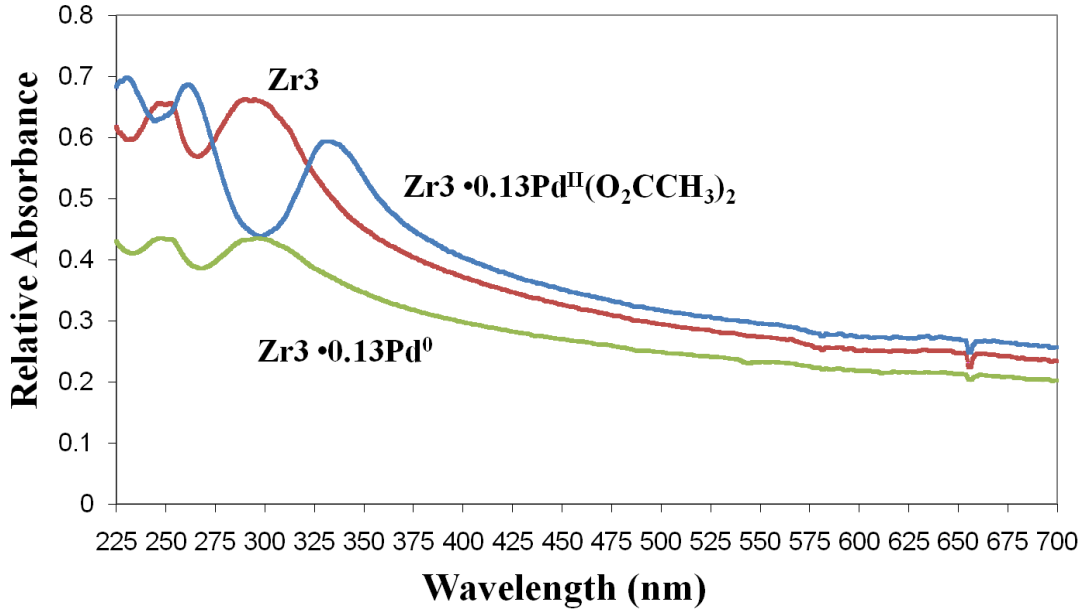

Figure 10 UV-Vis absorbtion spectra of Zr3 as-synthesized (red), loaded with Pd(O$_2$CCH$_3$)$_2$ (blue), and after treatment at 350 °C under 10% H$_2$ in N$_2$ to reduce the Pd(O$_2$CCH$_3$)$_2$ to Pd^0 nanoparticles

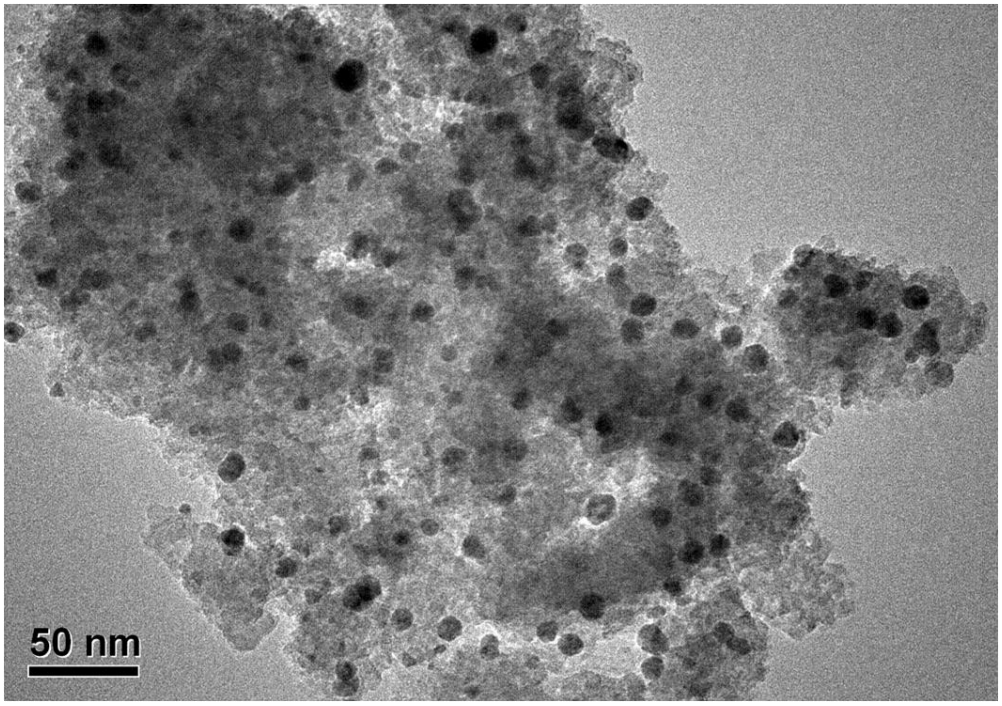

Figure 11 Sn3 with Pd^0 made by reflux in ethanol

At first it seems odd that the absorbance spectrum of the Pd-loaded material would show only two shifted peaks instead of two shifted and two unshifted peaks since only about 26% of the bipyridyl groups are actually chelating a Pd^{II} atom. One would naturally expect the peaks corresponding to the uncoordinated bipyridyl moieties to appear in the spectrum of the Pd-loaded material, since the remaining 74% of the bipyridyl groups are not bound to Pd^{II}. However, it must be remembered that since these materials are insoluble, the measurements were performed on suspensions of fine particles, the surfaces of which contain easily accessible bipyridyl sites for the coordination of Pd^{II}, while the interior of the particles holds the majority of the bipyridyl moieties which are inaccessible to dissolved $Pd(O_2CCH_3)_2$. Because light cannot penetrate into the interior of the particles, the measured spectrum only reflects what is on the surface of the particles, thus only the bipyridyl groups near the surface and capable of coordinating Pd^{II} are probed.

To vary the size of the nanoparticles, the Pd-loaded materials were refluxed in ethanol for several hours. The nanoparticles obtained were predominantly on the surface of the materials and fairly uniform, ranging in size from 10-15 nm (Figure 11). The reduction in ethanol may involve soluble species that allow the Pd to migrate to the surface, resulting in larger particles that are not limited by the pore structure.

Discussion

The subject of this chapter warrants at least a brief discussion on the nature of porosity in these Zr- and Sn-based pillared layered materials. Ideally, the structure is a

crystalline solid in which the pillars are aligned and packed next to one another in between the inorganic layers, but in this case there could be no porosity. According to this model, porosity can only be achieved by using a monophosphonate spacer unit. This would, presumably, interrupt the regular packing of the bisphosphonate to yield a network of interconnected pores. However, this work and that of others makes it apparent that porosity is achieved even without the use of spacer groups.[29] This can be explained by the poor solubility of these materials, which leads to low crystallinity and an enormous number of defects within the structure that interrupt the regular packing of the pillars and create pores.[90] The work herein shows that using a spacer unit increases the surface area, although probably not primarily in the way originally hypothesized. The inclusion of a spacer unit in the materials decreases the particle size and probably increases the number of defects. As a monophosphonate, the spacer is incapable of bridging between layers, and serves as a dead-end building block that inhibits particle growth, resulting in small, porous particles that pack together to create virtual internal surface. It should be pointed out that in the model compound for these layered materials, *α*-zirconium phosphate, individual layers grow faster in the lateral direction parallel to the layers, resulting in crystallites with large aspect ratios. In contrast, more crystalline versions of **Zr6**, prepared at 205 °C in the presence of HF, consist of nanocrystals that tend to grow more in the 'vertical' direction, perpendicular to the orientation of the layers (Figure 12). The *d*-spacing can be clearly seen in the TEM image. The fact that the crystals grow mostly in this direction shows how effectively a spacer group that

cannot bridge between the inorganic layers would disrupt the crystal growth, resulting in crystallites only a few nanometers across.

For the Zr compounds, there is a critical point at which the amount of spacer unit becomes too high (**Zr1** and **Zr2**), beyond which a mixture of two phases is obtained. One is probably similar in composition to **Zr3**, and the other is $Zr(O_3PCH_3)_2$, which can be detected by the presence of a peak in the PXRD at ~8.9 Å. The materials **Sn1**-**Sn6** are monophasic even to high ratios of spacer unit to bipyridyl crosslinker. The reason for this is not entirely clear, although in general it is the case that single phases are more likely to form when the ligands have similar solubility and hydrophilicity or hydrophobicity. In the present case, both the crosslinker and the spacer have high solubility in water, so some other phenomenon predominates. The higher solubility of Zr^{IV} than Sn^{IV} under these conditions allows for Ostwald ripening and annealing mechanisms to gradually produce the more ordered two-phase products for Zr, but not for Sn. It is likely that two phases would be obtained for the Sn materials if a sufficiently high ratio of spacer to crosslinker were used.

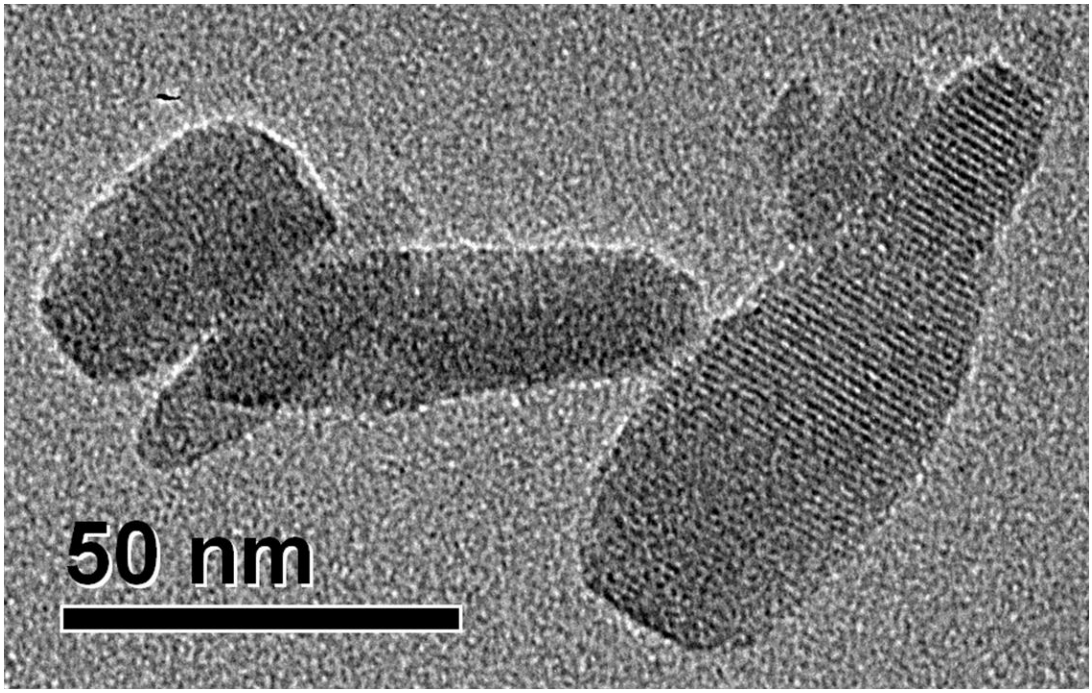

Figure 12 Zr6 prepared at 205 °C with HF as a solubilizing agent

Another significant difference between the Zr and Sn compounds is shown by their nitrogen sorption and desorption isotherms. While all of the compounds studied here show significant mesoporosity, the Zr compounds exhibit a pronounced hysteresis which indicates the presence of pore blocking phenomena and capillary effects of the pores. This type of hysteresis is indicative of multilayer adsorption in mesoporous materials. In the Sn compounds, the hysteresis is much smaller, matching the IUPAC classification of a type H4 hysteresis which indicates the presence of slit-shaped micropores. The Sn compounds also show a rapid increase in volume adsorbed at pressures close to P_0, due to the filling of the spaces between the tightly packed small particles. This was not observed for the Zr compounds. The closure of the hysteresis loops in both series of materials is not sharp, due to the wide range of pore sizes present.

Zr3 and **Zr6** take up significantly less Pd than the Sn compounds. This may be due to the higher crystallinity of the Zr compounds, i.e. fewer defects in the structure to allow access to bipyridyl sites as well as bipyridyl sites being packed too closely together for each of them to accommodate $Pd(O_2CCH_3)_2$. TEM shows small regions of ordered layers for the Zr compounds, but not for the Sn compounds. The ordered regions within the Zr materials may be too densely packed to allow for efficient uptake of Pd, whereas the less ordered nature of the Sn compounds provides more access to bipyridyl sites. It should still be noted that even in the most porous Sn sample (**Sn1**) only about 50% of the bipyridyl sites were occupied by $Pd(Oac)_2$. Higher loadings of $Pd(O_2CCH_3)_2$ were achieved by using the materials with more bipyridyl sites (**Zr6** and **Sn6**), although the percentage of occupied bipyridyl sites decreased. Higher loading of Pd results in

agglomerated nanoparticles of slightly larger size, which are densely arranged within the matrix. The particles were not dispersed enough to provide meaningful size distributions by SAXS.

It is worth emphasizing that heating the materials does not change the size of the nanoparticles. When the Pd is first reduced, it may initially have some mobility within the material, enabling it to contact and combine with other such small particles. Eventually, this process could lead to the nanoparticles seen by TEM and SAXS, which may be too large to move throughout the pore structure and combine with other nanoparticles. In this way, the sponge-like structure may be trapping the nanoparticles and preventing further agglomeration into larger particles without the use of stabilizing agents or surfactants.

ICP analyses performed after **Zr3 •0.13Pd** was loaded with $Pd(O_2CCH_3)_2$ for a second time indicate that the amount of Pd loaded during the second cycle is equal to the amount loaded in the first cycle, i.e. the presence of nanoparticles in the material does not inhibit further uptake of $Pd(O_2CCH_3)_2$. Multi-step chelation and reduction cycles could yield bimetallic alloy or core-shell type nanoparticles. For example, palladium could be taken into the material and reduced, and then the material could be used a second time to chelate platinum, which could then be reduced in a second cycle, creating an alloy or forming a platinum shell around the previously generated palladium nanoparticles.

Conclusion

Presented herein are porous, thermally robust Zr and Sn phosphonates that covalently incorporate at 2,2'-bipyridine moiety which is capable of coordinating Pd^{II} from solution, although only a fraction of the bipyridyl sites are occupied, which are mostly near the surface. Once $Pd(O_2CCH_3)_2$ has been loaded into the materials, it can be reduced by H_2 at elevated temperatures to form 2-4 nm particles or by reflux in ethanol to form 10-12 nm diameter particles. The nanoparticles are dispersed within the phosphonate matrix and do not aggregate upon heating, even in the absence of surfactants and stabilizing agents. Once the Pd has been reduced to form nanoparticles, the bipyridyl sites are vacant and available to again coordinate metal ions, which may allow for the preparation of alloy or core-shell type nanoparticles. Work is ongoing to synthesize bimetallic nanoparticles and to evaluate the catalytic activity of these supported nanoparticle systems.

CHAPTER IV

ZINC AND MANGANESE PHOSPHONOCARBOXYLATES: IN-SITU REACTIONS OF NITRILES AND BIMODAL ALKYLAMINE UPTAKE

Introduction

The incorporation of functional groups into layered phosphonates is an important step towards creating materials which may be useful. The series of layered compounds $M(O_3PR)(H_2O)$, where M = Zn, Mg, Mn, Ni, Cu, or Co and R = $-CH_3$ or $-C_6H_5$ has been known for some time.[20, 91] Mixed metal derivatives have also been reported.[92] The structures consist of inorganic layers decorated with pendant organic groups. Using this structure type as a model, it was our goal to synthesize the analogous layered material $M(O_3PC_6H_4CN)(H_2O)$, which would have nitrile groups extending into the interlayer space. These groups could undergo post-synthetic reactions to tailor the surface functionality of the material. By hydrothermal reactions, we obtained the compounds $Zn(O_3PC_6H_4CN)(H_2O)$ and $Mn(O_3PC_6H_4CN)(H_2O)$, in which the layers are isostructural with the previously reported methylphosphonates and phenylphosphonates. When we performed the reactions at a higher temperature, we were able to affect the in-situ hydrolysis of the nitrile to form a carboxylic acid, yielding $Zn(O_3PC_6H_4CO_2H)(H_2O)$ and $Mn(O_3PC_6H_4CO_2H)(H_2O)$ as single crystals. In these compounds the inorganic layers are again isostructural to the phenylphosphonates, and the carboxylic acids are engaged in interlayer hydrogen bonding, which keeps the layers ~18.5 Å apart.

There are a number of reported compounds of aryl phosphonoarylcarboxylates with divalent metals. In many of these the carboxylic acids are deprotonated and coordinate metal atoms,[93-99] but there are several examples which have free carboxylic acid groups which form hydrogen bonded pairs in the interlayer space, like the compounds we report herein.[45, 47, 51, 53, 100, 101] A number of related carboxyalkylphosphonates have also been reported.[44, 46, 48, 102]

Intrigued by the in-situ transformation of the nitrile that had occurred during the high-temperature syntheses, and aware of acid-catalyzed reactions of nitriles under supercritical conditions[103] that yield carboxylate esters, we repeated the syntheses at high temperature using methanol and ethanol as solvents. By holding the reactions at temperature for extended periods of time, we were able to obtain mixed products containing the esterified carboxylates, which analyzed as $Zn(O_3PC_6H_4CO_2CH_3)$ and $Mn(O_3PC_6H_4CO_2CH_3)$. The pure materials were obtained by solvothermally treating the products in the appropriate alcohol for a second time. The structure of $Mn(O_3PC_6H_4CO_2CH_3)$ was determined by single-crystal X-ray diffraction, and it was found that the layer structure was different than that of the other compounds. There is also a notable lack of the coordinated water molecule, most likely a consequence of the dry reaction environment.

The coordinated water molecule of M^{II} methylphosphonates and phenylphosphonates can be easily removed by heating which leaves an open coordination site at the metal. This reaction is reversible, and the materials will rehydrate upon exposure to water or moist air. When dehydrated, the metal can serve as a Lewis

acidic site which can interact with Lewis bases like amines. $Zn(O_3PCH_3)$ was shown to react with gas-phase amines to give the intercalation products $Zn(O_3PCH_3)(C_nH_{2n+1}NH_2)$, where n = 2-8.[104] The phenylphosphonates of Zn and Co were found to only take up ammonia from the gas phase, while larger alkylamines were calculated to be too large to fit in the space between the phenyl rings.[105] Further research showed that they could in fact be intercalated by contacting $Zn(O_3PC_6H_5)$ with liquid *n*-alkylamines for a few days. The structures of the propyl-, butyl-, and pentylamine intercalates were solved by PXRD, and it was found that the Zn atoms become tetrahedral as the structure shifts upon coordination of the amine.[106] *n*-Alkylamines as long as nonlyamine have been successfully intercalated into $Zn(O_3PC_6H_5)$.[107]

In this chapter we present the structural characterization of five new Zn and Mn phosphonates which are formed by the in-situ reaction of a nitrile phosphonate. We have explored the *n*-alkylamine uptake properties of $Zn(O_3PC_6H_4CO_2H)$, which has the ability two bind amines both at the open coordination site on the Zn atom and at the carboxylic acid in the interlayer space. The results of these studies will be discussed in context with those obtained for other layered phosphonates. We also claim that the in-situ reaction of nitriles to form carboxylic acids or carboxylate esters during solvothermal reactions is general and can be applied to other systems.

Experimental Details

Reagents were prepared or acquired as described in Chapter II. Water was distilled and deionized. Methanol, ethanol, and *n*-alkylamines were dried for at least two weeks over activated 3Å molecular sieves. Thermogravimetric analyses (TGA) were performed with a TA Instruments Q500-0215 analyzer. The samples were heated from ambient temperature to 1000 °C at a rate of 10 °C per minute under air. Elemental analyses were performed by Robertson Microlit, Inc., Madison, NJ, and Atlantic Microlabs, Inc., Norcross, GA. PXRD patterns from 4-40° in 2θ were obtained on a Bruker D8 Advance powder diffractometer using a rotating Cu anode (λ = 1.54184 Å) operated at 40 kV and 40 mA. Single crystal X-ray diffraction data were collected at 100 or 110 K on beamline 11.3.1 at Lawrence Berkeley National Laboratory using monochromatic synchrotron radiation (λ = .77490 Å). Absorption corrections were performed with SADABS,[108] and all structures were solved by direct methods and refined using SHELXL.[109]

Syntheses of Zn and Mn Phosphonates

$Zn(O_3PC_6H_4CN)(H_2O)$

$ZnSO_4 \cdot 7H_2O$ (0.3 mmol, 0.086 g) and $Et_2O_3PC_6H_4CN$ (0.3 mmol, 0.072 g) were placed with 8 ml H_2O in a 15 ml PTFE-lined steel reaction vessel and heated at 130 °C for 4 days. The crystalline white solid was collected by filtration and washed with ethanol. Yield: 0.021 g. Analysis calculated for $ZnO_4PC_7NH_6$: C, 31.79 %; H, 2.29 %; N, 5.30 %. Found: C, 31.86 %; H, 2.22 %; N, 5.20 %.

$Mn(O_3PC_6H_4CN)(H_2O)$

$MnCl_2 \cdot 4H_2O$ (0.3 mmol, 0.059 g) and $Et_2O_3PC_6H_4CN$ (0.3 mmol, 0.072 g) were placed with 8 ml ethanol in a 15 ml PTFE-lined steel reaction vessel and heated at 180 °C for 3 days. The crystalline white solid was collected by filtration and washed with ethanol. Yield: 0.057 g. Analysis calculated for $MnO_4PC_7NH_6$: C, 33.10 %; H, 2.38 %; N, 5.51 %. Found: C, 33.17 %; H, 2.45%; N, 4.93%.

$Zn(O_3PC_6H_4CO_2H)(H_2O)$

$ZnCl_2$ (0.6 mmol, 0.082 g) and $Et_2O_3PC_6H_4CN$ (0.3 mmol, 0.072 g) were placed with 8 ml H_2O in a 15 ml PTFE-lined steel reaction vessel and heated at 210 °C for 4 days. The crystalline white solid was collected by filtration and washed with ethanol. Yield: 0.031 g.

$Mn(O_3PC_6H_4CO_2H)(H_2O)$

$MnCl_2 \cdot 4H_2O$ (0.3 mmol, 0.059 g) and $Et_2O_3PC_6H_4CN$ (0.3 mmol, 0.073 g) in were placed with 8 ml H_2O in a 15 ml PTFE-lined steel reaction vessel and heated at 180 °C for 30 days. The crystalline white solid was collected by filtration and washed with ethanol. Yield 0.034 g. Analysis calculated for $MnO_6PC_7H_7$: C, 30.79 %; H, 2.58 %; N, 0.0 %. Found: C, 31.07 %; H, 2.12 %; N, < 0.02 %.

$Zn(O_3PC_6H_4CO_2CH_3)$

$Zn(SO_4) \cdot 7H_2O$ (0.3 mmol, 0.086 g) or $Zn(O_2CCH_3)_2 \cdot 2H_2O$ (0.3 mmol, 0.066 g) were heated with $Et_2O_3PC_6H_4CN$ (0.3 mmol, 0.073 g) and 8 ml methanol in a 15 ml PTFE-lined steel reaction vessel. The product obtained after heating at 180 °C for 30 days (or 210 °C for 10 days) was found to contain residual nitrogen from the unreacted nitrile. This material was again placed in a PTFE-lined steel reaction vessel with 8 ml methanol and heated at 210 °C for 7 days. The microcrystalline powder was found to be free of N and analyzed as $Zn(O_3PC_6H_4CO_2CH_3)$ by CHN analyses. Analyses calculated for $Zn(O_3PC_6H_4CO_2CH_3)$: C, 34.37%; H, 2.52 %; N, 0.00 %. Found: C, 34.22 %; H, 2.46 %; N, 0.0%.

$Mn(O_3PC_6H_4CO_2CH_3)$

$Mn(SO_4) \cdot 5H_2O$ (0.3 mmol, 0.072 g) or $Mn(O_2CCH_3)_2 \cdot 4H_2O$ (0.3 mmol, 0.074 g) were heated with $Et_2O_3PC_6H_4CN$ (0.3 mmol, 0.073 g) and 8 ml methanol in a 15 ml PTFE-lined steel reaction vessel. The product obtained after heating at 180 °C for 30

days (or 210 °C for 10 days) was found to contain residual nitrogen from the unreacted nitrile. This material was again placed in a PTFE-lined steel reaction vessel with 8 ml methanol and heated at 210 °C for 7 days. The microcrystalline powder was found to be free of N and analyzed as $Mn(O_3PC_6H_4CO_2CH_3)$ by CHN analyses.

Crystal Structures

Important structural details for the compounds described are given in Table 4.

$Zn(O_3PC_6H_4CN)(H_2O)$ and $Mn(O_3PC_6H_4CN)(H_2O)$ are isostructural, consisting of inorganic layers decorated by pendant benzonitrile groups which interpenetrate in the interlayer space (Figure 13). This allows the layers to come closer together than they would if the ligands on adjacent layers were directly opposite one another. The phenyl rings are rotationally disordered in both structures. The layer consists of octahedral M^{II} ions coordinated by phosphonate oxygen atoms and one solvent water molecule, which is essentially identical to the layer structure found in $Zn(O_3PC_6H_5)$. Although the nitrile groups interdigitate to avoid each other and fill available space, the *d*-spacing of ~16.3 Å is still larger than that of the phenylphosphonates.

A similar layer structure is present in $Zn(O_3PC_6H_4CO_2H)(H_2O)$ and $Mn(O_3PC_6H_4CO_2H)(H_2O)$, which are isostructural. The pendant carboxylic acid groups on the phenyl rings interact with other carboxylic acids on adjacent layers, forming doubly hydrogen bonded pairs (Figure 14). The interlayer distance is ~18.8 Å.

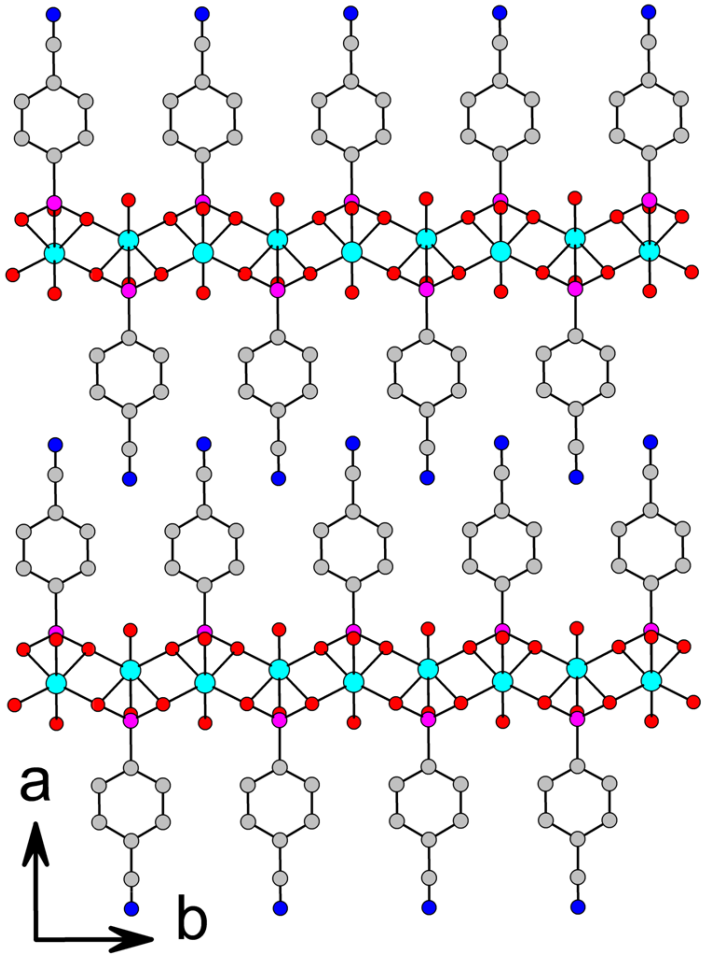

Figure 13 Layered structure of $Zn(O_3PC_6H_4CN)(H_2O)$ and $Mn(O_3PC_6H_4CN)(H_2O)$ viewed along the *c*-axis. The coordinating water molecules are between the benzonitrile groups on both sides of the layer.

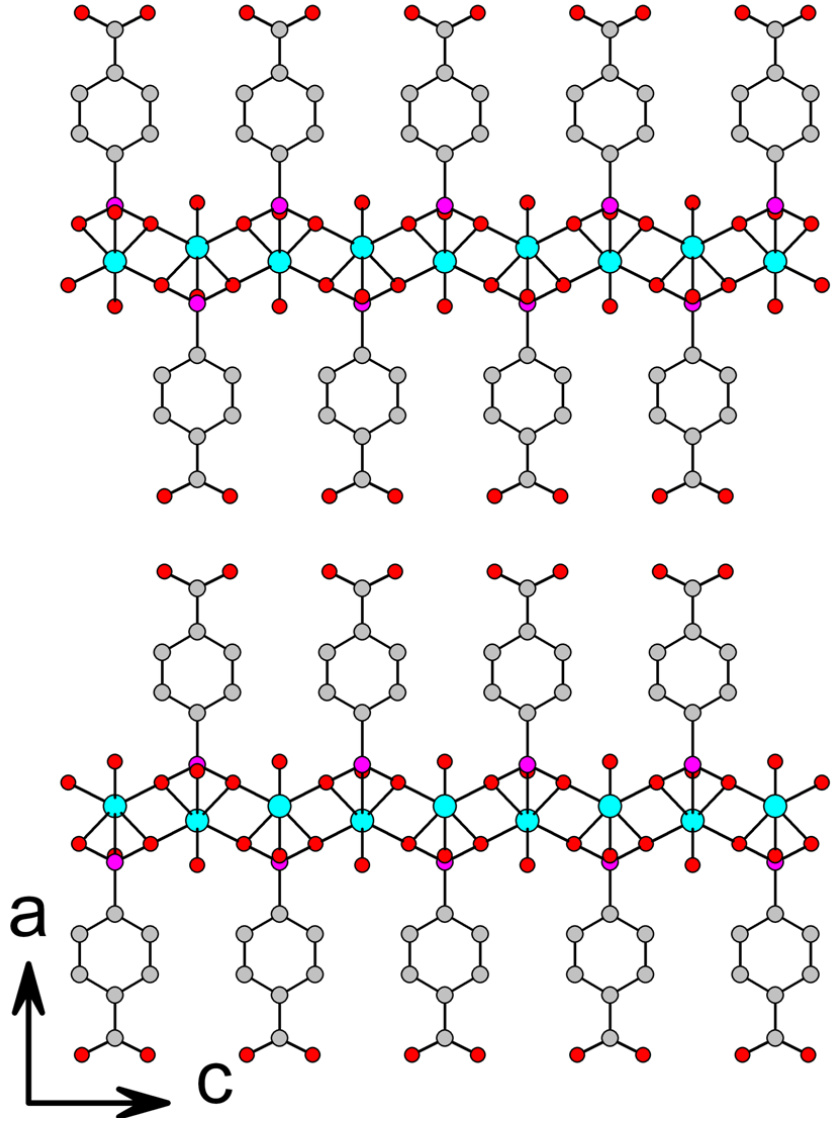

Figure 14 Pendant carboxylic acid groups form hydrogen-bonded pairs in in $Zn(O_3PC_6H_4CO_2H)(H_2O)$ and $Mn(O_3PC_6H_4CO_2H)(H_2O)$.

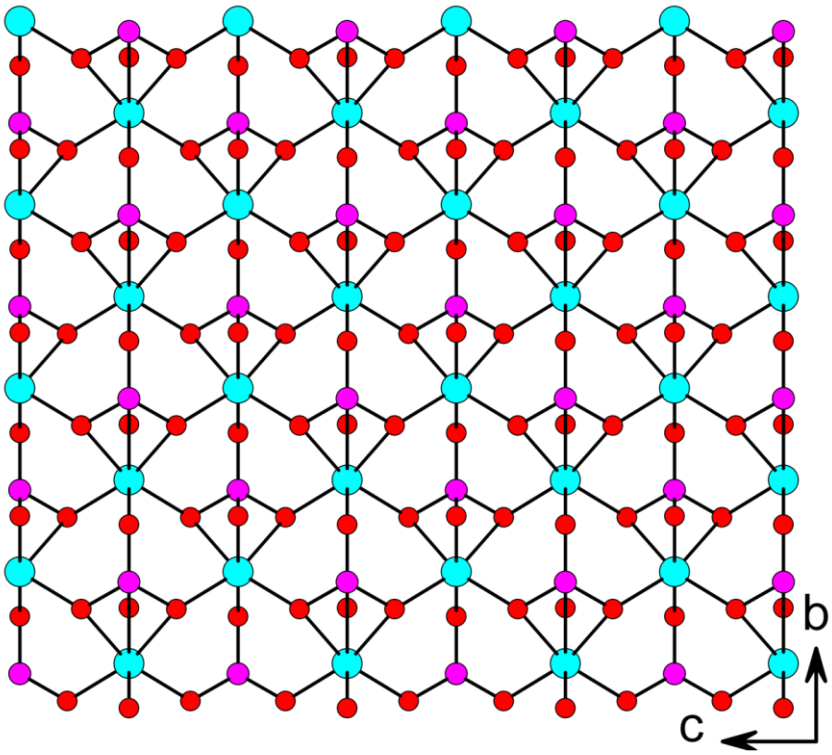

Figure 15 Inorganic layered structure common to divalent metal phosphonates. Octahedral metal ions are coordinated by five phosphonate oxygen atoms and one water molecule.

All four of the previously described compounds have isostructural layers in which the coordinating water molecules intersperse the pendant phosphonates. This layer structure is identical to that obtained for $Zn(O_3PCH_3)(H_2O)$ and $Zn(O_3PC_6H_5)(H_2O)$, and is shown in Figure 15.

A new layered structure was obtained for $Mn(O_3PC_6H_4CO_2CH_3)$ (Figure 16). In this compound, there are no coordinating water molecules and the Mn atoms are 5- and 6-coordinate. The structure still consists of pendant organic moieties decorating inorganic layers, but because the carboxylate is methylated, there is no hydrogen bonding between layers. The methyl groups on adjacent layers are somewhat staggered to allow the layers to come closer together.

The inorganic layer structure of $Mn(O_3PC_6H_4CO_2CH_3)$ is remarkably different than that of the nitrile and carboxylic acid compounds (Figure 17). This is probably due to the canted arrangement that the ligands must take to accommodate the additional bulk of the methyl groups. This structure is monoclinic, as opposed to orthorhombic like the other structures. Single crystals of the Zn analogue were not obtained, but the structure is probably similar, based on the *d*-spacing of the PXRD pattern (20.XX for Mn vs. 20.XX for Zn).

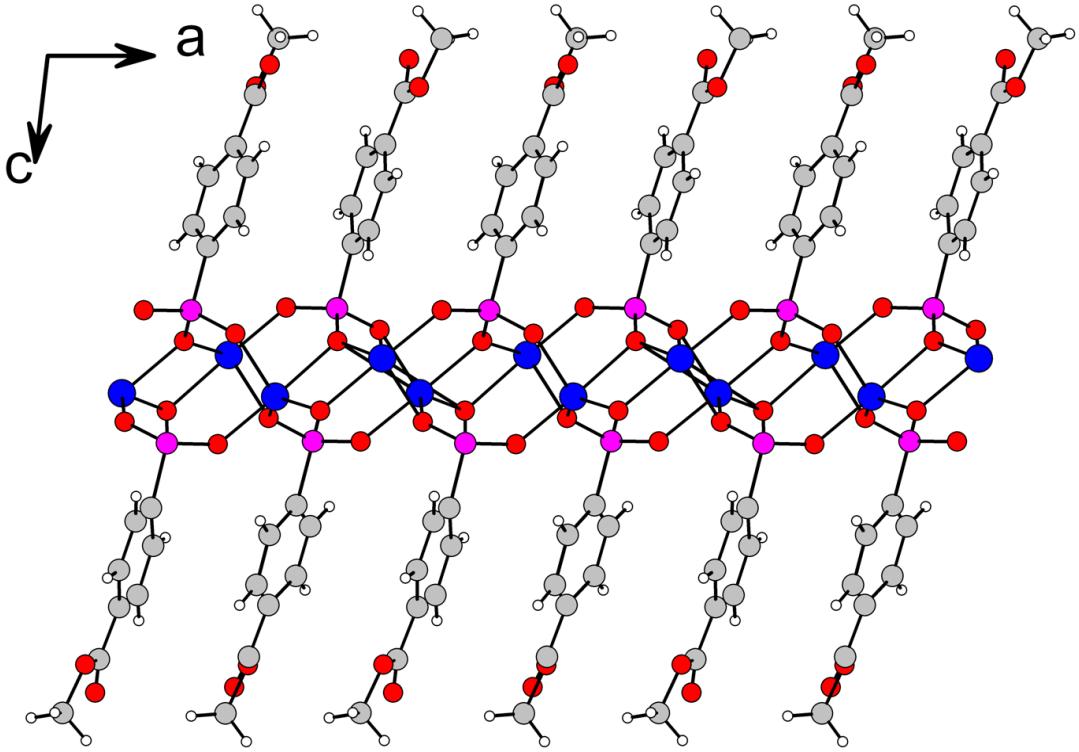

Figure 16 The layers of $Mn(O_3PC_6H_4COOCH_3)$ do not hydrogen bond with adjacent layers, and the organic groups cant in alternating directions to accommodate the methyl group

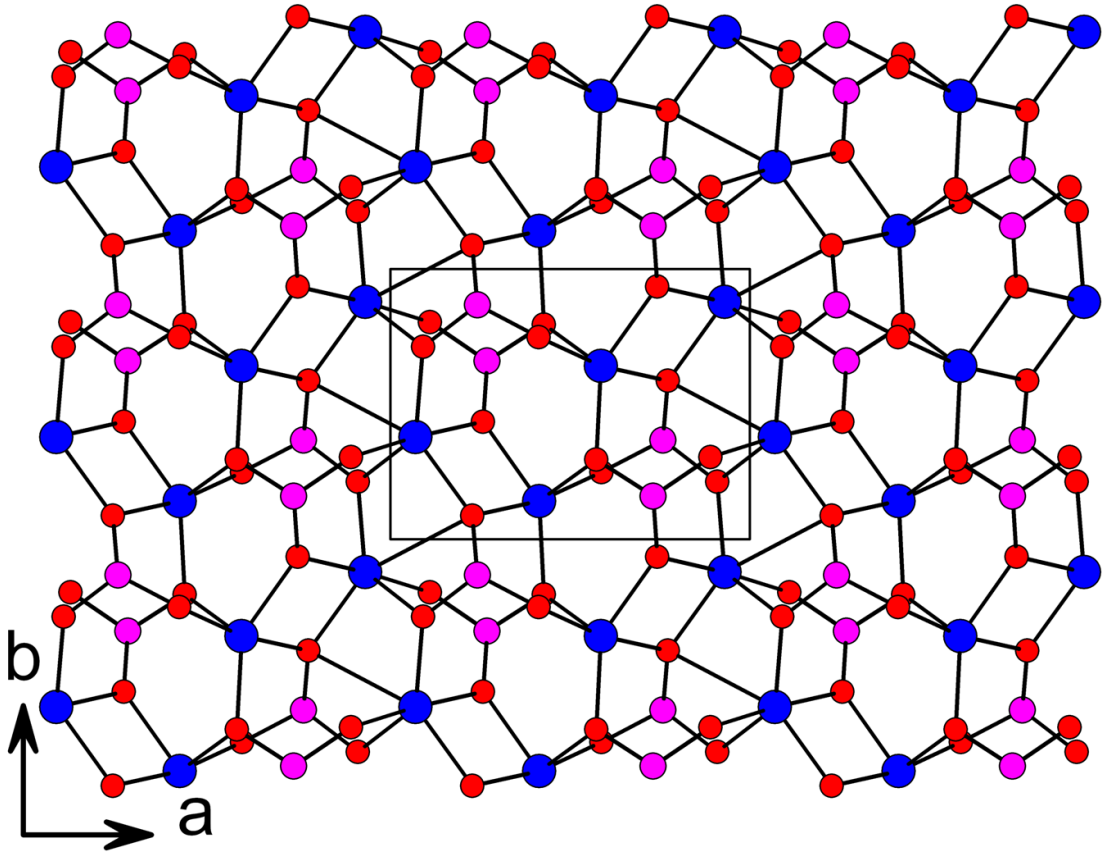

Figure 17 Inorganic layer structure of $Mn(O_3PC_6H_4CO_2CH_3)$. There are no solvent water molecules.

Table 4 Crystal structure details for the five compounds obtained as single crystals

	$Zn(O_3PC_6H_4CN)(H_2O)$	$Mn(O_3PC_6H_4CN)(H_2O)$	$Zn(O_3PC_6H_4CO_2H)(H_2O)$	$Mn(O_3PC_6H_4CO_2H)(H_2O)$	$Mn(O_3PC_6H_4CO_2CH_3)$
Formula mass	264.47	254.04	283.47	273.04	269.05
Crystal system	orthorhombic	orthorhombic	orthorhombic	orthorhombic	monoclinic
Space group	Pnma	Pnma	Pnnm	Pnnm	$P2_1$
a (Å)	32.547(4)	32.509(5)	38.225(14)	38.369(4)	7.874(2)
b (Å)	5.6492(7)	5.7491(9)	4.7725(18)	4.9072(5)	5.8616(17)
c (Å)	4.7934(6)	4.9135(7)	5.644(2)	5.7408(6)	20.125(6)
α (deg.)	90.00	90.00	90.00	90.00	90.00
β (deg.)	90.00	90.00	90.00	90.00	96.848(4)
γ (deg.)	90.00	90.00	90.00	90.00	90.00
Z	4	4	4	4	4
V ($Å^3$)	881.33(19)	918.3(2)	1029.6(7)	1080.90(19)	922.2(5)
Density (g/cm^3)	1.993	1.837	1.829	1.678	1.938
Measured reflections	8675	6255	7649	14654	12783
Unique reflections	1452	1515	1447	1785	5151
Parameters	112	139	167	158	274
$R_1 > 2\sigma(I)$, wR_2	0.0587, 0.1475	0.0545, 0.1324	0.0497, 0.1139	0.0305, 0.0757	0.0426, 0.1053
S (GooF) all data	1.222	1.136	1.004	1.184	1.029
Max/min Res. Dens. ($e/Å^3$)	2.764, -2.993	0.583, -1.341	1.536, -1.270	0.779, -0.808	0.888, -0.805

In-Situ Reaction of Nitriles

To explore the reaction of the nitrile under solvothermal conditions, experiments were carried out in which we varied the temperature, solvent, and metal salt used in the reaction. The reactions done in water were typically heated for 3 days, while those done in methanol and ethanol were heated for up to 10 days in an effort to obtain complete reaction of the nitrile. The products obtained were assigned a phase based on their *d*-spacing as determined by PXRD, which indicates the predominant crystalline phase. The presence of residual nitrile in the reaction was in some cases confirmed by CHN analyses. The results are summarized in Table 5.

In reactions performed at low temperatures, the nitriles were preserved for both Mn and Zn. The nitrile was stable with all metal salts when reacted at 130 °C for only 3 days. Higher temperatures (210 °C) resulted in the conversion of the nitrile to a carboxylic acid when the reactions were performed in water. Methyl carboxylate esters were formed for the Zn salts in methanol at reaction temperatures higher than 180 °C, but elemental analyses revealed that even after 30 days about 10% of the nitrile was still present. MnCl2 afforded no reaction between the nitrile and alcohols, even when reacted at 210 °C. This reveals that there is some role of the both the metal and the anion in the reaction of the nitrile. Higher proportions of ester could be obtained by taking the partially esterified products and solvothermally treating them again in methanol.

Table 5 Reaction products of $Et_2O_3PC_6H_4CN$ with various metal salts in water, methanol, and ethanol at specified temperatures.

	H_2O	Methanol	Ethanol
$MnCl_2 \cdot 4H_2O$	130 °C : CN; 180 °C: COOH	180 °C: CN; 210 °C: CN	180 °C: CN; 210 °C: CN
$Mn(SO_4) \cdot 5H_2O$	180 °C: COOH	210 °C: CN and CO_2CH_3	210 °C: CN, COOH, and $CO_2CH_2CH_3$
$Mn(O_2CCH_3) \cdot 4H_2O$	180 °C: COOH	210 °C: CN and CO_2CH_3	210 °C: CN, COOH, and $CO_2CH_2CH_3$
$ZnCl_2$	130 °C : CN; 180 °C: COOH	210 °C: CN and CO_2CH_3	210 °C: CN, COOH, and $CO_2CH_2CH_3$
$ZnSO_4 \cdot 7H_2O$	130 °C : CN; 180 °C: COOH	210 °C: CN and CO_2CH_3	210 °C: CN, COOH, and $CO_2CH_2CH_3$
$Zn(O_2CCH_3) \cdot 2H_2O$	180 °C: COOH	210 °C: CN and CO_2CH_3	210 °C: CN, COOH, and $CO_2CH_2CH_3$

Thermogravimetric Studies

TGA shows that $Zn(O_3PC_6H_4CN)(H_2O)$ and $Mn(O_3PC_6H_4CN)(H_2O)$ lose one mole of water at 80 and 150 °C, respectively. This is coincident with a decrease in the *d*-spacing of ~0.3 Å. This water loss is reversible by exposure to ambient air or contact with water. Similarly, $Zn(O_3PC_6H_4CO_2H)(H_2O)$ and $Mn(O_3PC_6H_4CO_2H)(H_2O)$ show a reversible loss of one mole of water at 60 and 140 °C, respectively. The d-spacing decreases by ~0.7 Å upon dehydration. Combustion of the organic moieties begins at ~400 °C for the carboxylate compounds and 550 °C for the nitrile compounds. By 1000 °C the compounds are converted to either $Zn_2(P_2O_7)$ or $Mn_2(P_2O_7)$.

TGA of $Zn(O_3PC_6H_4CO_2CH_3)$ and $Mn(O_3PC_6H_4CO_2CH_3)$ revealed that the compounds are stable to ~500 °C, at which point the organic portion of the material begins to combust, eventually leaving $Zn_2(P_2O_7)$ or $Mn_2(P_2O_7)$.

TGA was also performed on the *n*-alkylamine intercalates of $Zn(O_3PC_6H_4CO_2H)$. These graphs are included in Appendix B. The TGA curves were used to determine the amount of amine intercalated. The TGA curves were also useful in determining how the amine was intercalated into the material, i.e. at the metal site or in between the layers at the carboxylic acid groups, since alkylamines coordinated at different sites in the material (Lewis acidic Zn or the carboxylic acid) show different binding affinities. These results have been summarized in Table 6.

Table 6 *d*-Spacings and moles of amine taken up for various amine intercalates of $Zn(O_3PC_6H_4COOH)$. TGA was used to determine the amount of amines intercalated.

$Zn(O_3PC_6H_4CO_2H) \cdot nH_2N\text{-}R$	*d*-spacing (Å)
$n = 0$	18.1
$n = 2$, $R = C_3H_7$	19.6
$n = 1$, $R = C_4H_9$	18.4
$n = 1$, $R = C_5H_{11}$	18.4
$n = ?$, $R = C_6H_{13}$ (5 days)	18.5, 19.1, 32.2
$n = ?$, $R = C_6H_{13}$ (12 days)	19.1, 32.2
$n = 2.55$, $R = C_6H_{13}$ (23 days)	20.6, 12.0
$n = ?$, $R = C_7H_{15}$ (3 days)	18.4, 34.4
$n = ?$, $R = C_7H_{15}$ (12 days)	19.1, 34.0
$n = 1.8$, $R = C_7H_{15}$ (23 days)	19.8, 12.1
$n = 1.8$, $R = C_8H_{17}$	36.9
$n = 0.9$, $R = C_8H_{17}$, after heating	36.5
$n = 1.57$, $R = C_9H_{19}$	36.9
$n = 1$, $R = C_9H_{19}$, after heating	36.9

Intercalation of *n*-Alkylamines

$Zn(O_3PC_6H_4CO_2H)(H_2O)$ was dried in an oven at 150 °C for 12 hours to yield the anhydrous compound. About 0.05 g was placed in a vial to which was added 1 ml of *n*-alkylamine. After varying amounts of time the white solids were collected by filtration and washed with 200 ml dichloromethane. The products were air-dried on the filter. Some of the samples were dried at 80, 140, or 160 °C for 12 hours to study amine loss from the intercalates. To test the intercalation of longer chain alkylamines, $Zn(O_3PC_6H_4COOH)$ was left in contact with excess dodecylamine and octadecylamine dissolved in dichloromethane for 10 days, but no intercalation was detected by PXRD or TGA.

Intercalation of n-propylamine into $Zn(O_3PC_6H_4CO_2H)$ was complete in less than 48 hours. The PXRD pattern of the propylamine intercalate is shown in Figure 18. The d-spacing has increased to 19.7 Å, indicating that the amine has reacted with the carboxylic acid groups in the interlayer space. TGA shows that the compound has taken up two eq. of propylamine, which are lost in two steps at 125 and 200 °C.

PXRD patterns of the n-butylamine and n-pentylamine intercalates (Figure 19 and Figure 20, respectively) show a primary d-spacing of 18.4 Å, which is not different than that of the un-intercalated $Zn(O_3PC_6H_4CO_2H)$. TGA revealed that 0.9 eq. butylamine and 0.95 eq. pentylamine were intercalated. The butylamine intercalate lost the amine over a broad range between 100 and 250 °C, while pentylamine was lost in a single decomposition occurring at 250 °C. These intercalations were complete in 5 days, and longer exposure to the neat amines did not result in increased uptake.

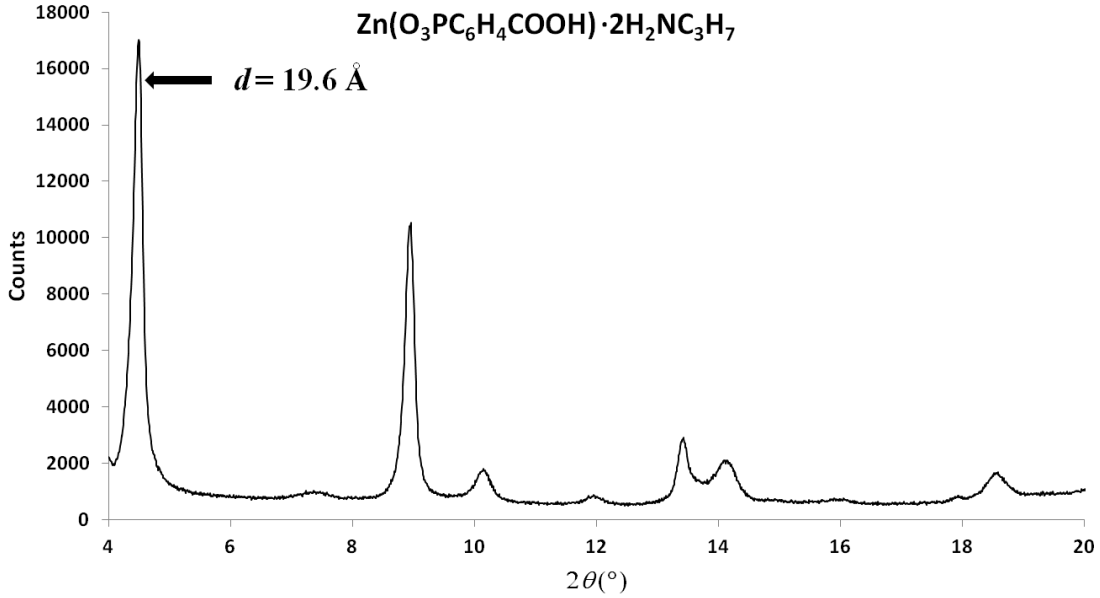

Figure 18 PXRD spectrum of the proplyamine intercalate of $Zn(O_3PC_6H_4CO_2H)$.

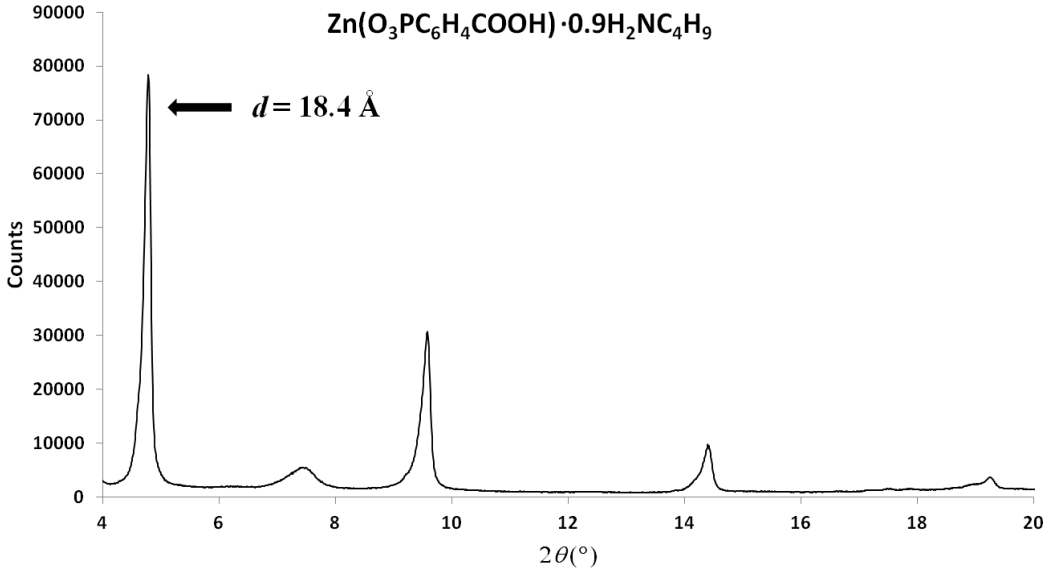

Figure 19 PXRD spectrum of the butylamine intercalate of $Zn(O_3PC_6H_4CO_2H)$.

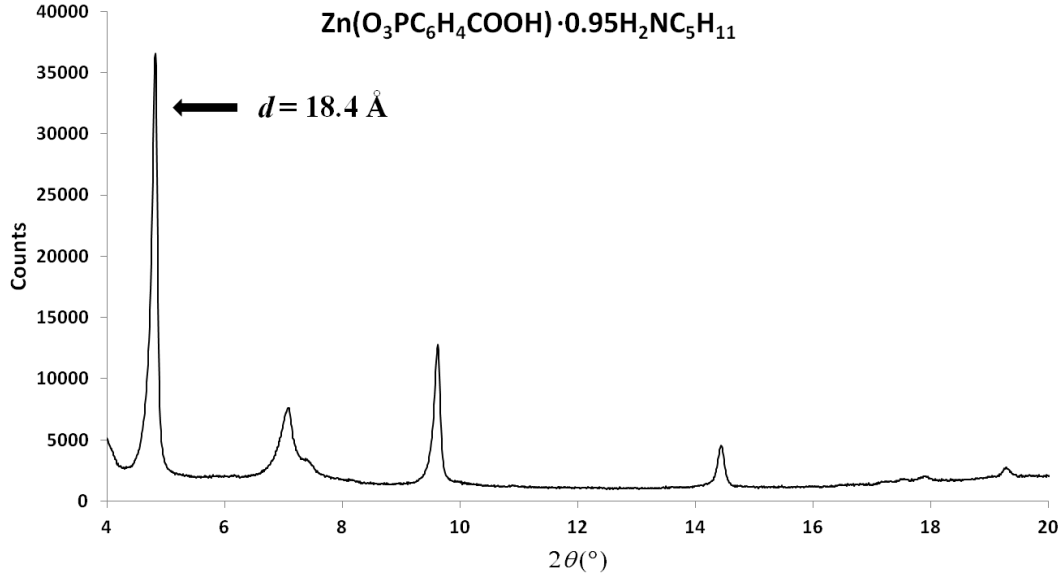

Figure 20 PXRD spectrum of the pentylamine intercalate of $Zn(O_3PC_6H_4CO_2H)$.

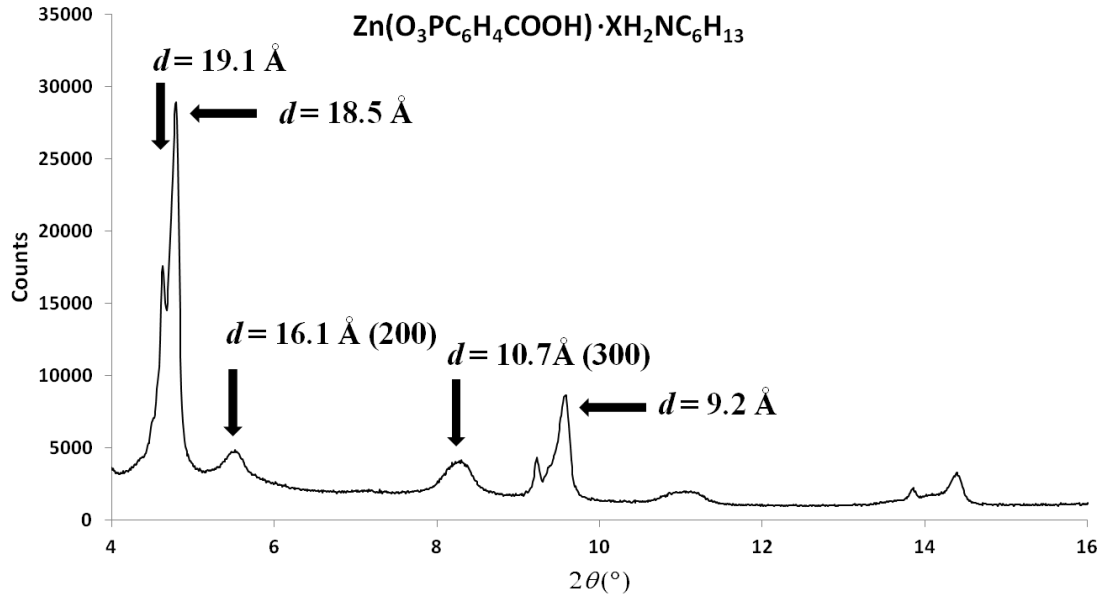

Figure 21 PXRD spectrum of the mixture of products obtained when $Zn(O_3PC_6H_4CO_2H)$ was exposed to hexylamine for 5 days.

The intercalation of hexylamine was much more complicated than the previously described cases. The PXRD pattern obtained after 5 days (Figure 21) shows the presence of at least 3 phases. Two sets of sharp peaks are present (d = 18.4 Å and d = 19.1 Å) in addition to one set of low intensity broad peaks (d = 32.1 Å). The 18.4 Å phase is most likely $Zn(O_3PC_6H_4CO_2H)$ which has not yet reacted with the amine. The presence of the 32.1 Å phase indicates that at least some of the interlayer carboxylic acids have reacted with the amine, resulting in expansion of the interlayer spacing. This will be discussed in more detail later. The nature of the 19.1 Å phase is unknown.

Increasing the reaction time to 12 days in attempt to let the system reach equilibrium resulted in the compound which gave the PXRD pattern shown in Figure 22. $Zn(O_3PC_6H_4CO_2H)$ is no longer present, as there is no peak at 18.4 Å. The compound is a mixture of the 19.1 Å phase, which is fairly crystalline, and a 32.2 Å phase, which is probably similar to the 32.1 Å phase obtained after 5 days. Letting the reaction equilibrate for 23 days resulted in the compound giving the PXRD pattern shown in Figure 23. TGA showed that this material had the composition $Zn(O_3PC_6H_4COOH)$ $\cdot 2.55H_2NC_6H_{13}$. The amount of amine present is in excess of the theoretical capacity of $Zn(O_3PC_6H_4COOH)$, and it is likely that a major structural change has occurred. Heating the material at 140 °C for 4 hours resulted in the composition $Zn(O_3PC_6H_4COOH)$ $\cdot 1.28H_2NC_6H_{13}$, and the PXRD pattern showed that the three low-angle peaks had disappeared, but that the narrow peak at 12 Å was still present (Figure 24).

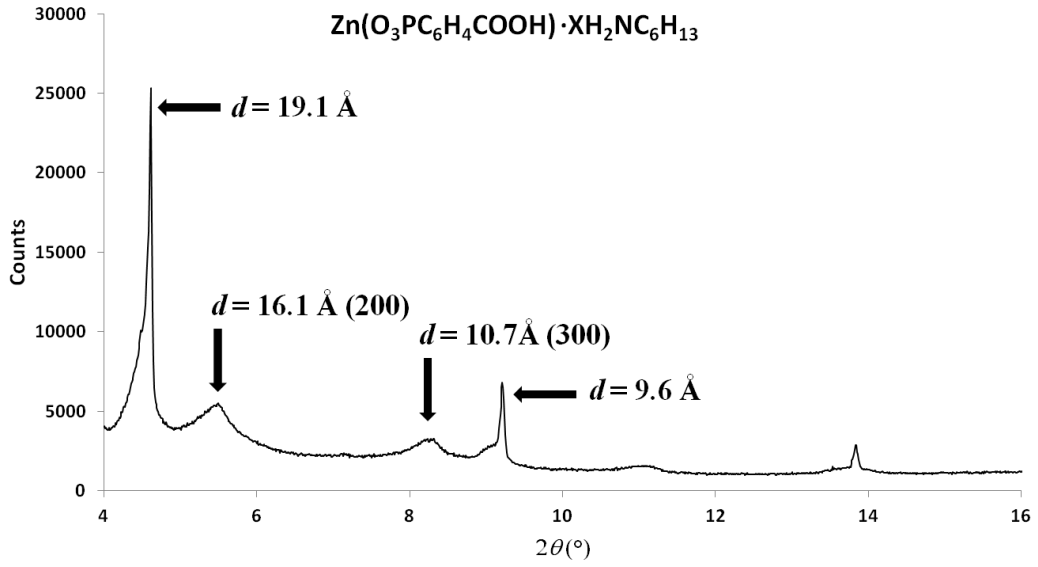

Figure 22 PXRD spectrum of $Zn(O_3PC_6H_4CO_2H)$ after 12 days exposure to hexylamine.

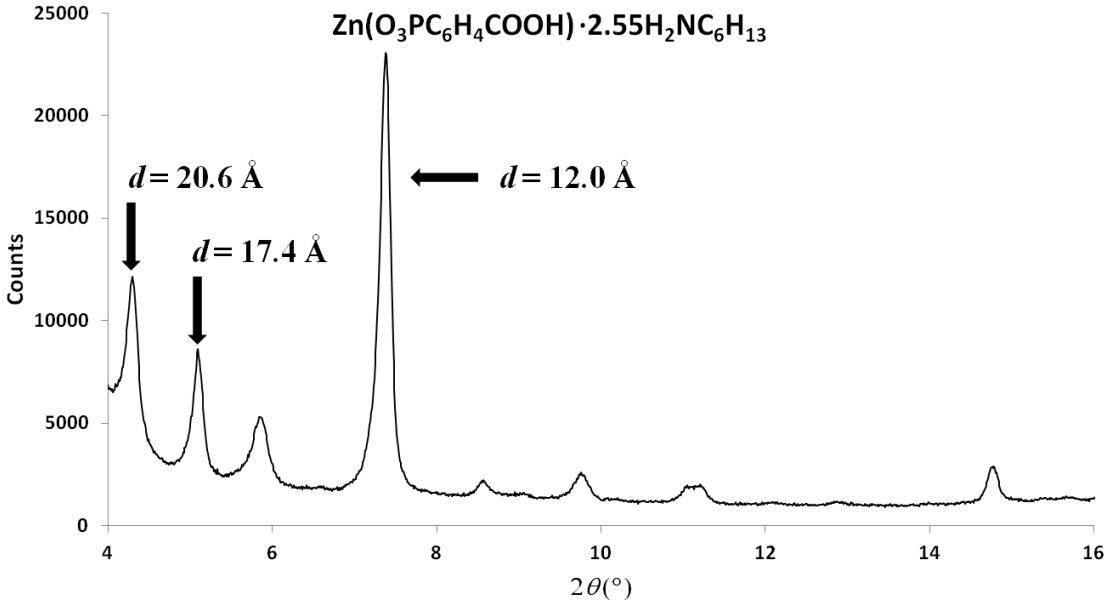

Figure 23 PXRD spectrum of $Zn(O_3PC_6H_4CO_2H)$ after 23 days exposure to hexylamine.

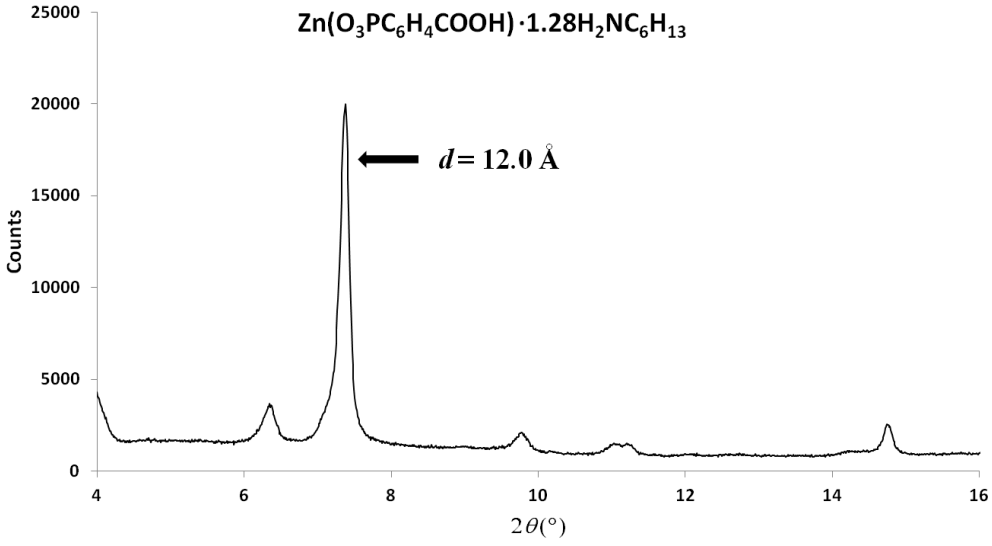

Figure 24 The hexylamine intercalate of $Zn(O_3PC_6H_4CO_2H)$ obtained after 23 days, heated at 140 °C to remove some of the amine.

The intercalation of n-heptylamine was similarly complicated. After 3 days, the product with the PXRD pattern shown in Figure 25 was obtained. It appears to be a mixture of two phases: The first (d = 18.5) is unreacted $Zn(O_3PC_6H_4COOH)$, and the second (d = 34.4 Å) is probably a phase in which the carboxylic acids have reacted with the amine, similar to the 32.2 Å phase obtained with *n*-hexylamine. The material obtained after 12 days (Figure 26) contains no unreacted $Zn(O_3PC_6H_4COOH)$, but is still a mixture of two phases. The first has a *d*-spacing of 19.2 Å and is probably related to the 19.1 Å phase obtained with hexylamine. The second has a d-spacing of 34 Å, and is probably similar in composition to the 34.4 Å phase obtained in the 3-day reaction.

After 17 days, all of these phases have completely disappeared (Figure 27). The PXRD pattern indicates the presence of a poorly crystalline material with a d-spacing of 19.9 Å, and a remarkably crystalline material with a major peak at 12.1 Å. It is likely that this phase is related to the product obtained in the 23-day reaction with n-hexylamine. TGA showed that this mixture had the overall composition $Zn(O_3PC_6H_4COOH) \cdot 1.8H_2NC_7H_{15}$.

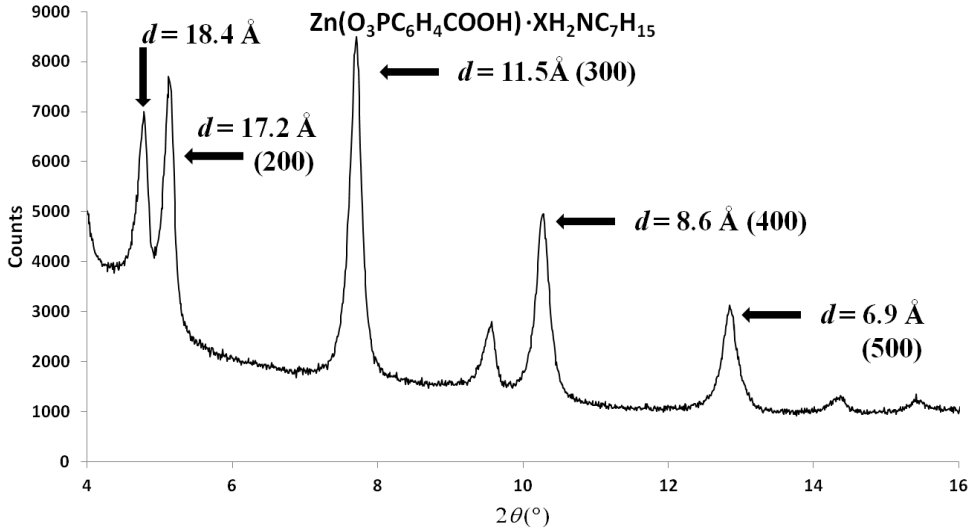

Figure 25 PXRD spectrum of $Zn(O_3PC_6H_4CO_2H)$ after exposure to heptylamine for 3 days.

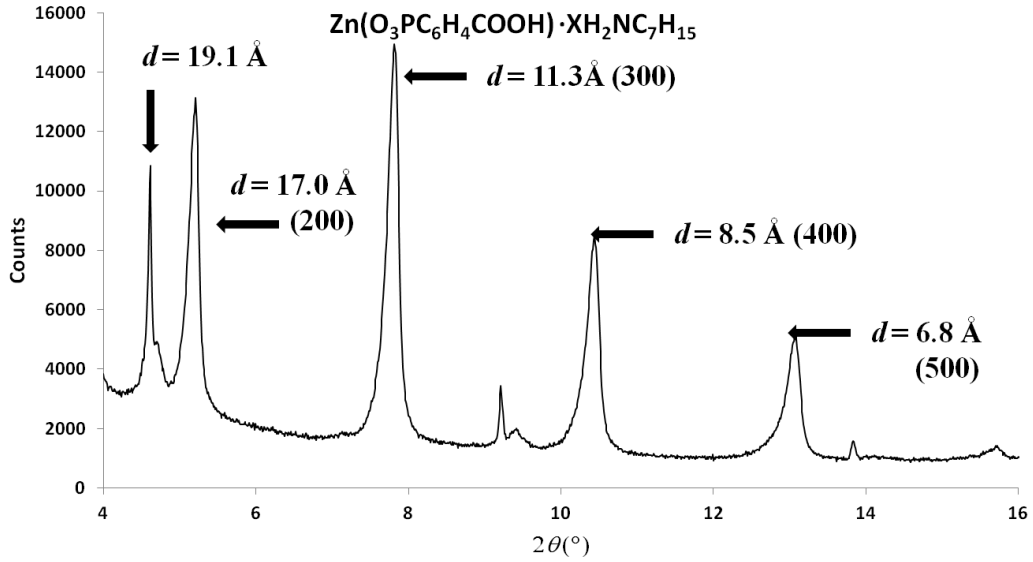

Figure 26 PXRD spectrum of $Zn(O_3PC_6H_4CO_2H)$ after exposure to heptylamine for 12 days.

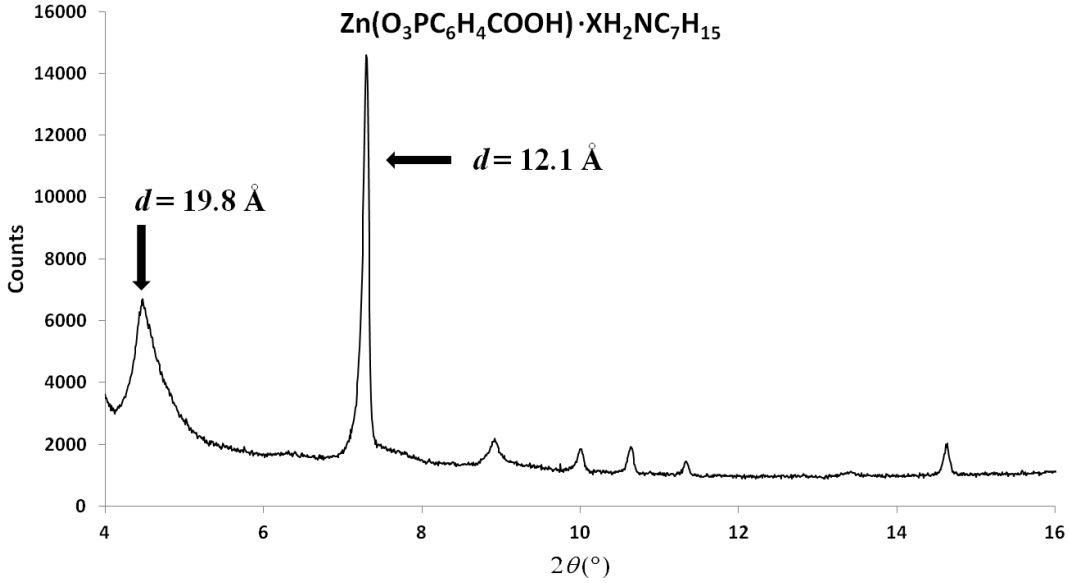

Figure 27 PXRD spectrum of $Zn(O_3PC_6H_4CO_2H)$ after exposure to heptylamine for 23 days.

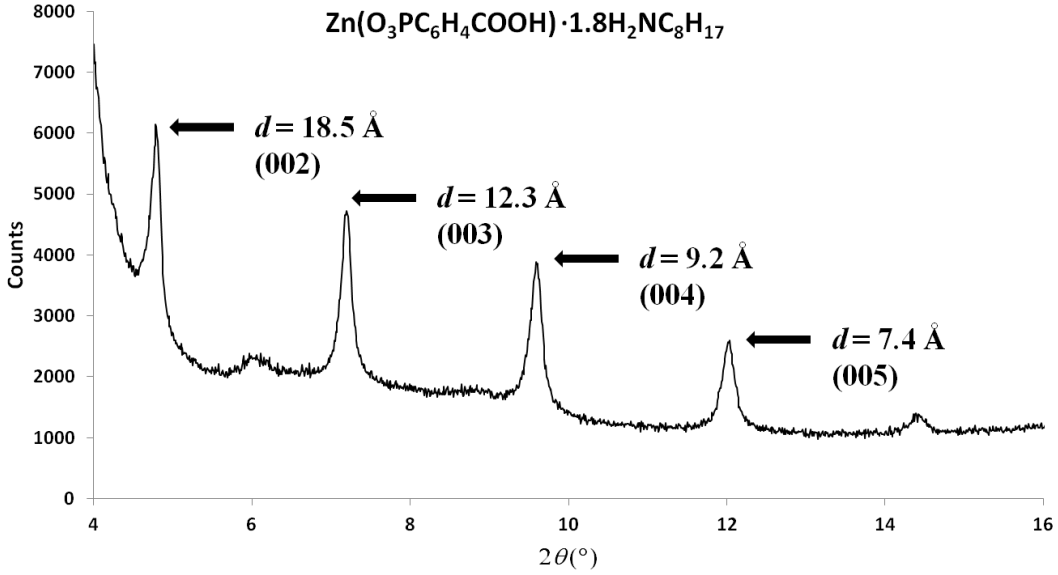

Figure 28 PXRD spectrum of the octylamine intercalate of $Zn(O_3PC_6H_4CO_2H)$ after 10 days.

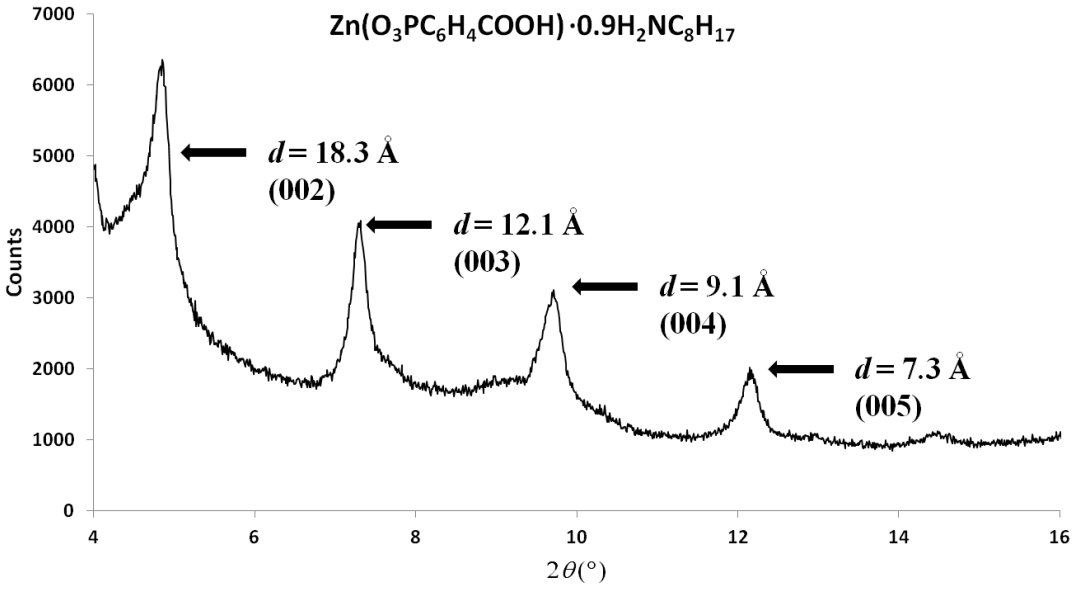

Figure 29 PXRD spectrum of the octylamine intercalate of $Zn(O_3PC_6H_4CO_2H)$ after heating to 140 °C to remove the amines bound at the metal site.

The product of the reaction between $Zn(O_3PC_6H_4COOH)$ and n-octylamine gave the PXRD pattern shown in Figure 28 after a reaction time of 10 days. TGA showed that the formula was $Zn(O_3PC_6H_4COOH) \cdot 1.8H_2NC_8H_{17}$. This material was apparently single-phase. The d-spacing of 36.9 Å indicates that the layers have spread apart to accommodate the presence of the octylamine molecules between the layers. There is also nearly complete uptake at the metal site, since the compound has taken up octylamine to 90% of the theoretical capacity. Interestingly, heating the compound at 140 °C for 12 hours did not cause a change in the PXRD pattern (Figure 29). TGA revealed that the formula of the heated compound was $Zn(O_3PC_6H_4COOH) \cdot 0.9H_2NC_8H_{17}$. The fact that the *d*-spacing is still 36.5 Å after driving off half of the intercalated amine supports the conclusion that the octylamine remaining in the compound is present in the interlayer space, interacting with the carboxylic acid groups, instead of at the metal site on the layer.

The intercalation of nonylamine was similar to that of octylamine, in that after 12 days reaction time a compound with a d-spacing of 36.9 Å was obtained (Figure 30). TGA showed that the composition was $Zn(O_3PC_6H_4COOH) \cdot 1.57H_2NC_9H_{19}$. Heating this compound at 150 °C for 12 hours resulted in the loss of about one-third of the amine. TGA of the compound after heating gave the composition $Zn(O_3PC_6H_4COOH) \cdot 1H_2NC_9H_{19}$, but the PXRD showed the presence of two phases (Figure 31). The phase with the peak at 36.9 Å was still present, indicating that at 150 °C, only the amines intercalated at the metal atoms are removed, leaving the amines intercalated at the carboxylic acids to hold the layers apart. The second phase had a *d*-spacing of 18.8 Å, which closely matches $Zn(O_3PC_6H_4COOH)(H_2O)$, although it may be from another unknown phase.

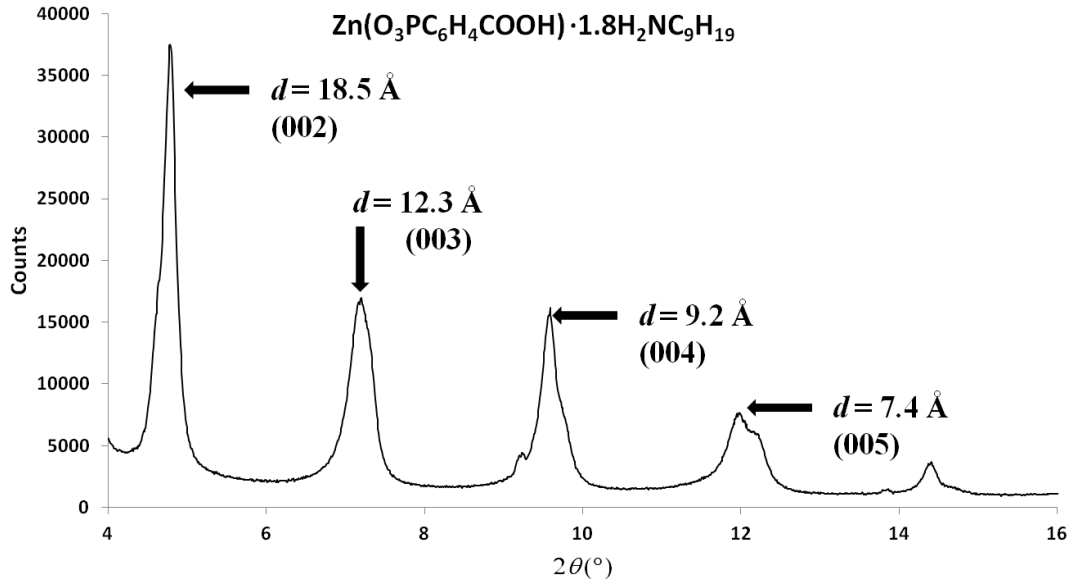

Figure 30 PXRD spectrum of the nonylamine intercalate of $Zn(O_3PC_6H_4CO_2H)$ after 12 days.

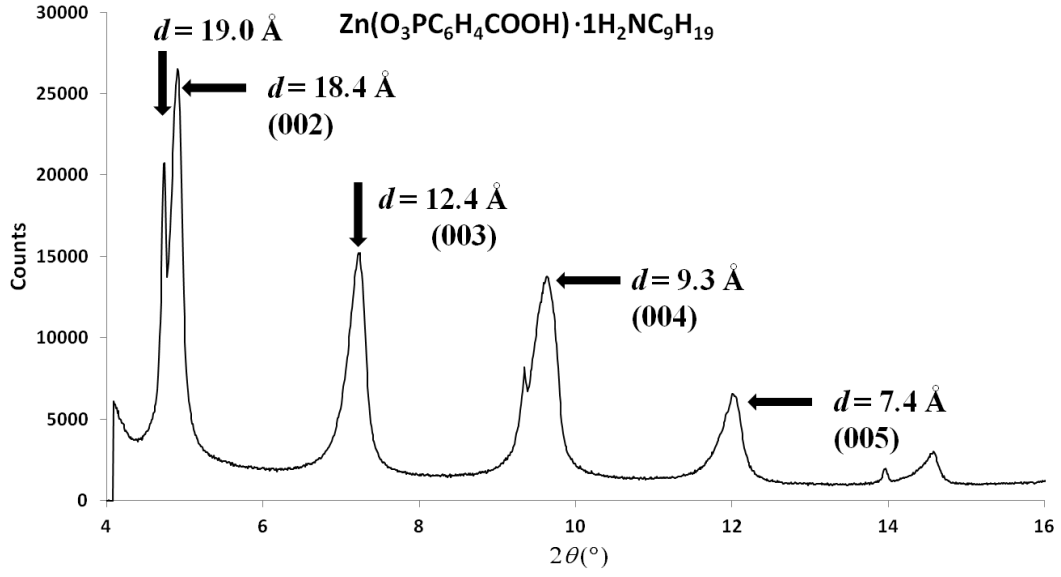

Figure 31 The nonylamine intercalate of $Zn(O_3PC_6H_4CO_2H)$ after heating to 160 °C to remove the amine bound at the metal. Note the presence of the second phase.

Discussion

Our studies on the conversion of the nitrile group to a carboxylic acid or a carboxylate ester in-situ showed some notable trends. First, the temperature of the reaction was an important factor. Reactions carried out at 130 °C did not result in any conversion of the nitrile, no matter which metal salt or solvent was used. Second, reactions with any metal salt in water at 180 °C resulted in the conversion of the nitrile to the carboxylic acid. This is most likely due to aicd-catalyzed catalysis from the increased auto-ionization of water at high temperatures, which has been reported to catalyze the decomposition of nitriles. [110, 111] Reactions performed at 210 °C in methanol resulted in incomplete conversion to the carboxylate methyl ester, except for when $MnCl_2 \cdot 4H_2O$ was used as the metal salt, in which case there was no reaction of the nitrile. For all other metal salts, elemental analyses showed that these reactions typically yielded about 90% conversion to the carboxylate ester. This was found to be an equilibrium state, as increasing the temperature or time of the reaction did not result in further conversion. These compounds appeared to be single-phase by PXRD, so it is likely that the remaining nitrile groups are interspersed with the carboxylate ester groups in the space between the layers, which are separated by ~20.2 Å. Treating these compounds again in methanol at 180 °C for 10 days resulted in the compounds $Zn(O_3PC_6H_4CO_2CH_3)$ and $Mn(O_3PC_6H_4CO_2CH_3)$. No coordinating water molecules are present in either compound. This was confirmed by TGA and the crystal structure of $Mn(O_3PC_6H_4CO_2CH_3)$, but a crystal structure of $Zn(O_3PC_6H_4CO_2CH_3)$ could not be obtained.

Performing the reactions in ethanol to effect the transformation of the nitrile to a carboxylate ethyl ester resulted in mixed phase materials in which nitrogen was still present. Research on the conversion of benzonitriles to benzoate esters in supercritical alcohols[103] has shown that the conversion in ethanol is much less efficient than that performed in methanol, because of a side reaction that results in the production of benzyl alcohol. Although the conditions used in the current research are not supercritical, a similar reaction is plausible.

The fact that the conversion of the nitrile does not occur in methanol when $MnCl_2 \cdot 4H_2O$ is used is interesting, because it shows that the metal and its anions play a role in catalyzing the reaction of the nitrile in non-aqueous systems. In water, the reaction is most likely catalyzed by the high concentrations of H_3O^+ which occur in water at 180 °C, due to increased auto-ionization. When the reaction is performed in dry methanol, this is no longer the case, so another mechanism must be responsible. The reaction systems are not completely dry, as the metal salts used are hydrates and the reactions were not loaded in a dry atmosphere. In addition, our experience with solvothermal reactions in alcohols at temperatures greater than 180 °C has shown that a significant amount of ethers are formed, which creates water as a by-product. Since the lack of water is not an issue, the metal atoms must be playing a role in the catalysis. However, the reaction proceeds when Zn salts are used, and also when Mn salts are used, just not $MnCl_2 \cdot 4H_2O$.

This may be explained by basic differences in the complex cations formed by Zn and Mn ions in solution. First, let us compare $ZnCl_2$, for which the reaction proceeds,

and $MnCl_2 \cdot 4H_2O$, for which it does not. At the relatively high concentrations of $ZnCl_2$ (~ 0.05 M) in methanol, the most predominant species would be $Zn(Cl)_2(OH_2)_x$, with x ranging from 0-4, depending on the amount of water present. These species are relatively acidic, especially the tetrahedral $Zn(Cl_2)(OH_2)_2$ ion. This acidity may be sufficient to catalyze the conversion of the nitrile to the methyl carboxylate by a mechanism similar to that of the Pinner reaction, which has been observed to occur in high-temperature aqueous solutions. Even low concentrations of $MnCl_2 \cdot 4H_2O$, however, tend to form $Mn(OH_2)_6^{2+}$ cations, due to the lower affinity of manganese for chloride ions. This species has a pKa ~10, which may not be sufficient to catalyze the decomposition of the nitrile.

While this reasoning may rationalize why the reaction proceeds for $ZnCl_2$ and not $MnCl_2 \cdot 4H_2O$, it does not explain why the reaction proceeds for the other manganese salts in methanol. It is likely that the complex ions formed in the presence of acetate or sulfate ions involve the direct coordination of the metal by these Lewis bases, since they are chelating ligands. As negatively charged ligands, they have stronger electron-donating capabilities that water molecules, which may increase the acidity of $Mn(O_2CCH_3)(OH_2)_4^+$ or $Mn(SO_4)(OH_2)_4$ relative to $Mn(OH_2)_6^{2+}$. This is in disagreement with the general rule based on coulombic effects which states that for complex ions, increased charge results in higher acidity. However, this rule does not take into account bonding effects of donor ligands which would significantly stabilize the deprotonated ion.

The compounds $Zn(O_3PC_6H_4CN)(H_2O)$ and $Zn(O_3PC_6H_4COOH)(H_2O)$, reported herein, would reasonably be expected to show dehydration and amine-uptake properties comparable to the previously reported compounds $Zn(O_3PCH_3)(H_2O)$ and $Zn(O_3PC_6H_4)(H_2O)$. However, there are some key differences that were found, primarily due to the presence of the carboxylic acid groups which form paired hydrogen bonds that hold the layers together.

$Zn(O_3PCH_3)(H_2O)$ shows a decrease of about 1.8 Å in the interlayer distance when the water molecule is removed. This is due to the methyl groups of one layer nesting in the space vacated by the water molecule. The compounds $Zn(O_3PC_6H_4CN)(H_2O)$ and $Zn(O_3PC_6H_4COOH)(H_2O)$ show a much smaller decrease in the interlayer spacing upon loss of the water molecule. This can be explained by the bulk of the phenyl rings, which do not allow the pendant organic groups from adjacent layers to approach closely and significantly decrease the space between the layers. For $Zn(O_3PC_6H_4COOH)$, the pairing of the carboxylic acids prevents the layers from being able to move closer together (Figure 32). The small decrease in *d*-spacing is most likely due to the canting of the benzonitrile and 4-carboxyphenyl groups into the vacant space next to them when the water is removed.

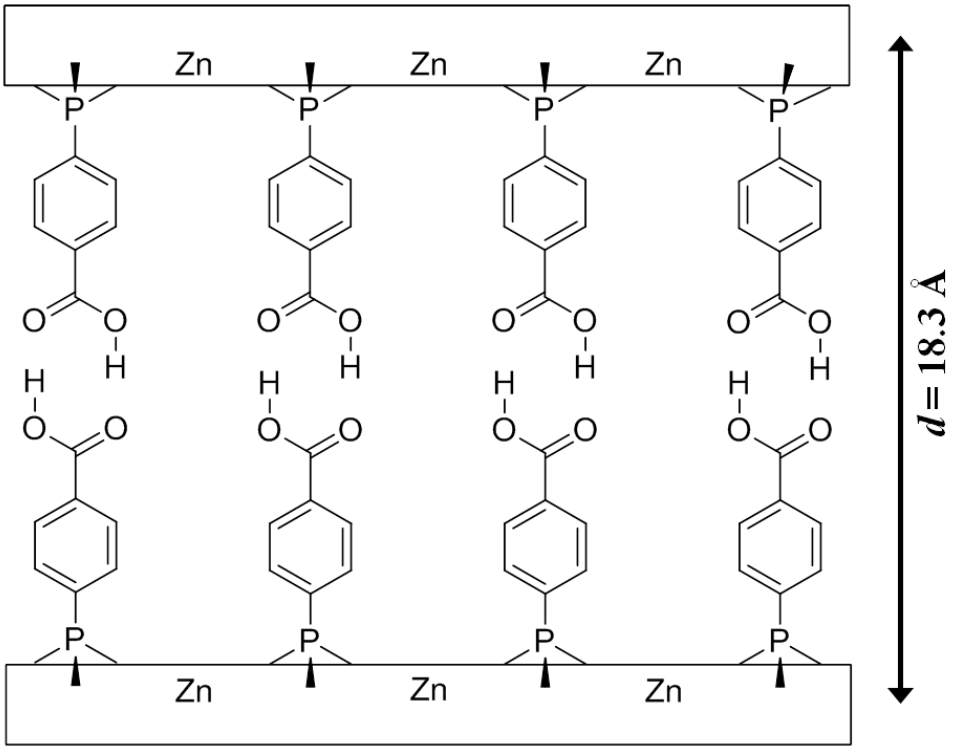

Figure 32 Depiction showing the arrangement of the paired carboxylic acids in $Zn(O_3PC_6H_4CO_2H)$ after removal of the coordinating water molecules.

Upon intercalation of propylamine, the *d*-spacing increases to ~19.6 Å, in contrast with the propylamine intercalate of $Zn(O_3PC_6H_4)$, which maintains its original d-spacing. The reason for this is that $Zn(O_3PC_6H_4)$ can only bind the amine at the metal atom in the layer, while $Zn(O_3PC_6H_4COOH)$ can bind an additional mole of propylamine with the pendant carboxylic acid group. The layers spread apart to accommodate the amines between the layers. A structural model for the propylamine intercalate must take into account the fact that 2 eq. of amine are intercalated and the d-spacing is larger than that of $Zn(O_3PC_6H_4COOH)$. A plausible arrangement is shown as a cartoon in Figure 33.

The butylamine and pentylamine intercalates of $Zn(O_3PC_6H_4COOH)$ have a d-spacing of 18.4 Å, which is less than that of the propylamine intercalate and approximately equal to that of the parent compound. TGA studies reveal that only one mole of butylamine is taken up. Because the interlayer spacing does not increase significantly, it seems that the amine only interacts with the metal atom in the layer, and not the catrboxylic acid group. This may be a consequence of the larger size of butylamine and pentylamine, which prevents them from being able to move between the layers and bind at the carboxylic acid. A possible structural model for the butlyamine and pentylamine intercalates is shown in Figure 34. The small increase in *d*-spacing observed is most likely due to a shift in the layer structure upon coordination of the amine. PXRD was used to solve the structures of some amine intercalates of $Zn(O_3PC_6H_4)$,[106] and it is reasonable to expect a similar shift in structure for $Zn(O_3PC_6H_4COOH)$, since the inorganic layers are isostructural.

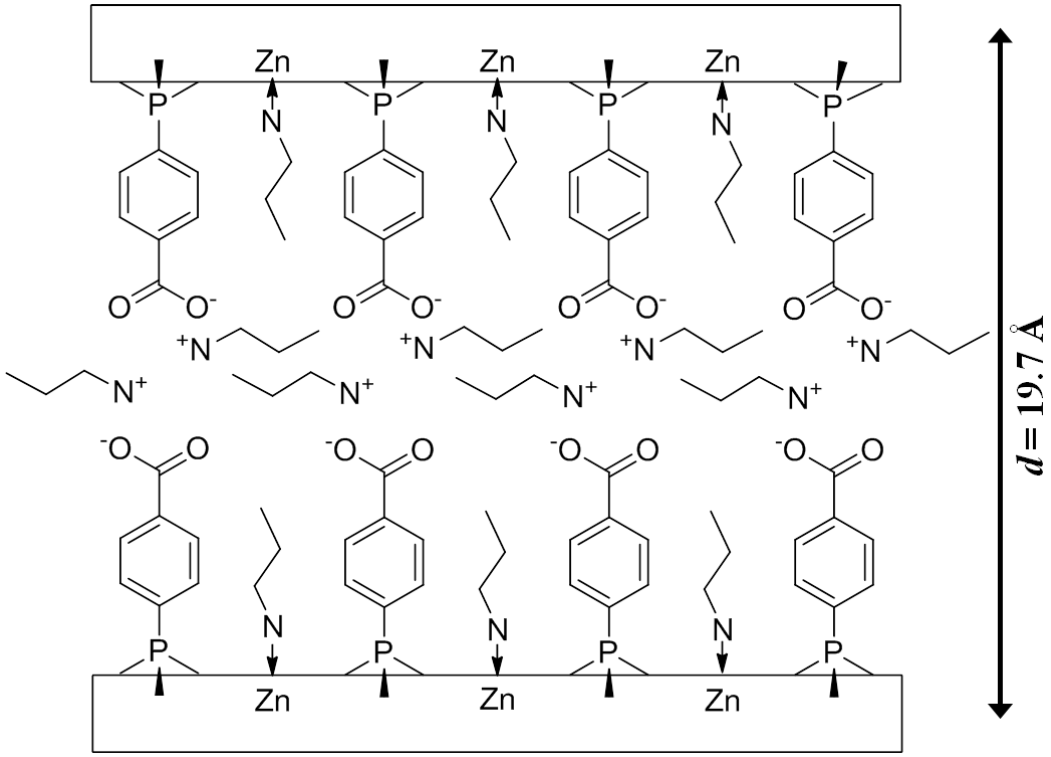

Figure 33 Possible arrangement of the propylamine molecules in $Zn(O_3PC_6H_4CO_2H) \cdot 2H_2NC_3H_7$.

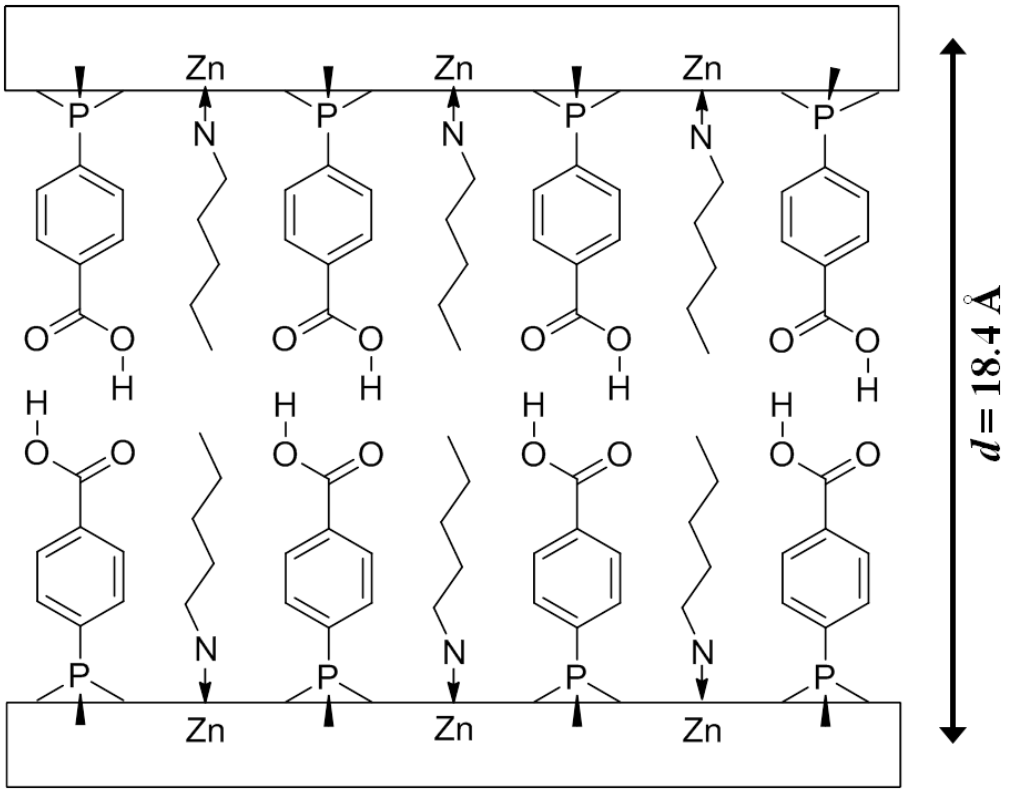

Figure 34 A depiction of the possible arrangement butylamine and pentylamine in their intercalates of $Zn(O_3PC_6H_4CO_2H)$.

This arrangement works for butylamine and pentylamine because when they are intercalated at the metal site, the alkyl chains are short enough that they fit between the benzoic acid groups and do not extend into the interlayer space. Hexylamine is too long to do this, and the layers would be pushed apart by the carbon chains extending past the benzoic acid groups. However, the hexylamine intercalate does not show just a small increase in interlayer spacing to accommodate the hydrophobic alkyl chains extending from hexylamine bound at the metal, but a large increase to 32.2 Å. We propose that this is because once the layers have been slightly pushed apart by the intercalation of hexylamine at the metal site, the hydrogen bonds holding the layers together are weakened, and more hexylamine can move into the space between the layers and interact with the carboxylic acid groups. The increase in interlayer spacing is good evidence that this binding occurs at the carboxylic acids. A model of a possible arrangement for this structure is shown in Figure 35.

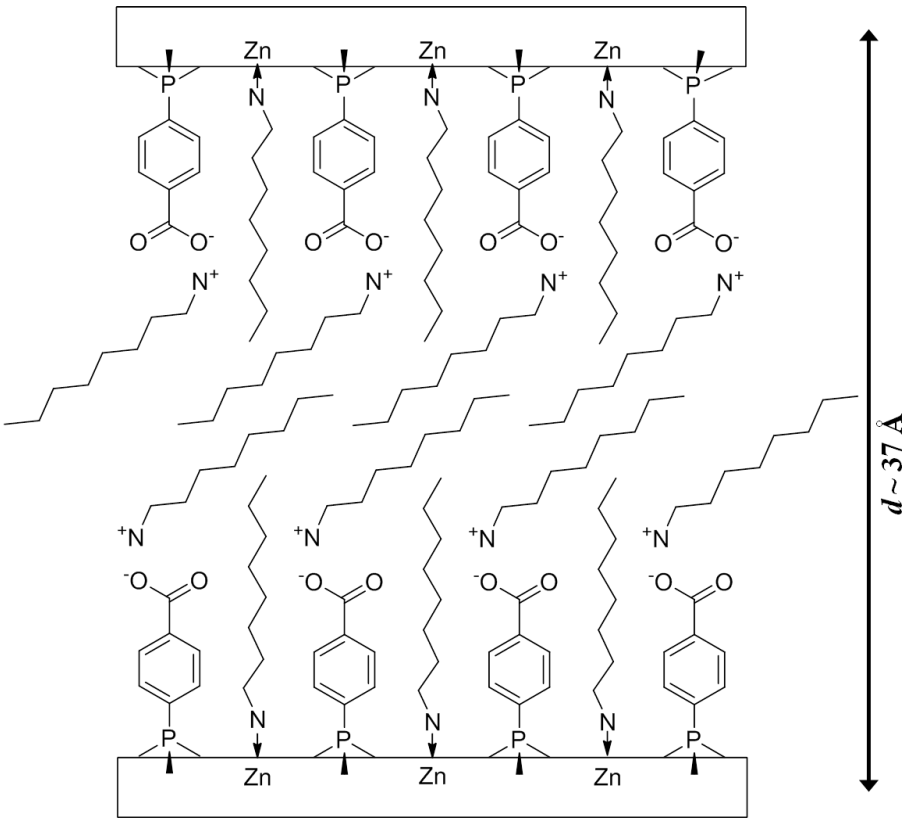

Figure 35 Depiction showing a possible arrangement for the amines in $Zn(O_3PC_6H_4CO_2H)$ intercalated with hexylamine, heptylamine, octylamine, and nonylamine.

The fact that TGA analyses show that more than 2 eq. of hexylamine is intercalated indicates that there are more complex phases which form, possibly involving non-coordinating amines filling the remainder of the interlayer space. A similar phenomenon occurs with the heptylamine and octylamine intercalates, which have *d*-spacings of 34.5 Å and 36.5 Å, respectively. The nonylamine intercalate has a *d*-spacing of 36.9 Å, which is close to that of the octylamine intercalate. This is probably because the compounds only bind these long amines at a fraction of the carboxylic acid sites, due to the crowding in the interlayer space. This allows the amines to adopt a canted arrangement, which results in much lower *d*-spacings than would be expected if they formed a true double layer.

This complicated behavior may be a consequence of the many different packing arrangements the long-chain alkylamines can take between the layers when they interact with the carboxylic acids. Obviously, as the amount of amine between the layer increases, the *d*-spacing should also increase. But there may be several stable phases which can coexist, as has been documented for alkylamine intercalates of zirconium phosphate.[112]

It is interesting that the octylamine and nonylamine intercalates can be heated to selectively remove the amines bound at the metal sites. This conclusion is supported by the fact that the heated compounds are shown to have less than 1 eq. of amine remaining, but their PXRD patterns still show that the interlayer distance is ~35 Å due to the remaining amine in the interlayer space. A depiction of a possible arrangement is shown in Figure 36.

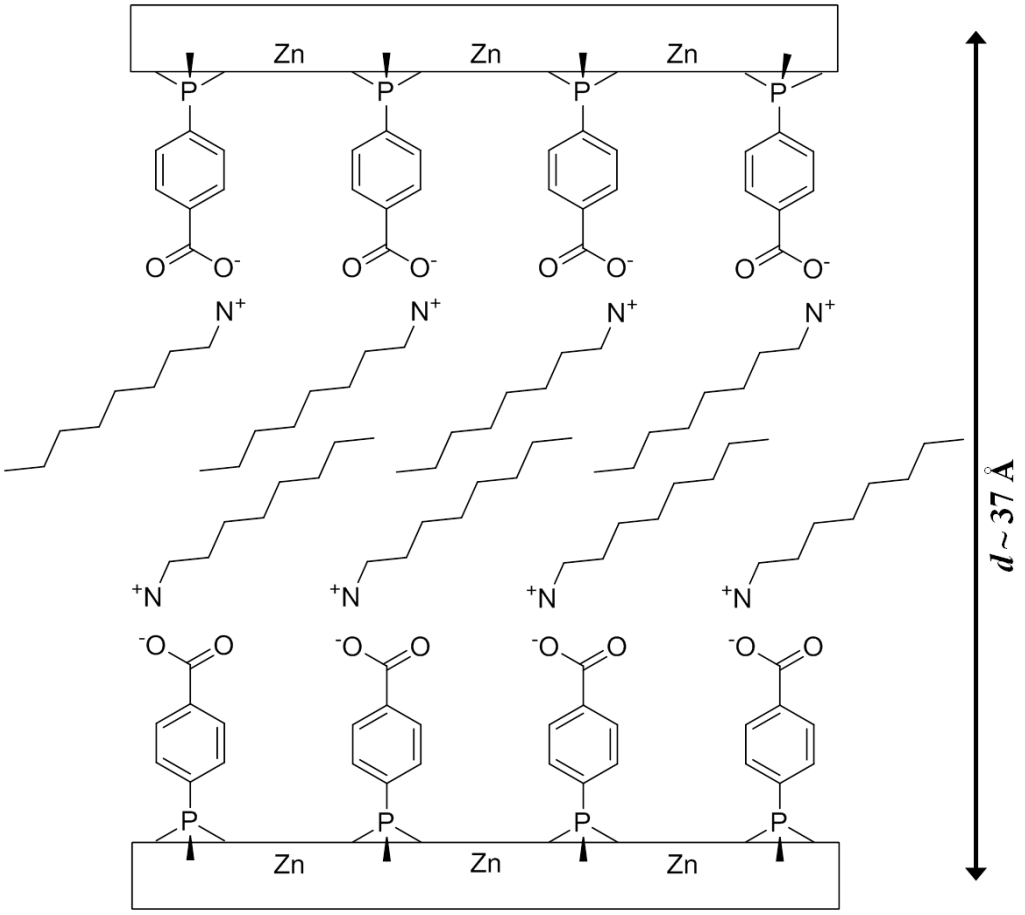

Figure 36 Representation of a possible structure of $Zn(O_3PC_6H_4CO_2H)$ $H_2NC_8H_{17}$ that accounts for the large d-spacing and the presence of 1 eq. of amine.

The structures of the alkylamine intercalates of $Zn(O_3PC_6H_5)$ were solved by powder XRD methods, and it was shown that the inorganic layer undergoes a solid-state rearrangement which widens the space between adjacent phenyl rings to allow room for the alkylamine chain. The Zn changes from five- to four-coordinate, and the amine chains are oriented nearly perpendicular to the plane of the layers. It is likely that the structures of the amine intercalates presented here undergo a similar transformation. Unfortunately, even intercalation of the amines into highly crystalline samples of $Zn(O_3PC_6H_4COOH)$ resulted in materials that gave very poor PXRD patterns which allowed only the observation of the d-spacing.

It should also be noted that the intercalations were carried out in neat amines because $Zn(O_3PC_6H_4COOH)$ is considerably soluble in water (unlike $Zn(O_3PC_6H_4)$), which prevented us from being able to add only stoichiometric amounts of amine to aqueous solutions. These intercalations are also much slower than those of $Zn(O_3PC_6H_4)$, so it is likely that intercalations with stoichiometric amounts of amine would take a very long time, given that reactions with neat amines take days or weeks in the absence of water competing for the Lewis acidic binding sites.

Conclusion

During hydrothermal and solvothermal syntheses, nitrile functional groups were maintained or converted to carboxylic acids or carboxylate methyl esters. This allowed for the syntheses of three different types of phosphonates using the same ligand, depending on the choice of solvent and temperature. In this work, complete conversion

to the carboxylic acid required heating at 180 °C in water for at least three days, while complete conversion to the methyl carboxylate ester was only obtained by two treatments at 180 °C in methanol. Using $MnCl_2 \cdot 4H_2O$ in methanol resulted in no reaction of the nitrile, which is probably due to the low acidity of $Mn(OH_2)_6^{2+}$, which is likely the predominant species in the reaction mixture. The ethyl carboxylates were not obtained as pure compounds even after two solvothermal treatments in ethanol. In-situ reactions of ligands in this manner may create new routes to functional materials. We are currently investigating applications of this reaction in tetravalent metal phosphonates.

$Zn(O_3PC_6H_4COOH)$ shows interesting amine-uptake properties, in that it binds primary amines in different quantities depending on the alkyl chain length. Propylamine binds both at the metal center and to the carboxylic acid, while butylamine and pentylamine bind only at the metal center because they are too large to fit between the layers and interrupt the hydrogen bonding betweeen pairs of carboxylic acids. Longer chain alkylamines first bind at the metal center, which leaves the hydrophobic tail extending into the interlayer space, where it interferes with the hydrogen bonds between carboxylic acid pairs. The layers move apart, which facilitates the secondary intercalation of amine into the interlayer space where it interacts with the carboxylic acids. The octylamine and nonylamine intercalates can be heated to selectively remove the amine from the metal site. This type of dual-character intercalation is unique to these layered phosphonates, and it may provide a basis for the syntheses of materials which show size-selectivity in amine uptake.

CHAPTER V

PHOSPHONATE-BASED HEPTANUCLEAR CLUSTERS

Introduction

Polynuclear metal clusters have been the subject of intense research, particularly for their potential as single-molecule magnets (SMM's). Most efforts in this field have been concentrated on oxo- and cyano-bridged Mn and Fe clusters of varying nuclearity. Many of these homo- and heteronuclear clusters incorporate carboxylate and alkoxide bridging ligands, but there is an increasing number of compounds reported which include phosphonate-based ligands.[57, 113-124] The Winpenny group has achieved additional success with mixed antimonate-phosphonate ligands.[125, 126] Phosphonates have been shown to facilitate weak magnetic coupling, and in these clusters the magnetic interactions are dominated by stronger magnetic couplers like carboxyates, azides, and alkoxides. Yet phosphonates are versatile ligands which have many different modes of coordination, allowing them to play an integral role in cluster topology and assembly.

A structurally interesting example of a phosphonate-based cluster was first reported in 2003 by Lei et al.,[127] $Zn_7L_6{\cdot}2Zn(H_2O)_6{\cdot}28H_2O$ (L = N-(phosphonomethyl)-N-glycine) contains a $[Zn_7(L)_6]^{4-}$ anion in which the central zinc ion is in an octahedral environment of oxygen atoms from the six phosphonate ligands. The six equivalent outer zinc ions are five-coordinate in an approximate trigonal bipyramidal arrangement and are bound to oxygen atoms from three phosphonates, a nitrogen atom from the amine, and another oxygen atom from the carboxylate. The six outer zinc ions form an

octahedron and the seventh zinc ion is in the center of the cluster. The 4- charge of the cluster is balanced by two $Zn(H_2O)_6^{2+}$ cations. Since this initial report, there have been other zinc clusters of the same topology reported that were synthesized from other multifunctional ligands such as N-(phosphonomethyl)proline,[128-130] hydroxy(2-pyridyl)methyl-phosphonic acid,[131] and N-(phosphonomethyl)pipecolinic acid.[132] In addition, such molecules have been incorporated into porous frameworks.[128, 129] Until the present study, only Zn^{II} has been observed to form these $[M_7L_6]^{4-}$ clusters, although other heptanuclear Co,[133-138] Mn,[139-145] Cu,[146-151] and Fe[152, 153] clusters of different topologies are well-documented in the literature. These clusters have been shown to exhibit interesting magnetic properties, including single-molecule magnetism.[120, 121] It is noteworthy that in many of these other clusters, the seven metal atoms are coplanar, while in the $[Zn_7L_6]^{4-}$ clusters the six exterior zinc ions are staggered above and below the horizontal plane that contains the central zinc ion.

The work presented in this chapter is based upon the trifunctional ligand 6-phosphonopyridine-2-carboxylic acid. When reacted with Zn^{II} salts, it produced a novel cluster with the $[Zn_7L_6]^{4-}$ topology. I then set out to determine if the $[M_7L_6]^{4-}$ clusters could be synthesized with other divalent metal ions, particularly Co and Mn.

The naming convention used in the remainder of this chapter will take the form *M(cation) symmetry*, where *M* denotes the metal in the cluster, *cation* denotes the charge-balancing species (DMA = dimethylammonium, DBA = dibenzylammonium, M = $M(H_2O)_4^{2+}$), and *symmetry* is the Schoenflies symbol for the virtual symmetry of the cluster (either S_6 or C_2). The first four compounds are isostructural, consisting of

$[M_7L_6]^{4-}$ clusters of virtual S_6 symmetry which are charge-balanced by dimethylammonium cations: $Zn_7(L)_6(Me_2NH_2)_4 \cdot 2(C_4H_9NO) \cdot H_2O$ (**Zn(DMA) *S*$_6$**), $Co_7(L)_6(Me_2NH_2)_4 \cdot 2(C_4H_9NO) \cdot H_2O$ (**Co(DMA) *S*$_6$**), $Mn_7(L)_6(Me_2NH_2)_4 \cdot 2(C_4H_9NO) \cdot H_2O$ (**Mn(DMA) *S*$_6$**), and $Mg_7(L)_6(Me_2NH_2)_4 \cdot 2(C_4H_9NO) \cdot H_2O$ (**Mg(DMA) *S*$_6$**) (L = 6-phosphonopyridine-2-carboxylate, C_4H_9NO = dimethylacetamide). The S_6 $[M_7L_6]^{4-}$ cluster unit has not been previously observed for manganese and cobalt.

The second group of compounds also have S_6 symmetry, but are charge-balanced by dibenzylammonium cations: **Zn(DBA) *S*$_6$, Co(DBA) *S*$_6$, Mn(DBA) *S*$_6$.** The larger cations affect the packing of the clusters, which can be all oriented in the same direction, in contrast with the clusters made with DMA.

Performing the reactions in the absence of base resulted in new Zn clusters that were not only of different virtual symmetry (C_2), but were charge-balanced by divalent metal ions which link the clusters through their pendant carboxylate groups. It was also found that if Co or Mn was included in the reaction mixture, partial substitution occurred at both the central site in the cluster and the bridging aqua cations, the only two octahedral sites in the structure. The compounds obtained were **Zn(Zn) *C*$_2$, Zn(Co) *C*$_2$,** and **Zn(Mn) *C*$_2$**, of which only the Co- and Mn-substituted compounds are isostructural.

The final compound obtained was a Zn cluster with S_6 symmetry, synthesized from water in the presence of triethylamine. The clusters are charge balanced by aqua cations that bridge the clusters through the pendant carboxylate groups. Again, two of the six carboxylate groups are protonated to achieve charge balance.

Experimental Details

Reagents and ligands used in the work presented in this chapter were prepared or acquired as described in Chapter II. Single crystal X-ray diffraction data for **Zn(Zn) *C*$_2$** were collected at 110 K on a Bruker-AXS GADDS MWPC three-circle X-ray Diffractometer equipped with a rotating Cu Kα (λ = 1.54178 Å) anode operated at 40 kV and 40 mA. Single crystal x-ray diffraction data for **Zn(Mn) *C*$_2$** were collected on a Bruker Smart APEX-II CCD diffractometer with a Mo Kα (λ = 0.71073 Å) source operated at 40 kV and 40 mA. Single crystal x-ray diffraction data for all other compounds were collected using synchrotron radiation (λ = 0.77490 Å) on beamline 11.3.1 at Lawrence Berkeley National Laboratory. Data reduction and cell refinement for all compounds were performed with SAINT.[154] SADABS[108] was used to obtain absorption corrected data. The structures were solved by direct methods using SHELXTL.[109]

Cluster Syntheses

Zn(DMA) S$_6$, Zn$_7$(O$_3$PC$_5$NH$_3$COO)$_6$(H$_2$NC$_2$H$_6$)$_4$ ·2C$_4$H$_9$NO ·H$_2$O

A mixture of $Zn(OOCCH_3)_2$•$2H_2O$ (0.7 mmol, 0.154 g) and 6-phosphonopyridine-2-carboxylic acid (0.6 mmol, 0.122 g) in 3 ml dimethylacetamide was placed in a PTFE-lined steel autoclave (internal volume 10 ml) and heated at 150 °C for six days. After cooling, colorless plate-shaped crystals of 1 were collected by vacuum filtration and washed with dimethylacetamide. Yield: 0.128 g, 63% based on Zn. Sample was dried to constant weight prior to elemental analyses. Analyses

calculated for $Zn_7(C_6NPO_5H_3)_6(Me_2NH_2)_4 \cdot(C_4H_9NO)$: C, 29.88%; H, 3.08%; N, 7.98%. Found: C, 30.37%; H, 2.90%; N, 8.00%.

Co(DMA) S_6, $Co_7(O_3PC_5NH_3COO)_6(H_2NC_2H_6)_4 \cdot 2C_4H_9NO \cdot H_2O$

A mixture of $CoCl_2 \cdot 6H_2O$ (0.7 mmol, 0.167 g) and 6-phosphonopyridine-2-carboxylic acid (0.6 mmol, 0.122 g) in 3 ml dimethylacetamide was placed in a PTFE-lined steel autoclave (internal volume 10 ml) and heated at 150 °C for six days. After cooling, blue plate-shaped crystals were collected by vacuum filtration and washed with dimethylacetamide. Yield: 0.158 g, 79% based on Co. Sample was dried to constant weight prior to elemental analyses. Analyses calculated for $Co_7(C_6NPO_5H_3)_6(Me_2NH_2)_4 \cdot(C_4H_9NO)$: C, 30.59%; H, 3.16%; N, 8.18%. Found: C, 30.18%; H, 3.45%; N, 8.00%.

Mn(DMA) S_6, $Mn_7(O_3PC_5NH_3COO)_6(H_2NC_2H_6)_4 \cdot 2C_4H_9NO \cdot H_2O$

A mixture of $Mn(OOCCH_3)_2 \cdot 4H_2O$ (0.7 mmol, 0.172 g) and 6-phosphonopyridine-2-carboxylic acid (0.6 mmol, 0.122 g) in 3 ml dimethylacetamide was placed in a PTFE-lined steel autoclave (internal volume 10 ml) and heated at 150 °C for six days. After cooling, pale yellow plate-shaped crystals were collected by vacuum filtration and washed with dimethylacetamide. Yield: 0.146 g, 74% based on Mn. Sample was dried to constant weight prior to elemental analyses. Analyses calculated for $Mn_7(C_6NPO_5H_3)_6(Me_2NH_2)_4 \cdot(C_4H_9NO)$: C, 31.05%; H, 3.20%; N, 8.30%. Found: C, 31.11%; H, 3.28%; N, 7.86%.

Mg(DMA) S_6, $Mg_7(O_3PC_5NH_3COO)_6(H_2NC_2H_6)_4 \cdot 2C_4H_9NO \cdot H_2O$

A mixture of $Mg(OOCCH3)_2 \cdot 4H_2O$ (0.35 mmol, 0.075 g) and 6-phosphonopyridine-2-carboxylic acid (0.3 mmol, 0.061 g) in 3 ml dimethylacetamide was placed in a PTFE-lined steel autoclave (internal volume 10 ml) and heated at 150 °C for six days. After cooling, colorless plate-shaped crystals were collected by vacuum filtration and washed with dimethylacetamide.

Zn(DBA) S_6, $Zn_7(O_3PC_5NH_3COO)_6(H_2NC_{14}H_{14})_4 \cdot 6.7H_2O$

A mixture of $Zn(OOCCH_3)_2 \cdot 2H_2O$ (0.35 mmol, 0.077 g) and 6-phosphonopyridine-2-carboxylic acid (0.3 mmol, 0.061 g) in 2 ml H_2O and 1 ml dibenzylamine was placed in a PTFE-lined steel autoclave (internal volume 10 ml) and heated at 180 °C for 3 days. After cooling, colorless plate-shaped crystals were collected by vacuum filtration and washed with ethanol.

Co(DBA) S_6, $Co_7(O_3PC_5NH_3COO)_6(H_2NC_{14}H_{14})_4 \cdot 4(H_2O)$

A mixture of $Co(OOCCH_3)_2 \cdot 4H_2O$ (0.35 mmol, 0.087 g) and 6-phosphonopyridine-2-carboxylic acid (0.3 mmol, 0.061 g) in 2 ml H_2O and 1 ml dibenzylamine was placed in a PTFE-lined steel autoclave (internal volume 10 ml) and heated at 180 °C for 3 days. After cooling, purple plate-shaped crystals of were collected by vacuum filtration and washed with ethanol.

Mn(DBA) S_6, $Mn_7(O_3PC_5NH_3COO)_6(H_2NC_{14}H_{14})_4 \cdot 2.8(H_2O)$

This compound was synthesized in ethanol (instead of water as done for **Zn(DBA) *S_6*** and **Co(DBA) *S_6***) to avoid the immediate precipitation of manganese hydroxide which occurs in basic aqueous solutions of Mn^{II}. A mixture of $Mn(OOCCH_3)_2 \bullet 4H_2O$ (0.7 mmol, 0.172 g), 6-phosphonopyridine-2-carboxylic acid (0.6 mmol, 0.122 g), and dibenzylamine (2.4 mmol, 0.385 g) in 2 ml H_2O was placed in a PTFE-lined steel autoclave (internal volume 10 ml) and heated at 160 °C for 3 days. After cooling, pale yellow plate-shaped crystals of were collected by vacuum filtration and washed with ethanol.

Zn(Zn) C_2, $Zn_7(O_3PC_5NH_3COO)_4(O_3PC_5NH_3COOH)_2Zn(H_2O)_4 \cdot 6H_2O$

$Zn(O_2CCH_3)_2$ $2H_2O$ (0.3 mmol, 0.066 g) and 6-phosphonopyridine-2-carboxylic acid (0.3 mmol, 0.061 g) was placed with 10 ml H_2O in a PTFE-lined steel autoclave (internal volume 15 ml) and heated at 180 °C for 4 days. The colorless crystals were collected by filtration and washed with ethanol.

Zn(Co) C_2, $Zn_{6.2}Co_{0.8}(O_3PC_5H_3NCOO)_4(O_3PC_5H_3NCOOH)_2Co(H_2O)_4 \cdot 5.5H_2O$

$Zn(NO_3)_2 \cdot 6H_2O$ (0.3 mmol, 0.089 g), $CoCl_2 \cdot 6H_2O$ (0.3 mmol, 0.071 g), and 6-phosphonopyridine-2-carboxylic acid (0.3 mmol, 0.061 g) was placed with 3 ml H_2O in a PTFE-lined steel autoclave (internal volume 10 ml) and heated at 180 °C for 3 days. The pale pink crystals were collected by filtration and washed with ethanol.

Zn(Mn) C_2, $Zn_{6.36}Mn_{0.64}(O_3PC_5NH_3COO)_4(O_3PC_5NH_3COO)_2Mn(H_2O)_4 \cdot 4H_2O$

$Zn(NO_3)_2 \cdot 6H_2O$ (0.3 mmol, 0.089 g), $Mn(SO_4) \cdot H_2O$ (0.3 mmol, 0.050 g), and 6-phosphonopyridine-2-carboxylic acid (0.3 mmol, 0.061 g) was placed with 10 ml H_2O in a PTFE-lined steel autoclave (internal volume 15 ml) and heated at 180 °C for 3 days. The colorless crystals were collected by filtration and washed with ethanol.

Zn(Zn) S_6, $Zn_7(O_3PC_5NH_3COO)_4(O_3PC_5NH_3COOH)_2Zn(H_2O)_4 \cdot 11H_2O$

$Zn(O_2CCH_3)_2$ $2H_2O$ (0.3 mmol, 0.066 g) and 6-phosphonopyridine-2-carboxylic acid (0.3 mmol, 0.061 g) was placed with 3 ml H_2O and 0.3 ml triethylamine in a PTFE-lined steel autoclave (internal volume 10 ml) and heated at 180 °C for 3 days. The colorless crystals were collected by filtration and washed with ethanol.

Table 7 Crystal structure information for Zn(DMA) S_6, Co(DMA) S_6, Mn(DMA) S_6, Mg(DMA) S_6, and Zn(DBA) S_6

	Zn(DMA) S_6	**Co(DMA) S_6**	**Mn(DMA) S_6**	**Mg(DMA) S_6**	**Zn(DBA) S_6**
Formula mass	2034.61	1989.53	1961.60	1747.19	2572.69
Crystal system	monoclinic	monoclinic	monoclinic	monoclinic	monoclinic
Space group	$P2_1/n$	$P2_1/n$	$P2_1/n$	$P2_1/n$	$P2_1/c$
a (Å)	17.1101(18)	16.9868(13)	17.2284(19)	17.0461(16)	13.6425(8)
b (Å)	24.353(3)	24.4833(19)	24.697(3)	24.547(2)	26.1753(15)
c (Å)	17.1744(18)	17.1557(13)	17.3344(19)	17.1940(16)	14.3175(8)
α (deg.)	90.00	90.00	90.00	90.00	90.00
β (deg.)	93.653(2)	93.496(2)	93.415	93.168(2)	94.051(2)
γ (deg.)	90.00	90.00	90.00	90.00	90.00
Z	4	4	4	4	2
V (Å^3)	7141.7(14)	7121.7(9)	7362.5(15)	7183.5(11)	5100.0(5)
Density (g/cm^3)	1.892	1.856	1.770	1.616	1.675
Measured reflections	100845	116402	107503	78398	72453
Unique reflections	13057	21654	22364	14717	15526
Parameters	1023	1023	1003	1023	712
$R_1 > 2\sigma(I)$, wR_2	0.0598, 0.1530	0.0356, 0.0721	0.0479, 0.1249	0.0453, 0.1129	0.0416, 0.1139
S (GooF) all data	1.052	0.999	1.020	1.015	1.070
Max/min Res. Dens. (e/Å^3)	1.343, -0.831	0.924, -0.625	1.088, -0.957	0.693, -0.496	0.991, -0.817

Crystal Structures

Zn(DMA) S_6, **Co(DMA) S_6**, **Mn(DMA) S_6**, and **Mg(DMA) S_6** are isostructural. The crystallographic information is given in Table 7. All of these structures are monoclinic, crystallizing in $P2_1/n$, with the unit cell volumes varying slightly with the size of the divalent metal used. The ligand is hexadentate and coordinates to four different metal atoms, three of which are external and one of which occupies a central position in the cluster (Figure 37). A single phosphonate oxygen atom bridges each external metal ion to the core metal ion, and O-P-O bridges connect each external metal ion to four others in addition to the central ion. The clusters have a 4- charge, which is balanced by four dimethylammonium cations formed by thermal decomposition of the dimethylacetamide. The dimethylammonium cations occupy the void spaces between the clusters along with interstitial H_2O molecules. The clusters readily dissolve in water, but are insoluble in diethyl ether, acetonitrile, dichloromethane, and ethanol.

The six external metal atoms alternate above and below the plane through the center of the cluster containing the central metal ion. The arrangement of the ligands gives the clusters virtual S_6 symmetry (Figure 38). The central metal ion is connected with the external metal ions through both oxo- and –O-P-O- bridges, while the external metal ions are bridged by only O-P-O groups. This may have consequences in the magnetic behavior of the Co and Mn versions of this cluster.

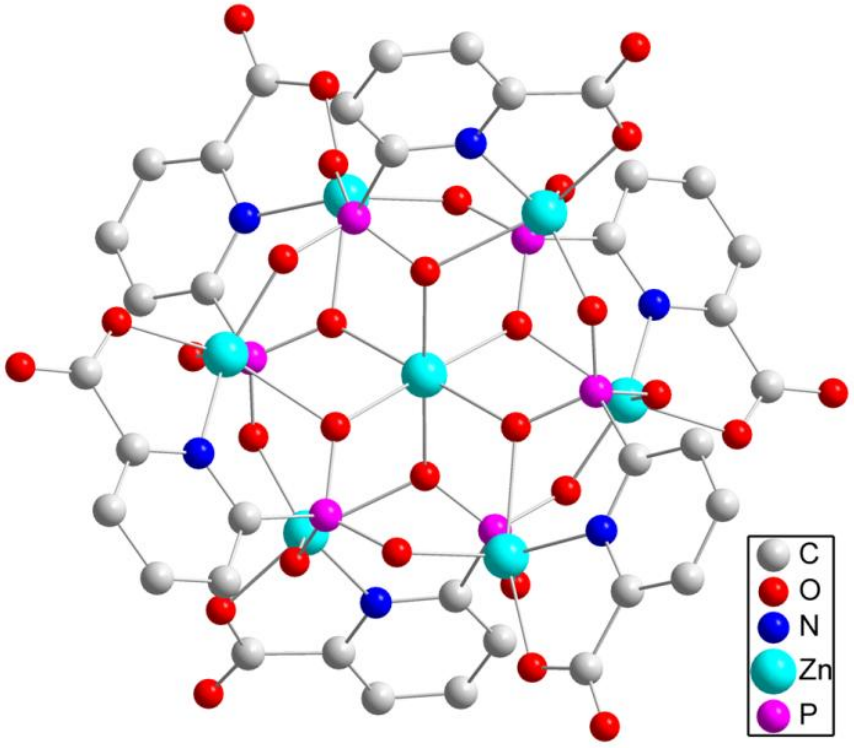

Figure 37 View of the $Zn_7(L)_6^{4-}$ cluster unit along the S_6 axis. Hydrogen atoms have been omitted for clarity. Mn, Co, or Mg ions can substitute for the Zn ions in isostructural compounds.

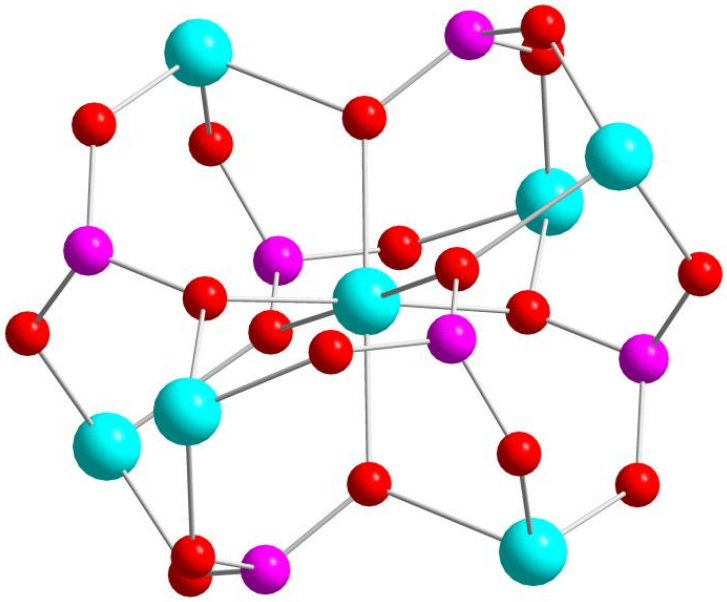

Figure 38 The core of the $[M^{II}_7(L)_6]^{4-}$ cluster with C, H, N, and carboxylate O atoms omitted to show the O and O-P-O bridging between M^{II} ions.

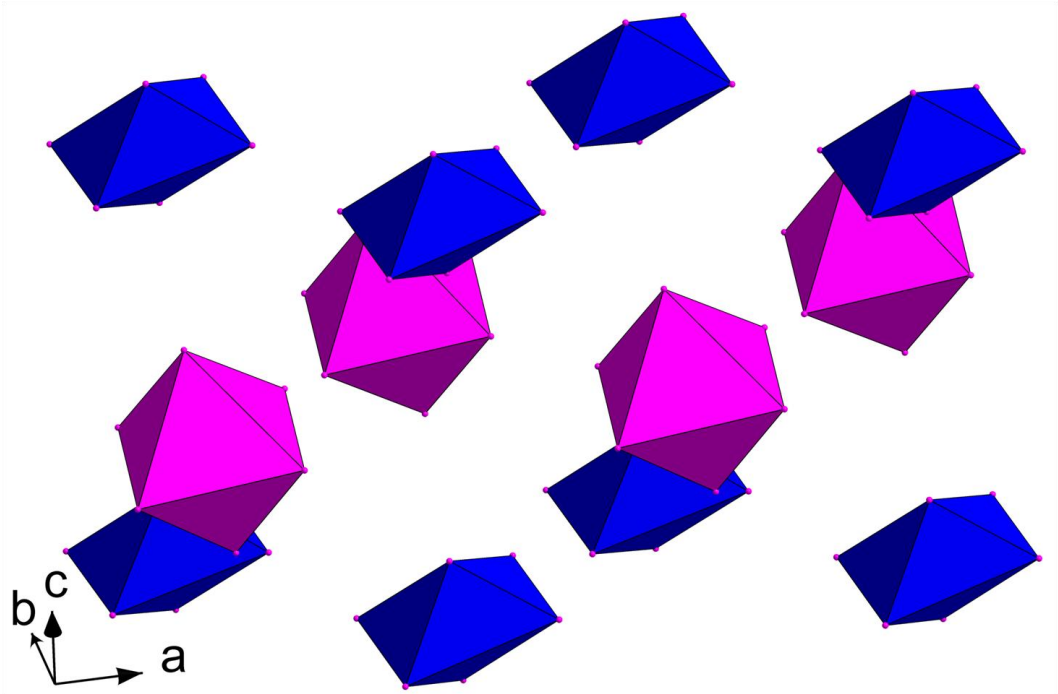

Figure 39 View of the Co(DMA) S_6 clusters showing the two different orientations of the clusters. Different orientations of the clusters are shown in two different colors. The polyhedra represent the Co atoms within the clusters.

In these compounds, the clusters are oriented in two different directions within the structure. This arrangement is shown in Figure 39. The presence of the dimethylammonium cation in the previously described compounds is due to the decomposition of the dimethylacetamide during the reaction. I hypothesized that the arrangement of the clusters would depend on the size and shape of the charge-balancing cations, and by changing solvent (to eliminate the presence of dimethylammonium) and including other amines that different arrangements could be obtained. I successfully synthesized the same cluster units with dibenzylammonium as the cation by performing the reactions in water (or ethanol for Mn^{II}) in the presence of dibenzylamine. By this method the compounds **Zn(DBA) *S*$_6$**, **Co(DBA) *S*$_6$**, and **Mn(DBA) *S*$_6$** were obtained. Crystallographic data are included in Table 7 and Table 8. Interestingly, only the Co and Mn derivatives are isostructural, crystallizing in the triclinic space group P-1. In these structures, which contain dibenzylammonium ions instead of dimethylammonium as the charge-balancing cations, the clusters are all oriented in the same direction in the crystal (Figure 40 and Figure 41). It is unclear why the Zn compound crystallizes in the monoclinic space group $P2_1/c$ and the clusters are in two different orientations (Figure 42 and Figure 43). This may be due to solubility or size differences between the metal cations, although no clear conclusions can be drawn.

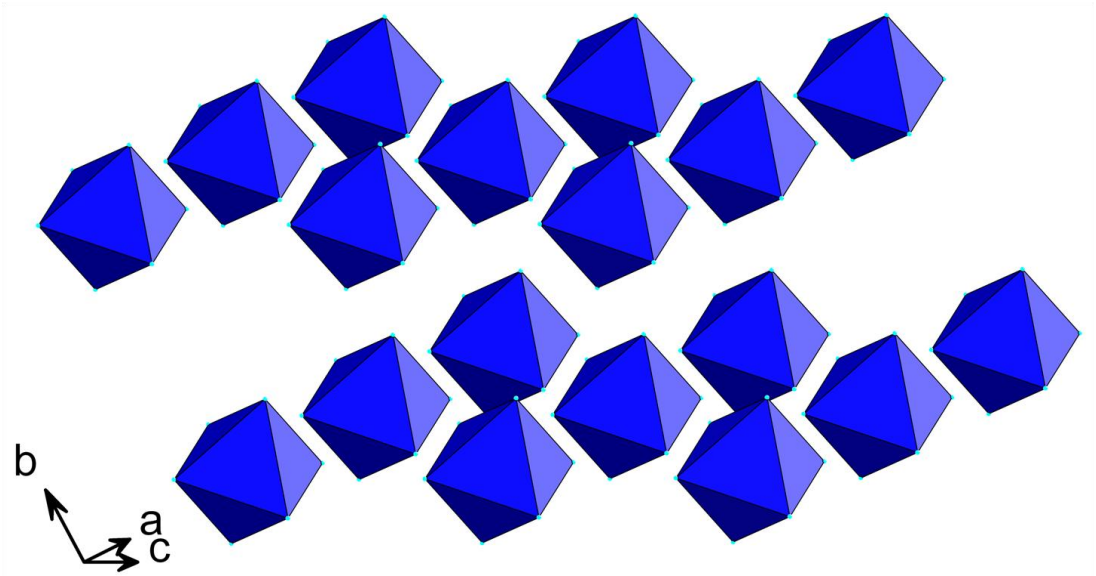

Figure 40 Triclinic Mn(DBA) S_6 and Co(DBA) S_6 clusters are oriented in the same direction. The polyhedra represent the Mn atoms within the clusters.

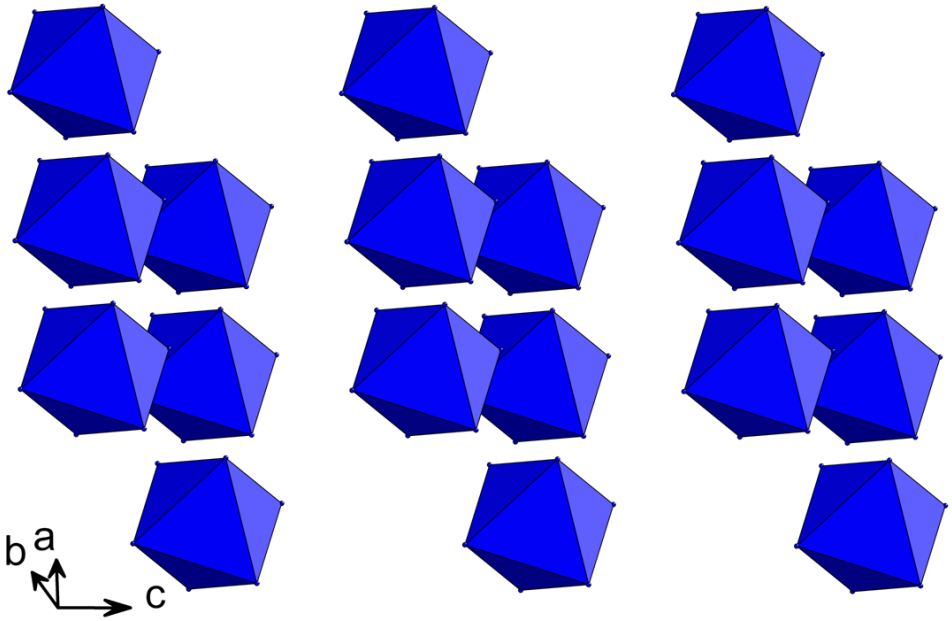

Figure 41 Triclinic Mn(DBA) S_6 and Co(DBA) S_6 clusters are oriented in the same direction. The polyhedra represent the Mn atoms within the clusters. The organic portion of the clusters and the dibenzylammonium cations occupy the space between layers of clusters.

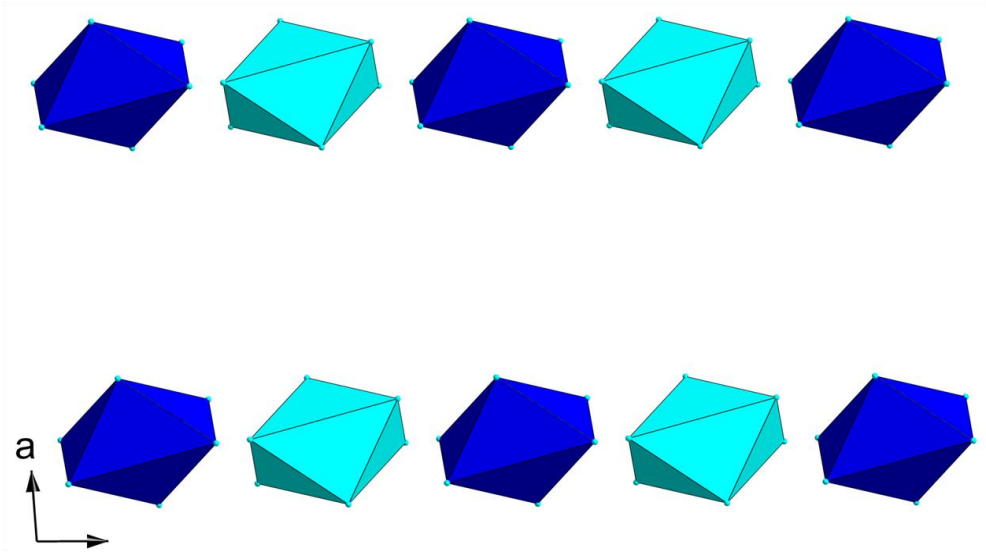

Figure 42 View of the Zn(DBA) S_6 clusters along the b-axis. Different orientations of the clusters are shown in two different colors. The polyhedra represent the Zn atoms within the clusters.

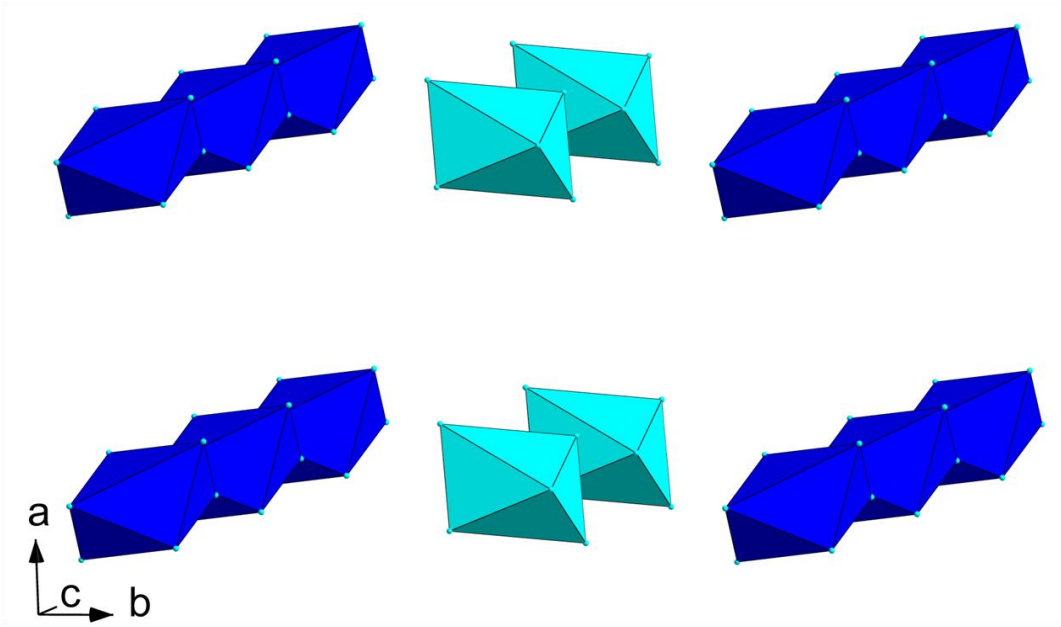

Figure 43 View of the Zn(DBA) S_6 clusters showing the two different orientations of the clusters. Different orientations of the clusters are shown in two different colors. The polyhedra represent the Zn atoms within the clusters.

Table 8 **Crystal data for Co(DBA) S_6, Mn(DBA) S_6, Zn(Zn) C_2, Zn(Co) C_2, Zn(Mn) C_2, and Zn(Zn)S_6**

	Co(DBA) S_6	**Mn(DBA) S_6**	**Zn(ZnH2) C_2**	**Zn(CoH2) C_2**	**Zn(MnH2) C_2**	**Zn(Zn) S_6**
Formula mass	2478.07	2428.52	1905.68	1885.86	1852.51	1995.76
Crystal system	triclinic	triclinic	triclinic	monoclinic	monoclinic	monoclinic
Space group	$P\bar{1}$	$P\bar{1}$	$P\bar{1}$	C_2/c	C_2/c	$P2_1/c$
a (Å)	10.7697(10)	11.0027(6)	12.911(3)	26.567(4)	26.486(5)	23.7294(17)
b (Å)	13.5836(12)	15.4672(8)	16.084(3)	18.213(3)	18.135(4)	12.0588(9)
c (Å)	18.0323(17)	16.2607(9)	16.191(3)	12.876(2)	12.876(3)	23.6791(17)
α (deg.)	105.140(2)	91.746(2)	69.01(2)	90.00	90.00	90.00
β (deg.)	102.784(2)	107.117(2)	71.72(3)	112.451	112.26(3)	115.431(2)
γ (deg.)	93.759(2)	110.768(2)	71.87(3)	90.00	90.00	90.00
Z	1	1	2	4	4	4
V (Å^3)	2461.9(4)	2444.5(2)	2904.7(10)	5758.2(2)	5724(2)	6119.2(8)
Density (g/cm^3)	1.685	1.650	1.640	1.638	1.618	1.631
Measured reflections	32303	36021	29409	34316	16806	88493
Unique reflections	12538	14712	9056	6622	6591	18660
Parameters	689	751	858	468	440	879
$R_1 > 2\sigma(I)$, wR_2	0.0377, 0.0958	0.0601, 0.1661	0.0976, 0.2431	0.0382, 0.0900	0.0435, 0.1090	0.0642, 0.1796
S (GooF) all data	1.026	1.022	0.958	1.023	1.044	0.988
Max/min Res. Dens. (e/Å^3)	0.880, -0.534	1.444, -0.692	2.436, -1.907	0.760, -0.792	1.590, -1.032	3.594, -2.684

I thought it would be interesting to synthesize the clusters in the absence of a charge-balancing dialkylammonium ion, which resulted in the compound **Zn(Zn) C_2**, which has Zn^{II} ions not included in the cluster as charge-balancing cations (Figure 44). Crystallographic data are included in Table 8. The clusters are topologically distinct from the previously described clusters although their overall composition is the same. Instead of S_6, these clusters have the virtual C_2 symmetry (Figure 45 and Figure 46). The reasons for the formation of this cluster instead of the other are unknown. Another key difference is that the clusters are protonated at two of the pendant carboxylate groups to achieve charge balance. In this structure, the clusters are oriented in two different directions as shown in Figure 47. The clusters are arranged with similarly oriented neighbors as chains along the *b*-axis.

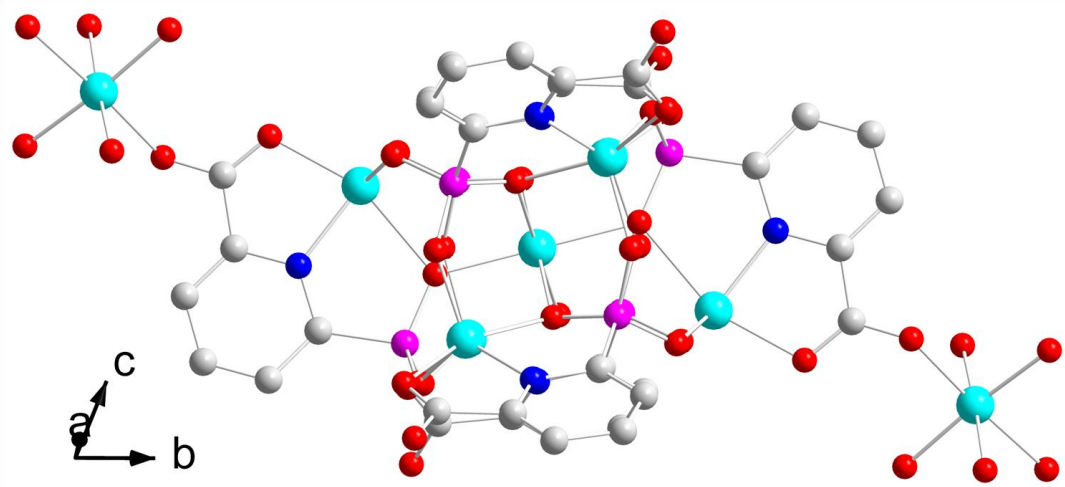

Figure 44 Zn(Zn) C_2 clusters are bridged by partially hydrated charge-balancing Zn^{2+} ions.

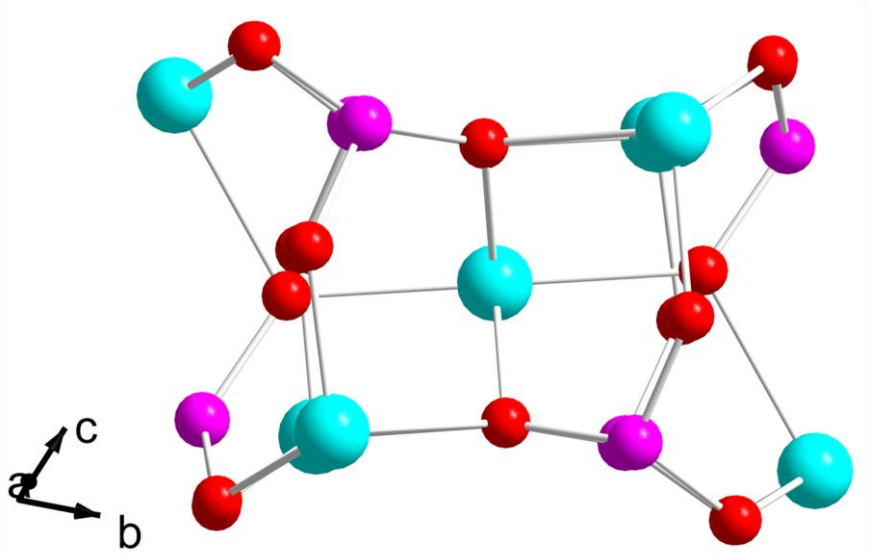

Figure 45 Zn(Zn) C_2 cluster viewed nearly along the C_2 axis. The pendant groups have been removed.

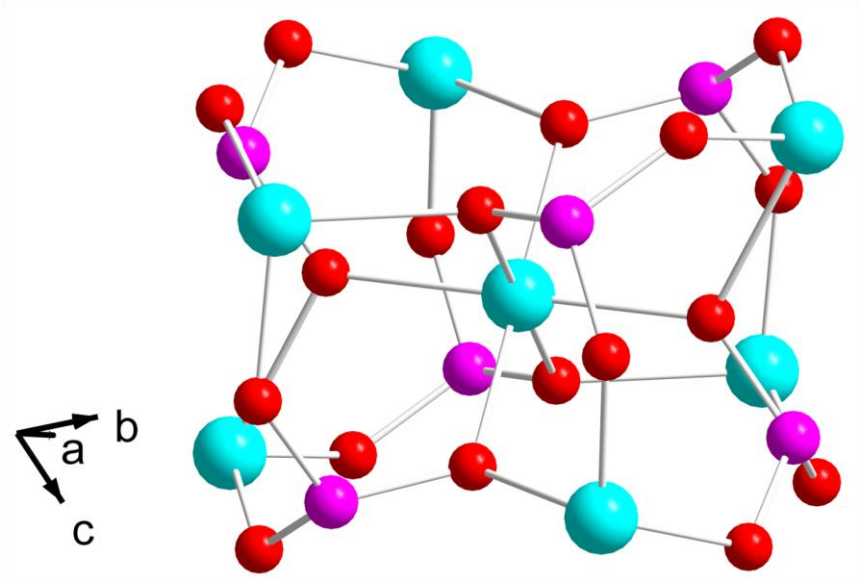

Figure 46 Zn(Zn) C_2 cluster with pendant groups removed.

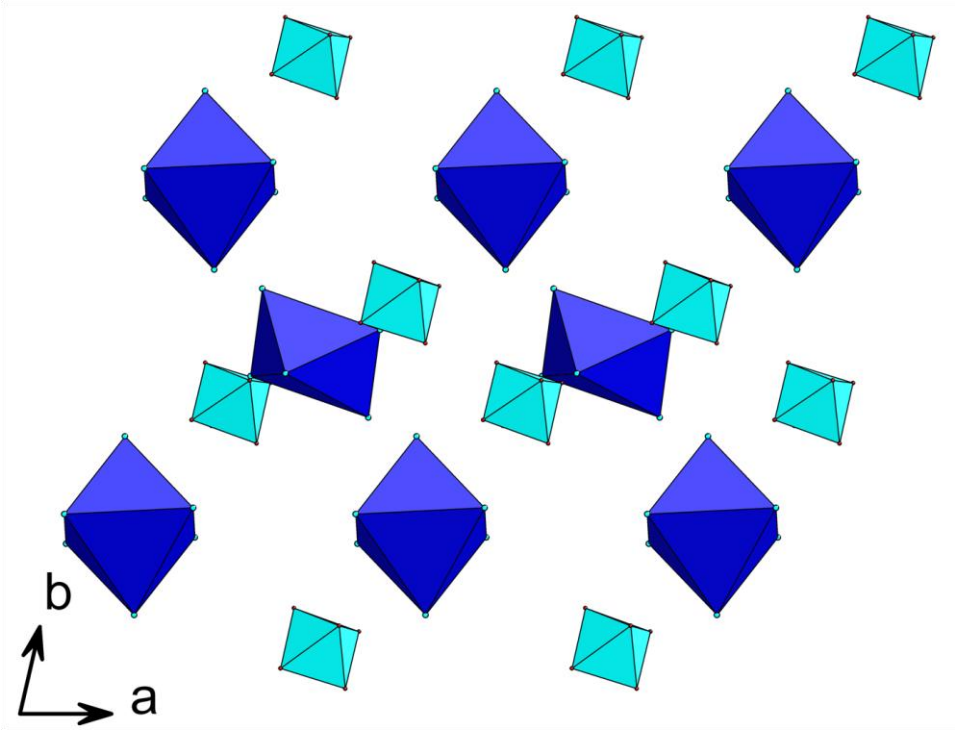

Figure 47 Zn(Zn) C_2 clusters viewed along the *c*-axis, showing the two different orientations of the cluster. The cluster-bridging $Zn(H_2O)_4$ units are shown as light blue polyhedra.

Reactions performed with only Co^{II} and Mn^{II} did not result in $[M_7L_6]^{4-}$ clusters. However, by including Co^{II} or Mn^{II} with Zn in the reactions, the clusters **Zn(Co) *C2*** and **Zn(Mn) *C2*** were obtained (crystallographic data are given in Table 8). In these compounds, both the central position in the cluster and the charge-balancing M^{II} cation are partially substituted by Co or Mn. The partial substitution occurs only at the octahedral sites, and it was determined by ICP-MS and crystallographic refinement that the central ion position is substituted completely and the bridging cation position is substituted at 80% for **Zn(Co) *C2*** and 64% for **Zn(Mn) *C2***. While the structures are similar, it is interesting that the compounds containing partial substitution of Co or Mn crystallize in the monoclinic space group C2/c as opposed to P-1 for the pure Zn compound. The reason for this is unclear, but the partial substitution of metals preferentially at the octahedral sites may provide for magnetically interesting compounds if this substitution is uniform throughout the compound, which cannot be accurately determined crystallographically or by ICP-MS. Electron microprobe indicated that the samples were inhomogeneous, with some regions richer in Mn or Co.

To further probe how reaction conditions affect the symmetry of the clusters and their packing in the solid state, I included triethylamine in the hydrothermal synthesis of the Zn clusters. The compound **Zn(Zn) S_6** was obtained, which does not include triethylammonium ions as would be expected from the inclusion of triethylamine in the reaction mixture. The clusters are charge-balanced by partially hydrated Zn^{II} cations which bridge the clusters through their ancillary carboxylate groups. In addition, two of these carboxylate oxygen atoms are protonated to achieve charge balance. The assignment of which oxygen atoms were protonated was made based on the C-O bond distances. Interestingly, these clusters are topologically identical to the ones obtained when they are synthesized in dimethylacetamide (Figure 37); they have S_6 symmetry. Because of the bridging tetra-aqua zinc ions, their arrangement in the crystal structure is evenly distributed over two different orientations (Figure 48 and Figure 49).

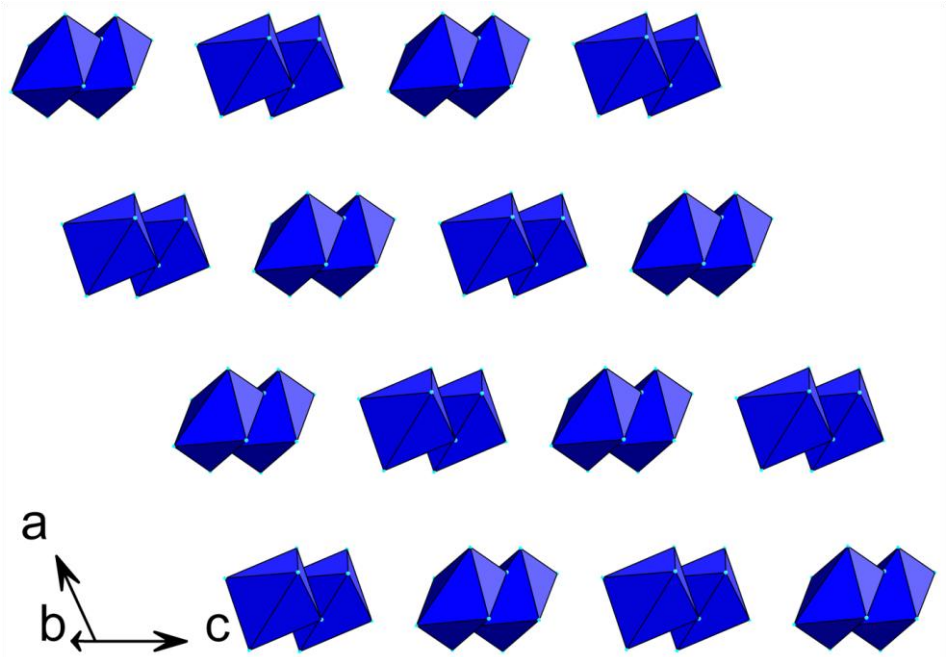

Figure 48 View of $Zn(ZnH_2)$ S_6 showing the two different orientations of the clusters. Polyhedra are Zn atoms of the cluster. All other atoms have been removed.

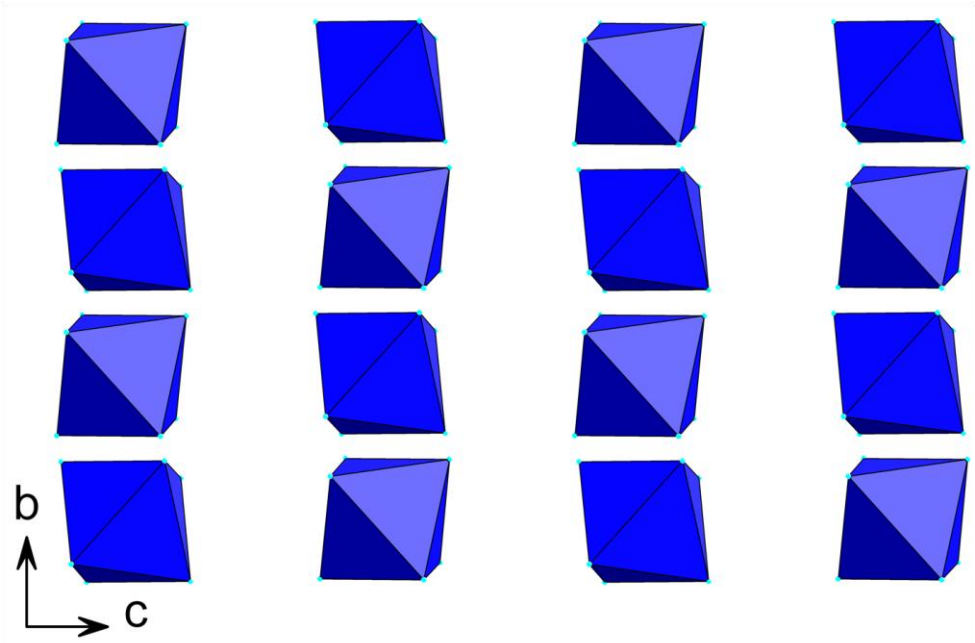

Figure 49 $Zn(ZnH_2)$ S_6 clusters viewed along the *a*-axis. Polyhedra are Zn atoms of the cluster. All other atoms have been removed.

Discussion

There were two main objectives in this research. The first, which was successful, was to control the packing of the clusters within the structure by using a different cation so that they were all oriented in the same direction. This could have profound effects on the magnetic properties of these materials, since a structure in which the clusters are all oriented in the same direction has greater anisotropy. Highly anisotropic compounds are more likely to exhibit better properties as SMM's None of the compounds presented in this chapter exhibited SMM behavior. The second goal was to incorporate Mn^{III} or Co^{III} into the clusters, which would have a more direct effect on the anisotropy since these ions themselves are highly anisotropic. If four of the normally divalent metals in the clusters were present as Mn^{III} or Co^{III}, then the clusters would be neutral, requiring no charge balancing anions and possibly being soluble in organic solvents. Unfortunately, no success was achieved on this front. Even by starting with various Mn^{III} or Co^{III} sources (including μ-3-oxo acetate clusters, Mn_{12}, and metal acetates) resulted in the same $[M_7L_6]^{4-}$ clusters. This is most likely due to the reducing conditions (alcohol solvents and the presence of amines) used during the syntheses. Even reactions of Mn^{III} salts with the ligand at room temperature resulted in the reduction of the Mn^{III} to Mn^{II}, and similar clusters were obtained. Further work towards the incorporation of these ions is warranted, since it is likely that cluster compounds incorporating Mn^{III} or Co^{III} would be highly interesting because of the single-ion anisotropy of the metal ions coupled with the orientation of the clusters.

Conclusion

In summary, two isostructural series of novel heptanuclear phosphonate-based M^{2+} clusters with the ligand 6-phosphonopyridine-2-carboxylic acid (M = Zn, Co, Mn, Mg) was prepared under solvothermal conditions. The charge-balancing cations were varied to control the orientation of the clusters in the solid state, and a single orientation was achieved for Mn and Co clusters with dibenzylammonium cations. The octahedral metal ions in the Zn clusters with C_2 symmetry could be selectively substituted with Co or Mn. This substitution was complete at the position of the charge-balancing cation, but only fractional at the central ion position in the core of the clusters. Attempts to incorporate the magnetically anisotropic ions Mn^{III} or Co^{III} into the cluster topology were unsuccessful due to the reducing conditions required during their syntheses. By increasing the magnetic anisotropy with the deliberate introduction of metal ions with strong single ion anisotropy, one may be able to engender SMM behavior in these molecules.

CHAPTER VI

STRUCTURAL VARIATIONS IN TIN PHOSPHONATES INFLUENCED BY BULKY PHOSPHONIC ACIDS

Introduction

The term 'hybrid material' is used to refer to a member of the broad class of materials that possess both inorganic and organic constituents. Included in this classification are crystalline 'metal-organic frameworks' (MOFs),[155-164] as well as semi-amorphous, pillared, layered compounds such as Zr 4,4'-biphenyldiylbisphosphonate and its Sn^{IV} analogue.[29, 37, 165] In both of these types of compounds, the inorganic units are covalently bound to the organic moieties of the structure, which can also contain other functional groups. Hybrid materials show great potential in a variety of applications including gas storage[166, 167], gas separations [168], catalysis [90, 165, 169], and ion exchange [170]. The viability of most of these applications depends on the nanoscale structural characteristics of the material. Compounds with potential in hydrogen storage or gas separation rely on the surface area or porosity as the main source of functionality. On the other hand, supported catalysts and ion exchangers require a chemically active moiety such as –COOH or $–NH_2$ to impart additional chemical properties. Chapter III discusses some materials of this type which have incorporated 2,2'-bipyridine functional groups. However, with some metals the inclusion of functional groups can also result in unanticipated structural variations in the materials obtained. Understanding how these

functional groups can influence the structure of metal phosphonates is important if we are to successfully incorporate them into functional phosphonates.

In this chapter I have taken a two-pronged approach to investigate structural variations in Sn^{II} phosphonates, using $Sn(O_3PC_6H_5)$ as a model. The first is by using a functional derivative of the ligand, in this particular case, the functional group is a pyridyl or nitrile group. The second approach was by systematically increasing the bulk of the phosphonate ligand, which required that new structures form to accommodate the larger ligands.

Divalent metal complexes and extended networks utilizing pyridylphosphonic acids have been the topic of a number of recent papers. Lin et al. synthesized and characterized several compounds of Zn, Co, Cu, and Cd with 3- and 4-pyridylphosphonic acids.[171] By using the hydrobromide of 3-pyridylphosphonic acid, they obtained a ladder structure in which the Zn atom is four-coordinate and the pyridyl nitrogen atom is protonated. The N atoms of the pyridyl ring in Co(4-pyridylphosphonate)$(H_2O)_3$ coordinate the Co atoms, which are also coordinated by three water molecules. The N-Co coordination links the chains of CoO_5N and PO_3C polyhedra, forming a 2-D grid network. Cu_2(4-pyridylphosphonate)$_2 \cdot 2H_2O$ forms a 3-D network that possesses open channels occupied by water molecules. An interesting Cd compound was obtained by using diethyl 4-pyridylphosphonate. By keeping the temperature low (70 °C), they avoided the complete hydrolysis of the ester and obtained the compound Cd(*O*-ethyl 4-pyridylphosphonate)$_2$, in which the ethyl groups occupy the voids within the 3-D network.

Anne Richards and her coworkers have prepared a variety of interesting compounds with Zn, Cd, Hg, and Ag, utilizing 2-pyridylphosphonic acid under mild conditions.[172] The compounds illustrate some of the many possible binding modes for phosphonates. $Cd(\mu\text{-}Cl)_2$(2-pyridylphosphonate) has chloride ions which bridge between Cd atoms. By reacting silver triflate with 2-pyridylphosphonic acid in ethanol they obtained a compound in which silver chains are coordinated by both phosphonate and triflate oxygen atoms.

Li-Min Zheng et al. have also used 2-pyridylphosphonic acid to prepare a trio of copper compounds.[173] In each of the structures, the pyridyl nitrogen atoms are bound to the Cu^{II} ions. $Cu(C_5H_4NPO_3H)_2$ forms chains, while $Cu_3(OH)_2(C_5H_4NPO_3)_2 \cdot 2H_2O$ and $Cu(C_5H_4NPO_3)$ form layered structures. They have also reported the syntheses of a Mn derivative of 2-pyridylphosphonic acid and a Zn derivative of 6-methyl-2-pyridylphosphonic acid by hydrothermal methods.[174] $Mn(C_5H_4NPO_3)_2(H_2O)$ and Zn(6-Me-2-$C_5H_4NPO_3$) are both layered compounds in which the pyridyl groups occupy the space between the layers.

Recently Konar et al. explored the compounds formed by Zn, Mn, and Cu with 4-pyridylphosphonic acid.[69] In the Zn compound, the tetrahedral Zn atoms are bound to two Cl atoms and two phosphonate O atoms. Two Zn atoms are bridged by O-P-O linkages to form eight-membered rings, but the two Cl atoms prevent the formation of ladders. The pyridyl nitrogen atoms are protonated and engage in hydrogen bonding with phosphonate oxygen atoms. The Mn compound forms layers which are linked by pendant pyridyl groups, while the Cu compound forms a 3-D network that contains

interpenetrating channels along all three crystallographic axes. The channels are filled with solvent water molecules that contribute to the stability of the compound.

Although pyridylphosphonic acids have yielded a panoply of coordination polymers with divalent metals, there have been no studies on the compounds they form with Sn^{II}. A variety of structural motifs have been observed for Sn^{II} phosphonates, including chains,[175] rings, ladders, and sheets.[66] Cheetham and coworkers[176] have developed a system of nomenclature for the inorganic units formed in these structure types, which describes them in terms of the number of Sn and P atoms in the Sn-O-P-O rings. The most prevalent rings are 4R's and 3R's, although 8R's and others have been observed. The Sn atoms in these structures are typically bound to 3 oxygen atoms resulting in a trigonal pyramidal geometric configuration. There have been examples published[177, 178] in which the Sn atoms are 4-coordinate; the additional bond is typically an oxygen atom at a distance of ~2.4 Å. Barrou and co-workers have synthesized a divalent Sn compound in which the Sn atom is coordinated by two oxygen atoms and two alkylamine nitrogen atoms.[179] However, prior to the work presented herein, there has not been a Sn^{II} phosphonate reported in which the Sn is additionally coordinated by a pyridyl nitrogen atom.

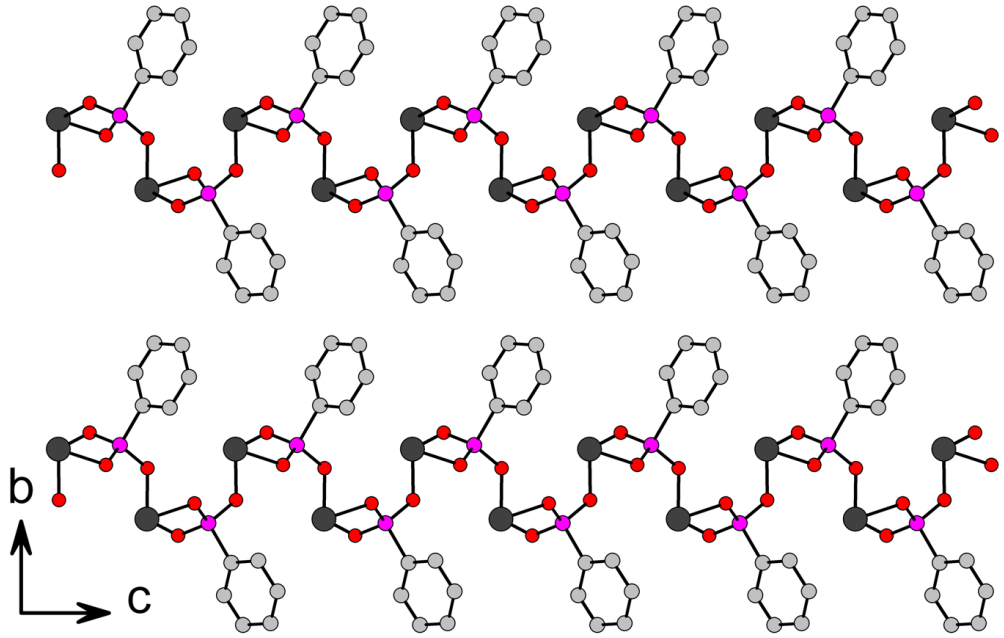

Figure 50 Layered structure in $Sn(O_3PC_6H_5)$. Note that the layers have the same directional quality.

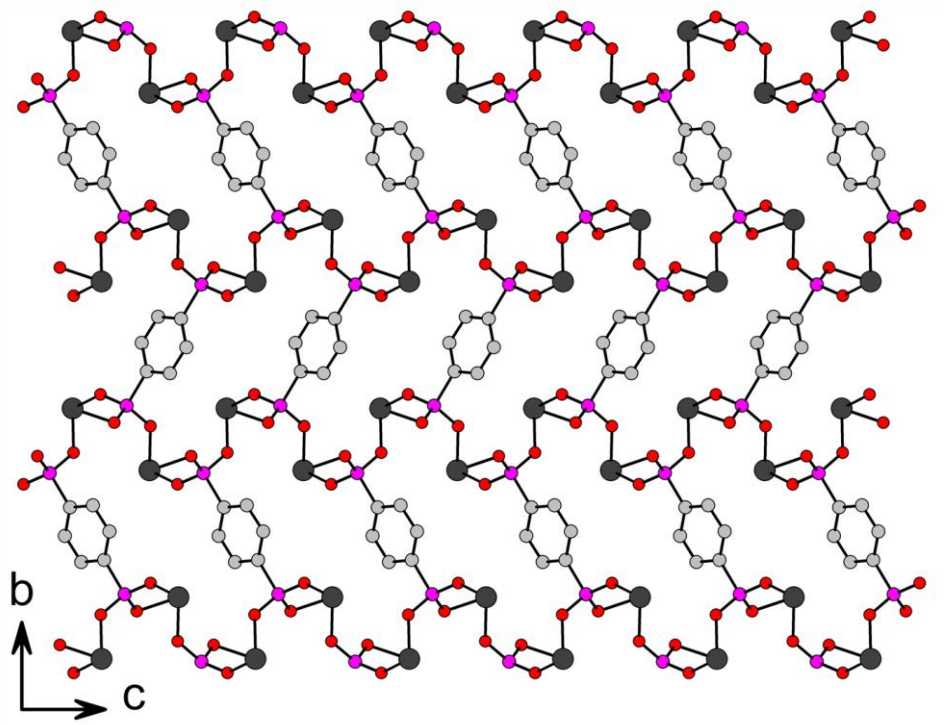

Figure 51 Crosslinked layers in $Sn_2(O_3PC_6H_4PO_3)$. The alternating arrangement of the layers is required for the bisphosphonate to bridge between them.

There have also been very few studies carried out which examined the effect of ligand bulk on the structures of Sn^{II} phosphonates. $Sn(O_3PC_6H_5)$ (Figure 50) was determined to be a layered compound,[180] and $Sn(O_3PC_6H_4PO_3)$ exhibits similar layers which are crosslinked (Figure 51).[66] To further explore this system I have attempted to systematically vary the bulk of the ligand and see what effects this has on the structure. An exhaustive investigation of even all phenylphosphonate derivatives was not practical, but the ligands chosen allow some general trends to be evaluated. Interestingly, even phosphonic acids with very large organic moieties form layered compounds, instead of chains which would allow more room for the bulky organic group. The comparison between $Sn(O_3PC_6H_4CH_3)$ and $Sn(O_3PC_6H_4CN)$ is interesting, because although the size of the organic groups are roughly the same, the tolyl derivative is layered, while the nitrile derivative has a chain structure. The only other chain compound obtained was the pyridyl derivative $Sn(O_3PC_5NH_4)$, in which interactions between the pyridyl nitrogen atoms and the Sn atoms may stabilize this structure. We have also structurally characterized a new type of structure that Sn^{II} can take with bisphosphonic acids. Instead of the double-layer structure observed for $Sn_2(O_3PC_6H_4PO_3)$, hereafter referred to as the α-phase, the new structure (β-type) consists of completely separated layers, capped by trigonal Sn^{II} atoms. This structure type may be exfoliable, which would provide a novel Lewis-basic functional surface. The α-type structure was also obtained with both biphenyl- and bipyridyl(bis)phosphonic acids, and it seems that the synthetic conditions determine which phase forms. The variations in the layered structures are discussed, as well as possible factors which may affect the type of structure obtained.

Experimental Details

The starting materials used in this work were prepared or acquired as stated in Chapter II. Thermogravimetric analyses (TGA) were performed with a TA Instruments Q500-0215 analyzer. The samples were heated from ambient temperature to 1000 °C at a rate of 10 °C per minute under air. Elemental analyses were performed by Robertson Microlit, Inc. of Madison, New Jersey, and Atlantic Microlabs Inc. of Norcross, Georgia.

X-Ray Crystallography

Single crystal x-ray diffraction data for $Sn(O_3PC_5NH_4)$ were collected at 110 K on a Bruker Smart CCD-1000 diffractometer with a Mo Kα (λ = 0.71073 Å) source operated at 40 kV and 40 mA. Single crystal X-ray diffraction data for $Sn_3O(O_3PC_5H_4N)_2$ and $Sn(O_3PC_{10}H_7)$ were collected at 110 K on a Bruker-AXS GADDS MWPC three-circle X-ray Diffractometer equipped with a rotating Cu Kα (λ = 1.54184 Å) anode operated at 40 kV and 40 mA. Single crystal X-ray diffraction data for all other compounds were collected at 110 K on a Bruker Smart APEX-II CCD diffractometer with a Mo Kα (λ = 0.71073 Å) source operated at 40 kV and 40 mA. Data reduction and cell refinement for all compounds were performed with SAINT[181]. SADABS[108] was used to obtain absorption corrected data. The structures were solved by direct methods using SHELXTL[109].

Syntheses of Sn^{II} Phosphonates

Tin(II) 3-pyridylphosphonate, $Sn(O_3PC_5NH_4)$

In a PTFE-lined autoclave with an internal volume of 15 ml, SnC_2O_4 (0.5 mmol, 0.103 g), 3-pyridylphosphonic acid (0.5 mmol, 0.08 g), and 10 ml H_2O were heated at 180 °C for five days under autogenous pressure. After cooling, colorless crystals were collected by filtration, washed with water and ethanol, and dried in an oven at 90 °C. Yield: 0.069 g, 62% based on Sn. Analyses calculated for $SnO_3PC_5NH_4$: C, 21.77%; H, 1.46%; N, 5.08%. Found: C, 21.78%; H, 1.06%; N, 5.18%.

Tri-tin(μ-3)oxo-bis(4-pyridylphosphonate), $Sn_3O(O_3PC_5NH_4)_2$

In a PTFE-lined autoclave with an internal volume of 15 ml, SnC_2O_4 (0.25 mmol, 0.052 g), 4-pyridylphosphonic acid (0.25 mmol, 0.04 g), 0.5 ml glacial acetic acid, and 10 ml H_2O were heated at 180 °C for four and a half days under autogenous pressure. After cooling, colorless crystals were collected by filtration, washed with water and ethanol, and dried in an oven at 90 °C. Yield: 0.036 g, 63% based on Sn. Analyses calculated for $Sn_3O_7P_2C_{10}N_2H_8$: C, 17.50%; H, 1.18%; N, 4.08%. Found: C, 17.47%; H, 1.03%; N, 3.94%.

Tin 6-methyl-2-pyridylphosphonatequadrahydrate, $Sn(O_3PC_5H_3NCH_3)\cdot 0.25H_2O$

In a PTFE-lined autoclave with an internal volume of 15 ml, SnC_2O_4 (0.40 mmol, 0.082g), 6-methyl-2-pyridylphosphonic acid (0.40 mmol, 0.070 g), and 10 ml H_2O were heated at 145 °C for 20 hours under autogenous pressure. After cooling, large

colorless crystals and a yellow powder were collected by filtration, washed with water and ethanol, and dried in an oven at 90 °C. The colorless crystals were separated from the yellow powder, which was not further analyzed. Yield: 0.087 g, 74% based on Sn. Analyses calculated for $Sn(O_3PC_5H_3NCH_3)$ •$0.25H_2O$: C, 24.49%; H, 2.23%; N, 4.76%. Found: C, 23.72%; H, 2.20%; N, 4.49%.

Tin(II) 4-cyanophenylphosphonate, $Sn(O_3PC_6H_4CN)$

In a PTFE-lined autoclave with an internal volume of 15 ml, SnC_2O_4 (0.30 mmol, 0.062g), diethyl 4-cyanophenylphosphonate (0.30 mmol, 0.072 g), and 10 ml H_2O were heated at 145 °C for 20 hours under autogenous pressure. After cooling, the white, crystalline solid was collected by filtration, washed with water and ethanol, and dried in an oven at 90 °C. Yield: 0.053 g. Reliable elemental analyses and TGA were not obtained because the sample consisted of multiple phases, as shown by powder x-ray diffraction and visual inspection of the material under a microscope. Manual separation of the phases was impractical, except for selecting a single crystal for x-ray diffraction.

Tin(II) p-tolylphosphonate $Sn(O_3PC_6H_4CH_3)$

SnC_2O_4 (0.3 mmol, 0.062 g) and *p*-tolylphosphonic acid (0.3 mmol, 0.052 g) were placed with 10 ml H_2O in a 15 ml PTFE-lined steel reaction vessel and heated for 4 days at 180 °C. The resulting off-white crystals were collected by filtration and washed with water and ethanol. Analyses calculated for $SnO_3PC_7H_7$: C, 29.11%; H, 2.44%. Found: C, 28.49%; H, 2.38%.

Tin(II) 3,5-dimethyl phenylphosphonate $Sn(O_3PC_6H_3(CH_3)_2)$

SnC_2O_4 (0.3 mmol, 0.062 g) and 3,5-dimethyl phenylphosphonic acid (0.3 mmol, 0.056g) were placed with 5 ml H_2O and 5 ml ethanol in a 15 ml PTFE-lined steel reaction vessel and heated for 24 hours at 140 C. The product was collected by filtration and washed with water and ethanol. Analyses calculated for $SnO_3PC_8H_9$: C, 31.73%; H, 3.00%. Found: C, 29.27%; H, 2.53%.

Tin(II) naphthylphosphonate $SnO_3PC_{10}H_7$

SnC_2O_4 (0.2 mmol, 0.041 g) and naphthylphosphonic acid (0.2 mmol, 0.042 g) were placed with 10 ml H_2O in a 15 ml PTFE-lined steel reaction vessel and heated for 4.5 days at 180 °C. The product was collected by filtration and washed with water and ethanol. Elemental analyses showed the product to be very high in carbon, indicating that unreacted ligand could not be washed out of the product.

Tin(II) p-tert-butyl phenylphosphonate $Sn(O_3PC_6H_4C(CH_3)_3)$

$SnCl_2 \cdot 2H_2O$ (1 mmol, 0.226 g) and p-t-butylphenylphosphonic acid (1 mmol, 0.214 g) were placed with 10 ml H_2O in a 15 ml PTFE-lined steel reaction vessel and heated for 3 days at 175 °C. The crystalline white solid was collected by filtration and washed with water and ethanol. Analyses calculated for $SnO_3PC_{10}H_{13}$: C: 36.30%, H: 3.96%. Found: C: 36.54%; H: 3.89%.

Tin(II) 2,2'-bipyridyl-5,5'-(bis)phosphonate

SnC_2O_4 (0.4 mmol, 0.082 g) bpyBPAE (0.2 mmol, 0.086 g) were placed with 9 ml H_2O and 0.4 ml HF (50% in H_2O) in a 15 ml PTFE-lined steel reaction vessel and heated for 3 days at 190 °C. The white solid was collected by filtration and washed with water and ethanol.

Tin(II) 4,4'-biphenyl(bis)phosphonate, β-$Sn_2(O_3PC_{12}H_8PO_3)$

SnC_2O_4 (0.4 mmol, 0.082 g) and 4,4'-biphenyl(bis)phosphonic acid (0.2 mmol, 0.085 g) were placed with 10 ml H_2O and 0.5 ml acetic acid in a 15 ml PTFE-lined steel reaction vessel and heated for 4.5 days at 180 °C. The off-white solid was collected by filtration and washed with water and ethanol. Analyses calculated for $Sn_2O_6P_2C_{12}H_8$: C: 26.32%, H: 1.47%. Found: C: 25.66%; H: 1.57%.

Crystal Structures

Crystallographic data are presented in Table 9 and Table 11.

Structure of $Sn(O_3PC_5NH_4)$

$Sn(O_3PC_5NH_4)$ crystallizes in space group $P2_1/c$, with $\beta = 93.616(2)°$. The Sn^{II} atoms are 3-coordinate with oxygen atoms from three separate phosphonate groups. Together, the Sn, O, and P atoms form ladders that extend along the *a*-axis. The ladders consist of fused 4-membered rings (4Rs) and are decorated on top and bottom by pendant pyridyl groups (Figure 52). The pyridyl groups are parallel to one another and canted at 35.5° from the direction of propagation of the ladder. When viewed along the *a*-axis, it can be seen that the ladders pack in a herringbone-type arrangement (Figure 53). This arrangement allows the nitrogen atom of each pyridyl group to interact with a Sn atom from a neighboring ladder at a distance of 2.606(3) Å. The nitrogen lone pair is directed toward the Sn atom, at a position that is in between two of the Sn-O bonds and the Sn^{II} lone pair. The Sn-O bond opposite the nitrogen atom is extended to 2.218(2) Å, while the other two Sn-O bonds are only 2.095(2) Å and 2.097(2) Å.

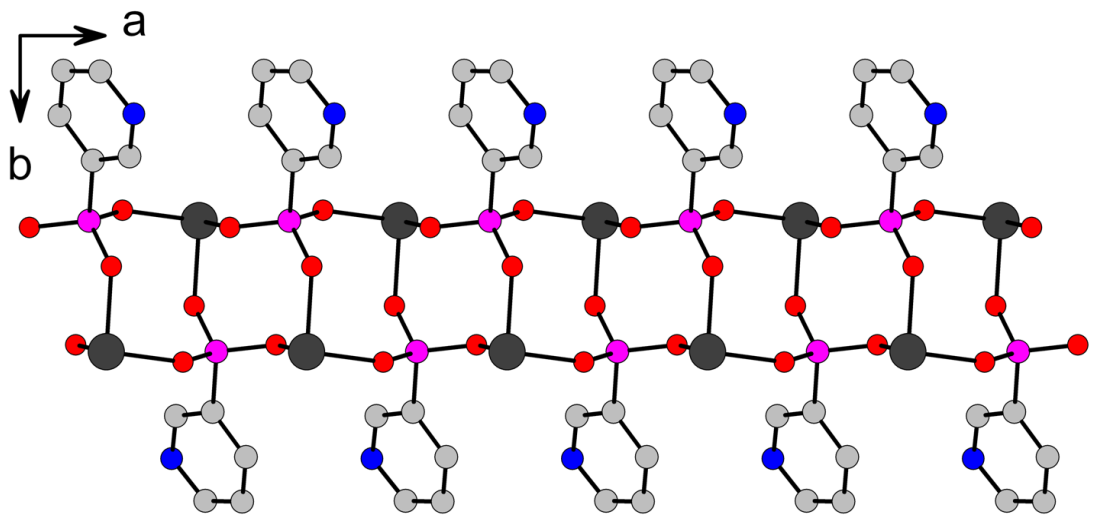

Figure 52 Chains in $Sn(O_3PC_5H_4N)$ are formed by fused 8-membered rings.

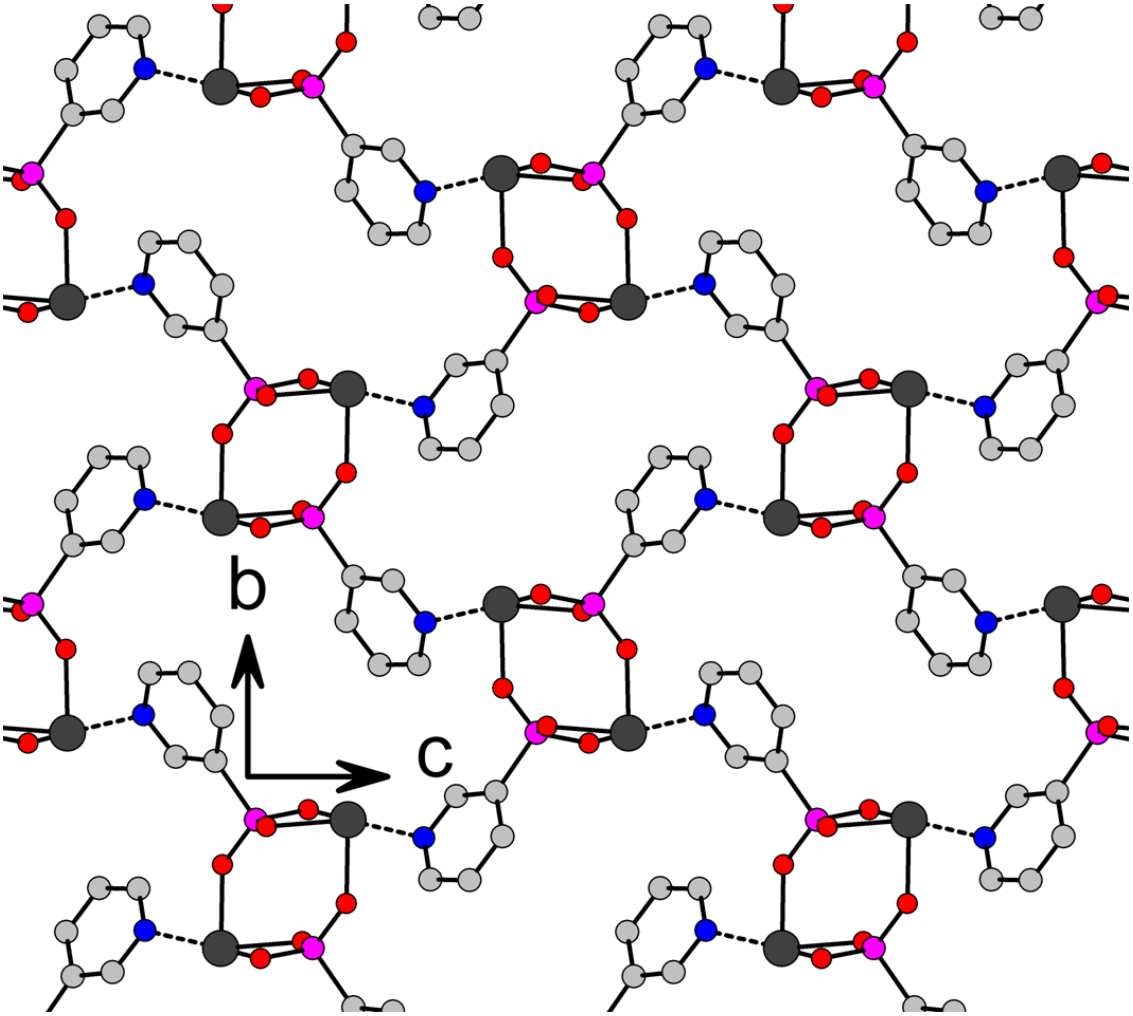

Figure 53 The chains of $Sn(O_3PC_5H_4N)$ pack in a herringbone-type arrangement to facilitate the Sn-N interaction at ~ 2.6 Å.

Table 9 Crystal data for the first five compounds presented in this chapter.

	$Sn(O_3PC_5NH_4)$	**$Sn_3O(O_3PC_5NH_4)_2$**	**$Sn(O_3PC_6NH_6)\bullet 0.25H_2O$**	**$Sn(O_3PC_7NH_4)$**	**$Sn(O_3PC_6H_4CH_3)$**
Formula mass	275.75	686.19	294.3	299.97	288.79
Crystal system	monoclinic	triclinic	orthorhombic	triclinic	monoclinic
Space group	$P2_1/c$	$P\bar{1}$	$Pna2_1$	$P\bar{1}$	$P2_1/c$
a(Å)	4.9595(8)	7.2406(14)	18.955(3)	5.0019(3)	4.7603(10)
b(Å)	10.7673(18)	9.9524(19)	9.7543(14)	8.4396(5)	29.169(6)
c(Å)	13.996(2)	12.604(3)	17.833(3)	10.3099(6)	6.7945(14)
α(deg.)	90.00	104.510(11)	90.00	90.352(3)	90.00
β(deg.)	93.616(2)	90.326(11)	90.00	94.894(3)	105.874(2)
γ(deg.)	90.00	110.897(11)	90.00	92.236(4)	90.00
Z	4	2	4	2	4
V ($Å^3$)	745.9(2)	816.9(3)	3297.2(9)	433.29(4)	907.5(3)
Density (g/cm^3)	2.456	2.790	2.367	2.298	2.114
Measured reflections	8139	6200	65018	6570	8086
Unique reflections	1635	2167	10881	1686	1531
Parameters	100	218	447	131	109
$R_1 > 2\sigma(I)$, wR_2	0.0224, 0.0381	0.0391, 0.1070	0.0300, 0.0625	0.0324, 0.0673	0.0773, 0.2308
S (GooF) all data	1.024	1.001	1.07	1.078	1.346
Max/min Res. Dens. ($e/Å^3$)	0.696, -0.550	1.105, -1.521	1.126, -1.071	0.837, -0.863	4.194, -3.483

Structure of $Sn_3O(O_3PC_5H_4N)_2$

$Sn_3O(O_3PC_5H_4N)_2$ crystallizes in space group P-1. There are two phosphonates for every three Sn atoms in the structure. Charge balance is achieved by the incorporation of an O^{2-} ion, which was not observed for any of the other compounds presented in this study. The Sn atoms are all coordinated by three oxygen atoms: the O^{2-} and two oxygen atoms from two different phosphonate groups. The O^{2-} is bonded to Sn1, Sn2, and Sn3 at distances of 2.080(6) Å, 2.083(6) Å, and 2.090(6) Å, respectively. Two of the Sn-O-Sn bond angles are similar (Sn2-O4-Sn3 = 121.87°, Sn1-O4-Sn3 = 121.09°), but one is relatively contracted (Sn1-O4-Sn2 = 112.52°). This creates a situation which requires the O^{2-} atom to be pyramidally distorted from trigonal planar geometry, and slightly pushed out of the plane formed by the three Sn atoms. The Sn, O, and P atoms form ladders that extend along the *c*-axis, which consist of fused 4R's and 3R's, with O4 and Sn3 being shared by two 3R's. The pyridyl groups extend above and below the ladders, at a slight angle to the next pyridyl group on the ladder (Figure 54). Nearest-neighbor pyridyl groups on the ladders are nearly perpendicular to one another, but next-nearest neighbor pyridyl groups are parallel. Each pyridyl group is oriented so that the N lone pair is directed toward a Sn atom from an adjacent ladder.

The Sn-N distances are 2.690(6) Å for Sn1-N1 and 2.618(6) Å for Sn2-N2. As in tin pyridylphosphonate the pyridyl nitrogen lone pairs are directed at the Sn atoms from a position in between two Sn-O bonds and the Sn^{II} lone pair. The Sn-O bonds opposite the Sn-N bonds are lengthened compared to the other Sn-O bonds: 2.225(6) Å for Sn1-O2 and 2.250(6) Å for Sn2-O6. The other Sn-O bond lengths are 2.080(6) Å, 2.118(6) Å, 2.083(6) Å, and 2.118(6) Å for Sn1-O4, Sn1-O1, Sn2-O4, and Sn2-O7, respectively.

The pyridyl groups from a single ladder interact with Sn atoms from four adjacent ladders. Consequently, the Sn atoms from a single ladder are coordinated by pyridyl nitrogen atoms from four different ladders. These interactions are most easily seen when the structure is viewed from along the *c*-axis (Figure 55). The pyridyl groups from different ladders are oriented parallel to and facing one another at a distance of ~3.5 Å, an indication that there is a reasonably strong π-π interaction (Figure 56).

Structure of $Sn(O_3PC_5H_3NCH_3) \cdot 0.25H_2O$

$Sn(O_3PC_5H_3NCH_3) \cdot 0.25H_2O$ crystallizes in orthorhombic space group $Pna2_1$. Each of the four distinct Sn atoms in the structure is four-coordinate: two are coordinated only by phosphonate oxygen atoms and two are coordinated by two phosphonate oxygen atoms and two pyridyl nitrogen atoms. The Sn-O and Sn-N bond distances are reported in Table 10. Each Sn atom has two short (~2.1 Å) Sn-O bonds and two longer bonds. For Sn1 and Sn3, the longer bonds are with nitrogen atoms, and for Sn2 and Sn4, the longer bonds are with two additional oxygen atoms. The Sn, O, and P atoms form 2-D sheets made of fused 4R's and 8R's (Figure 57). The pyridyl nitrogen atoms interact only with Sn atoms in the same layer, so there are no interlayer bonds holding the sheets together. The layers pack in an interlocking fashion so the methylpyridyl groups from one layer fit in between those of an adjacent layer (Figure 58). The single solvent water molecule is located between the layers. No other solvent water molecules could be located.

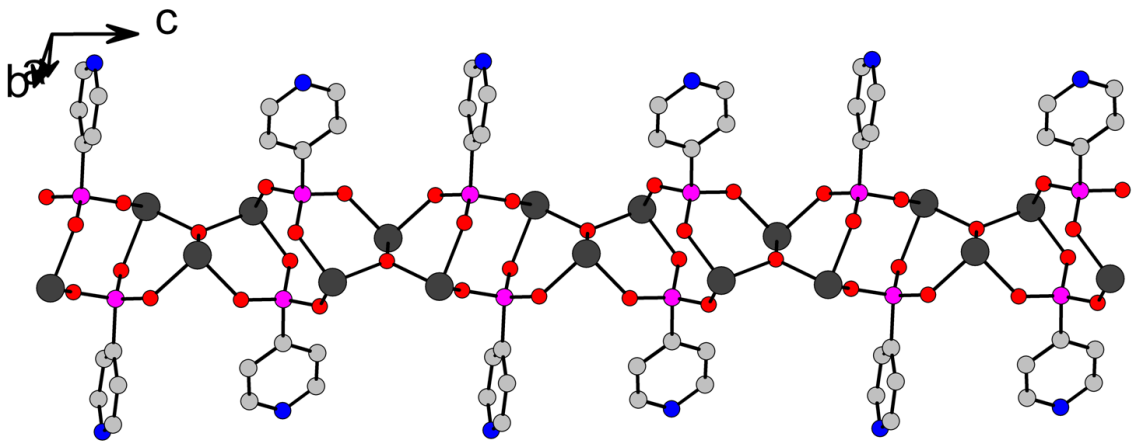

Figure 54 View of $Sn_3O(O_3PC_5H_4N)_2$ showing the ladders formed by fused rings. The 6-membered rings share the μ-3 oxygen and a tin atom.

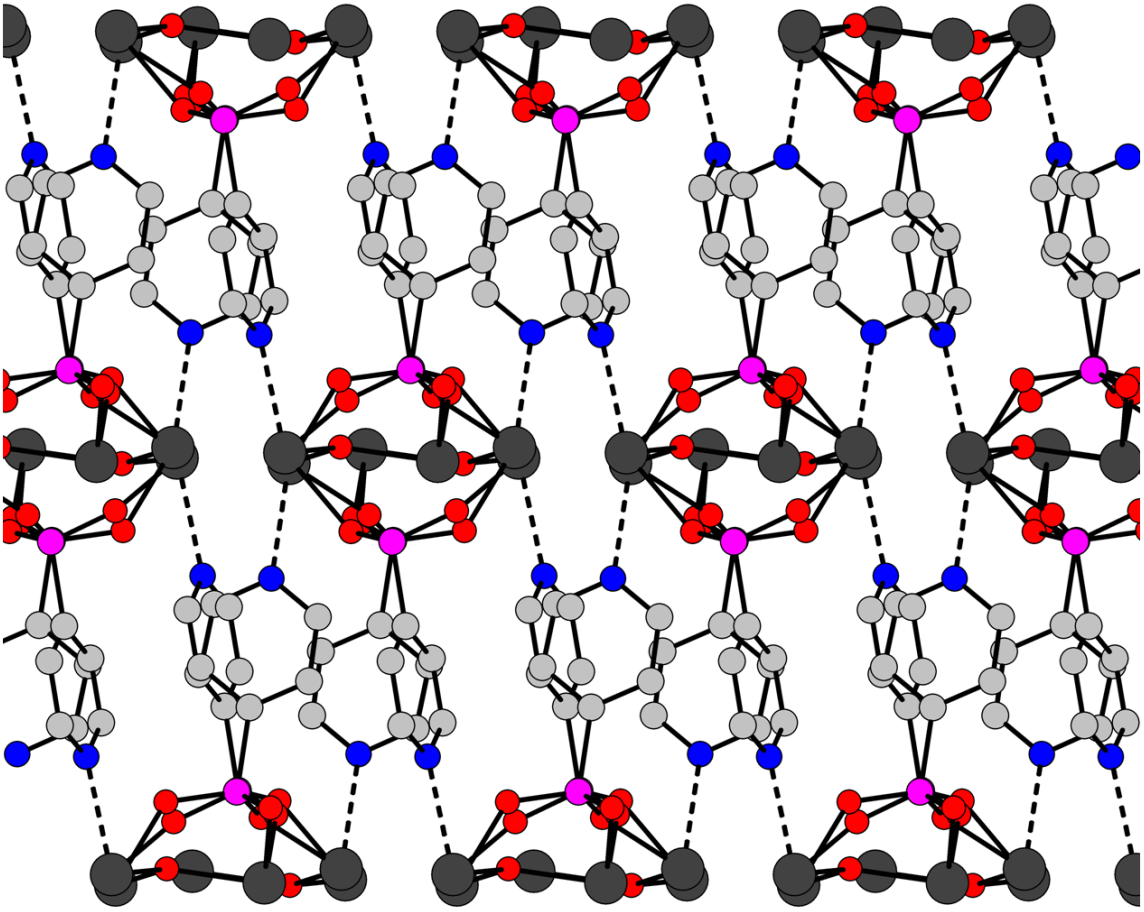

Figure 55 View along the *c*-axis of $Sn_3O(O_3PC_6H_4N)_2$. The Sn-N interactions are shown as dotted lines.

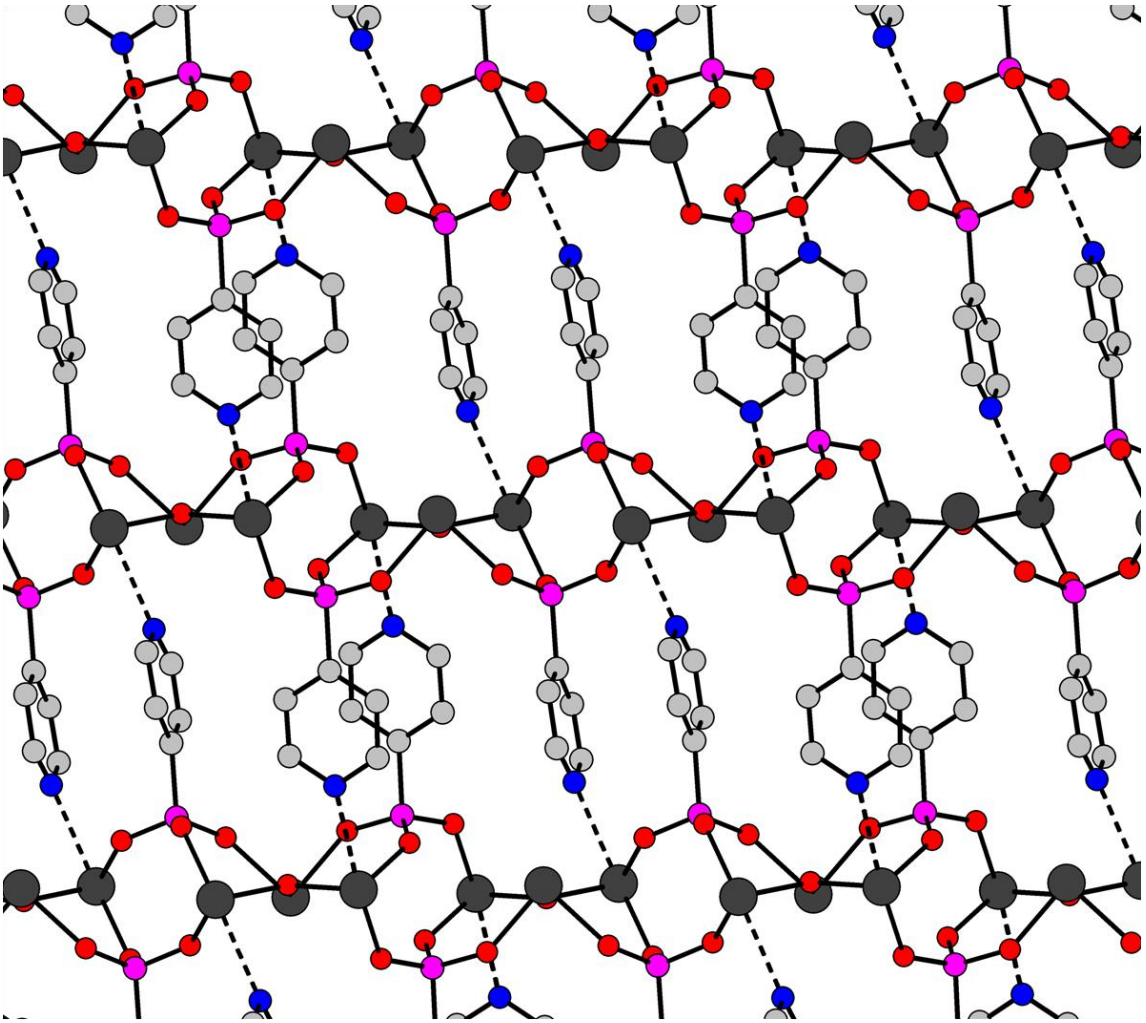

Figure 56 The Sn-N interactions between neighboring chains are shows as dotted lines. The π-π stacking arrangement of the rings is clearly visible.

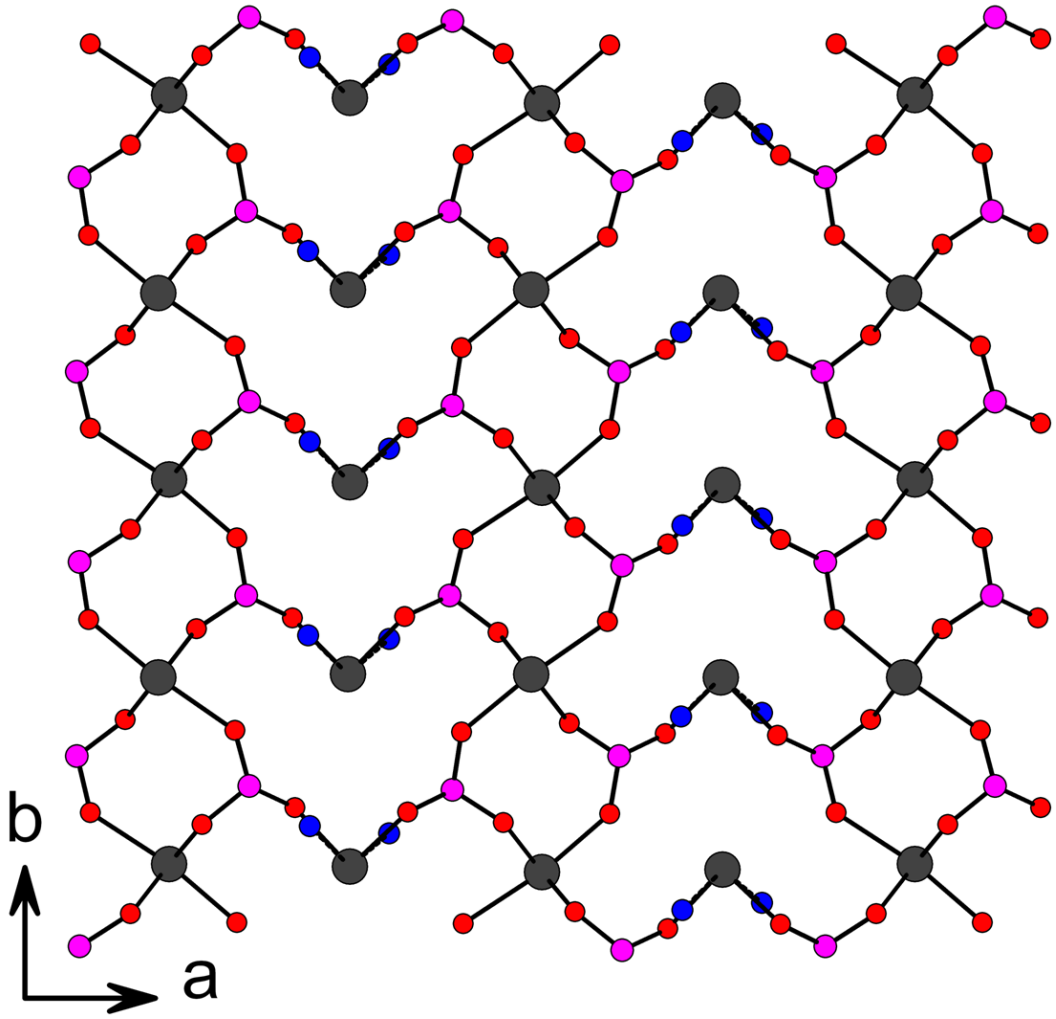

Figure 57 All tin atoms in $Sn(O_3PC_5H_3NCH_3)\cdot 0.25\ H_2O$ are 4-coordinate. The layer consists of fused 8-membered rings and 16-membered rings. The carbon and hydrogen atoms have been removed for clarity.

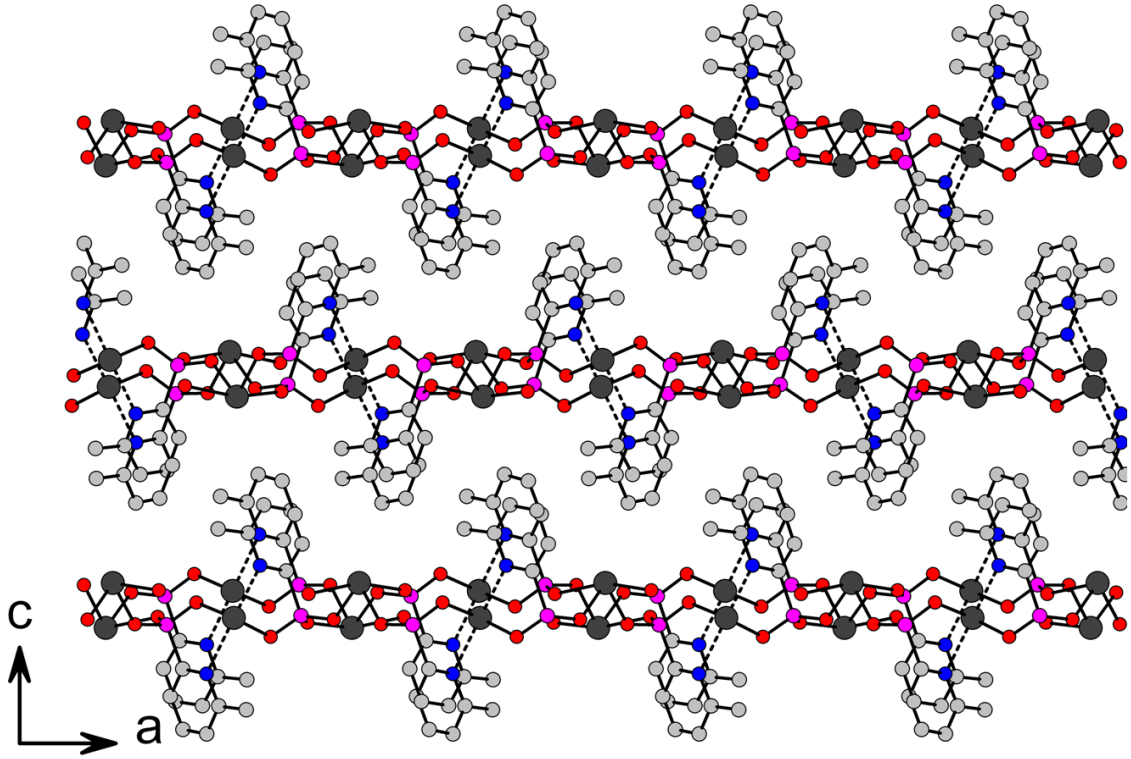

Figure 58 Interlocking layers in. $Sn(O_3PC_5H_3NCH_3)\cdot 0.25H_2O$. Solvent water has been removed for clarity.

Table 10 Selected bond distances for $Sn(O_3PC_5H_3NCH_3)\cdot 0.25H_2O$.

Atom pair	Distance (Å)	Atom pair	Distance (Å)
Sn1–O3	2.124(2)	Sn3–O12	2.138(2)
Sn1–O4	2.134(2)	Sn3–O8	2.141(2)
Sn1–N1	2.454(3)	Sn3–N4	2.469(3)
Sn1–N2	2.620(3)	Sn3–N3	2.555(3)
Sn2–O2	2.101(2)	Sn4–O7	2.096(2)
Sn2–O5	2.105(2)	Sn4–O11	2.108(2)
Sn2–O10	2.279(2)	Sn4–O1	2.317(2)
Sn2–O9	2.423(2)	Sn4–O6	2.397(2)

Structure of $Sn(O_3PC_6H_4CN)$

This compound crystallizes in space group P-1. The phenyl ring is rotationally disordered around the C1-C4 axis, with each component contributing equally to the total occupancy. Each Sn atom is 3-coordinate with oxygen atoms from three different phosphonate groups, and the Sn, O, and P atoms form ladders that extend along the *a*-axis, as in $Sn(O_3PC_5H_4N)$. The ladders are essentially identical to those of $Sn(O_3PC_5H_4N)$, with the major difference being the pendant organic moieties that decorate the top and bottom of the ladders (Figure 59). In $Sn(O_3PC_5H_3NCH_3)$ •$0.25H_2O$, all three Sn-O bonds are similar; 2.103(3) Å, 2.118(3) Å, and 2.132(4) Å for Sn1–O2, Sn1–O3, and Sn1–O1, respectively. The fact that they are all relatively short indicates that there is not a Sn-N interaction that lengthens one Sn-O bond, and indeed, when the packing arrangement of the ladders is viewed from along the *a*-axis, it can be seen that the ladders pack in a manner different from that observed in $Sn(O_3PC_5H_4N)$. The nitrile lone pairs do not point directly at the Sn atoms, and the ladders pack in a side-by-side manner that does not facilitate a Sn-N interaction (Figure 60). The shortest Sn-N distance is > 3.2 Å, which supports the hypothesis that there is no Sn-N interaction as observed in $Sn(O_3PC_5H_4N)$.

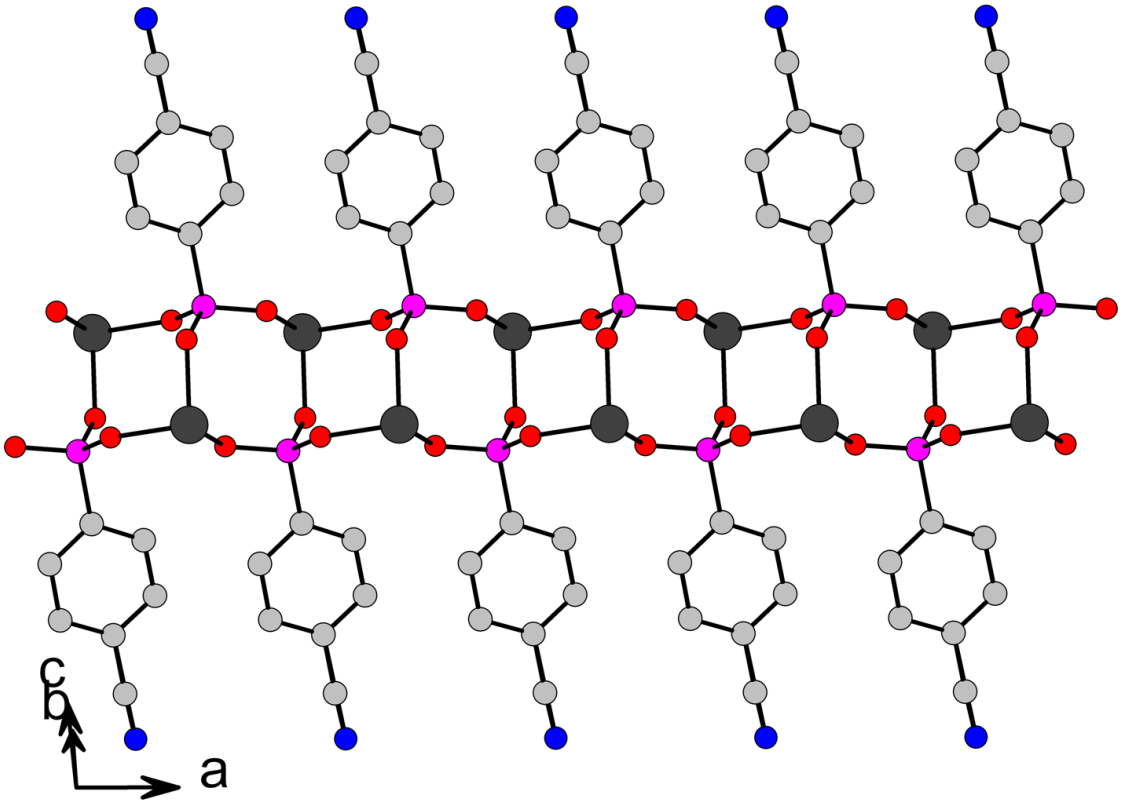

Figure 59 Chains in $Sn(O_3PC_6H_4CN)$ are essentially identical to those in $Sn(O_3PC_5H_4N)$, except for the identity of the pendant organic group.

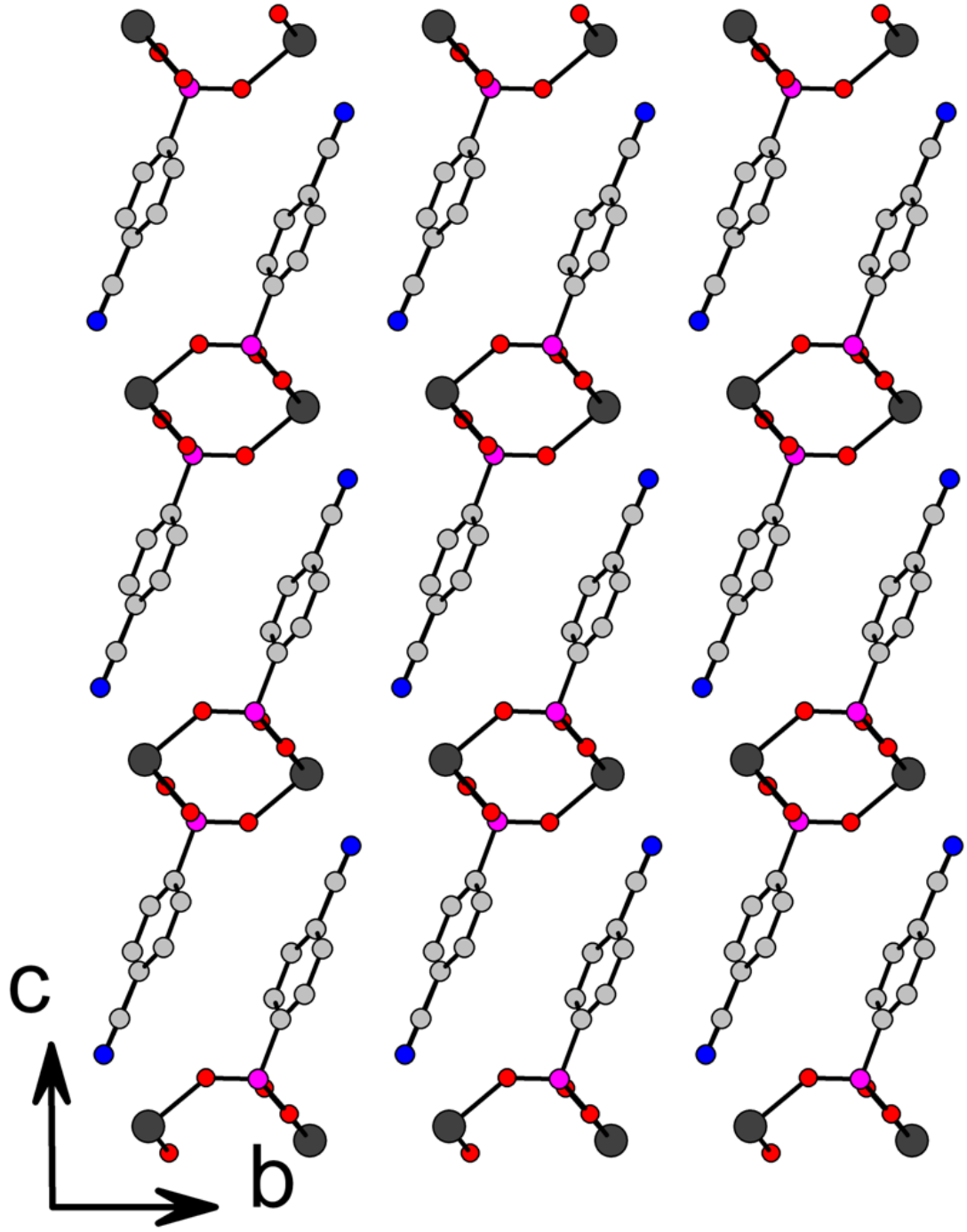

Figure 60 The packing arrangement of the chains in $Sn(O_3PC_6H_4CN)$. Note the lack of a direct Sn-N interaction. Only one position of the rotationally disordered phenyl ring is shown.

Structure of $Sn(O_3PC_6H_4CH_3)$

The structure of $Sn(O_3PC_6H_4CH_3)$ consists of alternating inorganic layers decorated by pendant organic groups (Figure 61). The tolyl groups are offset from one another, which allows the them to interpenetrate, but the interlayer distance is still larger than that of $Sn(O_3PC_6H_5)$. The Sn atoms are 3-coordinate, and the inorganic portion of the layer is made from edge-sharing 6R's (Figure 62). Upon inspection it becomes apparent that the layers have a directional quality, in that the Sn atoms in adjacent layers are oriented at 180° from each other. From this perspective, it is not difficult to envision how a bisphosphonic acid could crosslink the layers. This directionality is also seen in $Sn(O_3PC_6H_5)$, but in that structure the layers are all oriented in the same direction, which would not allow crosslinking of the layers (Figure 50). The methyl group may pack better in the alternating layer structure, but the ultimate reason as to why the layers alternate is unknown.

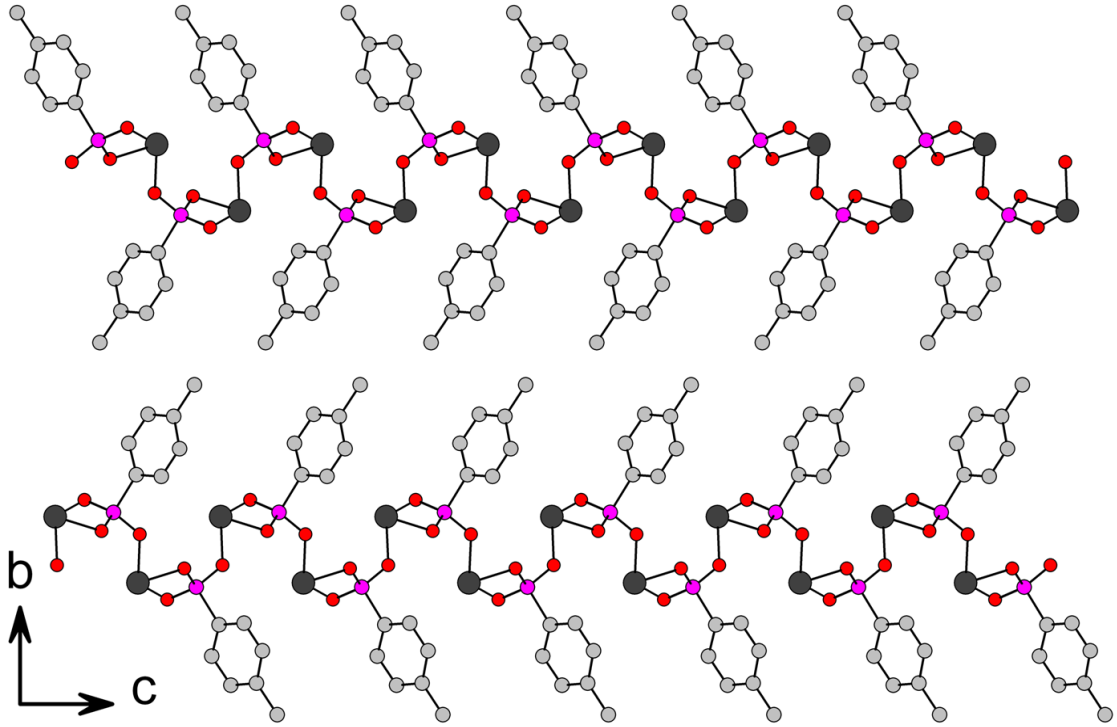

Figure 61 Double layered structure of $Sn(O_3PC_6H_4CH_3)$.

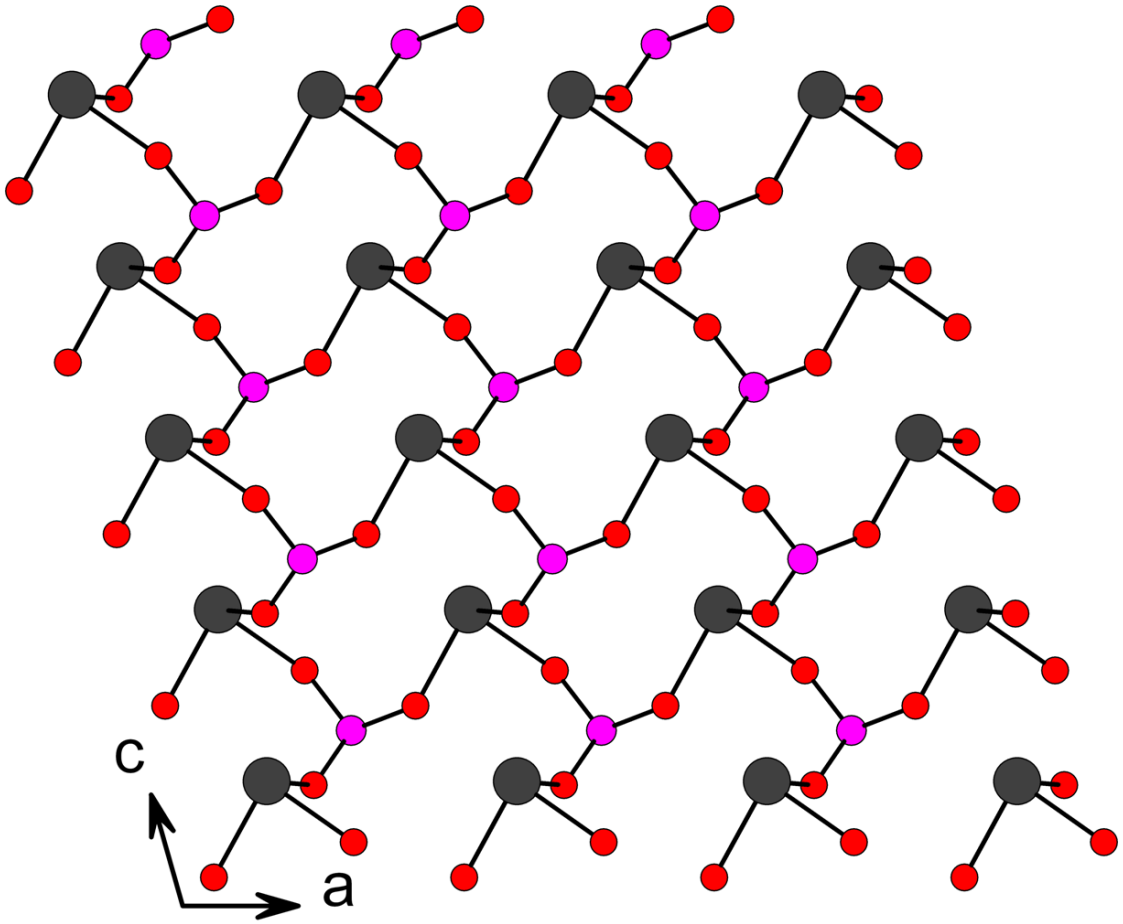

Figure 62 View of the inorganic portion of the double layer structure of $Sn(O_3PC_6H_4CH_3)$. The carbon and hydrogen atoms have been removed.

Structure of $Sn(O_3PC_6H_3(CH_3)_2)$

Increasing the bulk of the phenylphosphonate by adding two methyl groups makes it so that the organic moieties can no longer pack on the layer surface in the manner observed in $Sn(O_3PC_6H_5)$ and $Sn(O_3PC_6H_4CH_3)$. $Sn(O_3PC_6H_3(CH_3)_2)$ is still a layered compound, but the ligand must be oriented so that the methyl groups do not interfere with the packing, and this is shown in Figure 63. From this angle it appears that there may be π-π interactions between the aromatic rings, but viewed from another angle it is apparent that this is not the case (Figure 64). While the methyl groups on the phenyl rings are large enough to prevent the simple layer structure obtained for $Sn(O_3PC_6H_5)$ from forming, they do not necessitate the formation of chains to accommodate the additional bulk. The structure of the inorganic layer is considerably different, consisting of corrugated layers which facilitate the staggered packing of the 3,5-dimethylphenyl groups. This layer is made up of edge sharing 4R's and 8R's and the Sn atoms are all 3-coordinate (Figure 65).

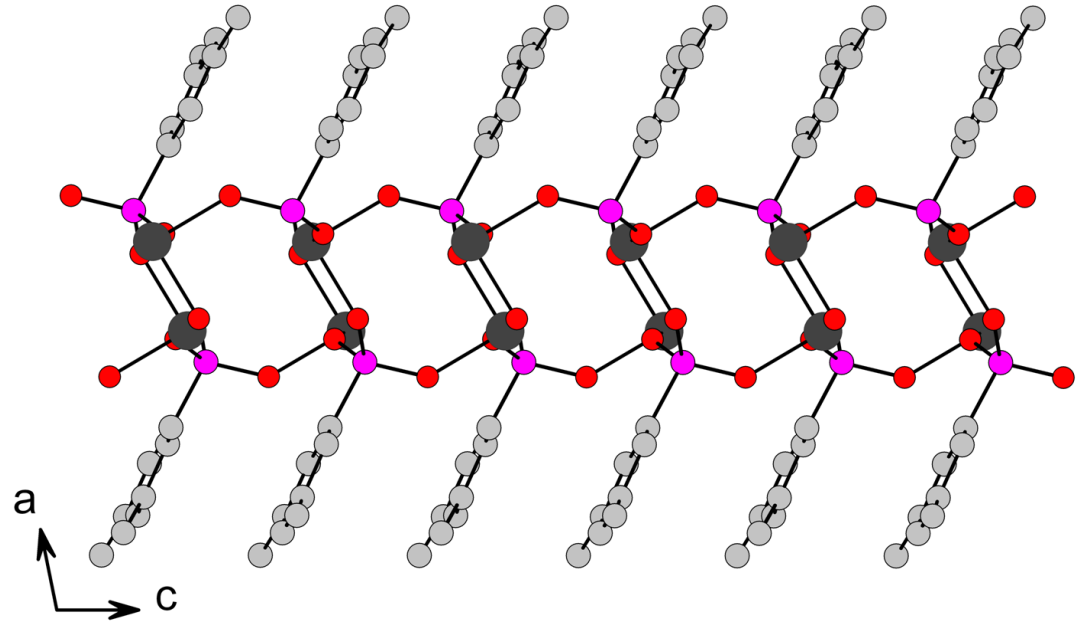

Figure 63 View of $Sn(O_3PC_6H_3(CH_3)_2)$ along the *b*-axis. Note the parallel arrangement of the aromatic rings.

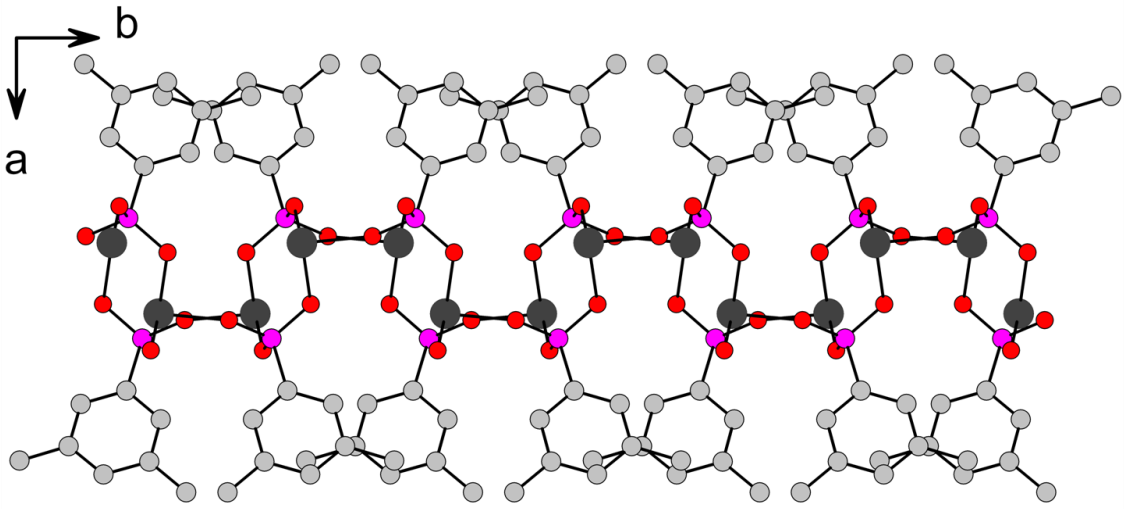

Figure 64 The staggered layers of $Sn(O_3PC_6H_3(CH_3)_2)$ are apparent when the structure is viewed along the *c*-axis.

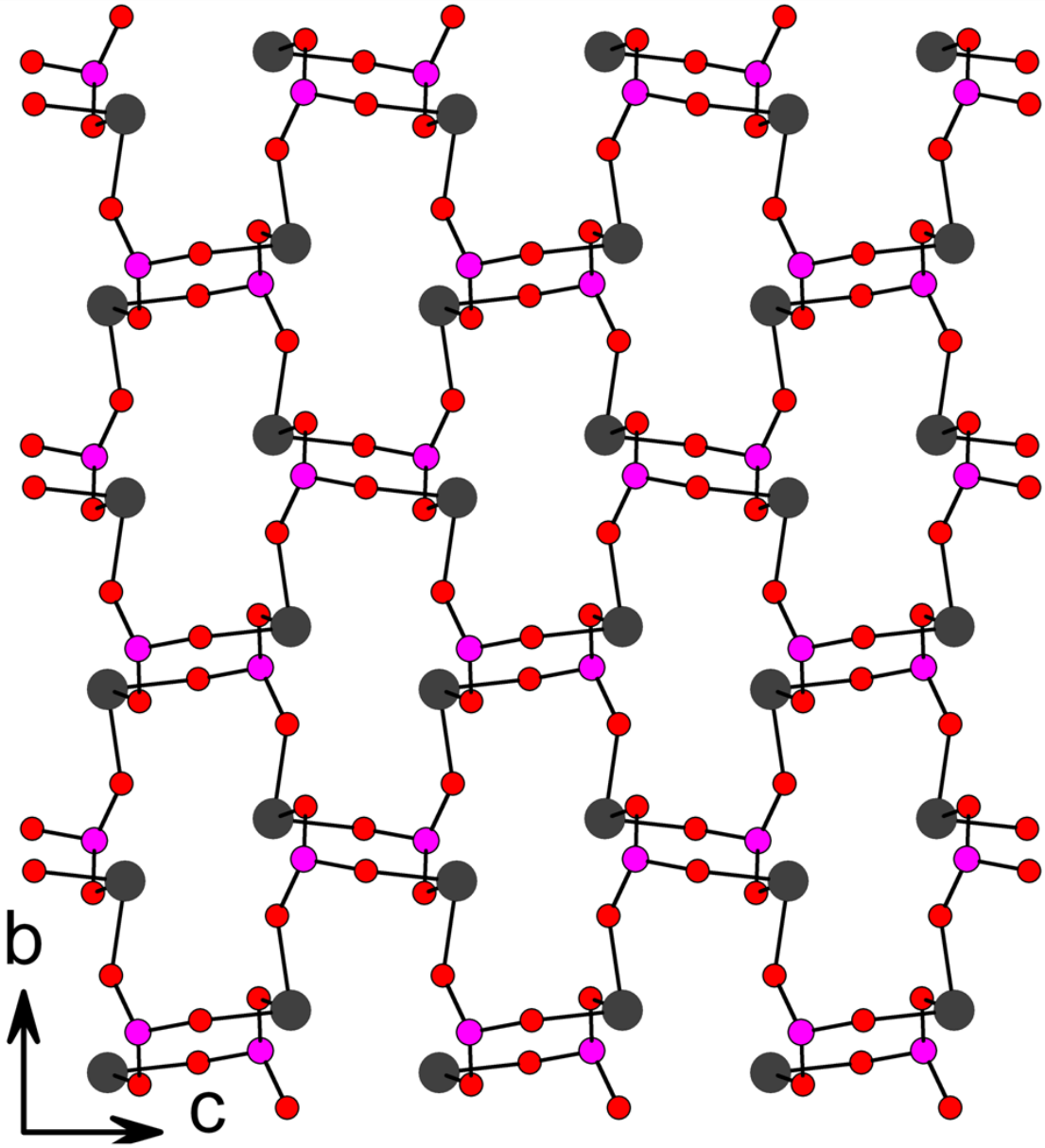

Figure 65 The inorganic portion of $Sn(O_3PC_6H_3(CH_3)_2)$. The layers consist of fused 8- and 16-membered rings.

Table 11 Crystal data for the last five compounds presented in this chapter.

	$Sn(O_3PC_6H_3(CH_3)_2)$	$Sn(O_3PC_{10}H_7)$	$Sn(O_3PC_6H_4C(CH_3)_3)$	$Sn_2(O_3PC_{10}N_2H_6PO_3)$	$Sn_2(O_3PC_{12}H_8PO_3)$
Formula mass	302.81	324.84	330.89	549.53	547.50
Crystal system	monoclinic	monoclinic	triclinic	monoclinic	triclinic
Space group	$P2_1/c$	$P2_1/c$	$P\bar{1}$	$P2_1/c$	$P\bar{1}$
a (Å)	15.385(8)	16.836(3)	7.7198(15)	4.7570(10)	4.889(2)
b (Å)	8.4194(15)	8.3010(18)	9.2648(19)	21.983(4)	4.948(3)
c (Å)	7.434(2)	15.828(3)	16.621(3)	6.8470(14)	16.069(8)
α (deg.)	90.00	90.00	92.06(3)	90.00	81.244(6)
β (deg.)	101.44(2)	113.421(12)	94.41(3)	105.36(3)	85.491(7)
γ (deg.)	90.00	90.00	91.23(3)	90.00	63.262(5)
Z	4	8	4	2	1
V ($Å^3$)	943.9(6)	2029.9(7)	1184.1(4)	690.4(2)	343.1(3)
Density (g/cm^3)	2.131	2.132	1.856	2.643	2.650
Measured reflections	3380	10696	3962	4595	2953
Unique reflections	2177	3156	1900	996	2090
Parameters	129	121	271	100	199
$R_1 > 2\sigma(I)$, wR_2	0.0471, 0.1208	0.1289, 0.3356	0.0958, 0.2337	0.0216, 0.0620	0.0609, 0.1484
S (GooF) all data	0.998	1.379	0.965	1.205	1.051
Max/min Res. Dens. ($e/Å^3$)	1.372, -1.096	3.830, -4.195	2.089, -1.583	1.246, -0.858	2.286, -1.760

Structure of $Sn(O_3PC_{10}H_7)$

This compound exhibits marked differences from the previously described structures, most notably the presence of 4-coordinate Sn atoms in the absence of N-donors. $Sn(O_3PC_{10}H_7)$ has a layered structure, and the naphthyl groups are oriented to facilitate π-π interactions between the aromatic rings (Figure 66). The inorganic layer structure is quite complicated, consisting of edge-sharing 3R's, 4R's, and 6R's (Figure 67). There are also 4-membered rings consisting of two Sn atoms bridged by two phosphonate oxygen atoms. The 4-coordinate Sn atom is in a bonding environment similar to those seen for 4-coordinate Sn in other systems, having two short bonds (2.132(16) Å and 2.176(16) Å) and two long bonds (2.302(17) Å and 2.504(15) Å).

Structure of $Sn(O_3PC_6H_4C(CH_3)_3)$

$Sn(O_3PC_6H_4C(CH_3)_3)$ acid forms a layered structure, similar to the other compounds presented herein in that the pendant organic groups decorate the surface of the inorganic sheets (Figure 68). The *p-tert*-butylphenyl groups cannot pack in the same arrangement as the phenyl or tolyl groups because of steric interactions. The inorganic portion of the layer consists of an edge-sharing network of 4R's and 8R's, with additional 4-membered rings made of two Sn atoms and two phosphonate oxygen atoms (Figure 69). Half of the Sn atoms are 4-coordinate, and these are in bonding environments of two shorter (2.083(14) Å and 2.061(16) Å) and two longer bonds (2.155(13) Å and 2.159(15) Å). The longer bonds are considerably shorter than those observed in other 4-coordinate Sn^{II} phosphonates.

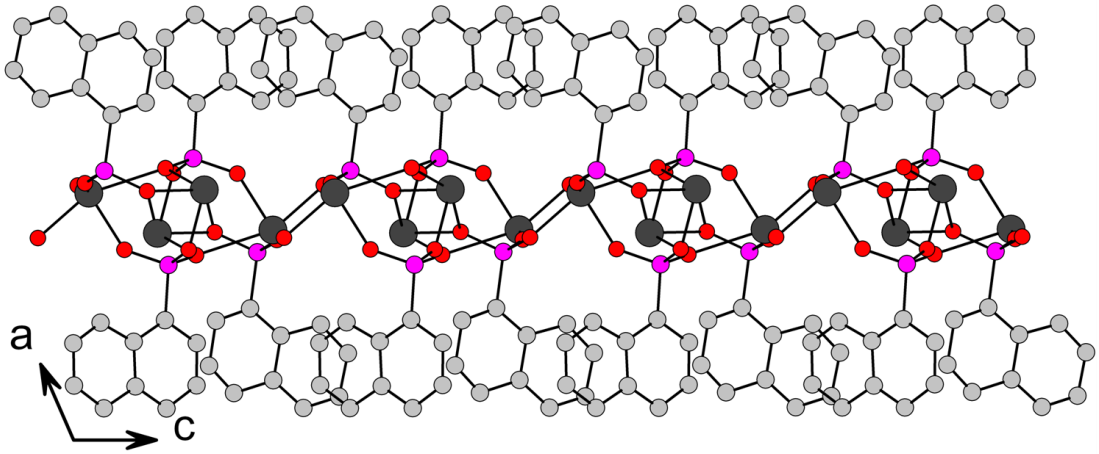

Figure 66 The layers in $Sn(O_3PC_{10}H_7)$ adopt a new connectivity to accommodate the bulk of the aromatic ring system.

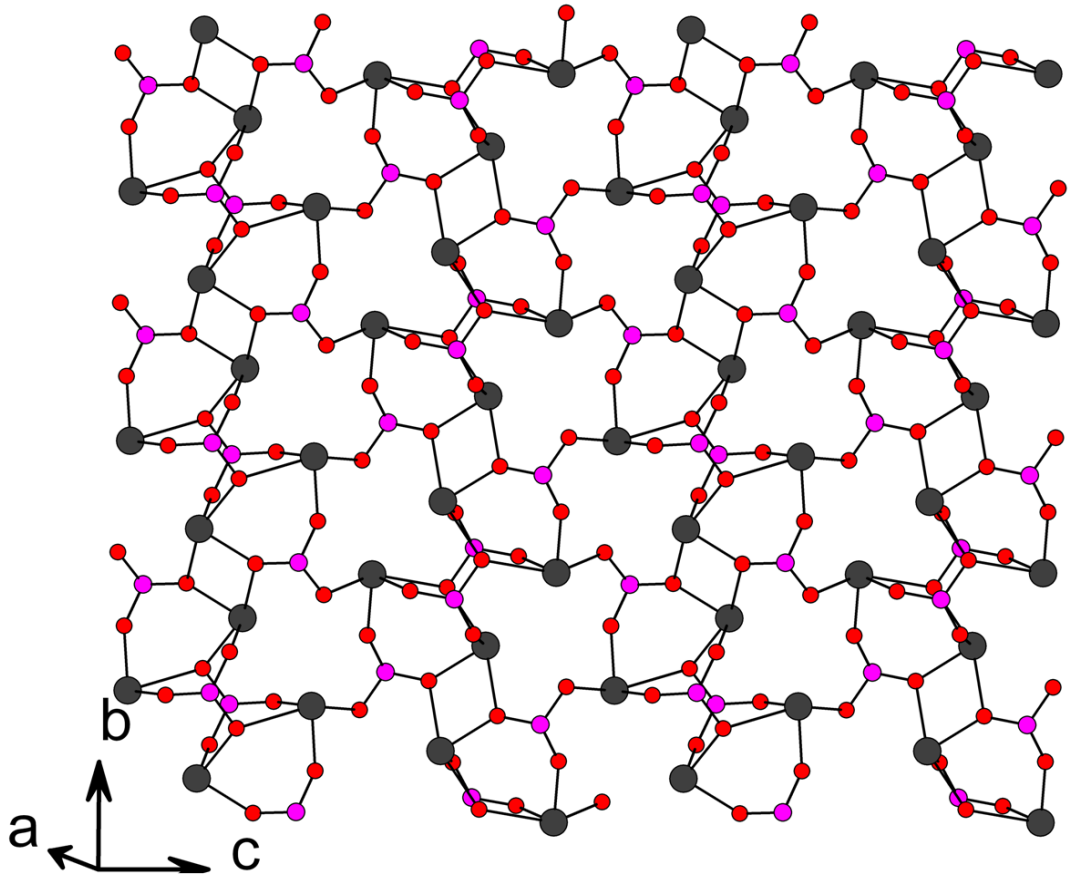

Figure 67 The inorganic portion of $Sn(O_3PC_{10}H_7)$. All of the Sn^{II} atoms are four-coordinate.

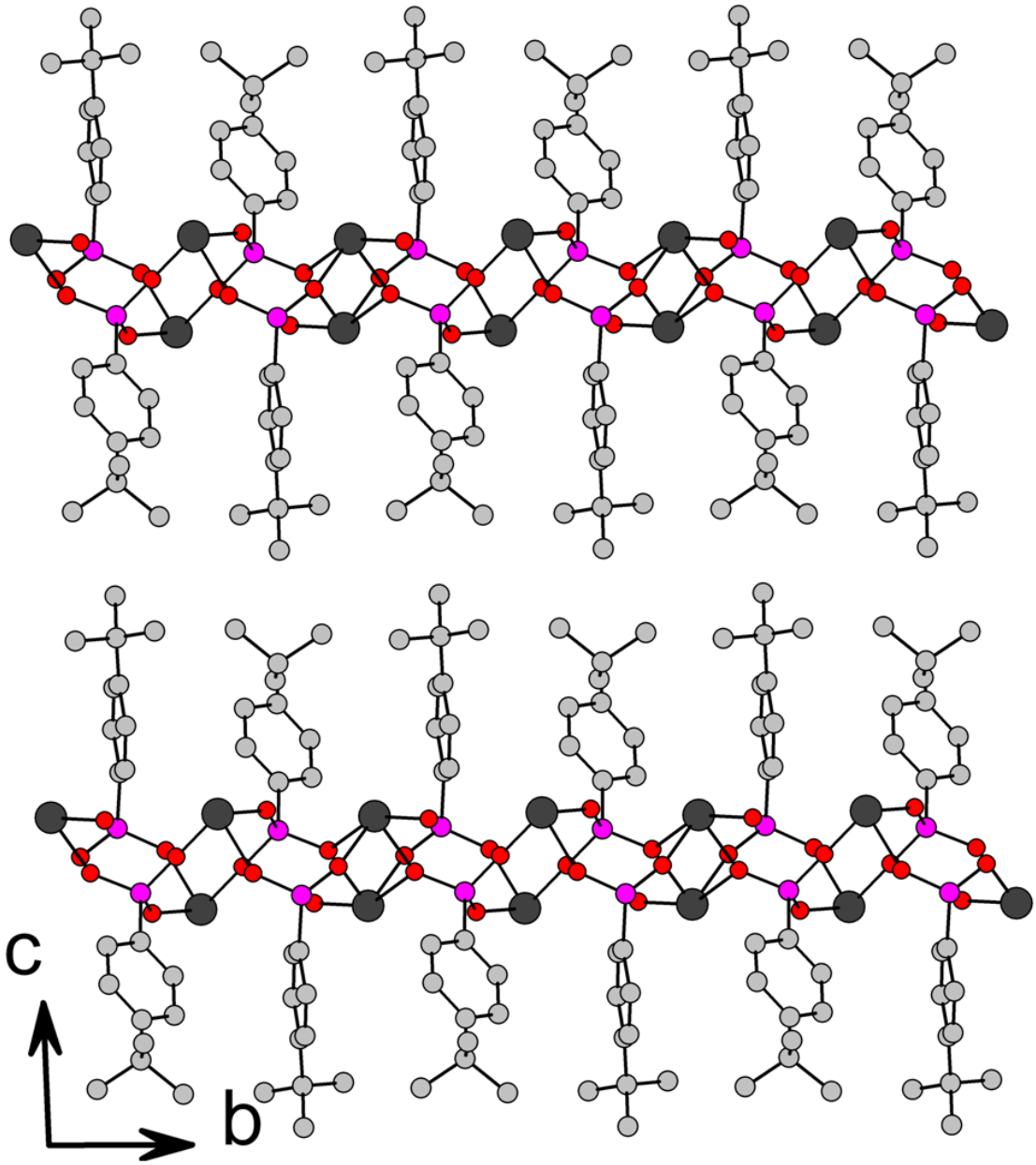

Figure 68 Layered structure of $Sn(O_3PC_6H_4C(CH_3)_3)$. The phenyl rings cannot pack side-by-side due to the bulk of the *tert*-butyl groups.

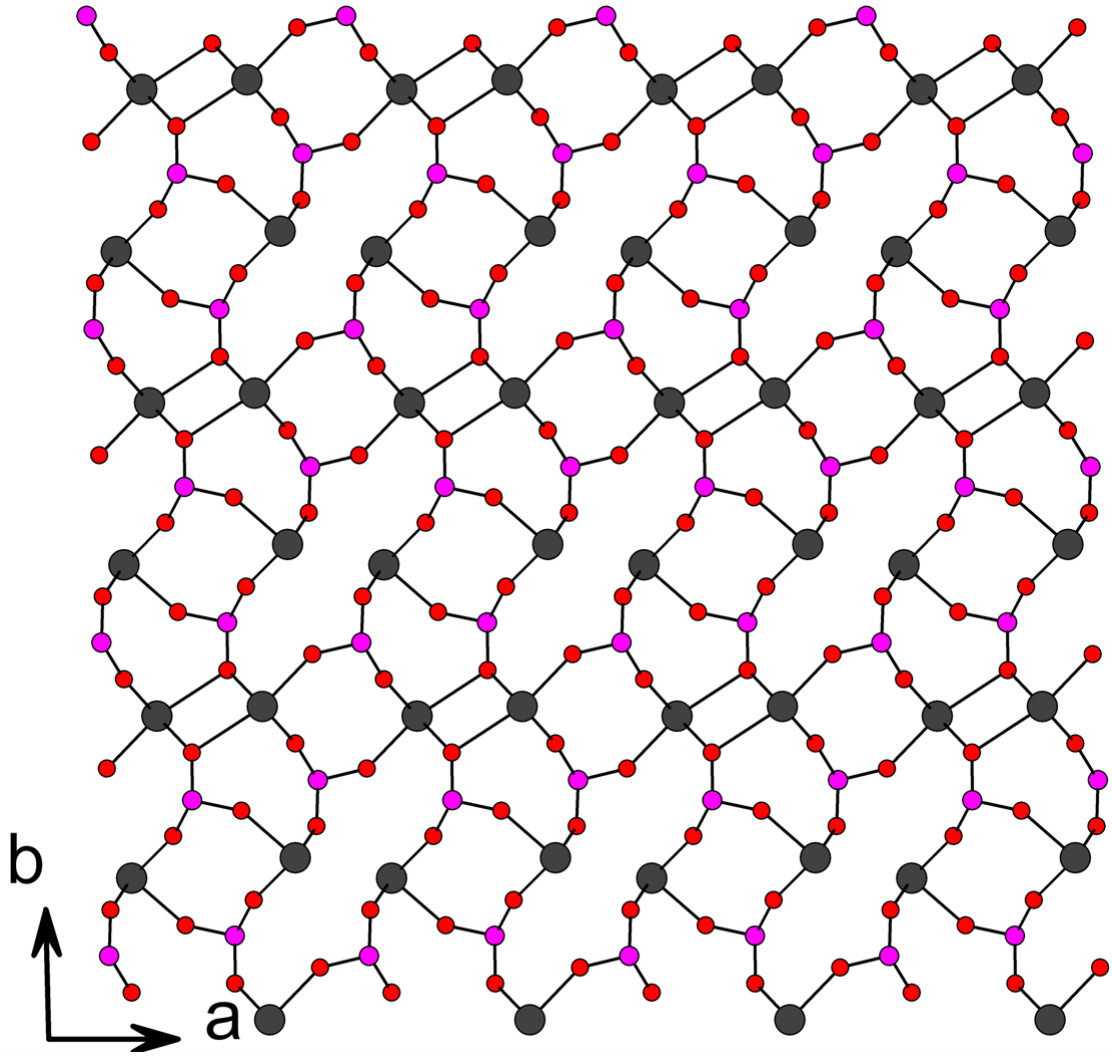

Figure 69 The inorganic layer of $Sn(O_3PC_6H_4C(CH_3)_3)$ consists of fused 4-, 8-, and 16-membered rings. Half of the Sn^{II} atoms are four-coordinate.

Structure of α-$Sn_2(O_3PC_{10}N_2H_6PO_3)$

α-$Sn_2(O_3PC_{10}N_2H_6PO_3)$ is a layered crosslinked compound which is closely related to $Sn_2(O_3PC_6H_4PO_3)$. The double layers of Sn atoms are in alternating directions in adjacent layers, allowing the ligand to effectively crosslink the layers (Figure 70). The d-spacing of this compound is 13.7 Å. All of the Sn atoms are 3-coordinate and the connectivity of the inorganic layers is identical to that in $Sn(O_3PC_6H_4PO_3)$ (Figure 71).

Structure of β-$Sn_2(O_3PC_{12}H_8PO_3)$

A new structure type for Sn phosphonates was found with 4,4'-biphenyl(bis)phosphonic acid, referred to as β-$Sn_2(O_3PC_{12}H_8PO_3)$. In this structure, the layers are no longer crosslinked, but instead capped by the trigonal 3-coordinate Sn atoms (Figure 72). The lone pairs of the Sn atoms are interdigitated in the interlayer space to avoid direct interactions. The inorganic layers consist of edge-sharing 12-membered rings, and all of the Sn atoms are 3-coordinate (Figure 73). This structure has a *d*-spacing of 16 Å, about 2 Å larger than the interlayer spacing of the compound obtained with the isomorphic ligand 2,2'-bipyridyl(bis)phosphonate. Varying the reaction conditions produced microcrystalline compounds with a d-spacing of ~13.9 Å, indicative of the α-phase. Unfortunately, single crystals of α-$Sn_2(O_3PC_{12}H_8PO_3)$ were not obtained, but its presence was confirmed by the PXRD spectra and elemental analyses. Under some conditions, reactions yielded mixtures of both the α- and β-phases. The formation of the β-phase may be related to the poor solubility of 4,4'-biphenyl(bis)phosphonic acid compared to 2,2'-bipyridyl(bis)phosphonic acid.

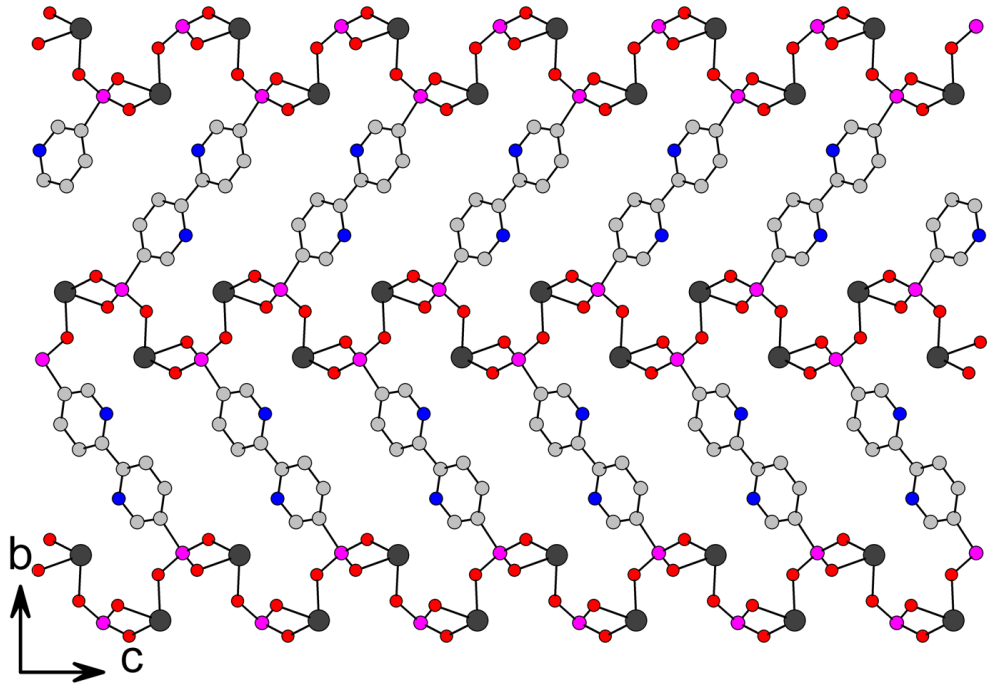

Figure 70 Crosslinked layered structure of $Sn_2(O_3PC_{10}N_2H_6PO_3)$. This is similar to the reported structure of $Sn_2(O_3PC_6H_4PO_3)$.

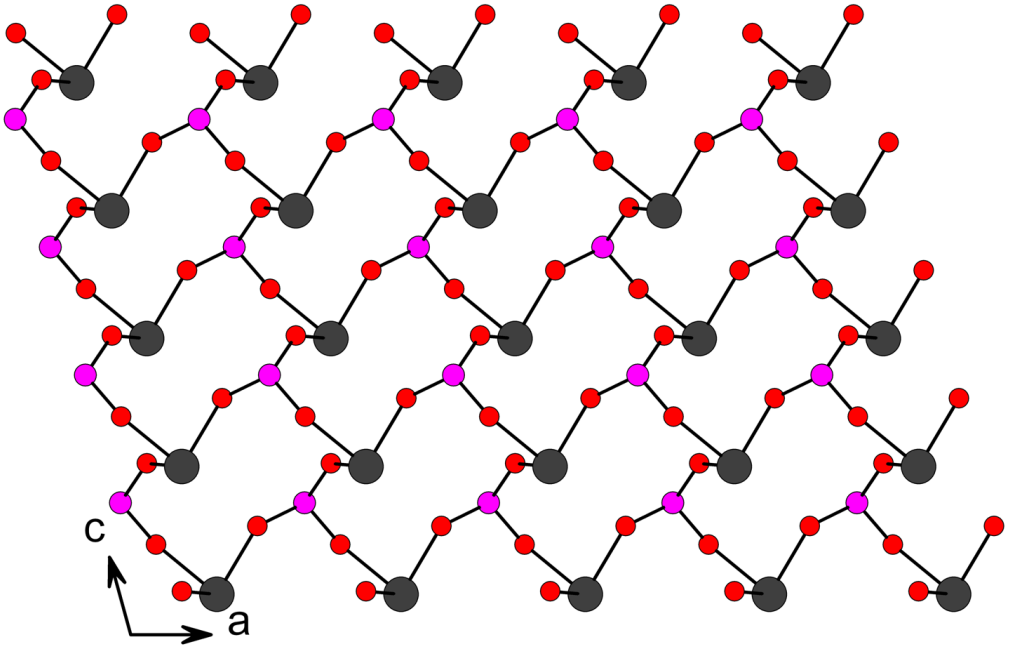

Figure 71 View of the layers in the crosslinked compound $Sn_2(O_3PC_{10}N_2H_6PO_3)$ with the organic groups removed. The layer consists of fused 12-membered rings.

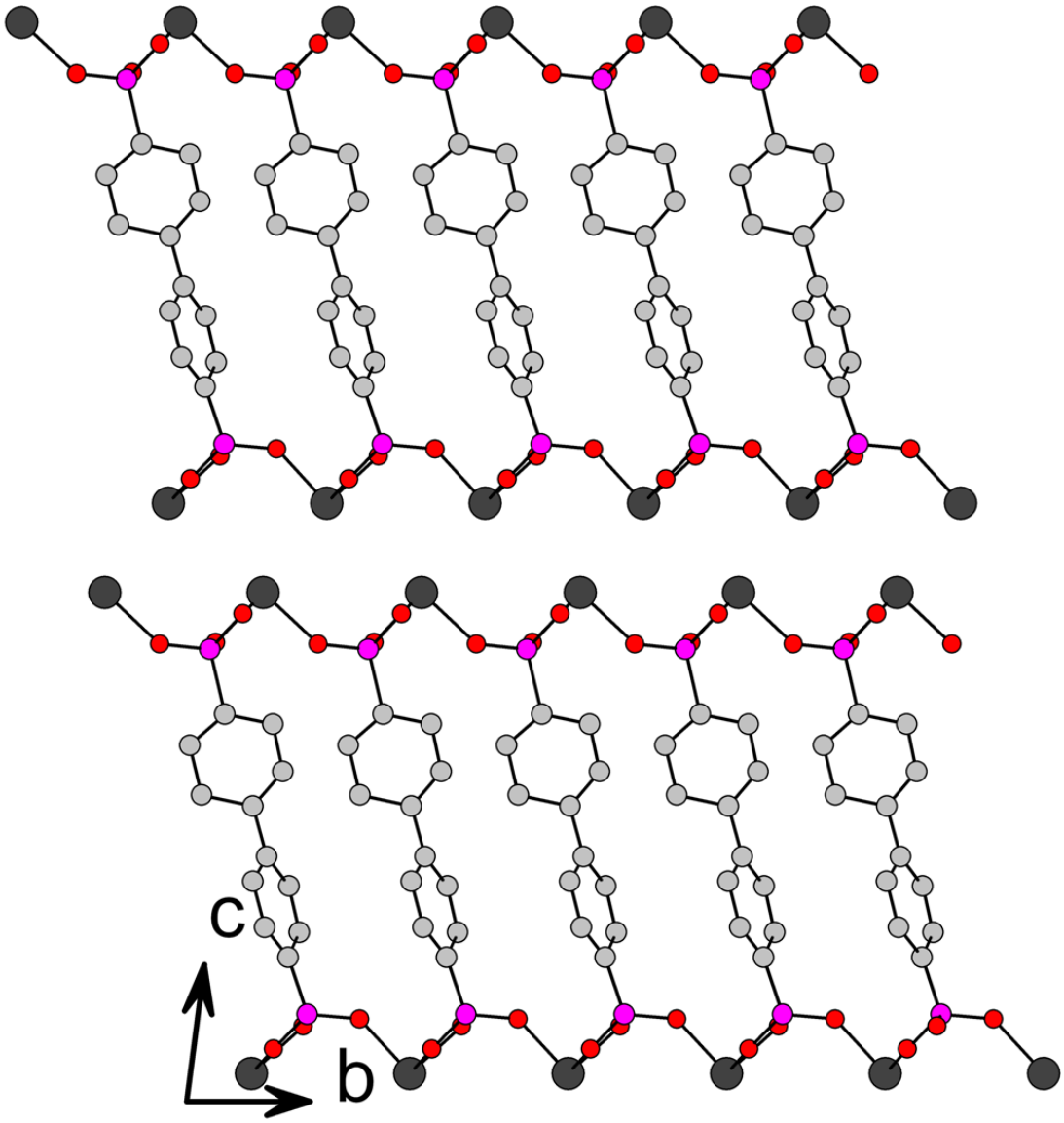

Figure 72 The capped layer structure of $Sn_2(O_3PC_{12}H_8PO_3)$. The Sn^{II} atoms are arranged so as to avoid the direct interaction of their lone pairs.

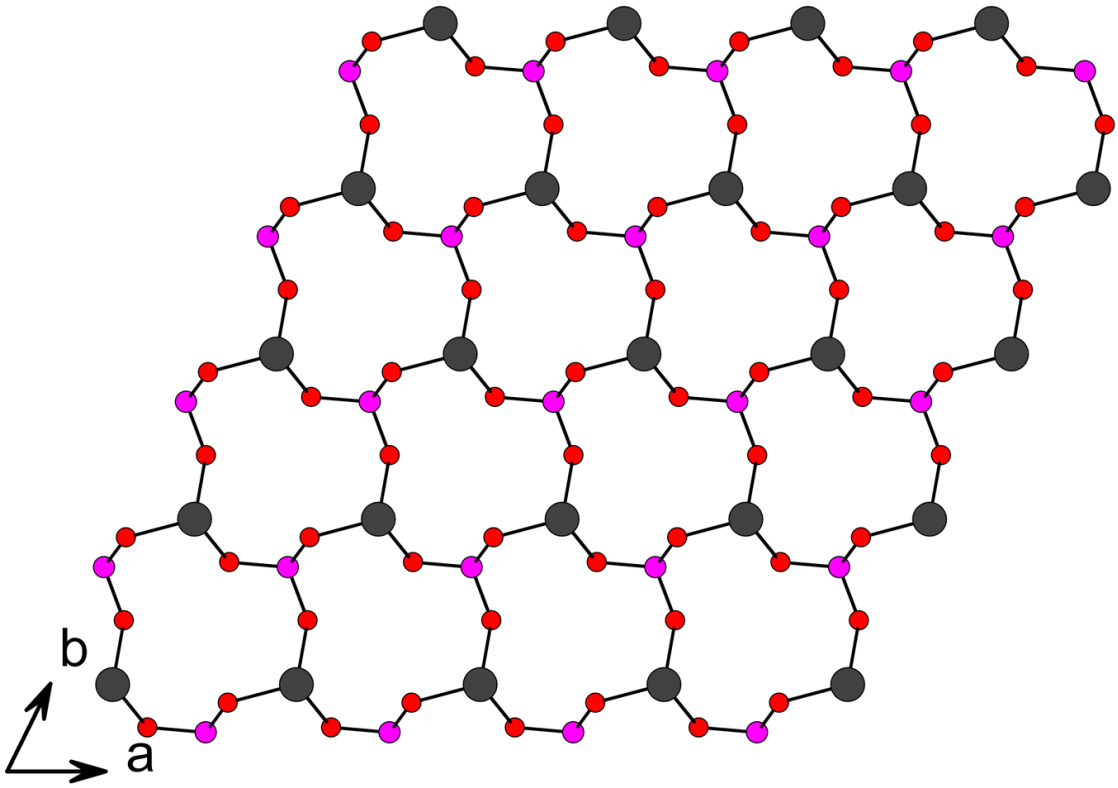

Figure 73 The inorganic layers of $Sn_2(O_3PC_{12}H_8PO_3)$ also consist of fused 12-membered rings, but the Sn^{II} atoms are all oriented in the same direction.

Thermogravimetric Studies

TGA were performed on compounds that were isolated as pure phases. The samples were ground with a mortar and pestle prior to heating. Weight loss and derivative weight loss curves upon heating to 1000 °C are included in Appendix B.

$Sn(O_3PC_5H_4N)$ shows no evidence of decomposition until ~325°C, at which point a weight increase is seen, corresponding to the oxidation of Sn^{II} to Sn^{IV} and the concurrent uptake of oxygen from the air. The organics combust between 450 °C and 650 °C, before the final weight loss event occurs over a large range centered at ~800 °C. The observed weight loss is 19.75%, which is in agreement with the calculated weight loss for the complete conversion to an equimolar mixture of SnO_2 and $Sn(P_2O_7)$, 19.61%.

$Sn_3O(O_3PC_5H_4N)_2$ shows its first weight loss at ~500 °C, due to the combustion of the pyridyl rings. The oxidation of Sn^{II} occurs during this step, as evidenced by a large negative spike in the derivative weight change at ~525 °C. The second major weight loss at ~750 °C corresponds to the phosphonate groups splitting out water and forming $P_2O_7^{4-}$. The calculated weight loss for the complete conversion to $2SnO_2$ and $Sn(P_2O_7)$ is 13.43%, which is close to the observed loss of 14.19%.

$Sn(O_3PC_5H_3NCH_3) \cdot 0.25H_2O$ gradually loses ¼ of a water molecule per formula unit as it is heated from 25 °C to 400 °C, corresponding with a loss of 1.53%. The organic groups combust in two steps between 400 °C and 600 °C, and the material undergoes a final decomposition step centered at ~800 °C as the pyrophosphate forms and water is split out. The observed weight loss of 23.64% is reasonably consistent with

the calculated loss of 24.70% for the complete conversion to an equimolar mixture of SnO_2 and $Sn(P_2O_7)$.

It is worthy of note that the oxidation of Sn^{II} and the accompanying weight increase in $Sn(O_3PC_5H_3NCH_3) \cdot 0.25H_2O$ occurs slightly before the decomposition of the organic groups. This is also observed for $Sn(O_3PC_5NH_4)$, but in that case, the increase is broad and drawn out over a range between 300 °C and 500 °C. The oxidation of Sn^{II} in compound $Sn(O_3PC_5H_3NCH_3) \cdot 0.25H_2O$ is rapid, occurring between 400 °C and 450 °C. We suspected that the broadness of the increase for $Sn(O_3PC_5H_4N)$ relative to that of $Sn(O_3PC_5H_3NCH_3) \cdot 0.25H_2O$ was perhaps due to a larger average particle size caused by variations in sample preparation. However, the TGAs were repeated after carefully and fully grinding the samples and the same results were obtained.

β-$Sn_2(O_3PC_{12}H_8PO_3)$ was observed to be thermally stable up to temperatures in excess of 550 °C. This is remarkable, considering the nature of the organic groups present within the compound. It is also interesting that no oxidation of the Sn^{II} occurs prior to this temperature, as in some of the other compounds in this study.

Discussion

One of the initial aims of this work was to create a layered compound possessing Lewis base functionality in the form of pyridyl groups, which would extend between the layers and be available to coordinate and sequester metal ions. In Sn^{II} phenylphosphonate, phenyl groups decorate both sides of infinite Sn-O-P layers. It seemed plausible that by substituting a pyridylphosphonic acid for phenylphosphonic

acid, we could create an isostructural compound having pyridyl nitrogen lone pairs directed into the space between the layers. This material could then coordinate and sequester nitrophilic metals, which might lead to useful catalytic or ion-exchange properties. However, the structure of Sn^{II} 3-pyridylphosphonate was vastly different than that of Sn^{II} phenylphosphonate. Instead of 2-D sheets, the structure of Sn^{II} 3-pyridylphosphonate consisted of fused-ring ladders decorated by pendant pyridyl groups. We noticed that the Sn-N distance was relatively short (~2.6 Å), and realized that there was an interaction between the two atoms. Changing the position of the nitrogen from 3- to 4- within the pyridyl ring resulted in a different structure.

The ladders in $Sn(O_3PC_5NH_4)$ are arranged so that the pyridyl nitrogen lone pairs can donate to the Sn atoms of adjacent ladders. The Sn-O bond opposite to the pyridyl N-donor is lengthened by more than 0.1 Å, reflecting the Sn-O antibonding character of the Sn-N bonding orbital. This is observed in $Sn(O_3PC_5NH_4)$, $Sn_3O(O_3PC_5H_4N)_2$, and $Sn(O_3PC_5H_3NCH_3)$ •$0.25H_2O$. In these instances, Sn^{II} is acting as a Lewis acid, which is an unusual role for a metal that, in the divalent state, usually acts as a Lewis base by donating its 5s lone pair. We tested the strength of this tendency by incorporating a nitrile group into the phosphonic acid, which yielded $Sn(O_3PC_5H_4N)$. In this compound, there is no Sn-N interaction, perhaps because nitrile is a much weaker base than pyridyl. The same ladder motif forms in both $Sn(O_3PC_5NH_4)$ and $Sn(O_3PC_5H_4N)$, but in $Sn(O_3PC_5NH_4)$, the ladders are packed in a herringbone-type arrangement to allow for the Sn-N interaction. In $Sn(O_3PC_5H_4N)$, the absence of this interaction allows the ladders to pack in a simple side-by-side fashion. We have not determined why

$Sn(O_3PC_5H_4N)$ adopts a ladder structure instead of a layered structure. This may be a result of the relatively mild synthetic conditions used in the preparation, but this is difficult to test since the nitrile group is prone to decomposition at elevated temperatures and at low pH. The fact that the same ladders are packed differently in $Sn(O_3PC_5H_4N)$ and $Sn(O_3PC_5H_4N)$ show that the Sn-N interaction is strong enough to alter the final structure of Sn phosphonates, which are typically robust, stable materials.

This work is the first example of a Sn^{II} phosphonate in which the Sn atoms are four-coordinate with three O atoms and one pyridyl N atom, as seen in the compounds ($Sn(O_3PC_5NH_4)$ and $Sn_3O(O_3PC_5H_4N)_2$). Another novel coordination environment occurs in $Sn(O_3PC_5H_3NCH_3)$ $\bullet 0.25H_2O$, in which the Sn^{II} is four coordinate with two O atoms and two N atoms from pyridyl rings.

We attempted to interrupt the Sn-N interaction by including acetic acid in the reaction mixture. The compound obtained was identical to that obtained without acetic acid. Although no acetate was included in the structure, a greater fraction of the material obtained was crystalline, and the crystals were larger than those obtained without acetic acid. It may be that the acetic acid helps to dissolve the SnC_2O_4, which is only sparingly soluble in pure water. Hydrothermal reactions carried out with $SnCl_2$ $\bullet 2H_2O$ (as a source of HCl to protonate the pyridine) instead of SnC_2O_4 were not successful, resulting only in liquids that failed to yield crystals upon slow evaporation. We are continuing efforts to interrupt the Sn-N interaction and more completely understand the structure-directing influences at work. If the Sn-N interaction can be selectively interrupted, then it may be possible to use the ladders as secondary building units in more complex materials.

We could not find any published examples of Sn phosphonates that contain the Sn_3(μ-3)-oxo unit that is present in compound $Sn(O_3PC_5H_3NCH_3)$ •$0.25H_2O$. However, Davies and coworkers reported the structure of tritin(II) dihydroxide oxide sulphate, which contains the $[Sn_3O(OH)_2]^{2+}$ cation. In that structure, the oxygen atom is central and coordinated only by three Sn atoms at distances of 2.062(7) Å, 2.063(7) Å, and 2.094(8) Å. These distances are similar to the Sn-O distances reported herein for compound III: 2.080(6) Å, 2.083(6) Å, and 2.090(6) Å. In addition, Natarajan and Cheetham[182] encountered the Sn_3(μ-3)-oxo unit in the structure of $[NH_4]^+[(Sn_3O_2)(PO_4)_3]^-$. They report similar values for the Sn-O distances. Like $Sn(O_3PC_5H_3NCH_3)$ •$0.25H_2O$, both of these compounds were obtained from reactions in water, so it is likely that the solvent is the source of the O^{2-} incorporated into the structure.

The bulk of the R-group has a profound influence on the structure of the inorganic layers formed in Sn phosphonates. As these materials are possible candidates for catalysts, this could be important because in some structures it makes the electron lone pairs of the Sn atoms more accessible. This application for the materials presented herein is not likely, since the organic groups block access to the layers, but it may be possible for small molecules to selectively interact with the Sn atoms.

The structure of β-$Sn_2(O_3PC_{12}H_8PO_3)$ is interesting, because the layers are not crosslinked and are functionalized by the Sn lone pairs on their surface. It may be possible to exfoliate the layers using an appropriate Lewis base. Because the compound is thermally stable to 550 °C, there may be applications in catalysis if the layers can be

pillared in the same manner as layered double hydroxides or clays. It is also likely that appropriate reaction conditions could yield β-phases of other Sn^{II} bisphosphonates, which would have similar properties. Decreasing the size of the layer by using phenyl(bis)phosphonic acid or short chain alkyl α,ω-(bis)phosphonic acids could provide materials more amenable to exfoliation.

The main factor which seemed to determine whether the *α*- or *β*-phase formed was the temperature at which the reaction was performed. The *β*-phases formed for $Sn_2(O_3PC_{12}H_8PO_3)$ and $Sn_2(O_3PC_{10}N_2H_8PO_3)$ when the reactions were done below 190 °C (Figure 74). Above this temperature, the *α*-phase or mixtures of both phases were obtained (Figure 75). This threshold temperature was lowered when the overall solubility of the compound was increased by using $SnCl_2 \cdot 2H_2O$ or including HF as a solubilizing agent.

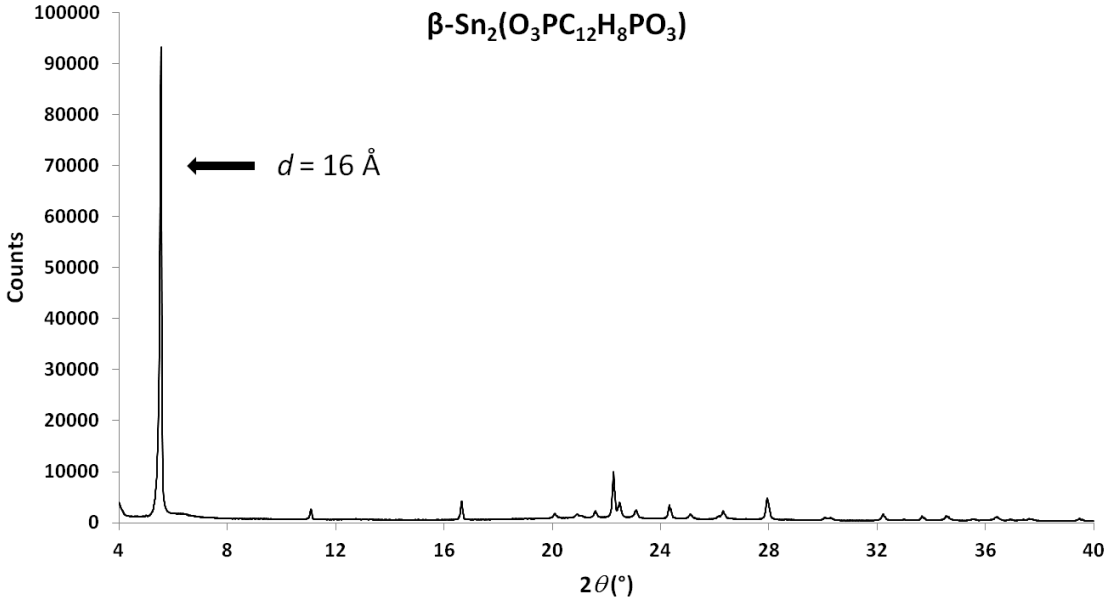

Figure 74 PXRD of *β*-$Sn_2(O_3PC_{12}H_8PO_3)$ synthesized in water at 180 °C.

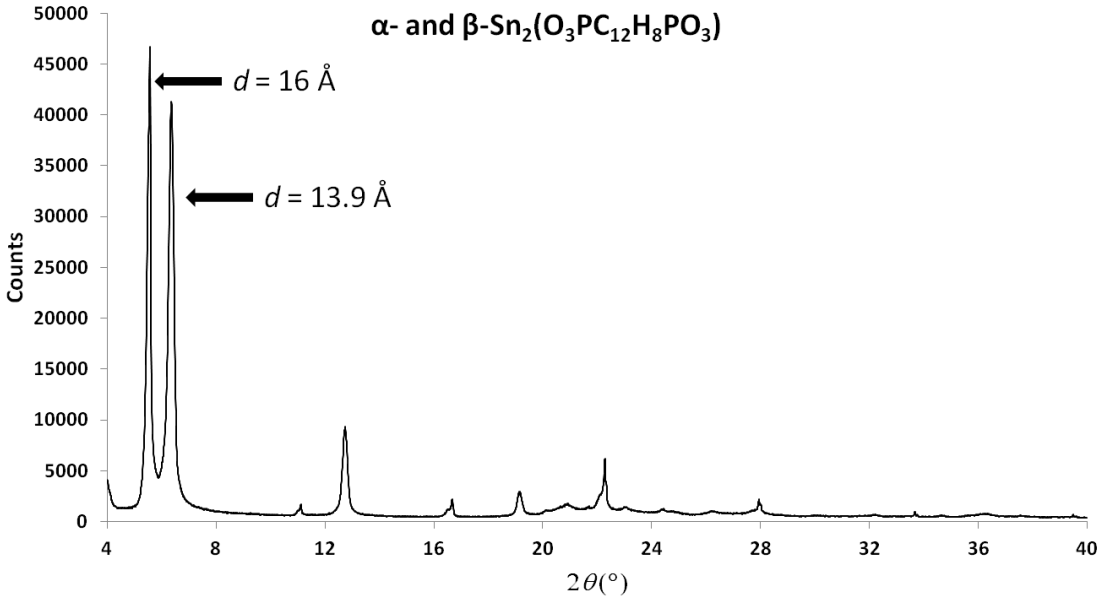

Figure 75 Reactions of SnC_2O_4 and 4,4'-biphenyl(bis)phosphonic acid performed at temperatures greater than 190 °C or with solubilizing agents resulted in mixtures of *α*- and *β*-$Sn_2(O_3PC_{12}H_8PO_3)$. The *β*-phase has the 16 Å *d*-spacing.

Conclusion

In conclusion, we have presented crystal structures and TGAs of 10 Sn^{II} phosphonates. The first series of compounds was used to explore Sn-N interactions which can affect the structures. When 3-pyridylphosphonate or 4-pyridylphosphonate is incorporated into the structures, the compounds form ladders, and the nitrogen atoms from the pendant pyridyl groups of one ladder interact with Sn atoms on neighboring ladders at distances of ~2.6 Å. In this instance, Sn^{II} is acting as a Lewis acid, which is an unusual role for a metal that, in the divalent state, is normally a Lewis base. Tri-tin(μ-3)oxo-bis(4-pyridylphosphonate contains a rare Sn_3(μ-3)-oxo unit never before observed in a Sn^{II} phosphonate. When 6-methyl-2-pyridylphosphonate is utilized, 2-D sheets form, and two of the four distinct Sn atoms are coordinated by two pyridyl nitrogen atoms (in addition to two O atoms) at distances ranging from ~2.45 Å to ~2.62 Å. In Sn^{II} 4-cyanophenylphosphonate, the structure consists of chains similar to those formed in Sn^{II} 3-pyridylphosphonate, but the lack of a Sn-N interaction allows the chains to pack differently in the bulk structure. The influence of the nitrogen position within the pyridyl ring on the crystal structure demonstrates the profound and unanticipated effects that a subtle change in the ligand can have on the formation of metal organic frameworks.

The second series of compounds was studied to determine the effects of ligand bulk on the structures of Sn^{II} phosphonates. Even with very bulky phosphonates, the compounds tended to form layers. A new structure type for Sn^{II} bisphosphonates was structurally characterized. In this compound, β-$Sn_2(O_3PC_{12}H_8PO_3)$, the Sn^{II} atoms cap layers formed by parallel stacks of the phosphonate ligand. The layers are not bonded to

one another, and have surfaces which consist of Sn^{II} atoms. This type of material may be exfoliable if an appropriate Lewis acid is used to interact with the lone pairs on the Sn atoms. The α-form of $Sn_2(O_3PC_{12}H_8PO_3)$ was not isolated as single crystals, but it was prepared as a powder. The isostructural compound α-$Sn_2(O_3PC_{10}N_2H_8PO_3)$ was obtained as single crystals and its structure determined. Solubility seems to the main factor in determining which phase forms. The structural chemistry of Sn^{II} phosphonates is rich, and further study may yield more interesting, if not useful, materials.

CHAPTERVIII

SUMMARY

The previous chapters have given examples of some of the many ways that functionality can be built into metal phosphonates. Tetravalent phosphonates have the inherent advantages of insolubility and thermal stability, which may be useful if these materials are to be used as supports in catalytic materials, like the Zr and Sn phosphonates presented in Chapter III. Crystalline layered materials like the carboxylate-functionalized Mn and Zn phosphonates discussed in Chapter IV have much more ordered structures, which could be useful in the selective uptake of amines. Discrete cluster units like the heptanuclear clusters presented in Chapter V may prove to be magnetically interesting materials if anisotropic metal ions can be included in their topology. Sn^{II} phosphonates, like the compounds discussed in Chapter VI, show myriad structural variations which can be affected by the size of the ligand as well as the presence of additional functional groups. This may allow for the syntheses of framework materials that have accessible Sn^{II} sites. These types of materials could be useful as heterogeneous solid-acid catalysts.

REFERENCES

1. Clearfield, A.; Blessing, R. H.; Stynes, J. A., *Journal of Inorganic and Nuclear Chemistry* **1968,** *30* (8), 2249-58.
2. Clearfield, A.; Smith, G. D., *Journal of Inorganic and Nuclear Chemistry* **1968,** *30* (1), 327-9.
3. Clearfield, A.; Stynes, J. A., *Journal of Inorganic and Nuclear Chemistry* **1964,** *26* (1), 117-29.
4. Clearfield, A.; Smith, G. D., *Inorganic Chemistry* **1969,** *8* (3), 431-6.
5. Inoue, Y., *Journal of Inorganic and Nuclear Chemistry* **1964,** *26* (12), 2241-53.
6. Piret, J.; Henry, J.; Balon, G.; Beaudet, C., *Bulletin de la Societe Chimique de France* **1965,** (12), 3590-6.
7. Dines, M. B.; DiGiacomo, P. M., *Inorganic Chemistry* **1981,** *20* (1), 92-7.
8. Maya, L., *Journal of Inorganic and Nuclear Chemistry* **1981,** *43* (2), 400.
9. Clearfield, A., *Journal of Molecular Catalysis* **1984,** *27* (1-2), 251-62.
10. Alberti, G.; Costantino, U.; Kornyei, J.; Giovagnotti, M. L. L., *Reactive Polymers, Ion Exchangers, Sorbents* **1985,** *4* (1), 1-10.
11. Burwell, D. A.; Thompson, M. E., *Chemistry of Materials* **1991,** *3* (4), 730-7.
12. Alberti, G.; Casciola, M.; Costantino, U.; Peraio, A.; Montoneri, E., *Solid State Ionics* **1992,** *50* (3-4), 315-22.
13. Alberti, G.; Casciola, M.; Vivani, R.; Biswas, R. K., *Inorganic Chemistry* **1993,** *32* (21), 4600-4.

14. Alberti, G.; Costantino, U.; Marmottini, F.; Vivani, R.; Zappelli, P., *Angewandte Chemie* **1993,** *105* (9), 1396-8 (See also Angew Chem , Int Ed Engl , 1993, 32(9), 1357-9).

15. Alberti, G.; Murcia-Mascaros, S.; Vivani, R., *Materials Chemistry and Physics* **1993,** *35* (3-4), 187-92.

16. Vermeulen, L. A.; Snover, J. L.; Sapochak, L. S.; Thompson, M. E., *Journal of the American Chemical Society* **1993,** *115* (25), 11767-74.

17. Wang, J. D.; Clearfield, A.; Pen, G., *Materials Chemistry and Physics* **1993,** *35* (3-4), 208-16.

18. Poojary, D. M.; Vermeulen, L. A.; Vicenzi, E.; Clearfield, A.; Thompson, M. E., *Chemistry of Materials* **1994,** *6* (10), 1845-9.

19. Thompson, M. E., *Chemistry of Materials* **1994,** *6* (8), 1168-75.

20. Cao, G.; Lee, H.; Lynch, V. M.; Mallouk, T. E., *Inorganic Chemistry* **1988,** *27* (16), 2781-5.

21. Le Bideau, J.; Jouanneaux, A.; Payen, C.; Bujoli, B., *Journal of Materials Chemistry* **1994,** *4* (8), 1319-23.

22. Le Bideau, J.; Payen, C.; Bujoli, B.; Palvadeau, P.; Rouxel, J., *Journal of Magnetism and Magnetic Materials* **1995,** *140-144* (Pt. 3), 1719-20.

23. Poojary, D. M.; Zhang, B.; Cabeza, A.; Aranda, M. A. G.; Bruque, S.; Clearfield, A., *Journal of Materials Chemistry* **1996,** *6* (4), 639-44.

24. Poojary, D. M.; Zhang, B.; Clearfield, A., *Journal of the American Chemical Society* **1997,** *119* (51), 12550-12559.

25. Hix, G. B.; Harris, K. D. M., *Journal of Materials Chemistry* **1998,** *8* (3), 579-584.

26. Petruska, M. A.; Talham, D. R., *Chemistry of Materials* **1998,** *10* (11), 3672-3682.

27. Bellitto, C., *Magnetism Molecules to Materials II* **2001**, 425-456.

28. Clearfield, A., *Curr. Opin. Solid State Mater. Sci.* **2003,** *6* (6), 495-506.

29. Clearfield, A., *Dalton Transactions* **2008,** (44), 6089-6102.

30. Clearfield, A.; Sharma, C. V. K.; Zhang, B., *Chemistry of Materials* **2001,** *13* (10), 3099-3112.

31. Demadis, K. D., *Solid State Chemistry Research Trends* **2007**, 109-172.

32. Kamecka, A.; Kurzak, B., *Wiadomosci Chemiczne* **2003,** *57* (9-10), 797-825.

33. Maeda, K., *Microporous and Mesoporous Materials* **2004,** *73* (1-2), 47-55.

34. Mutin, P. H.; Guerrero, G.; Vioux, A., *Journal of Materials Chemistry* **2005,** *15* (35-36), 3761-3768.

35. Shimizu, G. K. H.; Vaidhyanathan, R.; Taylor, J. M., *Chemical Society Reviews* **2009,** *38* (5), 1430-1449.

36. Subbiah, A.; Pyle, D.; Rowland, A.; Huang, J.; Narayanan, R. A.; Thiyagarajan, P.; Zon, J.; Clearfield, A., *Journal of the American Chemical Society* **2005,** *127* (31), 10826-10827.

37. Cabeza, A.; Gomez-Alcantara, M. d. M.; Olivera-Pastor, P.; Sobrados, I.; Sanz, J.; Xiao, B.; Morris, R. E.; Clearfield, A.; Aranda, M. A. G., *Microporous and Mesoporous Materials* **2008,** *114* (1-3), 322-336.

38. Kirumakki, S.; Huang, J.; Subbiah, A.; Yao, J.; Rowland, A.; Smith, B.; Mukherjee, A.; Samarajeewa, S.; Clearfield, A., *Journal of Materials Chemistry* **2009,** *19* (17), 2593-2603.

39. Medoukali, D.; Mutin, P. H.; Vioux, A., *Journal of Materials Chemistry* **1999,** *9* (10), 2553-2557.

40. Kirumakki, S.; Samarajeewa, S.; Harwell, R.; Mukherjee, A.; Herber, R. H.; Clearfield, A., *Chemical Communications* **2008,** (43), 5556-5558.

41. Conceicao Cruz Costa, M.; Johnstone, R. A. W.; Whittaker, D., *Journal of Molecular Catalysis A Chemical* **1998,** *129* (1), 79-89.

42. Clearfield, A.; Wang, Z.; Bellinghausen, P., *Journal of Solid State Chemistry* **2002,** *167* (2), 376-385.

43. Wang, Z.; Heising, J. M.; Clearfield, A., *Journal of the American Chemical Society* **2003,** *125* (34), 10375-10383.

44. Bestaoui, N.; Ouyang, X.; Fredoueil, F.; Bujoli, B.; Clearfield, A., *Acta Crystallographica, Section B Structural Science* **2005,** *B61* (6), 669-674.

45. Fang, C.; Chen, Z.; Liu, X.; Yang, Y.; Deng, M.; Weng, L.; Jia, Y.; Zhou, Y., *Inorganica Chimica Acta* **2009,** *362* (7), 2101-2107.

46. Fredoueil, F.; Evain, M.; Massiot, D.; Bujoli-Doeuff, M.; Janvier, P.; Clearfield, A.; Bujoli, B., *Journal of the Chemical Society, Dalton Transactions* **2002,** (7), 1508-1512.

47. Gomez-Alcantara, M. M.; Aranda, M. A. G.; Olivera-Pastor, P.; Beran, P.; Garcia-Munoz, J. L.; Cabeza, A., *Dalton Transactions* **2006,** (4), 577-585.

48. Gomez-Alcantara, M. M.; Cabeza, A.; Aranda, M. A. G.; Guagliardi, A.; Mao, J. G.; Clearfield, A., *Solid State Sciences* **2004,** *6* (5), 479-487.

49. Hou, S.-Z.; Cao, D.-K.; Liu, X.-G.; Li, Y.-Z.; Zheng, L.-M., *Dalton Transactions* **2009,** (15), 2746-2750.

50. Song, J.-L.; Mao, J.-G.; Sun, Y.-Q.; Zeng, H.-Y.; Kremer, R. K.; Clearfield, A., *Journal of Solid State Chemistry* **2004,** *177* (3), 633-641.

51. Stock, N.; Bein, T., *Journal of Materials Chemistry* **2005,** *15* (13), 1384-1391.

52. Stock, N.; Karaghiosoff, K.; Bein, T., *Zeitschrift fuer Anorganische und Allgemeine Chemie* **2004,** *630* (13-14), 2535-2540.

53. Svoboda, J.; Zima, V.; Benes, L.; Melanova, K.; Trchova, M.; Vlcek, M., *Solid State Sciences* **2008,** *10* (11), 1533-1542.

54. Christou, G., *Polyhedron* **2005,** *24* (16-17), 2065-2075.

55. Murray, K. S., *Australian Journal of Chemistry* **2009,** *62* (9), 1081-1101.

56. Du, Z.-Y.; Prosvirin, A. V.; Mao, J.-G., *Inorganic Chemistry* **2007,** *46* (23), 9884-9894.

57. Konar, S.; Bhuvanesh, N.; Clearfield, A., *J. Am. Chem. Soc.* **2006,** *128* (30), 9604-9605.

58. Konar, S.; Clearfield, A., *Inorganic Chemistry* **2008,** *47* (13), 5573-5579.

59. Konar, S.; Clearfield, A., *Inorganic Chemistry* **2008,** *47* (9), 3489-3491.

60. Maheswaran, S.; Chastanet, G.; Teat, S. J.; Mallah, T.; Sessoli, R.; Wernsdorfer, W.; Winpenny, R. E. P., *Angewandte Chemie, International Edition* **2005,** *44* (32), 5044-5048.

61. Serre, C.; Stock, N.; Bein, T.; Ferey, G., *Inorganic Chemistry* **2004,** *43* (10), 3159-3163.

62. Stock, N.; Bein, T., *Angewandte Chemie, International Edition* **2004,** *43* (6), 749-752.

63. Shiina, I.; Fukui, H. In *Sn(II) and Sn(IV) Lewis acids*, Wiley-VCH Verlag GmbH & Co. KGaA: 2008; pp 517-550.

64. Natarajan, S.; Attfield, M. P.; Cheetham, A. K., *Angew. Chem., Int. Ed. Engl.* **1997,** *36* (9), 978-980.

65. Natarajan, S.; Cheetham, A. K., *Chem. Commun.* **1997,** (12), 1089-1090.

66. Subbiah, A.; Bhuvanesh, N.; Clearfield, A., *Journal of Solid State Chemistry* **2005,** *178* (4), 1321-1325.

67. Zapf, P. J.; Rose, D. J.; Haushalter, R. C.; Zubieta, J., *J. Solid State Chem.* **1997,** *132* (2), 438-442.

68. Romero, F. M.; Ziessel, R., *Tetrahedron Lett.* **1995,** *36* (36), 6471-4.

69. Konar, S.; Zon, J.; Prosvirin, A. V.; Dunbar, K. R.; Clearfield, A., *Inorganic Chemistry* **2007,** *46* (13), 5229-5236.

70. Chen, D.; Martell, A. E.; Motekaitis, R. J.; McManus, D., *Canadian Journal of Chemistry* **1998,** *76* (4), 445-451.

71. Penicaud, V.; Odobel, F.; Bujoli, B., *Tetrahedron Lett.* **1998,** *39* (22), 3689-3692.

72. Alberti, G.; Bein, T.; Editors, *Comprehensive Supramolecular Chemistry, Volume 7: Solid-State Supramolecular Chemistry: Two-and Three-Dimensional Inorganic Networks*. Pergamon, Oxford, U.K.: 1996; p 837 pp.

73. Kumar, C. V.; Bhambhani, A.; Hnatiuk, N. In *Layered α-zirconium phosphates and phosphonates*, Marcel Dekker, Inc., New York: 2004; pp 313-372.

74. Vivani, R.; Alberti, G.; Costantino, F.; Nocchetti, M., *Microporous Mesoporous Mater.* **2007,** *107* (1-2), 58-70.

75. Poojary, M. D.; Hu, H. L.; Campbell, F. L., III; Clearfield, A., *Acta Crystallogr., Sect. B: Struct. Sci.* **1993,** *B49* (6), 996-1001.

76. Beck, S.; Brough, A. R.; Bochmann, M., *J. Mol. Catal. A: Chem.* **2004,** *220* (2), 275-284.

77. Curini, M.; Rosati, O.; Costantino, U., *Curr. Org. Chem.* **2004,** *8* (7), 591-606.

78. Hu, A.; Ngo, H. L.; Lin, W., *J. Am. Chem. Soc.* **2003,** *125* (38), 11490-11491.

79. Rocha, G. M. S. R. O.; Santos, T. M.; Bispo, C. S. S., *Catal. Lett.* **2011,** *141* (1), 100-110.

80. Alberti, G.; Casciola, M. In *Membranes for medium temperature PEFC based on Nafion filled with layered metal phosphates and phosphonates*, Wiley-VCH Verlag GmbH & Co. KGaA, Weinheim, Germany: 2008; pp 97-122.

81. Furman, B. R.; Wellinghoff, S. T.; Laine, R. M.; Chan, K. S.; Nicolella, D. P.; Rawls, H. R., *J. Appl. Polym. Sci.* **2009,** *114* (2), 993-1001.

82. Tsai, T.-Y.; Wu, Y.-J.; Hsu, F.-J., *J. Phys. Chem. Solids* **2007,** *69* (5-6), 1379-1382.

83. Lanari, D.; Montanari, F.; Marmottini, F.; Piermatti, O.; Orru, M.; Vaccaro, L., *J. Catal.* **2010,** *277* (1), 80-87.

84. Odobel, F.; Bujoli, B.; Massiot, D., *Chemistry of Materials* **2001,** *13* (1), 163-173.

85. Bloch, E. D.; Britt, D.; Lee, C.; Doonan, C. J.; Uribe-Romo, F. J.; Furukawa, H.; Long, J. R.; Yaghi, O. M., *J. Am. Chem. Soc.* **2010,** *132* (41), 14382-14384.

86. Byrd, H.; Clearfield, A.; Poojary, D.; Reis, K. P.; Thompson, M. E., *Chemistry of Materials* **1996,** *8* (9), 2239-2246.

87. Konarev, P. V.; Volkov, V. V.; Sokolova, A. V.; Koch, M. H. J.; Svergun, D. I., *J. Appl. Crystallogr.* **2003,** *36* (5), 1277-1282.

88. Ha, K., *Z. Kristallogr. - New Cryst. Struct.* **2010,** *225* (4), 665-666.

89. Ivanova, E. V.; Puzyk, M. V.; Balashev, K. P., *Opt. Spectrosc.* **2009,** *107* (1), 101-105.

90. Clearfield, A.; Wang, *Z.*, *Journal of the Chemical Society, Dalton Transactions* **2002,** No. 15, 2937-2947.

91. Martin, K. J.; Squattrito, P. J.; Clearfield, A., *Inorg. Chim. Acta* **1989,** *155* (1), 7-9.

92. Culp, J. T.; Fanucci, G. E.; Watson, B. C.; Nicole, M. A.; Backov, R.; Ohnuki, H.; Meisel, M. W.; Talham, D. R., *J. Solid State Chem.* **2001,** *159* (2), 362-370.

93. Adelani, P. O.; Oliver, A. G.; Albrecht-Schmitt, T. E., *Cryst. Growth Des.* **2011,** *11* (7), 3072-3080.

94. Chen, Z.; Zhou, Y.; Weng, L.; Yuan, C.; Zhao, D., *Chemistry – An Asian Journal* **2007,** *2* (12), 1549-1554.

95. Li, J.-T.; Cao, D.-K.; Liu, B.; Li, Y.-Z.; Zheng, L.-M., *Cryst. Growth Des.* **2008,** *8* (8), 2950-2953.

96. Li, J.-T.; Guo, L.-R.; Shen, Y.; Zheng, L.-M., *CrystEngComm* **2009,** *11* (8), 1674-1678.

97. Li, J.-T.; Keene, T. D.; Cao, D.-K.; Decurtins, S.; Zheng, L.-M., *CrystEngComm* **2009,** *11* (7), 1255-1260.

98. Liao, T.-B.; Ling, Y.; Chen, Z.-X.; Zhou, Y.-M.; Weng, L.-H., *Chem. Commun. (Cambridge, U. K.)* **2010,** *46* (7), 1100-1102.

99. Wang, P.-F.; Duan, Y.; Cao, D.-K.; Li, Y.-Z.; Zheng, L.-M., *Dalton Trans.* **2010,** *39* (19), 4559-4565.

100. Bauer, S.; Bein, T.; Stock, N., *Inorg. Chem.* **2005,** *44* (16), 5882-5889.

101. Zima, V.; Svoboda, J.; Benes, L.; Melanova, K.; Trchova, M.; Ruzicka, A., *J. Solid State Chem.* **2009,** *182* (11), 3155-3161.

102. Hix, G. B.; Turner, A.; Kariuki, B. M.; Tremayne, M.; MacLean, E. J., *J. Mater. Chem.* **2002,** *12* (11), 3220-3227.

103. Kamitanaka, T.; Yamamoto, K.; Matsuda, T.; Harada, T., *Tetrahedron* **2008,** *64* (24), 5699-5702.

104. Cao, G.; Mallouk, T. E., *Inorg. Chem.* **1991,** *30* (7), 1434-8.

105. Frink, K. J.; Wang, R. C.; Colon, J. L.; Clearfield, A., *Inorganic Chemistry* **1991,** *30* (7), 1438-41.

106. Poojary, D. M.; Clearfield, A., *Journal of the American Chemical Society* **1995,** *117* (45), 11278-84.

107. Zhang, Y.; Scott, K. J.; Clearfield, A., *Journal of Materials Chemistry* **1995,** *5* (2), 315-18.

108. Sheldrick, G. M. *SADABS, Program for Absorption Correction of Area Detector Frames*, Bruker AXS, Inc.: Madison, WI.

109. Sheldrick, G. M., *Acta Crystallographica, Section A Foundations of Crystallography* **2008,** *A64* (1), 112-122.

110. Akiya, N.; Savage, P. E., *Chem. Rev.* **2002,** *102* (8), 2725-2750.

111. Izzo, B.; Harrell, C. L.; Klein, M. T., *AIChE Journal* **1997,** *43* (8), 2048-2058.

112. Clearfield, A.; Tindwa, R. M., *J. Inorg. Nucl. Chem.* **1979,** *41* (6), 871-8.

113. Baskar, V.; Shanmugam, M.; Sanudo, E. C.; Shanmugam, M.; Collison, D.; McInnes, E. J. L.; Wei, Q.; Winpenny, R. E. P., *Chem. Commun.* **2007,** No. 1, 37-39.

114. Breeze, B. A.; Shanmugam, M.; Tuna, F.; Winpenny, R. E. P., *Chem. Commun.* **2007,** No. 48, 5185-5187.

115. Khanra, S.; Helliwell, M.; Tuna, F.; McInnes, E. J. L.; Winpenny, R. E. P., *Dalton Trans.* **2009,** No. 31, 6166-6174.

116. Khanra, S.; Konar, S.; Clearfield, A.; Helliwell, M.; McInnes, E. J. L.; Tolis, E.; Tuna, F.; Winpenny, R. E. P., *Inorganic Chemistry* **2009,** *48* (12), 5338-5349.

117. Konar, S.; Clearfield, A., *Inorganic Chemistry* **2008,** *47* (13), 5573-5579.

118. Konar, S.; Clearfield, A., *Inorganic Chemistry* **2008,** *47* (9), 3489-3491.

119. Konar, S.; Zon, J.; Prosvirin, A. V.; Dunbar, K. R.; Clearfield, A., *Inorganic Chemistry* **2007,** *46* (13), 5229-5236.

120. Langley, S.; Helliwell, M.; Sessoli, R.; Teat, S. J.; Winpenny, R. E. P., *Inorganic Chemistry* **2008,** *47* (2), 497-507.

121. Li, J.-T.; Ma, Y.-S.; Li, S.-G.; Cao, D.-K.; Li, Y.-Z.; Song, Y.; Zheng, L.-M., *Dalton Trans.* **2009,** No. 25, 5029-5034.

122. Ma, Y.-S.; Song, Y.; Li, Y.-Z.; Zheng, L.-M., *Inorganic Chemistry* **2007,** *46* (14), 5459-5461.

123. Shanmugam, M.; Chastanet, G.; Mallah, T.; Sessoli, R.; Teat, S. J.; Timco, G. A.; Winpenny, R. E. P., *Chem.--Eur. J.* **2006,** *12* (34), 8777-8785.

124. Wang, M.; Ma, C.; Chen, C., *Dalton Trans.* **2008,** No. 34, 4612-4620.

125. Ali, S.; Baskar, V.; Muryn, C. A.; Winpenny, R. E. P., *Chem. Commun.* **2008,** No. 47, 6375-6377.

126. Ali, S.; Muryn, C. A.; Tuna, F.; Winpenny, R. E. P., *Dalton Trans.* **2010,** *39* (1), 124-131.

127. Lei, C.; Mao, J.-G.; Sun, Y.-Q.; Zeng, H.-Y.; Clearfield, A., *Inorganic Chemistry* **2003,** *42* (20), 6157-6159.

128. Liu, H.-Y.; Zhang, Z.-J.; Shi, W.; Zhao, B.; Cheng, P.; Liao, D.-Z.; Yan, S.-P., *Dalton Trans.* **2009,** No. 23, 4416-4419.

129. Liu, H.-Y.; Zhao, B.; Shi, W.; Zhang, Z.-J.; Cheng, P.; Liao, D.-Z.; Yan, S.-P., *Eur. J. Inorg. Chem.* **2009,** No. 18, 2599-2602.

130. Yang, B.-p.; Mao, J.-g.; Sun, Y.-q.; Zhao, H.-h.; Clearfield, A., *Eur. J. Inorg. Chem.* **2003,** No. 23, 4211-4217.

131. Cao, D.-K.; Li, Y.-Z.; Zheng, L.-M., *Inorganic Chemistry* **2005,** *44* (9), 2984-2985.

132. Guo, Y.-Q.; Yang, B.-P.; Song, J.-L.; Mao, J.-G., *Cryst. Growth Des.* **2008,** *8* (2), 600-605.

133. Alley, K. G.; Bircher, R.; Waldmann, O.; Ochsenbein, S. T.; Guedel, H. U.; Moubaraki, B.; Murray, K. S.; Fernandez-Alonso, F.; Abrahams, B. F.; Boskovic, C., *Inorganic Chemistry* **2006,** *45* (22), 8950-8957.

134. Brechin, E. K.; Graham, A.; Parkin, A.; Parsons, S.; Seddon, A. M.; Winpenny, R. E. P., *Dalton* **2000,** No. 19, 3242-3252.

135. Chibotaru, L. F.; Ungur, L.; Aronica, C.; Elmoll, H.; Pilet, G.; Luneau, D., *J. Am. Chem. Soc.* **2008,** *130* (37), 12445-12455.

136. Clemente-Juan, J. M.; Coronado, E.; Forment-Aliaga, A.; Galan-Mascaros, J. R.; Gimenez-Saiz, C.; Gomez-Garcia, C. J., *Inorganic Chemistry* **2004,** *43* (8), 2689-2694.

137. Wang, X.-T.; Wang, B.-W.; Wang, Z.-M.; Zhang, W.; Gao, S., *Inorg. Chim. Acta* **2008,** *361* (14-15), 3895-3902.

138. Zhang, Y.-Z.; Wernsdorfer, W.; Pan, F.; Wang, Z.-M.; Gao, S., *Chem. Commun.* **2006,** (31), 3302-3304.

139. Abbati, G. L.; Cornia, A.; Fabretti, A. C.; Caneschi, A.; Gatteschi, D., *Inorganic Chemistry* **1998,** *37* (7), 1430-1431.

140. Bolcar, M. A.; Aubin, S. M. J.; Folting, K.; Hendrickson, D. N.; Christou, G., *Chem. Commun.* **1997,** No. 16, 1485-1486.

141. Harden, N. C.; Bolcar, M. A.; Wernsdorfer, W.; Abboud, K. A.; Streib, W. E.; Christou, G., *Inorganic Chemistry* **2003,** *42* (22), 7067-7076.

142. Liu, C.-M.; Zhang, D.-Q.; Zhu, D.-B., *Inorganic Chemistry* **2009,** *48* (3), 792-794.

143. Mishra, A.; Wernsdorfer, W.; Abboud, K. A.; Christou, G., *Inorganic Chemistry* **2006,** *45* (25), 10197-10206.

144. Stamatatos, T. C.; Poole, K. M.; Foguet-Albiol, D.; Abboud, K. A.; O'Brien, T. A.; Christou, G., *Inorganic Chemistry* **2008,** *47* (15), 6593-6595.

145. Wang, J.; Bi, D.; Niu, J., *CrystEngComm* **2007,** *9* (9), 740-742.

146. Blake, A. J.; Gould, R. O.; Grant, C. M.; Milne, P. E. Y.; Reed, D.; Winpenny, R. E. P., *Angewandte Chemie (International ed. in English)* **1994,** *33* (2), 195-197.

147. Chandrasekhar, V.; Azhakar, R.; Senapati, T.; Thilagar, P.; Ghosh, S.; Verma, S.; Boomishankar, R.; Steiner, A.; Koegerler, P., *Dalton Trans.* **2008,** No. 9, 1150-1160.

148. Chandrasekhar, V.; Kingsley, S., *Angew. Chem., Int. Ed.* **2000,** *39* (13), 2320-2322.

149. Chandrasekhar, V.; Nagarajan, L., *Dalton Trans.* **2009,** No. 34, 6712-6714.

150. Chandrasekhar, V.; Nagarajan, L.; Clerac, R.; Ghosh, S.; Senapati, T.; Verma, S., *Inorganic Chemistry* **2008,** *47* (12), 5347-5354.

151. Chandrasekhar, V.; Nagarajan, L.; Clerac, R.; Ghosh, S.; Verma, S., *Inorganic Chemistry* **2008,** *47* (3), 1067-1073.

152. Gatteschi, D.; Sessoli, R.; Cornia, A., *Chem. Commun.* **2000,** No. 9, 725-732.

153. Oshio, H.; Hoshino, N.; Ito, T.; Nakano, M.; Renz, F.; Gutlich, P., *Angew. Chem., Int. Ed.* **2003,** *42* (2), 223-225.

154. *SAINT, Program for Reduction of Area Detector Data*, Version 6.63; Bruker AXS, Inc.: Madison, WI.

155. Barthelet, K.; Marrot, J.; Riou, D.; Ferey, G., *Angewandte Chemie, International Edition* **2002,** *41* (2), 281-284.

156. Caskey, S. R.; Wong-Foy, A. G.; Matzger, A. J., *Inorganic Chemistry* **2008,** *47* (17), 7751-7756.

157. Chae, H. K.; Siberio-Perez, D. Y.; Kim, J.; Go, Y. B.; Eddaoudi, M.; Matzger, A. J.; O'Keeffe, M.; Yaghi, O. M., *Nature* **2004,** *427* (6974), 523-527.

158. Eddaoudi, M.; Kim, J.; Rosi, N.; Vodak, D.; Wachter, J.; O'Keeffe, M.; Yaghi Omar, M., *Science* **2002,** *295* (5554), 469-72.

159. Ferey, G., *Science* **2001,** *291* (5506), 994-995.

160. Ferey, G.; Mellot-Draznieks, C.; Serre, C.; Millange, F., *Acc. Chem. Res.* **2005,** *38* (4), 217-225.

161. Ferey, G.; Mellot-Draznieks, C.; Serre, C.; Millange, F.; Dutour, J.; Surble, S.; Margiolaki, I., *Science* **2005,** *309* (5743), 2040-2042.

162. Millange, F.; Serre, C.; Ferey, G., *Chemical Communications* **2002,** No. 8, 822-823.

163. Rowsell, J. L. C.; Millward, A. R.; Park, K. S.; Yaghi, O. M., *Journal of the American Chemical Society* **2004,** *126* (18), 5666-5667.

164. Yaghi, O. M.; O'Keeffe, M.; Ockwig, N. W.; Chae, H. K.; Eddaoudi, M.; Kim, J., *Nature* **2003,** *423* (6941), 705-714.

165. Wang, Z.; Heising, J. M.; Clearfield, A., *Journal of the American Chemical Society* **2003,** *125* (34), 10375-10383.

166. Furukawa, H.; Miller, M. A.; Yaghi, O. M., *Journal of Materials Chemistry* **2007,** *17* (30), 3197-3204.

167. Li, Y.; Yang Ralph, T., *Langmuir* **2007,** *23* (26), 12937-44.

168. Mueller, U.; Schubert, M.; Teich, F.; Puetter, H.; Schierle-Arndt, K.; Pastre, J., *Journal of Materials Chemistry* **2006,** *16* (7), 626-636.

169. Ingleson, M. J.; Barrio, J. P.; Bacsa, J.; Dickinson, C.; Park, H.; Rosseinsky, M. J., *Chemical Communications* **2008,** No. 11, 1287-1289.

170. Wu, J.; Hou, H.; Han, H.; Fan, Y., *Inorganic Chemistry* **2007,** *46* (19), 7960-7970.

171. Ayyappan, P.; Evans, O. R.; Foxman, B. M.; Wheeler, K. A.; Warren, T. H.; Lin, W., *Inorganic Chemistry* **2001,** *40* (23), 5954-5961.

172. Fry, J. A.; Samanamu, C. R.; Montchamp, J.-L.; Richards, A. F., *European Journal of Inorganic Chemistry* **2008,** No. 3, 463-470.

173. Chen, B.; Liang, C.; Yang, J.; Contreras, D. S.; Clancy, Y. L.; Lobkovsky, E. B.; Yaghi, O. M.; Dai, S., *Angewandte Chemie, International Edition* **2006,** *45* (9), 1390-1393.

174. Shanmugam, M.; Shanmugam, M.; Chastanet, G.; Sessoli, R.; Mallah, T.; Wernsdorfer, W.; Winpenny, R. E. P., *Journal of Materials Chemistry* **2006,** *16* (26), 2576-2578.

175. Zapf, P. J.; Rose, D. J.; Haushalter, R. C.; Zubieta, J., *Journal of Solid State Chemistry* **1996,** *125* (2), 182-185.

176. Adair, B. A.; Neeraj, S.; Cheetham, A. K., *Chemistry of Materials* **2003,** *15* (7), 1518-1529.

177. Adair, B.; Natarajan, S.; Cheetham, A. K., *Journal of Materials Chemistry* **1998,** *8* (6), 1477-1479.

178. Stock, N.; Stucky, G. D.; Cheetham, A. K., *Chemical Communications* **2000,** No. 22, 2277-2278.

179. Zemlyansky, N. N.; Borisova, I. V.; Kuznetsova, M. G.; Khrustalev, V. N.; Ustynyuk, Y. A.; Nechaev, M. S.; Lunin, V. V.; Barrau, J.; Rima, G., *Organometallics* **2003,** *22* (8), 1675-1681.

180. Lansky, D. E.; Zavalij, P. Y.; Oliver, S. R. J., *Acta Crystallographica, Section C: Crystal Structure Communications* **2001,** *57* (9), 1051-1052.

181. Meng, L.; Sun, Z.; Dong, D.; Chen, H.; Zhu, Y.; Zhang, J.; Zhao, Y.; You, W., *Journal of Coordination Chemistry* **2007,** *60* (17-19), 2075-2083.

182. Natarajan, S.; Cheetham, A. K., *Journal of Solid State Chemistry* **1997,** *134* (1), 207-210.

APPENDIX A

NITROGEN SORPTION AND DESORPTION ISOTHERMS

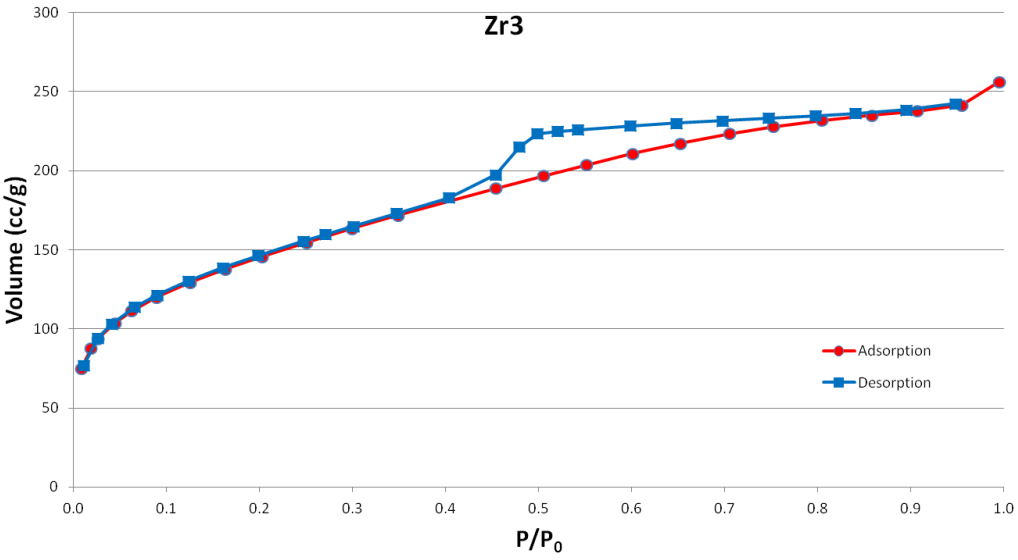

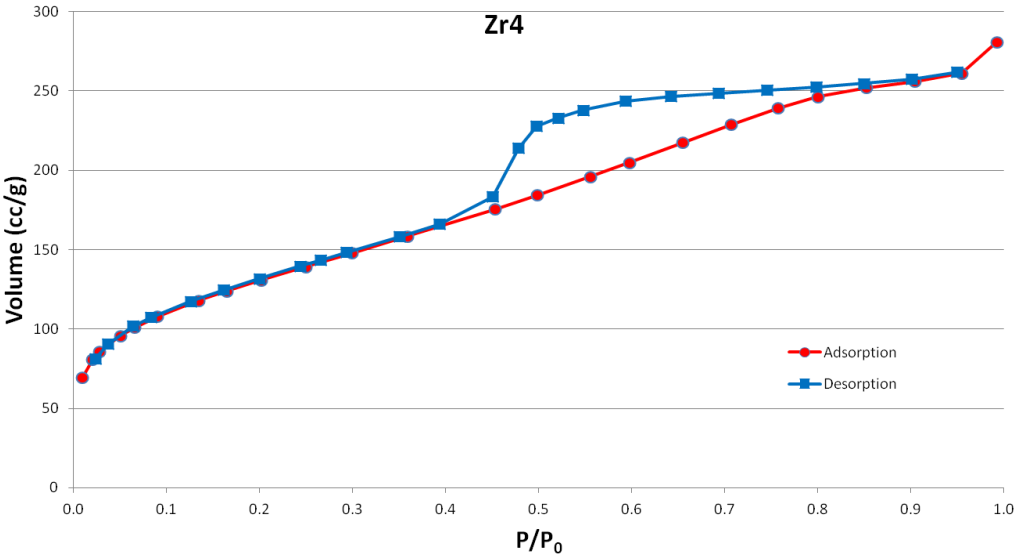

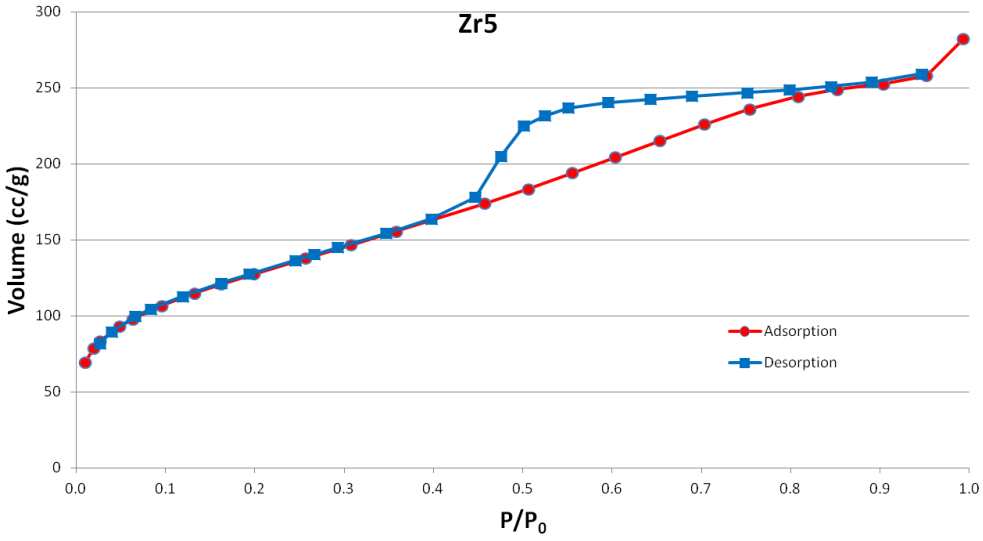
Zr5
Volume (cc/g)
P/P0
Adsorption
Desorption
0
50
100
150
200
250
300
0.0
0.1
0.2
0.3
0.4
0.5
0.6
0.7
0.8
0.9
1.0

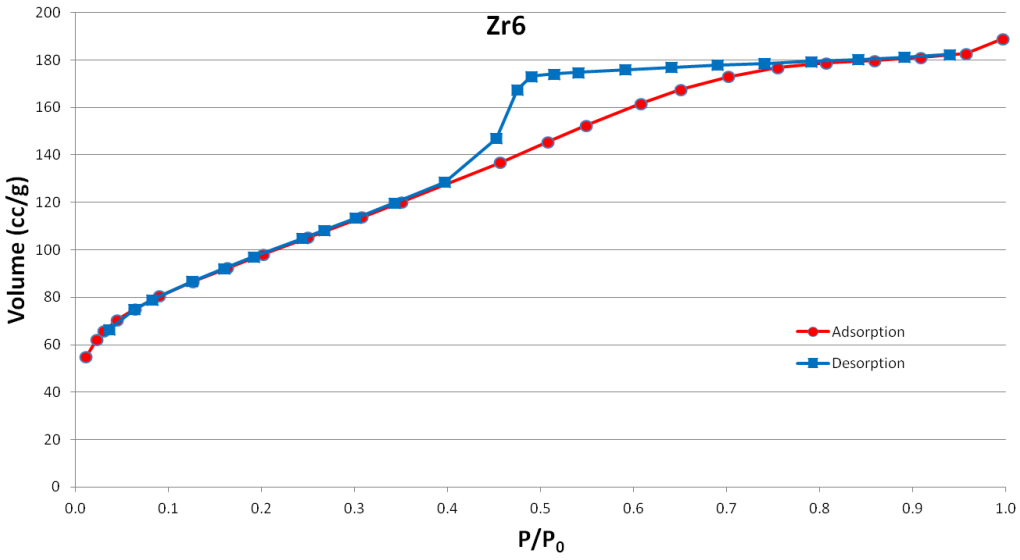
Zr6
Volume (cc/g)
P/P0
Adsorption
Desorption
0
20
40
60
80
100
120
140
160
180
200
0.0
0.1
0.2
0.3
0.4
0.5
0.6
0.7
0.8
0.9
1.0

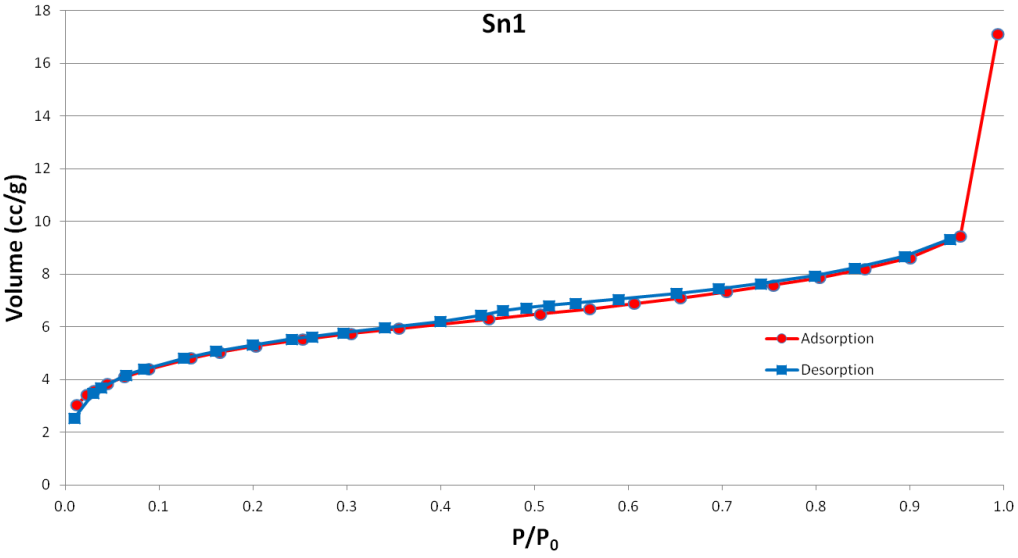
Sn1
Volume (cc/g)
P/P0
Adsorption
Desorption
0
2
4
6
8
10
12
14
16
18
0.0
0.1
0.2
0.3
0.4
0.5
0.6
0.7
0.8
0.9
1.0

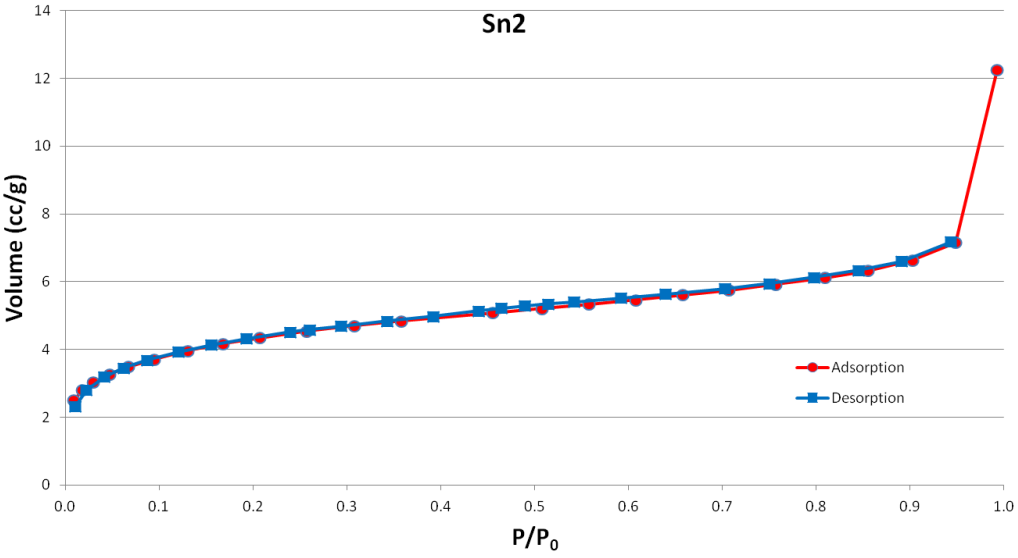
Sn2
Volume (cc/g)
P/P0
Adsorption
Desorption
0
2
4
6
8
10
12
14
0.0
0.1
0.2
0.3
0.4
0.5
0.6
0.7
0.8
0.9
1.0

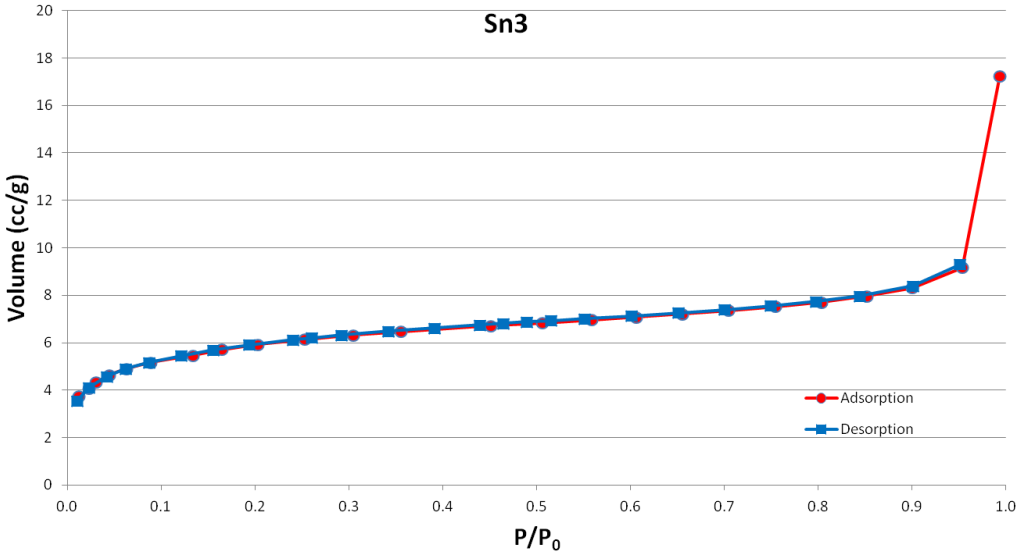
Sn3
Volume (cc/g)
P/P0
Adsorption
Desorption
0
2
4
6
8
10
12
14
16
18
20
0.0
0.1
0.2
0.3
0.4
0.5
0.6
0.7
0.8
0.9
1.0

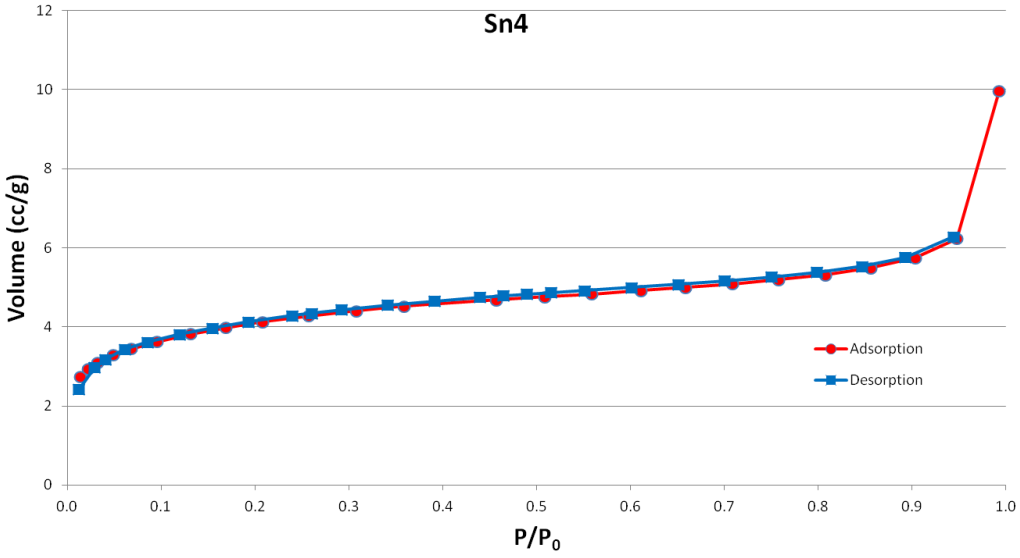
Sn4
Volume (cc/g)
P/P0
Adsorption
Desorption
0
2
4
6
8
10
12
0.0
0.1
0.2
0.3
0.4
0.5
0.6
0.7
0.8
0.9
1.0

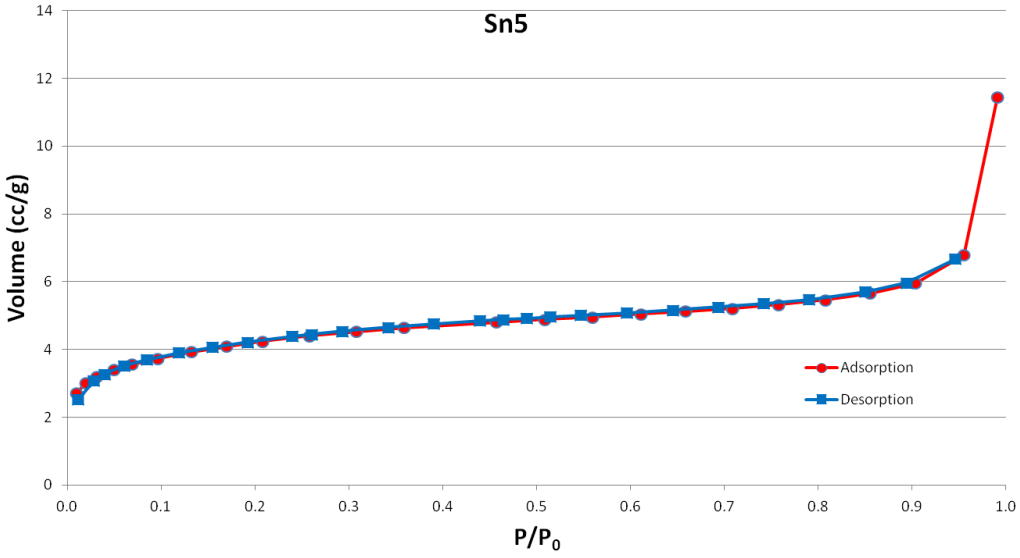
Sn5
Volume (cc/g)
P/P0
Adsorption
Desorption
0
2
4
6
8
10
12
14
0.0
0.1
0.2
0.3
0.4
0.5
0.6
0.7
0.8
0.9
1.0

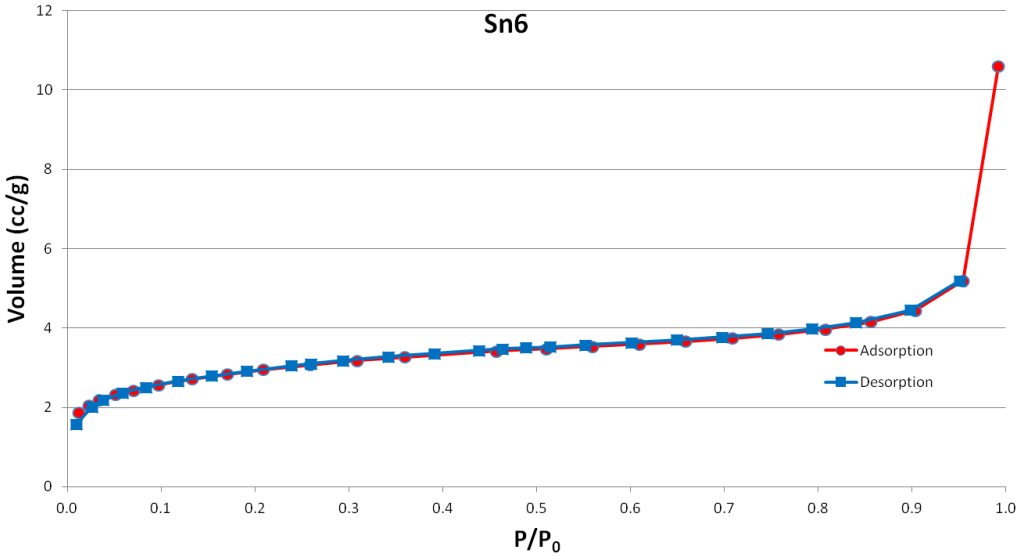
Sn6
Volume (cc/g)
P/P0
Adsorption
Desorption
0
2
4
6
8
10
12
0.0
0.1
0.2
0.3
0.4
0.5
0.6
0.7
0.8
0.9
1.0

APPENDIX B

THERMOGRAVIMETRIC ANALYSES

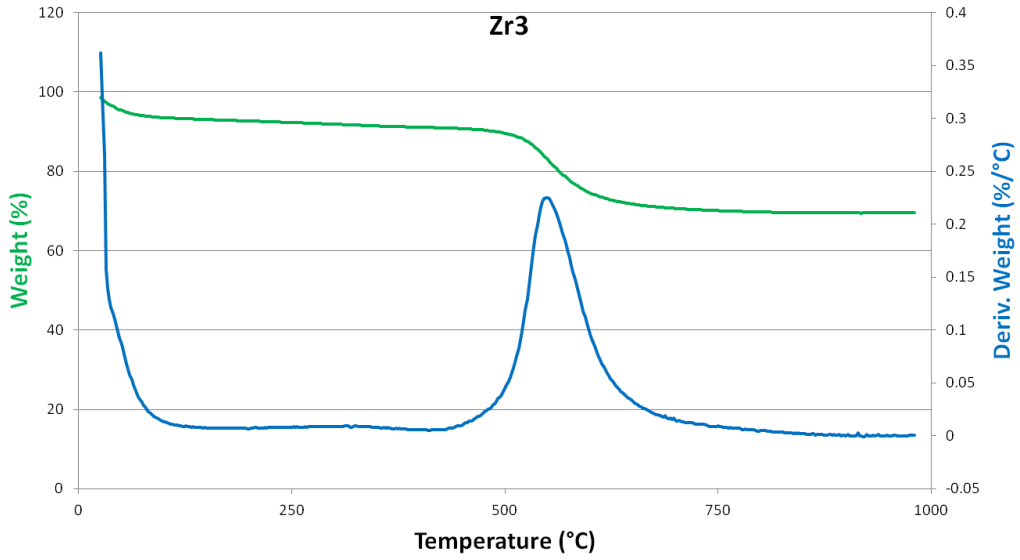

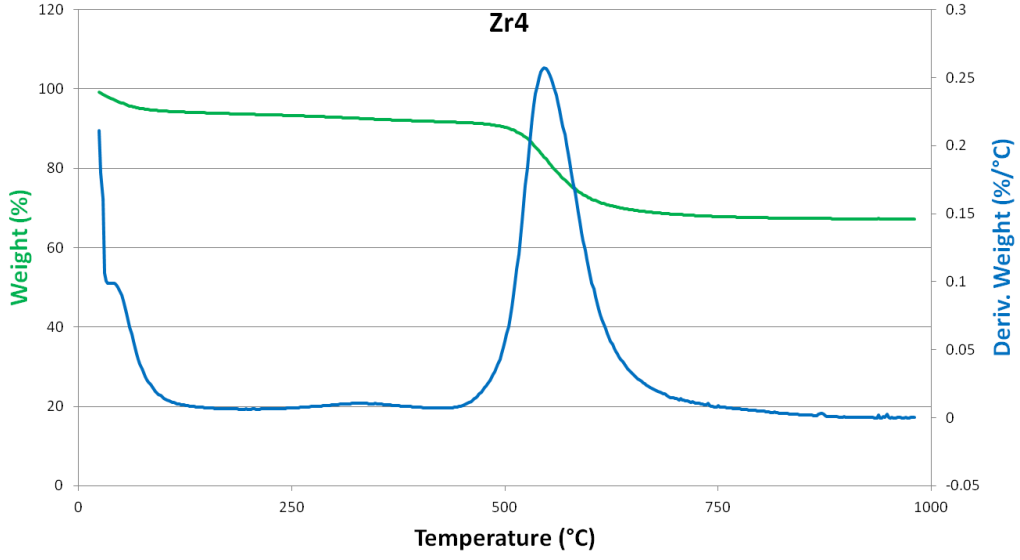

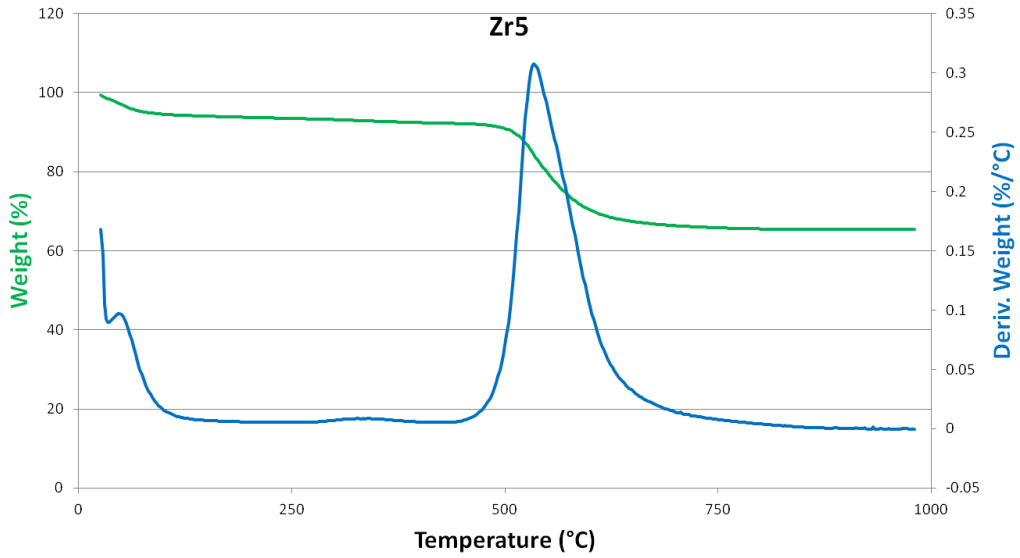
Zr5
Weight (%)
Deriv. Weight (%/°C)
Temperature (°C)
120
100
80
60
40
20
0
0.35
0.3
0.25
0.2
0.15
0.1
0.05
0
-0.05
0
250
500
750
1000

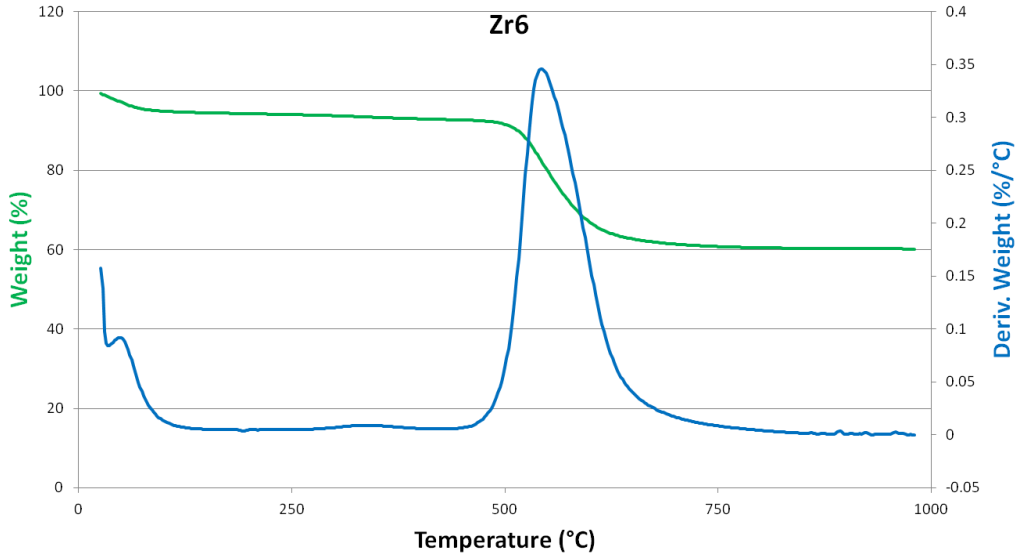
Zr6
Weight (%)
Deriv. Weight (%/°C)
Temperature (°C)
120
100
80
60
40
20
0
0.4
0.35
0.3
0.25
0.2
0.15
0.1
0.05
0
-0.05
0
250
500
750
1000

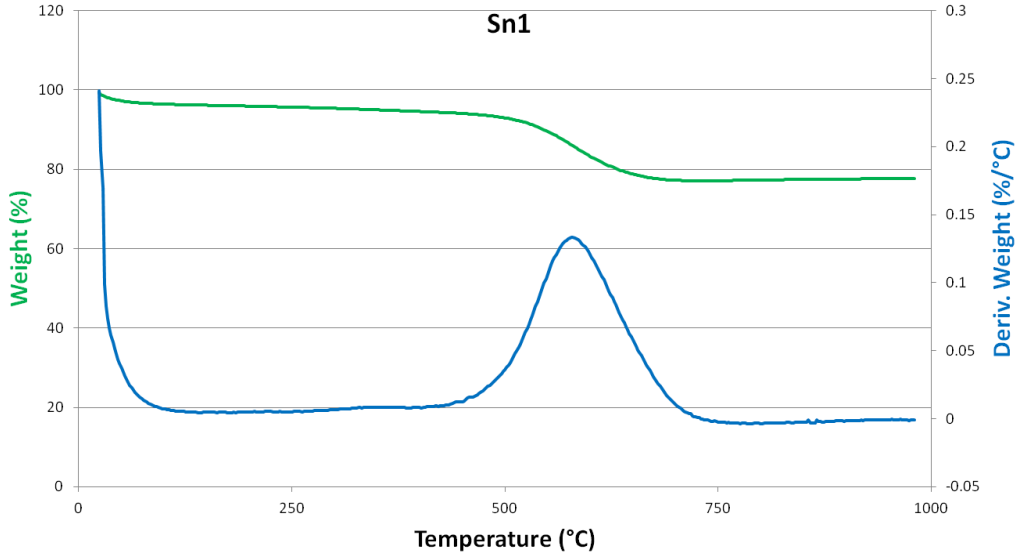
Sn1
Weight (%)
Deriv. Weight (%/°C)
Temperature (°C)
120
100
80
60
40
20
0
0.3
0.25
0.2
0.15
0.1
0.05
0
-0.05
0
250
500
750
1000

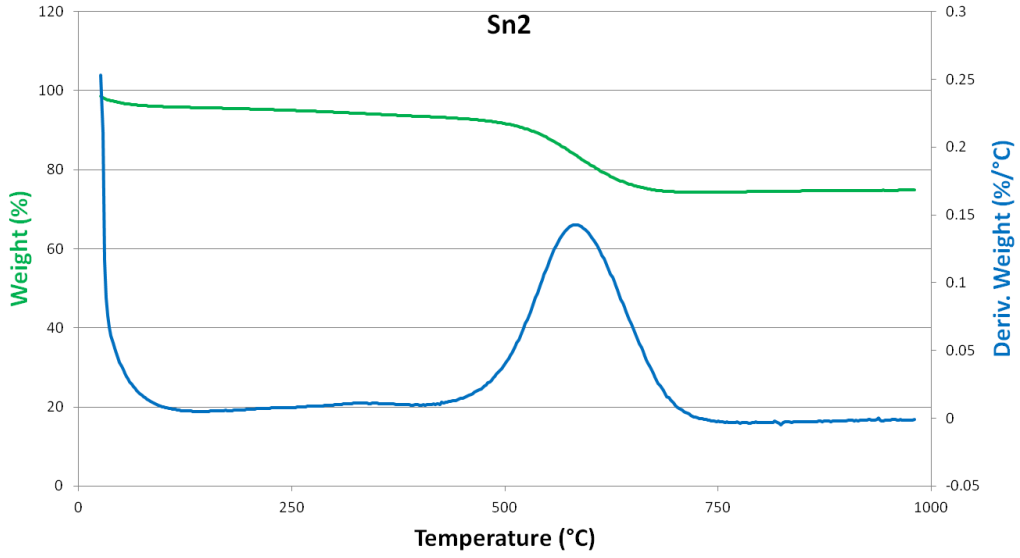
Sn2
Weight (%)
Deriv. Weight (%/°C)
Temperature (°C)
120
100
80
60
40
20
0
0.3
0.25
0.2
0.15
0.1
0.05
0
-0.05
0
250
500
750
1000

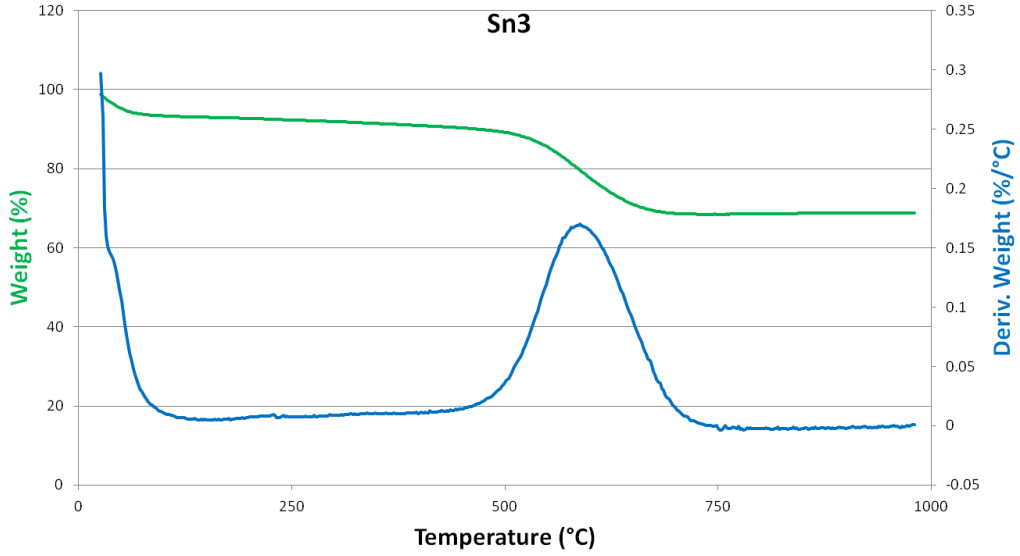
Sn3
Weight (%)
Deriv. Weight (%/°C)
Temperature (°C)
120
100
80
60
40
20
0
0.35
0.3
0.25
0.2
0.15
0.1
0.05
0
-0.05
0
250
500
750
1000

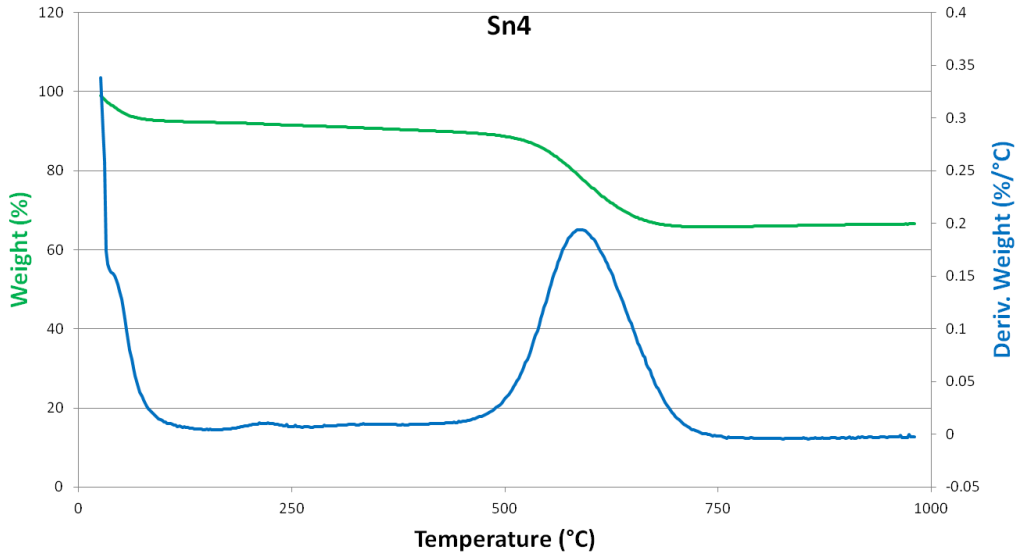
Sn4
Weight (%)
Deriv. Weight (%/°C)
Temperature (°C)
120
100
80
60
40
20
0
0.4
0.35
0.3
0.25
0.2
0.15
0.1
0.05
0
-0.05
0
250
500
750
1000

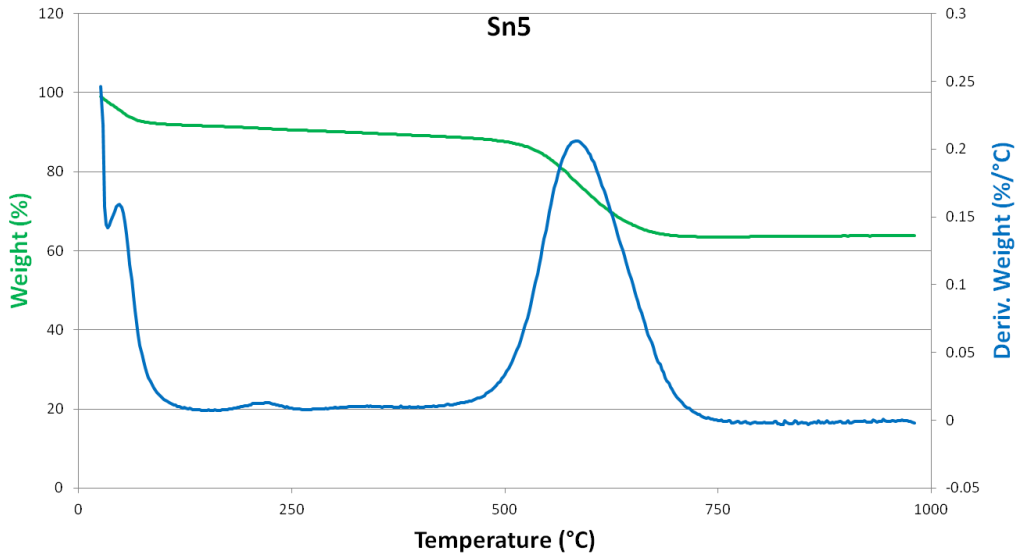
Sn5
Weight (%)
Deriv. Weight (%/°C)
Temperature (°C)
120
100
80
60
40
20
0
0.3
0.25
0.2
0.15
0.1
0.05
0
-0.05
0
250
500
750
1000

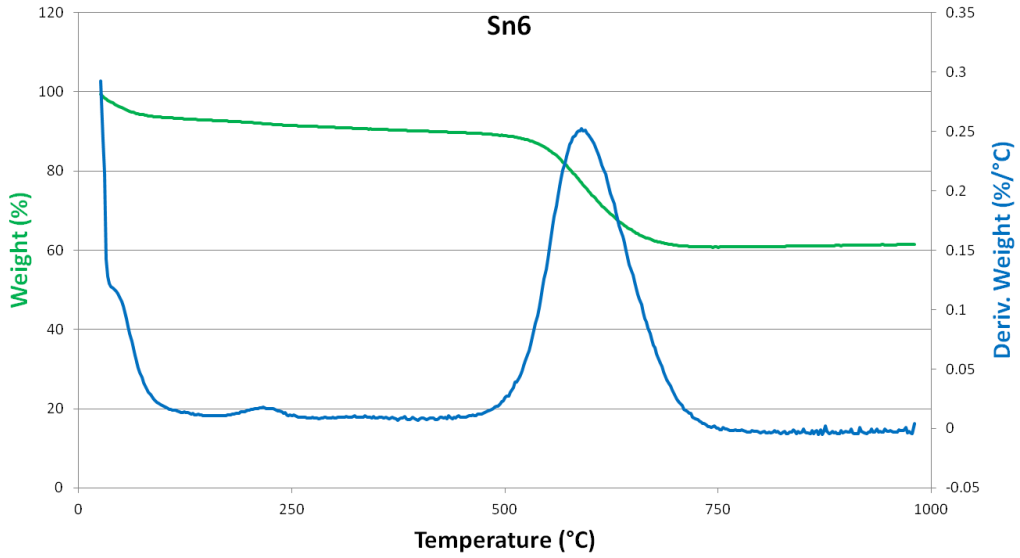
Sn6
Weight (%)
Deriv. Weight (%/°C)
Temperature (°C)
120
100
80
60
40
20
0
0.35
0.3
0.25
0.2
0.15
0.1
0.05
0
-0.05
0
250
500
750
1000

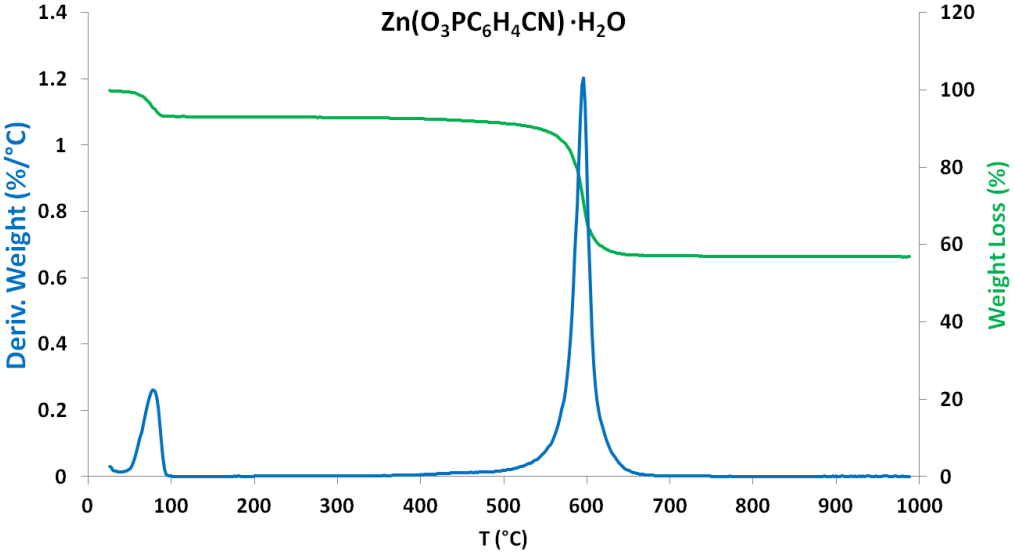
Zn(O3PC6H4CN)·H2O
Deriv. Weight (%/°C)
Weight Loss (%)
T (°C)
1.4
1.2
1
0.8
0.6
0.4
0.2
0
120
100
80
60
40
20
0
0
100
200
300
400
500
600
700
800
900
1000

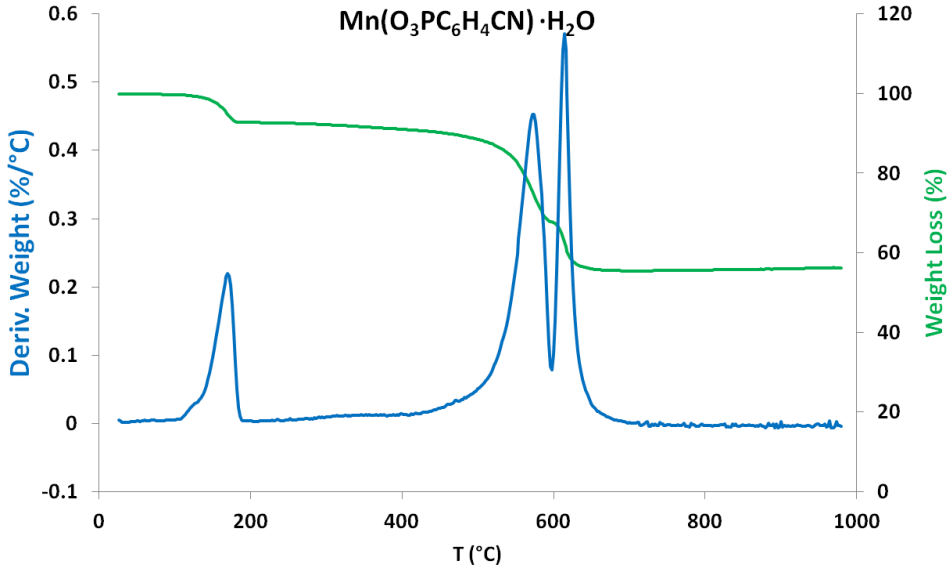
Mn(O3PC6H4CN)·H2O
Deriv. Weight (%/°C)
Weight Loss (%)
T (°C)
0.6
0.5
0.4
0.3
0.2
0.1
0
-0.1
120
100
80
60
40
20
0
0
200
400
600
800
1000

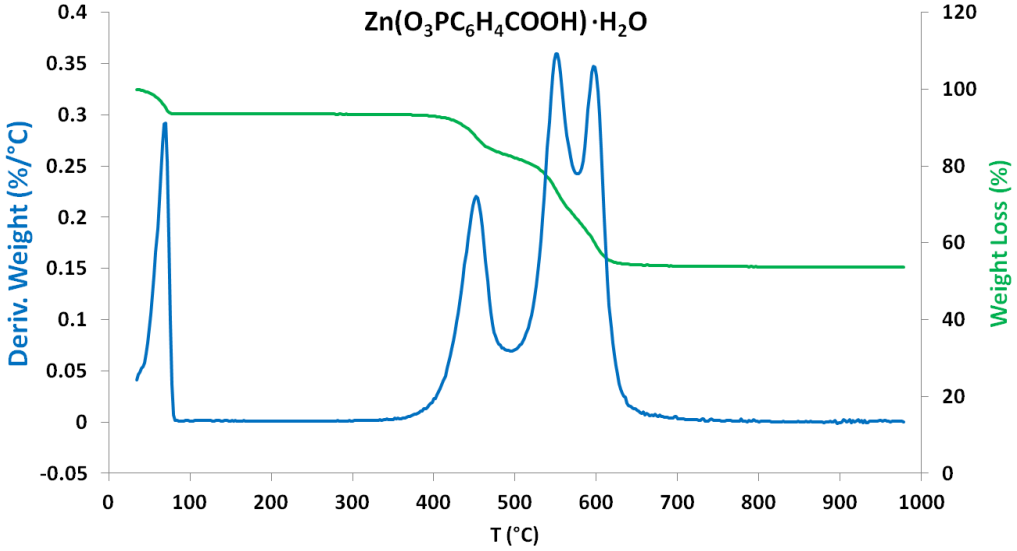
Zn(O3PC6H4COOH)·H2O
Deriv. Weight (%/°C)
Weight Loss (%)
T (°C)
0.4
0.35
0.3
0.25
0.2
0.15
0.1
0.05
0
-0.05
120
100
80
60
40
20
0
0
100
200
300
400
500
600
700
800
900
1000

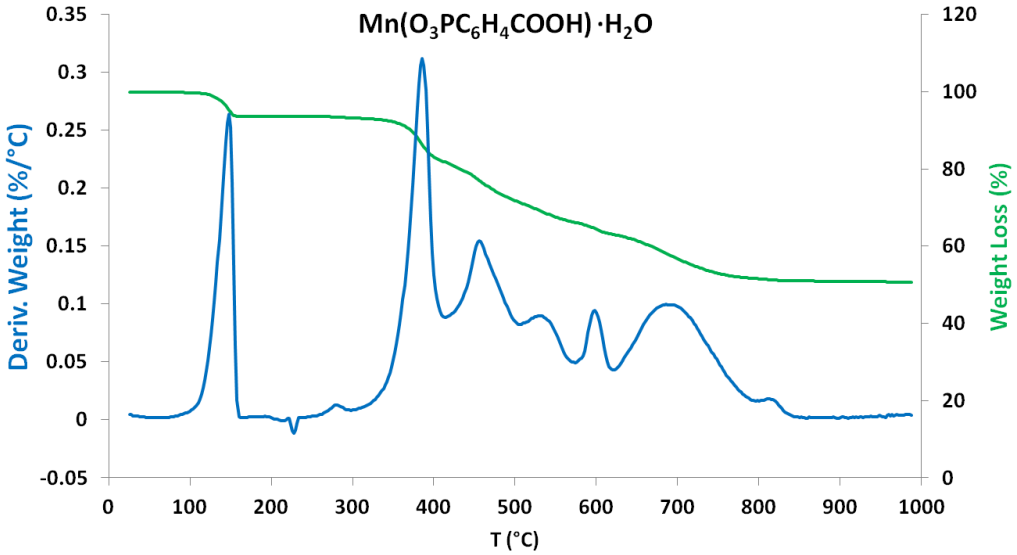
Mn(O3PC6H4COOH)·H2O
Deriv. Weight (%/°C)
Weight Loss (%)
T (°C)
0.35
0.3
0.25
0.2
0.15
0.1
0.05
0
-0.05
120
100
80
60
40
20
0
0
100
200
300
400
500
600
700
800
900
1000

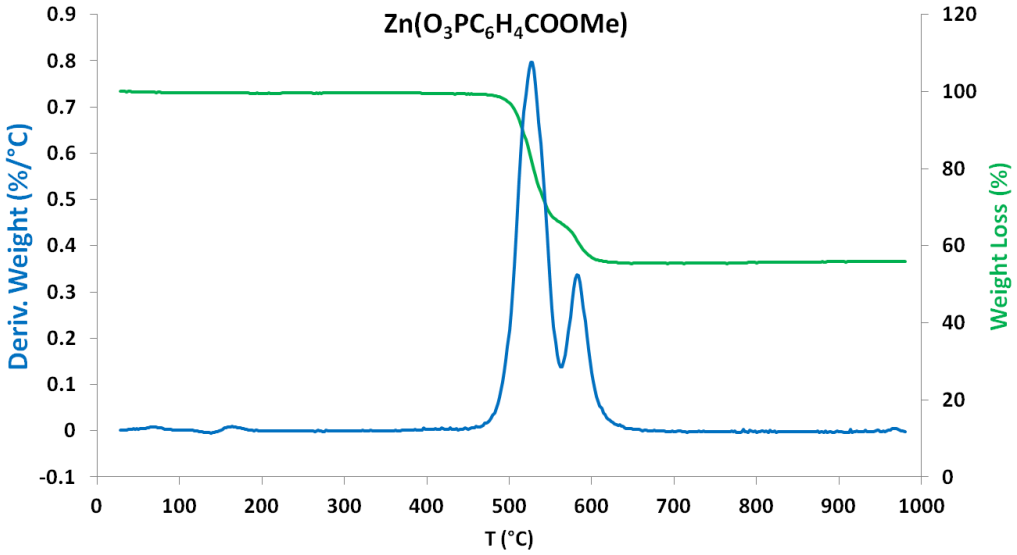
Zn(O3PC6H4COOMe)
Deriv. Weight (%/°C)
Weight Loss (%)
T (°C)
0.9
0.8
0.7
0.6
0.5
0.4
0.3
0.2
0.1
0
-0.1
120
100
80
60
40
20
0
0
100
200
300
400
500
600
700
800
900
1000

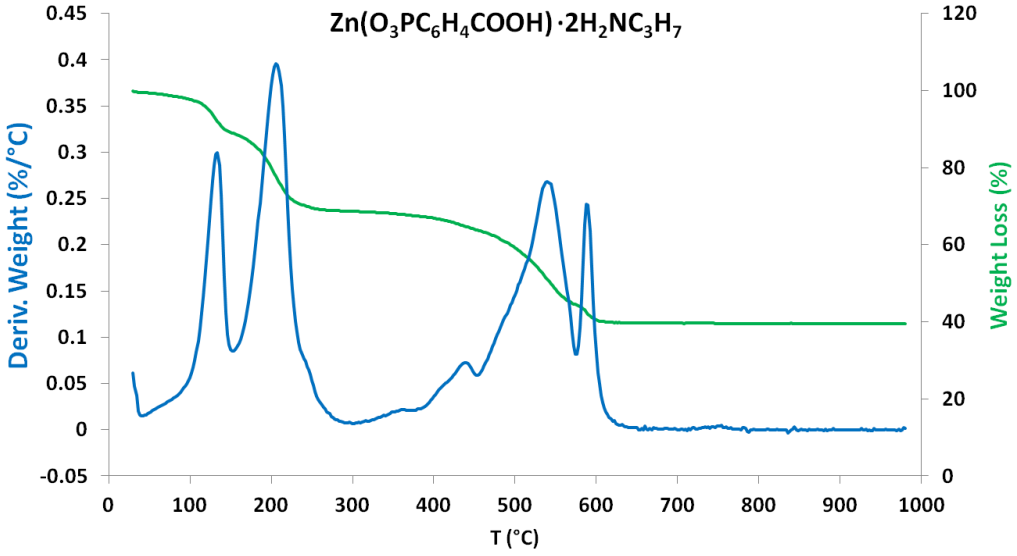
Zn(O3PC6H4COOH)·2H2NC3H7
Deriv. Weight (%/°C)
Weight Loss (%)
T (°C)
0.45
0.4
0.35
0.3
0.25
0.2
0.15
0.1
0.05
0
-0.05
120
100
80
60
40
20
0
0
100
200
300
400
500
600
700
800
900
1000

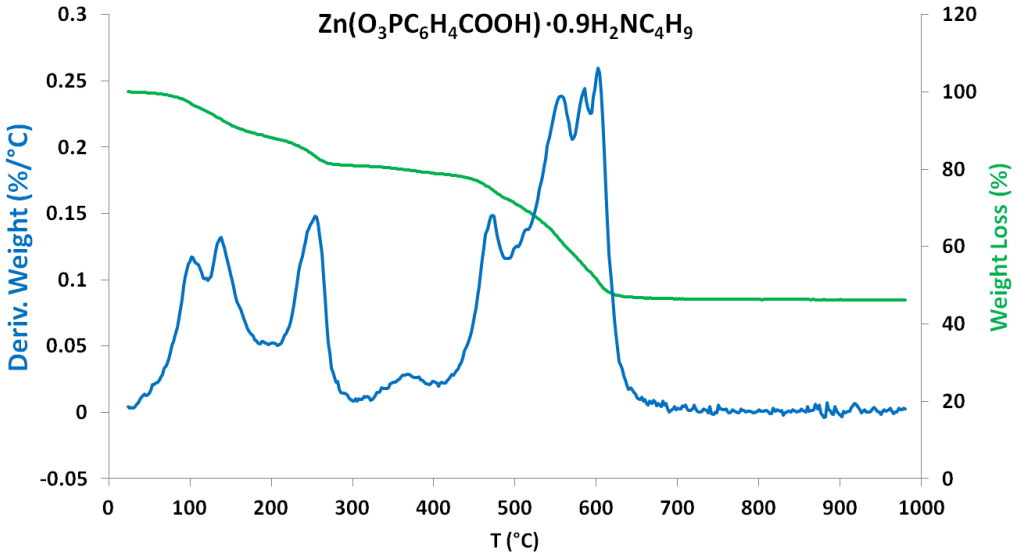
Zn(O3PC6H4COOH)·0.9H2NC4H9
Deriv. Weight (%/°C)
Weight Loss (%)
T (°C)
0.3
0.25
0.2
0.15
0.1
0.05
0
-0.05
120
100
80
60
40
20
0
0
100
200
300
400
500
600
700
800
900
1000

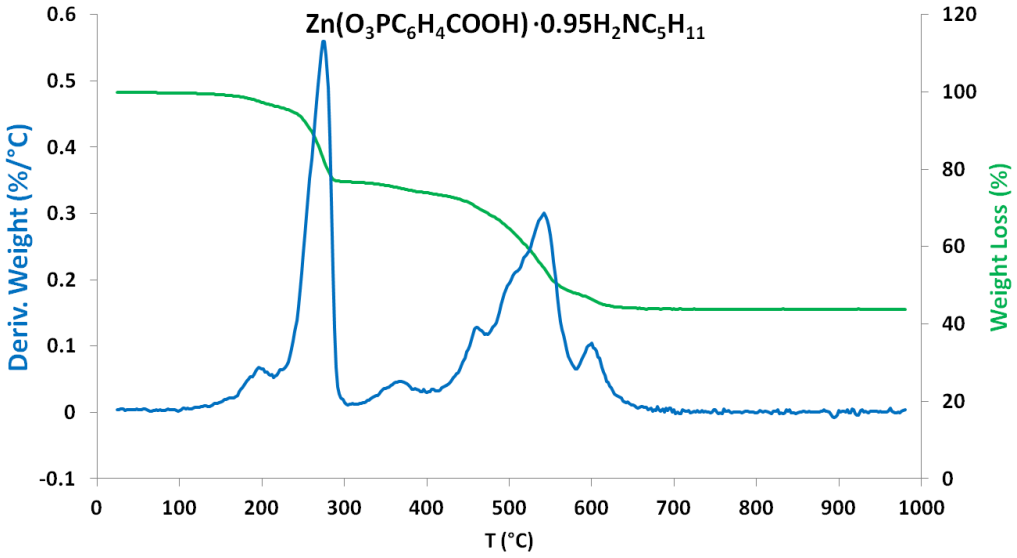
Zn(O3PC6H4COOH)·0.95H2NC5H11
Deriv. Weight (%/°C)
Weight Loss (%)
T (°C)
0.6
0.5
0.4
0.3
0.2
0.1
0
-0.1
120
100
80
60
40
20
0
0
100
200
300
400
500
600
700
800
900
1000

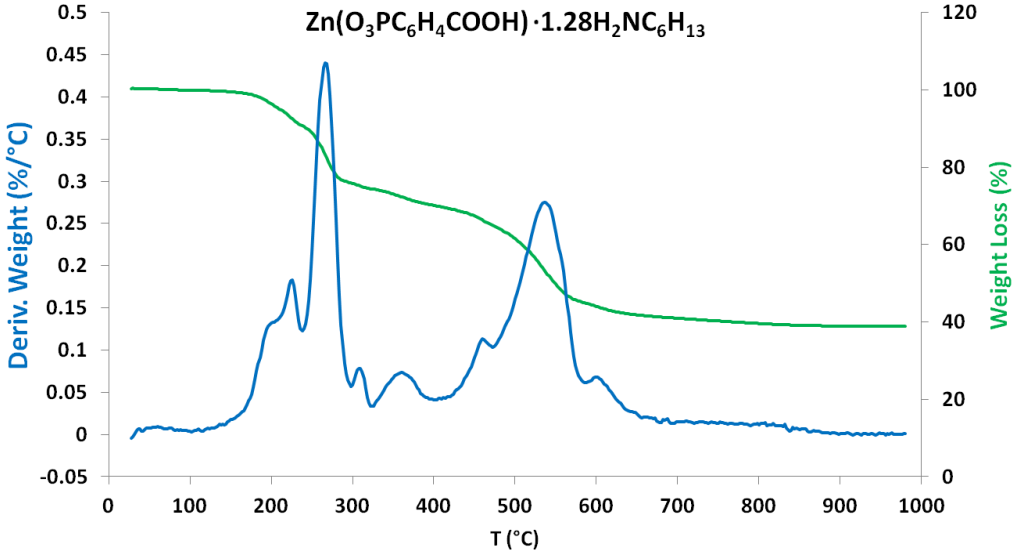
Zn(O3PC6H4COOH)·1.28H2NC6H13
Deriv. Weight (%/°C)
Weight Loss (%)
T (°C)
0.5
0.45
0.4
0.35
0.3
0.25
0.2
0.15
0.1
0.05
0
-0.05
120
100
80
60
40
20
0
0
100
200
300
400
500
600
700
800
900
1000

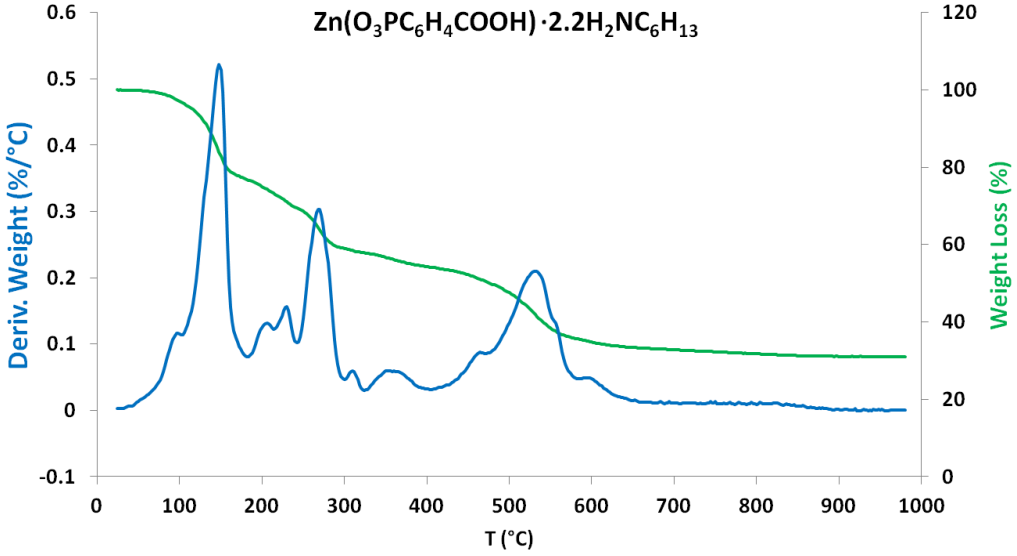
Zn(O3PC6H4COOH)·2.2H2NC6H13
Deriv. Weight (%/°C)
Weight Loss (%)
T (°C)
0.6
0.5
0.4
0.3
0.2
0.1
0
-0.1
120
100
80
60
40
20
0
0
100
200
300
400
500
600
700
800
900
1000

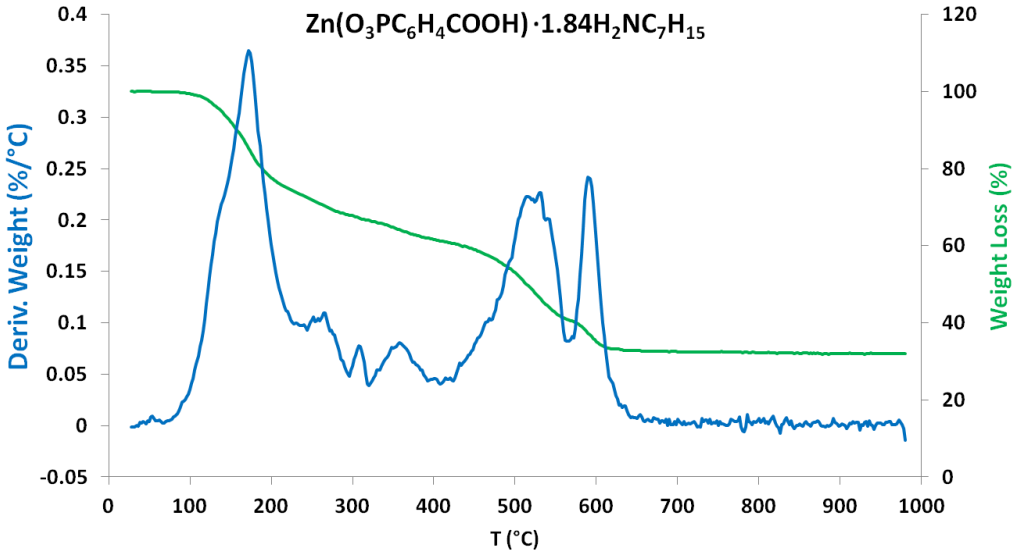
Zn(O3PC6H4COOH)·1.84H2NC7H15
Deriv. Weight (%/°C)
Weight Loss (%)
T (°C)
0.4
0.35
0.3
0.25
0.2
0.15
0.1
0.05
0
-0.05
120
100
80
60
40
20
0
0
100
200
300
400
500
600
700
800
900
1000

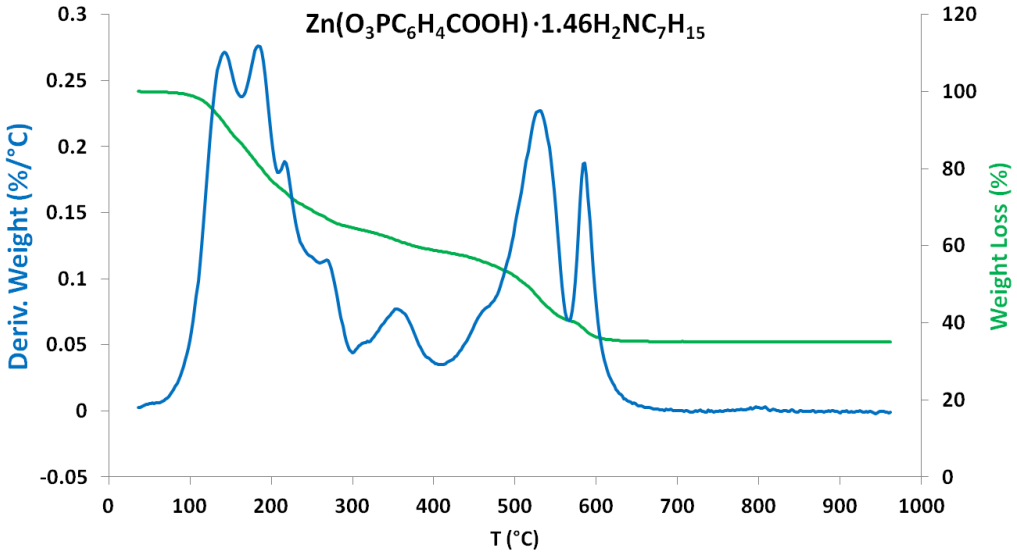
Zn(O3PC6H4COOH)·1.46H2NC7H15
Deriv. Weight (%/°C)
Weight Loss (%)
T (°C)
0.3
0.25
0.2
0.15
0.1
0.05
0
-0.05
120
100
80
60
40
20
0
0
100
200
300
400
500
600
700
800
900
1000

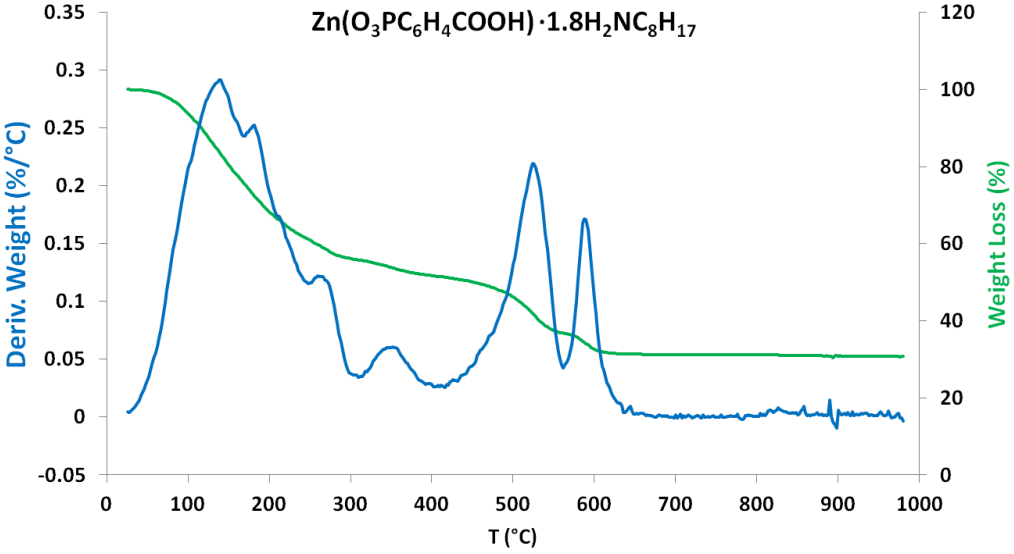
Zn(O3PC6H4COOH)·1.8H2NC8H17
Deriv. Weight (%/°C)
Weight Loss (%)
T (°C)
0.35
0.3
0.25
0.2
0.15
0.1
0.05
0
-0.05
120
100
80
60
40
20
0
0
100
200
300
400
500
600
700
800
900
1000

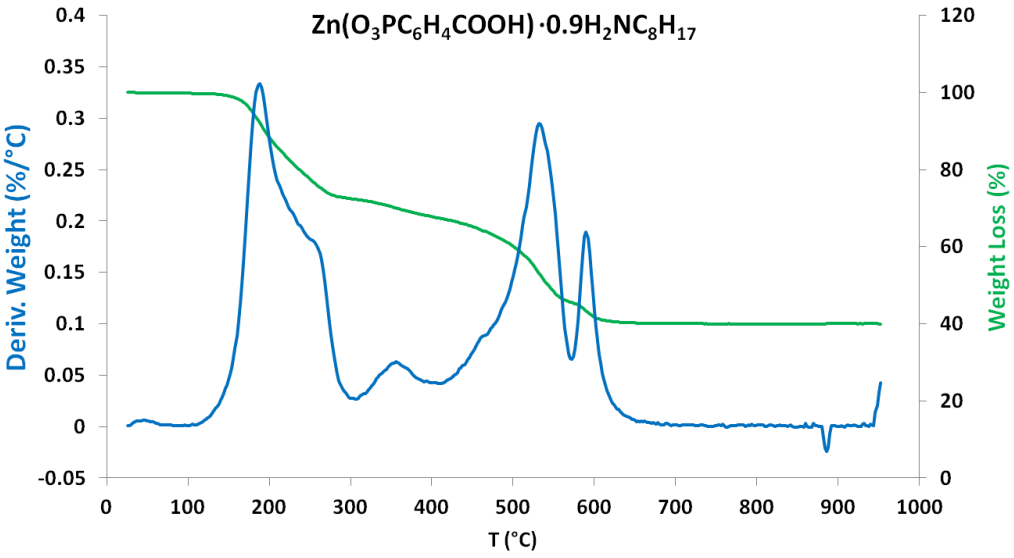
Zn(O3PC6H4COOH)·0.9H2NC8H17
Deriv. Weight (%/°C)
Weight Loss (%)
T (°C)
0.4
0.35
0.3
0.25
0.2
0.15
0.1
0.05
0
-0.05
120
100
80
60
40
20
0
0
100
200
300
400
500
600
700
800
900
1000

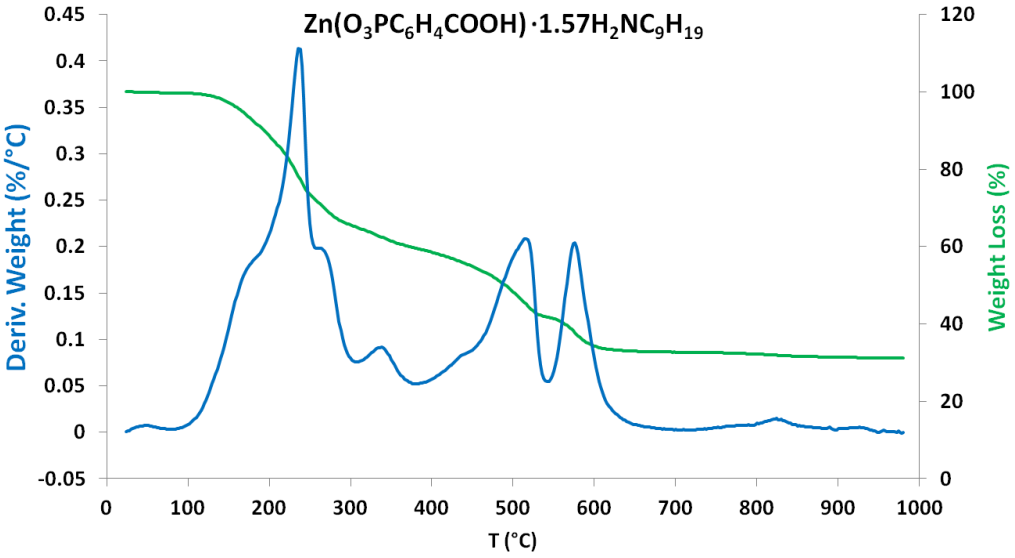
Zn(O3PC6H4COOH)·1.57H2NC9H19
Deriv. Weight (%/°C)
Weight Loss (%)
T (°C)
0.45
0.4
0.35
0.3
0.25
0.2
0.15
0.1
0.05
0
-0.05
120
100
80
60
40
20
0
0
100
200
300
400
500
600
700
800
900
1000

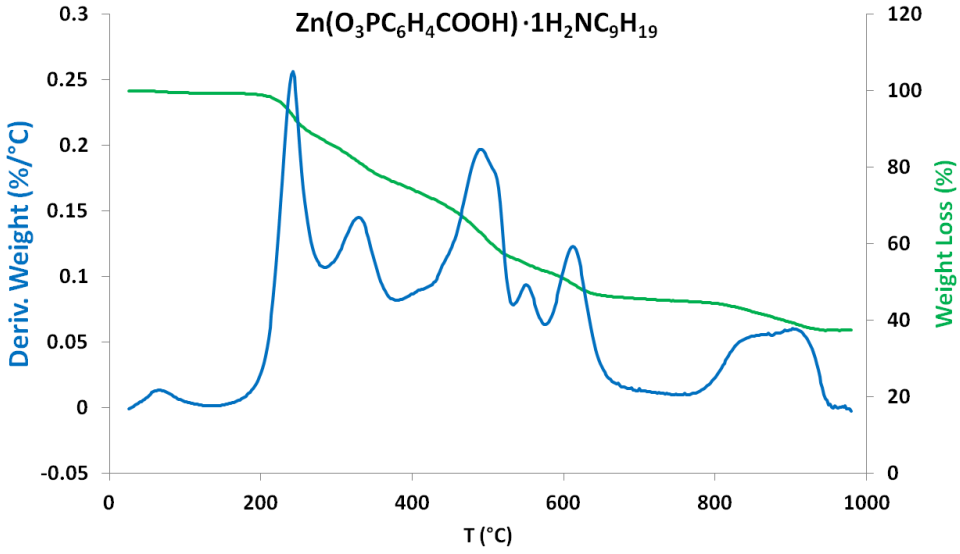
Zn(O3PC6H4COOH)·1H2NC9H19
Deriv. Weight (%/°C)
Weight Loss (%)
T (°C)
0.3
0.25
0.2
0.15
0.1
0.05
0
-0.05
120
100
80
60
40
20
0
0
200
400
600
800
1000

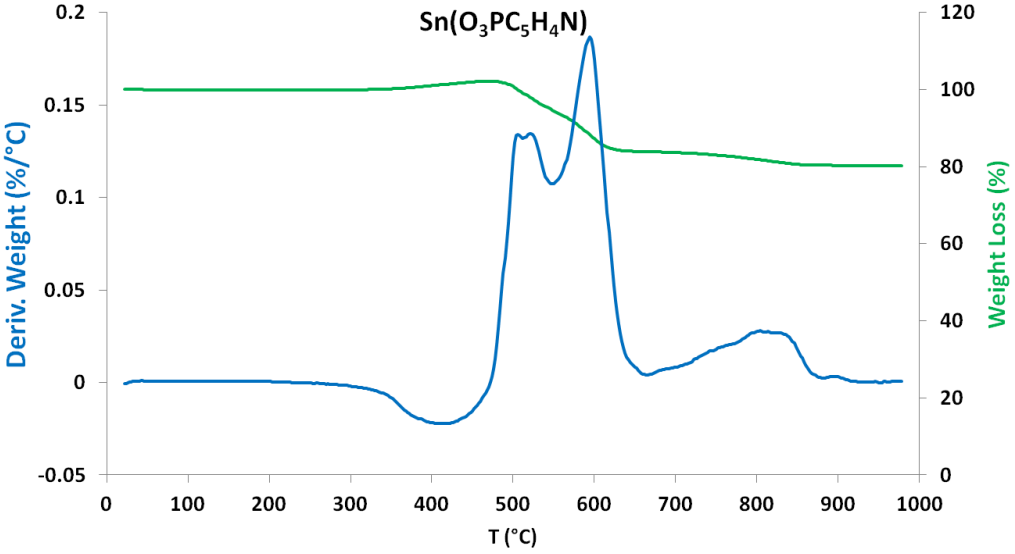
Sn(O3PC5H4N)
Deriv. Weight (%/°C)
Weight Loss (%)
T (°C)
0.2
0.15
0.1
0.05
0
-0.05
120
100
80
60
40
20
0
0
100
200
300
400
500
600
700
800
900
1000

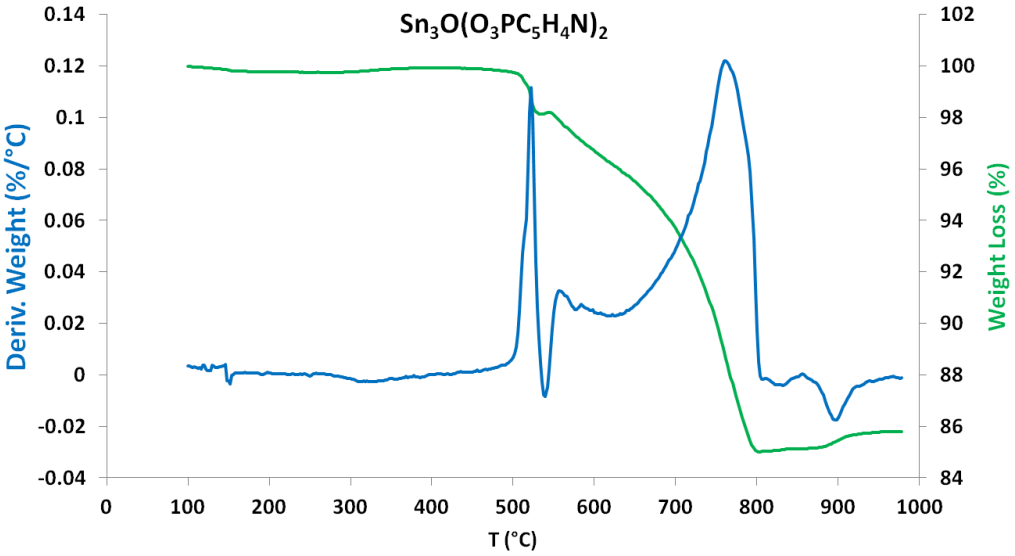
Sn3O(O3PC5H4N)2
Deriv. Weight (%/°C)
Weight Loss (%)
T (°C)
0.14
0.12
0.1
0.08
0.06
0.04
0.02
0
-0.02
-0.04
102
100
98
96
94
92
90
88
86
84
0
100
200
300
400
500
600
700
800
900
1000

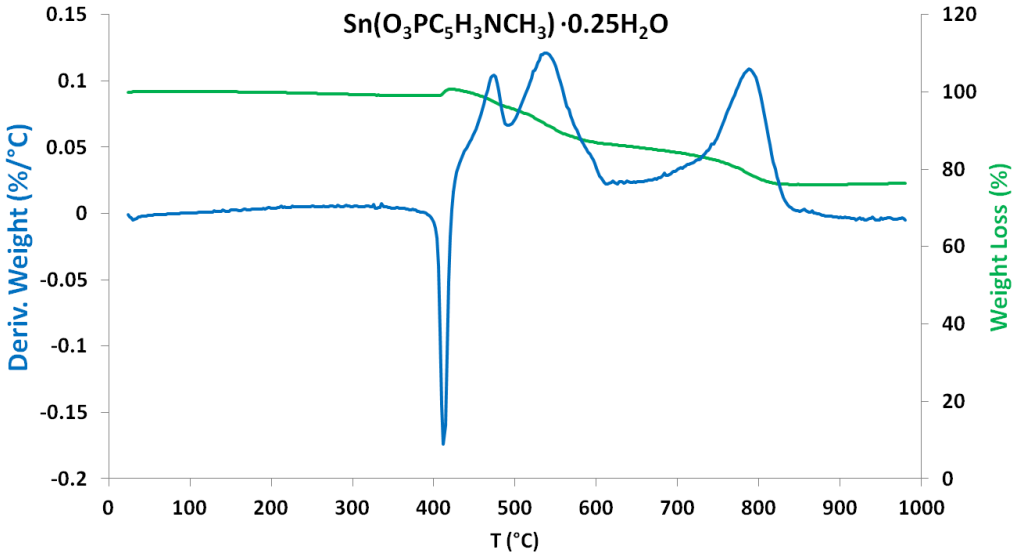
Sn(O3PC5H3NCH3)·0.25H2O
Deriv. Weight (%/°C)
Weight Loss (%)
T (°C)
0.15
0.1
0.05
0
-0.05
-0.1
-0.15
-0.2
120
100
80
60
40
20
0
0
100
200
300
400
500
600
700
800
900
1000

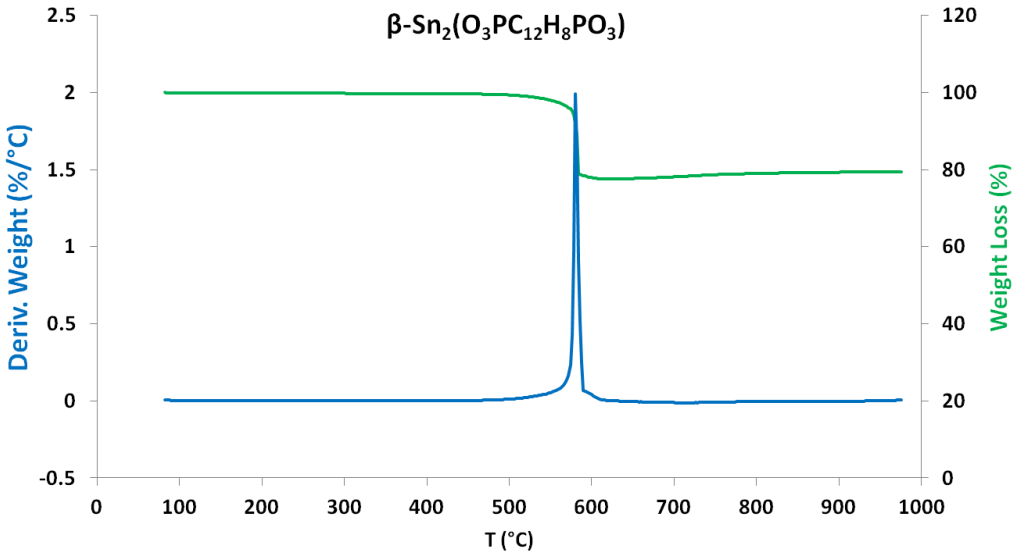
β-Sn2(O3PC12H8PO3)
Deriv. Weight (%/°C)
Weight Loss (%)
T (°C)
2.5
2
1.5
1
0.5
0
-0.5
120
100
80
60
40
20
0
0
100
200
300
400
500
600
700
800
900
1000

VITA

Name:	Houston Phillipp Perry
Address:	Chemistry Dept, c/o Dr. Clearfield, Texas A&M University, College Station, TX 77843-3255
Email Address:	hpperry@gmail.com
Education:	B.S., Chemistry, Texas A&M University, 2005 Ph.D., Chemistry, Texas A&M University, 2011